NWRF 37-0660-035

METEOROLOGICAL ASPECTS
of
RADIO-RADAR PROPAGATION

U.S. NAVY WEATHER RESEARCH FACILITY
NORFOLK, VIRGINIA

June 1960

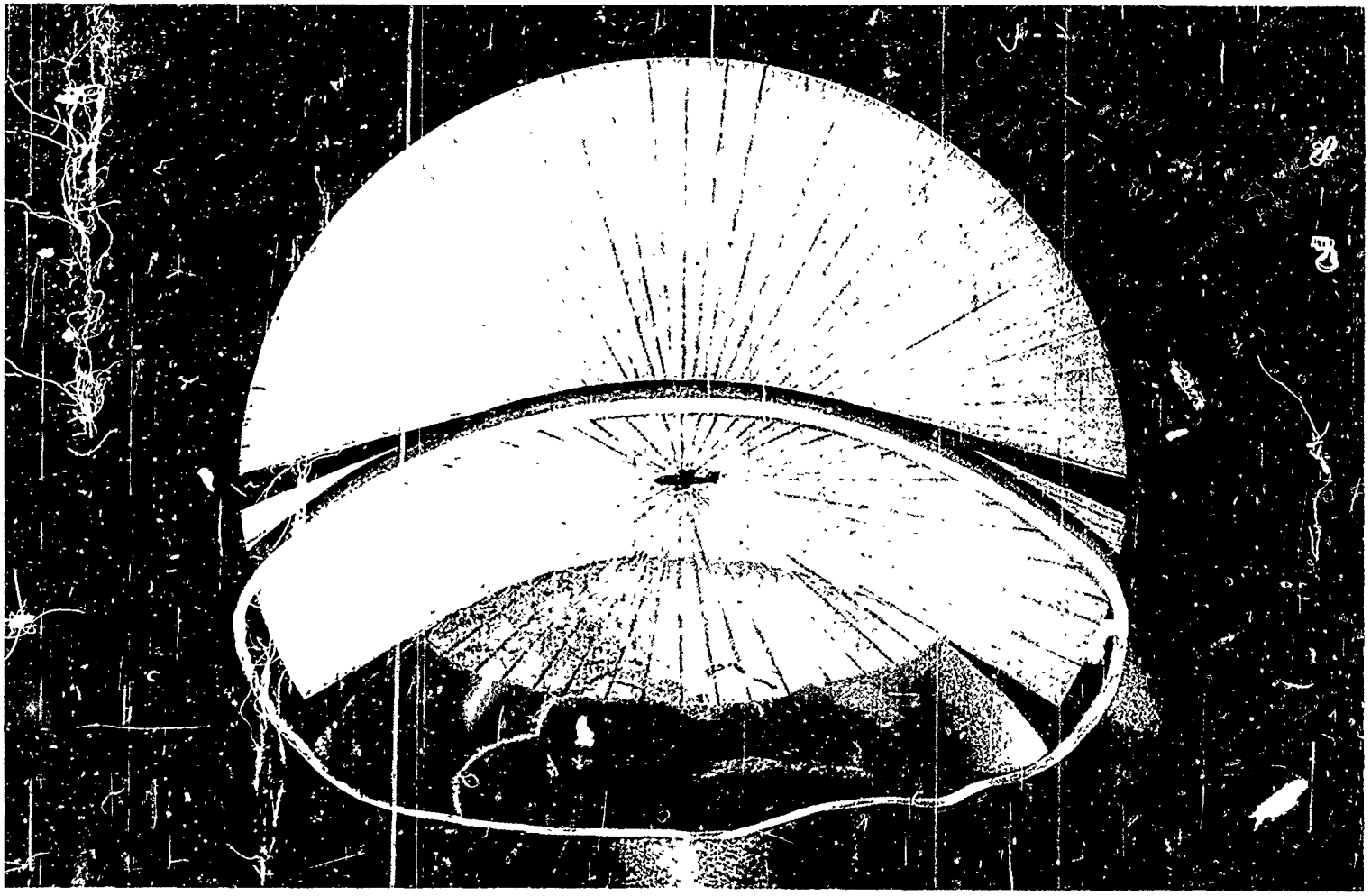

FRONTISPIECE - The Radar Hole.

METEOROLOGICAL ASPECTS

OF

RADIO-RADAR PROPAGATION

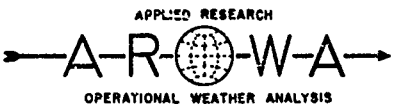

U. S. NAVY WEATHER RESEARCH FACILITY
BUILDING R-48
U. S. NAVAL AIR STATION
NORFOLK 11, VIRGINIA

June 1960

FOREWORD

This report has been prepared under Task 31, "Meteorological Aspects of Refraction and Propagation of Radar Waves," which was assigned to the U. S. Navy Weather Research Facility for the purpose of developing new techniques for predicting atmospheric propagation parameters. Fleet and field units, operating microwave radio and radar equipment, require atmospheric information in order to evaluate and predict the performance of naval communications and detection systems.

This publication is intended as a comprehensive reference in radio-radar meteorology for Naval Weather Service personnel. It is not a procedural manual and, more often than not, suggests several solutions to a given problem without prescribing the "best one". Our objective has been to assemble sufficient general information so as to facilitate the solution of new, as well as routine, problems as they arise in the field. In an era of rapid technological advance and of ever-changing concepts as to the tactical employment of radio and radar systems, new problems must be dealt with on an almost daily basis.

The central ideas presented herein are largely the result of research, supported in part by the U. S. Navy Weather Research Facility, at Smyth Research Associates in San Diego, California and at the Boulder Laboratories of the National Bureau of Standards in Boulder, Colorado. Chapters 5, 6, and 7 were taken almost wholly from a manuscript written under contract by Mr. L. J. Anderson of Smyth Research Associates. Chapters 8 and 9 were taken almost wholly from technical reports prepared by Mr. B. R. Bean and associates at the Boulder Laboratories of the National Bureau of Standards. Chapters 1, 2, 3, and 4 were assembled by the undersigned from current literature.

The research program, which laid the foundations for this report, was organized under the direction of Comdr. J. P. King, USN, with the assistance of Mr. Paul L. Hexter. Excellent editorial assistance was provided during the assembly of this publication by Mr. John M. Mercer.

DANIEL F. REX
Commander, U. S. Navy
Officer in Charge
Navy Weather Research Facility

TABLE OF CONTENTS

TABLE OF CONTENTS (Continued)

TABLE OF CONTENTS (Continued)

TABLE OF CONTENTS (Continued)

LIST OF FIGURES, TABLES, AND CHARTS

Page

Figures (80) (Continued):

Page

Figures (80) (Continued):

Page

Tables (6):

Charts (7): In Envelope Inside Back Cover.

INTRODUCTION

A specific responsibility of the meteorological officer, as stated in U. S. Navy Regulations[1], is to provide "the information necessary for evaluation of the effects of sea and atmospheric conditions on radar and sonar performance." In order to provide this information (insofar as it relates to radar performance) the weather officer must:

1. Understand the effects of atmospheric variables on (radio and) radar performance.

2. Know the fleet requirements for atmospheric information in terms of current operational employment.

3. Collect the necessary data, and make those analyses pertinent to a description of existing atmospheric propagation conditions.

4. Describe the propagation conditions that will be encountered at some future time.

It should perhaps be emphasized that success can only be achieved by taking each of these four actions.

It is the aim of this manual to provide the Naval Weather Service officer with information of direct assistance in connection with items 1, 3, and 4 above. A knowledge of fleet requirements (item 2) can only be obtained from experience and through frequent and detailed discussions with command and operational personnel. The weather officer must take the initiative in order to fully inform himself concerning fleet (operational) requirements.

It should be mentioned here that since the material in this manual was gathered from many sources, the letters and symbols used in the text and equations are not necessarily uniformly defined throughout the entire manual; i.e., the symbols may only be consistent in meaning within the section where they are used.

In part I of this manual, some of the basic principles of radio-

[1] U. S. Navy Regulations, Chapter 9, Article 0928.

radar propagation are presented in order to familiarize the reader with the nature of electromagnetic energy and how it propagates through the atmosphere. No attempt has been made to present a complete treatise on the subject; only that information considered to be essential to an elementary understanding of the subject has been included. Part II contains a rather general discussion of atmospheric refraction, the methods available for obtaining refractive index data, and the various modified indices in common use. In part III, working methods for computing radio-radar performance are presented, together with numerical examples (in some cases) intended to clarify the procedures used. In order to apply the methods of part III intelligently, the reader should become as familiar as possible with the background material presented in parts I and II.

The final section of this manual, part IV, presents information available from various climatological and synoptic studies of atmospheric refractivity. This material has been included not only because of its interest in connection with planning problems, but more particularly because of its importance in predicting future refractive conditions. It seems unlikely that our ability to forecast pressure, temperature, and humidity will improve rapidly enough within the next decade to permit one to predict future propagation conditions from direct forecasts of these parameters. Refractivity forecasts will more probably be made, within the foreseeable future, from a consideration of the expected climatological and synoptic influences on present (observed) conditions.

In concluding this introduction it may be well to mention that abnormal radio-radar performance may be the result of improper or abnormal functioning of the radar equipment, or it may be the result of atmospheric effects. In the first instance the electronics (or radar) officer must take action. In the second instance, the weather officer and the electronics officer must take joint, coordinated action in order to minimize detrimental (and to take advantage of favorable) atmospheric conditions. Work with your electronics - CIC - radar teammates!

PART I

BASIC PRINCIPLES

1. ELECTROMAGNETIC PROPAGATION

1.1 Characteristics of Electromagnetic Waves

The wave nature of visible light was first demonstrated by Thomas Young in 1801. James Clerk Maxwell, after a study of Faraday's scientific papers, published several mathematic treatises on the electromagnetic theory of light in the late 1860's. It was not, however, until 1873 that this theory appeared in a fully developed form in his "Electricity and Magnetism". Maxwell reduced all electric and magnetic phenomena to stresses and motions of a material medium and proved that electromagnetic waves in a homogeneous, transmitting medium tend to propagate in straight lines with a velocity equal to

$$v = \frac{c}{\sqrt{\mu k}} , \tag{1.1}$$

where c is the velocity of light, μ is the magnetic permeability, and k is the dielectric constant of the medium.

Since Maxwell's time it has been found that there is an entire spectrum of electromagnetic waves, covering at least 20 decades of wavelength, over which the physical characteristics of the waves are identical, except for wavelength itself. A representation of a simple wave motion is shown in figure 1.1. In this figure a periodic variable, A, is plotted graphically as a function of time, t. For the case of an electromagnetic wave the quantity A may be considered to be either the electric field strength or the magnetic field strength at some fixed point in space. If we define one wavelength, λ, as the distance from crest to crest (or trough to trough) and the frequency, f, as the number of cycles completed per unit time; i.e., the number of wavelengths which pass a fixed point in unit time, the velocity of propagation, v, is equal to

$$v = \lambda f , \tag{1.2}$$

or, from equation (1.1)

$$\lambda f = \frac{c}{\sqrt{\mu k}} . \tag{1.3}$$

In a homogeneous medium the quantity $\frac{c}{\sqrt{\mu k}}$ is a constant (i.e., the propagation velocity is constant) so that either wavelength or frequency, which are inversely related, may be used to uniquely describe any par-

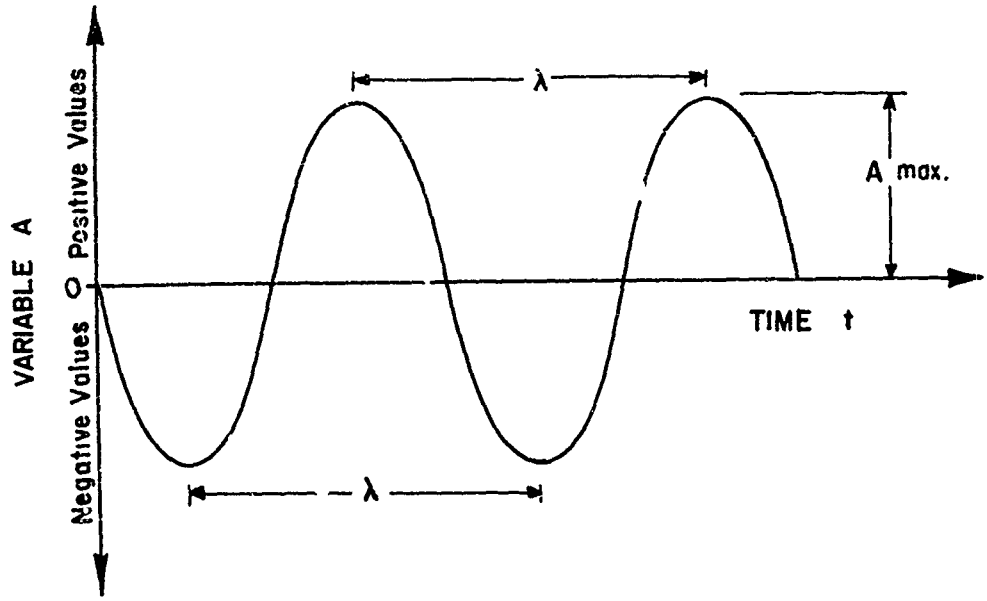

Figure 1.1. A Simple Sine Wave.

ticular electromagnetic wave.

Electromagnetic energy propagates best in a vacuum, where both μ and k equal unity; however, most gases and some solids are transparent to it as well. The velocity of propagation in a vacuum is identical over the entire wavelength spectrum and is equal to the velocity of light (3.0×10^8 cm./sec.). One of the basic axioms of physics is that this is the maximum velocity attainable by energy or matter.

In some of its properties electromagnetic energy behaves as though it consisted of energy packets (quanta) instead of waves. This has given rise to the branch of physics known as "quantum mechanics", which has done much to clarify many of the puzzling phenomena which have been observed, particularly at extremely short wavelengths. For the purposes of this manual however, one may regard electromagnetic energy as being purely a wave phenomenon. In the radio-radar spectrum, the wave nature of the energy is sufficiently general to describe all the phenomena with which we are concerned.

1.2 The Electromagnetic Spectrum

Figure 1.2 is a representation of the entire electromagnetic spectrum as it is now recognized. It is divided into numerous wavelength bands as shown. The boundaries are somewhat arbitrary because overlapping occurs, particularly at shorter wavelengths, but the figure illustrates the variety of phenomena to which the name "electromagnetic energy" is properly applied. The wavelength and frequency scales are logarithmic. The vertical lines are divided into increments, each of which represents a tenfold change in wavelength. The units commonly used to designate wavelength and frequency are shown just to the left and to the right of the vertical lines.

The narrow band just below the 1 micron (μ) line represents the visible spectrum which covers the range of sensitivity of the human eye. Late in the last century the remainder of the vast spectrum (nonvisual) shown in figure 1.2 was discovered, resulting in a flood of new knowledge and techniques whose usefulness is now gradually being exploited.

The portion of the spectrum discussed in this manual is that shown above the far infrared band in figure 1.2, particularly the region above the 1-centimeter wavelength line. This is the radio-radar spectrum in which waves are generated by coherent electronic transmitters of various kinds.

1.3 Wave Fronts and Rays

In dealing with the behavior of electromagnetic energy it is often convenient to employ the concepts of wave fronts and rays. The Dutch scientist Huyghens in 1690 stated the principle which leads to a simple geometrical construction of the wave front, and which allows us to deal with a wave motion as a straight-line propagation.

In figure 1.3 the point P represents a point source of energy from which electromagnetic waves are proceeding through a homogeneous medium with equal speeds in all directions. At the end of a certain time the disturbance will have arrived at all points which lie on the spherical surface S_1. Since the points are all equidistant from P, the locus of such points is a sphere, and this sphere represents the initial wave front. According to Huyghens' principle every point on the wave front becomes immediately a new source from which secondary waves

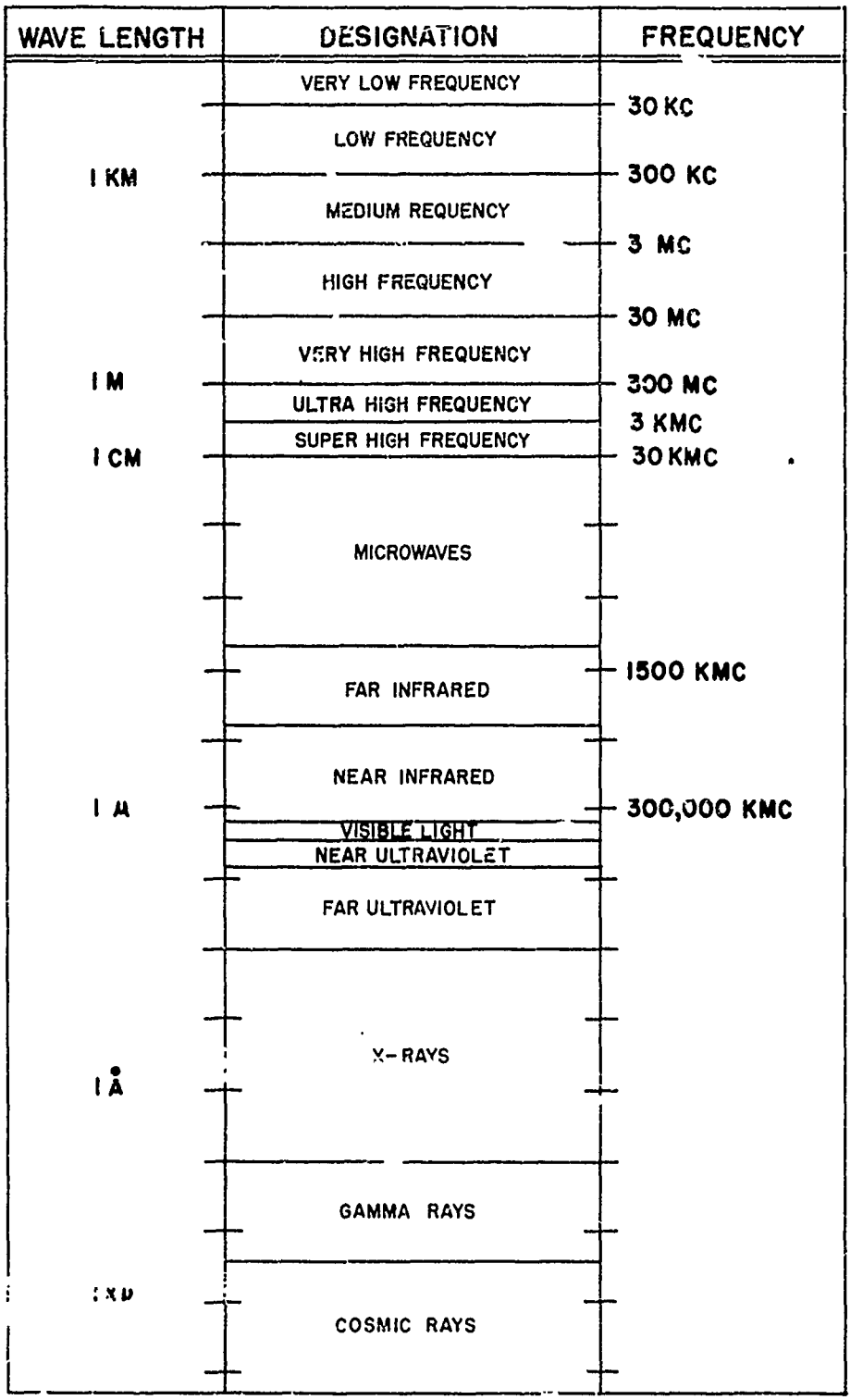

Figure 1.2. The Electromagnetic Spectrum.

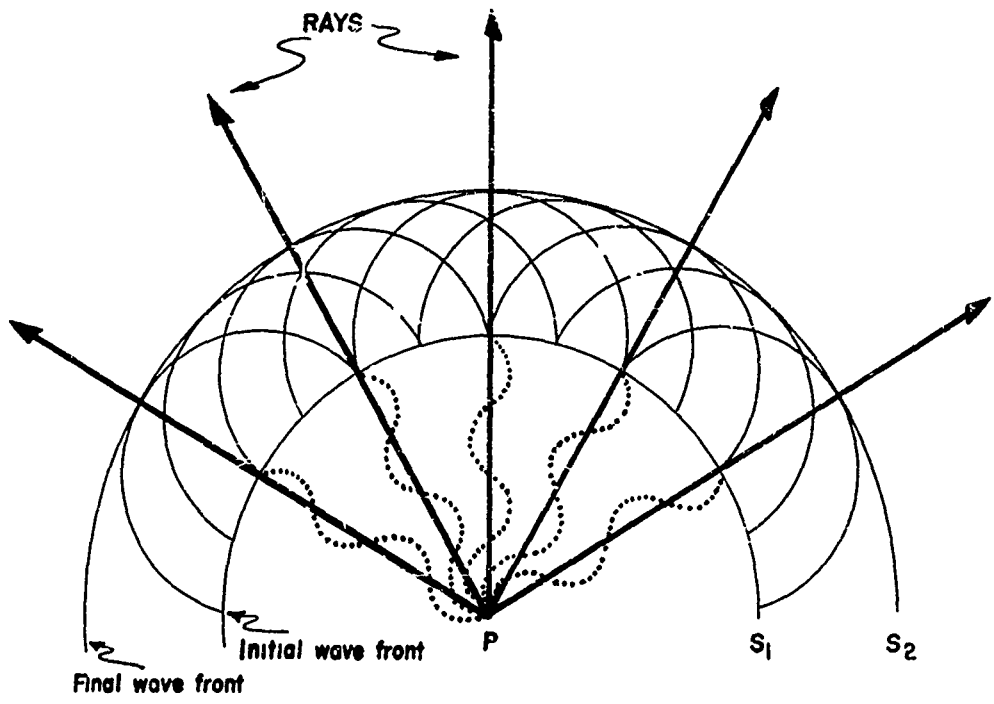

Figure 1.3. Huyghens' Construction of the Wave Front.

or wavelets spread out in all directions. By construction then, let us draw circles of equal radius from each point on the surface $\underline{S_1}$ representing the wavelets. These innumerable wavelets, starting together from all points influenced by the principal wave, overlap and interfere with each other so that their resultant effect is produced only at the points in the resultant surface which at any instant envelop all the secondary wave fronts. Thus, the new principal wave front will be $\underline{S_2}$, which is the enveloping surface or envelope of the wavelets. The tangent surface, constructed from the wavelets according to Huyghens' principle, thus gives the position of the wave front at a later time. The result is the same as if the old wave front $\underline{S_1}$ had expanded into a new wave front $\underline{S_2}$, the disturbance progressing in straight lines in all directions.

It can be seen that in a homogeneous medium (i.e., propagation velocity constant at all points in the medium) the enveloping surface or wave front emanating from a point source will be a sphere concentric with all other earlier and later wave fronts, and that straight lines or rays, radiating out from the center, will be the paths of the disturbance. The ray (see fig. 1.3), which is the path of the disturbance, is

thus normal to the wave front, which is the envelope of the disturbance.

1.4 Propagation Characteristics in Free Space

It is convenient to begin our study of electromagnetic propagation characteristics with a consideration of the behavior of electromagnetic waves in free space; i.e., in a vacuum and without the presence of discrete bodies.

1.4.1 Free Space Fields

A fundamental factor governing the behavior of electromagnetic waves is the inverse distance spreading of energy. If a transmitting source emits a given amount of energy per second, $\mathscr{P}_t$, when one is at distance r from the transmitter this energy is spread out over the surface of a sphere of radius r and area $4\pi r^2$ (see fig. 1.3). Thus, the power received $\mathscr{P}_r$ at distance r from a point source P is

$$\mathscr{P}_r = \frac{\mathscr{P}_t}{4\pi r^2} \tag{1.4}$$

watts per unit area. The power decreases as the square of the distance from the source (or transmitter), and the electromagnetic field strength, which is proportional to the square root of power, decreases as the first power of the distance. This decrease is known as the "free space attentuation" of the field, since it occurs even in a vacuum and without the earth present. It is a direct consequence of the fundamental law of the conservation of energy, and applies both in free space and in the terrestrial environment.

1.4.2 Interference

Whenever two (or more) wave trains travelling over different paths impinge (intersect) at a point in space, the phenomenon known as interference occurs. If the two waves arrive at the point in question in phase they reinforce one another and produce a resultant field strength greater than either of the two component waves taken alone. If the two waves arrive at the point in question out of phase they partially cancel one another and produce a weaker resultant field strength. This phenomenon is fundamental to all wave motion and occurs both in free space and in the terrestrial environment. Figure 1.4 illustrates the phenomenon of interference for two simple sine waves of the same frequency (or wavelength). The figure shows the time variation of the electro-

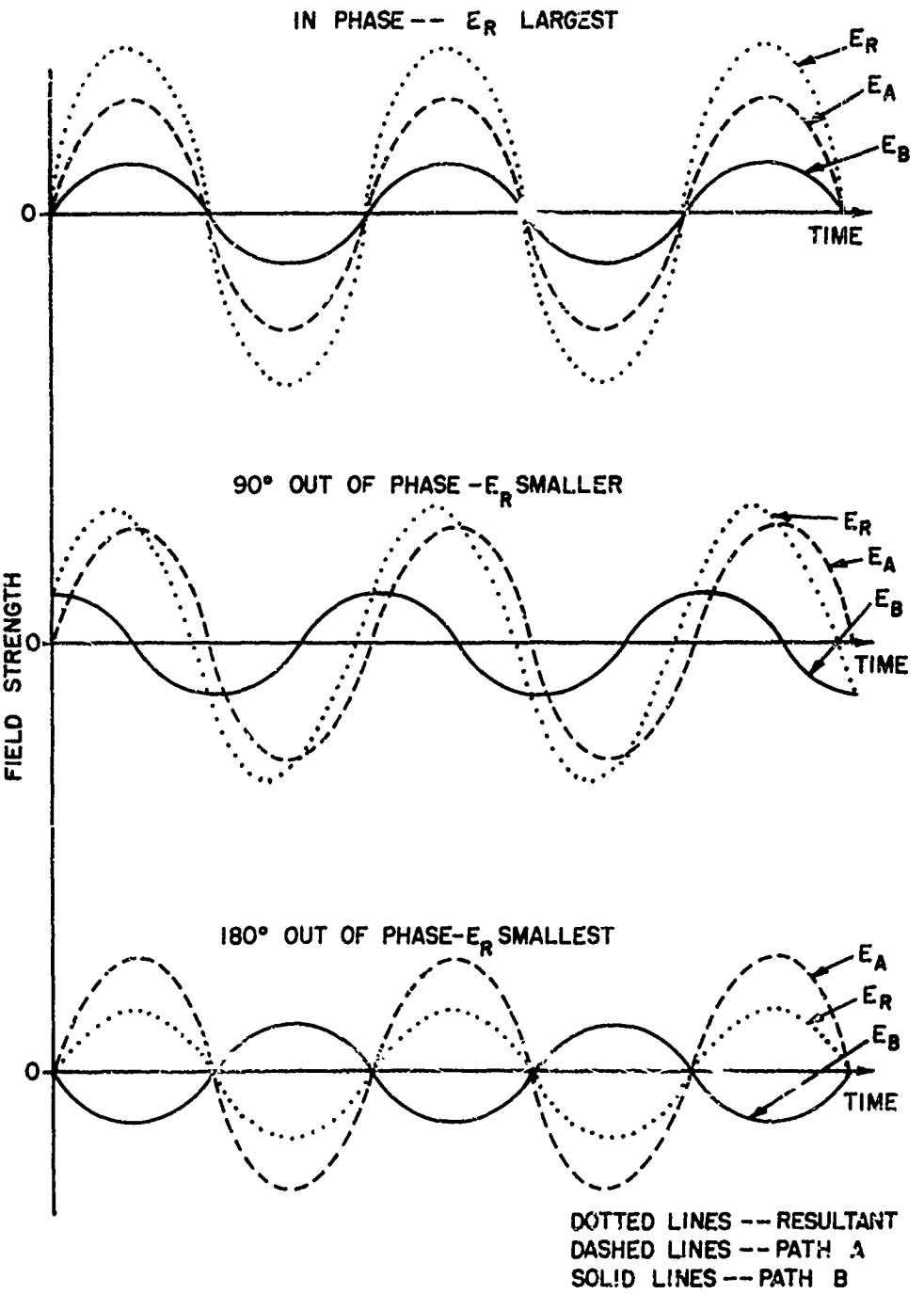

Figure 1.4. The Interference of Two Wave Trains.

magnetic field strength, $\underline{E}_R$, at a point in space, which results from the interference of two waves of equal frequency and with field strengths $\underline{E}_A$ and $\underline{E}_B$. The component waves $\underline{E}_A$ and $\underline{E}_B$ are shown in phase, 90° out of phase, and 180° out of phase.

2. RADIO-RADAR PROPAGATION

2.1 The Radio-Radar Spectrum

That portion of the electromagnetic spectrum utilized for communication extends from millimeter wavelengths to those thousands of meters long. This broad zone covers all the frequencies of radio and radar transmission (see fig. 2.1). Because the effect of tropospheric variables is most pronounced on the shorter wavelengths, our primary interest in this manual will be focused on the short-wave end of the radio-radar spectrum from about 1 centimeter to 10 meters. At longer wavelengths, the ionosphere becomes the controlling influence, rather than the comparatively thin troposphere. At wavelengths shorter than 1 centimeter, on the other hand, the atmosphere becomes relatively opaque for at least two decades of wavelength, and long distance propagation is impractical.

2.2 Atmospheric Effects

When Marconi demonstrated in 1901 that radio signals could be transmitted across the Atlantic Ocean, investigations were soon initiated to account for the presence of signals beyond the horizon. Four principal mechanisms were proposed; diffraction, atmospheric refraction, atmospheric scattering, and reflection from an elevated layer of ionized gases. The reflecting layer hypothesis, proposed by Kennelly and Heaviside in 1902 and proven by Watson in 1919, is generally accepted as the primary mechanism which permits extended range transmission at wavelengths greater than about 10 meters. Although communication at these longer wavelengths is subject to various anomalies (fading, holes, etc.) which may become serious problems in practice, the principles of ionospheric transmission lie outside the scope of this manual.

In the 1930's new developments in electronic oscillators made shorter wavelengths useable for practical communication. It was soon observed that signals shorter than about 10 meters were often not received at ranges greatly exceeding the horizon distance. The shorter the wavelength the more transparent the Kennelly-Heaviside layer becomes to incident radiation, and the ionospheric reflection mechanism becomes relatively unimportant in explaining transmission beyond the horizon. Once again the attention of researchers was focused on the phenomena of diffraction, refraction, and scattering as the mechanisms

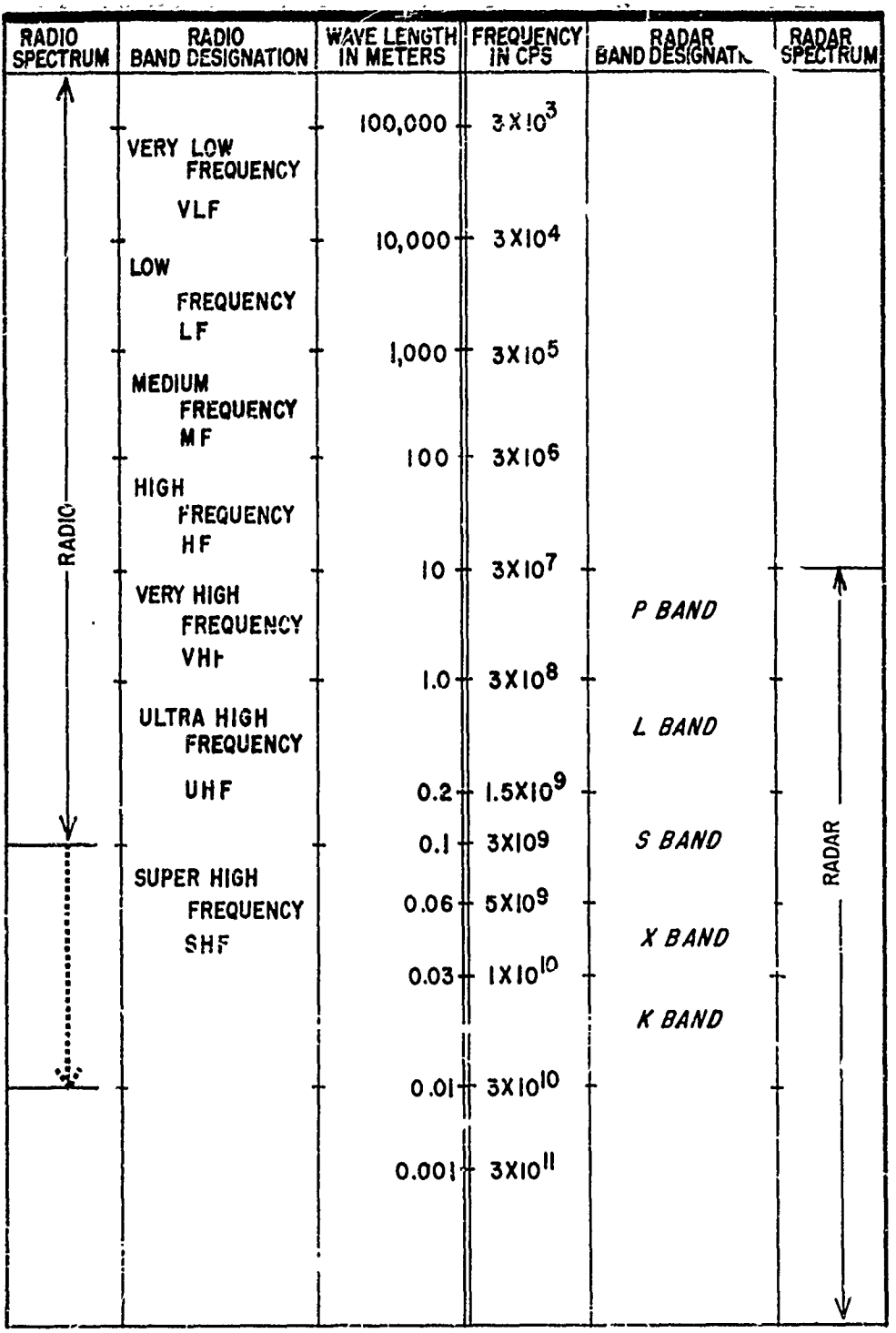

Figure 2.1. The Radio-Radar Spectrum.

which might explain extended-range, short-wave (<10 m.) communication.

With the development of radar in the 1940's (on even shorter wavelengths), it was found that the shorter the wavelength in use the more frequent were occurrences of propagation well beyond the radio horizon. Surface objects were often observed at distances many times greater than the visual range, and these occurrences were found to be associated with unusual distributions of temperature and relative humidity in the layers near the earth's surface. This phenomenon is known as "ducting" or "trapping". It is, in effect, an extreme case of superrefraction, or atmospheric refraction greater than normal.

The phenomenon of superrefraction was observed even prior to 1940 for radio propagation in the range of 1.6 to 5 meters; comprehensive studies of superrefraction have been principally stimulated, however, by the development of radar during and after World War II. The 7-meter and 1.5-meter radar sets established at coastal sites along the Mediterranean reported superrefraction effects much more intense than those reported on the same wavelengths around the British Isles. The entire coast of Sicily, for example, could frequently be seen with 1.5-meter radars on Malta, and from time to time echoes from Greece and Sardinia at ranges on the order of 650 kilometers were obtained. Ships were sometimes plotted to a range of 300 kilometers in locations where the geometrical horizon was less than 30 kilometers away. Perhaps the most distant targets ever observed were seen on a 1.5-meter radar at Bombay, India [13], which received echoes from points in Arabia at a distance of 2,700 kilometers. Although meteorological effects usually act to extend surface radar coverage, it should be mentioned here that subrefraction also does occur. On several occasions, radar equipment on Fisher's Island, New York, was unable for many hours to pick up Block Island despite the fact that it is only 35 kilometers away and visible to the naked eye.

In the years following World War II with the continuously increasing application of airborne radar, an even more disturbing phenomenon has been frequently observed, the "radar hole". This effect, produced by the presence of superrefractive layers aloft, may at times drastically reduce the effectiveness of airborne search radar (see Fron-tispiece).

2.3 Propagation Characteristics in the Terrestrial Environment

In order to find an explanation for the anomalies described in the foregoing paragraphs we shall consider in some detail those phenomena which control propagation in the troposphere; (1) the absorption of radiant energy, (2) the interference of waves, resulting in regions where two waves enhance and in adjacent regions where they cancel each other, (3) the diffraction of waves around the earth and other objects, and (4) the variations in propagation velocity caused by changes in pressure, temperature, and humidity; which give rise to refractive, reflective, and scattering effects.

2.3.1 Absorption

Whenever electromagnetic radiation propagates through a real medium (be it solid, liquid, or gaseous), a fraction of the incident energy is absorbed in passing through each increment of the medium. The energy absorbed is imparted to the atomic or molecular structure of the medium and, in most cases, is eventually given up as heat. The effect may be thought of as a kind of frictional loss.

Any particular substance does not absorb radiation of different wavelengths equally, nor do different substances absorb radiation of one particular wavelength equally -- as anyone familiar with the spectrograph will know. The particular absorption characteristics of a medium (e.g., air), therefore, depend upon its composition, upon the atomic and molecular structure of each constituent, and upon the physical characteristics of the incident radiation.

Fortunately, in practice the absorption mechanism does not often produce serious performance anomalies in the operation of radio or radar equipment. Absorption may, however, become an important design consideration in selecting the wavelength to be used in a radar system; e.g., for air search radar one would avoid selecting a wavelength close to one of the water vapor absorption bands, since water vapor is present in the natural atmosphere.

2.3.2 Interference

In the radio-radar spectrum interference produces very pronounced fluctuations in signal strength (see fig. 1.4). These are not only produced by electromagnetic wave trains from two or more sources (transmitters) arriving at a particular point in space (receiver), but also by wave trains from a single source arriving at a particular point,

having travelled over different transmission paths. For example, two different ray paths from source to receiver might be the direct, line-of-sight ray and a reflected ray from the transmitting antenna to the earth's surface and thence to the receiving antenna (see fig. 2.3).

Interference between signals of different wavelengths from two or more sources is eliminated by the "tuning section" of the receiver which is nothing more than a sharply tuned bypass filter. The filter rejects all signals except those having frequencies within a very narrow band centered on the frequency to which the receiver is "tuned". Any electromagnetic wave (signal) having a frequency within the bypass band will be "passed" on through the amplification and detection stages of the receiver; waves having other frequencies are rejected.

Signals of the same (or nearly the same) frequency, whether from several sources or from a single source, produce interference which cannot be eliminated by a filter (tuner). The case of two or more sources is of practical importance in connection with electronic counter measures (ECM) but will not be discussed further here. The case of interference produced by surface reflections from a single source will be developed more fully in the following paragraphs.

A spherical earth enveloped by a homogeneous atmosphere is shown in figure 2.2. In this figure, as in all others depicting curved earth geometry, the height scale has been greatly exaggerated compared to the horizontal distance scale. Assume that a radio transmitter is located at R at height H above the earth. Since the atmosphere is homogeneous, energy will leave the antenna in straight rays. If one now draws a straight ray from R tangent to the earth's surface, this line defines the horizon distance D and the horizon height h at point P which is at a distance d beyond the tangent point. Referring to figure 2.2,

$$a^2 + D^2 = (a + H)^2 \; ; \tag{2.1}$$

expanding, we have

$$D^2 = 2\,a\,H + H^2 \; . \tag{2.2}$$

Since H is much smaller than 2 a, the second order term in the above equation may be neglected. Therefore,

$$D \cong \sqrt{2\,a\,H} \; , \tag{2.3}$$

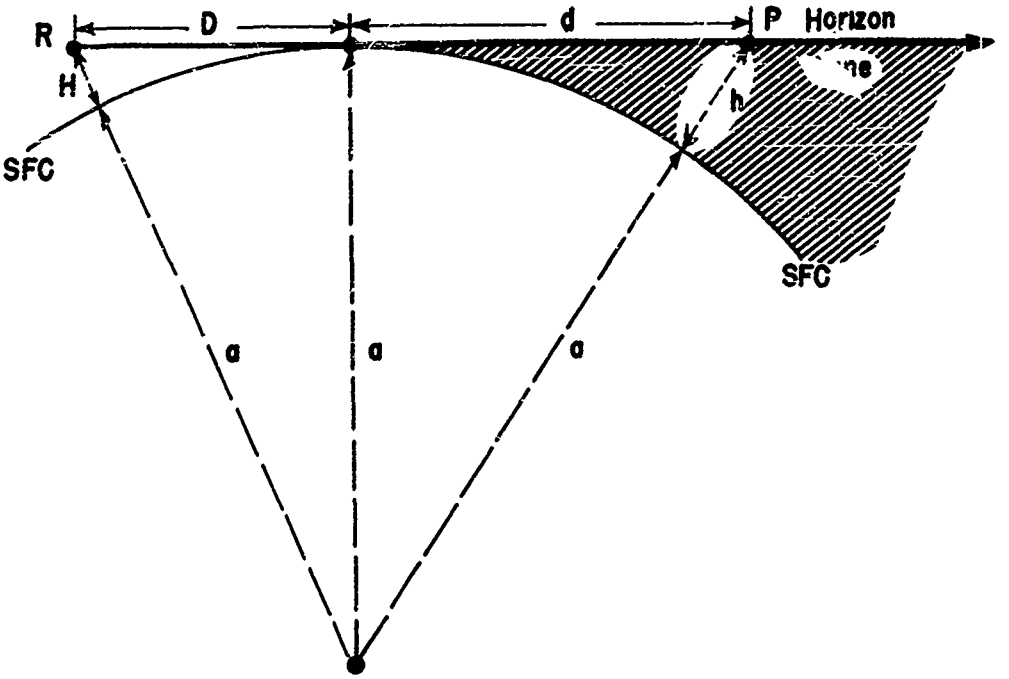

Figure 2.2. Ray Geometry for Spherical Earth--Homogeneous Atmosphere.

and similarly,

$$d \cong \sqrt{2\,a\,h} \quad . \tag{2.4}$$

The horizon line beyond the tangent point divides radio space into two regions. The region above the line is always illuminated directly by the transmitter and is called the interference region; the region below the line is not directly illuminated and is generally called the diffraction region (shaded in fig. 2.2). The illuminated region is referred to as the interference region because the radio field strength at a given point above the horizon line is determined by the interference between two rays, as described in section 1.4.2. One is the direct ray from the transmitter to the point; the other is a ray reflected from the earth's surface to the point. Since the reflected ray path is somewhat longer, the ray arrives at the point somewhat later than the direct ray. If it arrives half a wavelength behind (180° out of phase) the two waves will tend to cancel each other, and if they are of equal strength the resultant field at the point will be zero. On the other hand, if the point is higher,

so that the reflected wave arrives a full wavelength behind the direct wave, the two will be in phase, and the field strength will be intensified. This alternate cancellation and enhancement in the field strength as the path-length differences are increased, gives rise to a vertical interference pattern, consisting of a series of narrow fingers or "lobes" of strong field strength with weaker fields in between (see fig. 6.1).

In figure 2.3, showing a spherical earth surrounded by a homogeneous atmosphere, the path difference, δ, between the direct and reflected waves may be shown to be

$$\delta \simeq \frac{2 H_R H_T}{d}, \tag{2.5}$$

where H_R and H_T are the heights of the transmitter at point R and of the target at point P above the reflecting plane and d is the direct path distance. The reflection plane is tangent to the earth at the point of reflection, such that the angle of incidence θ, equals the angle of reflection θ.

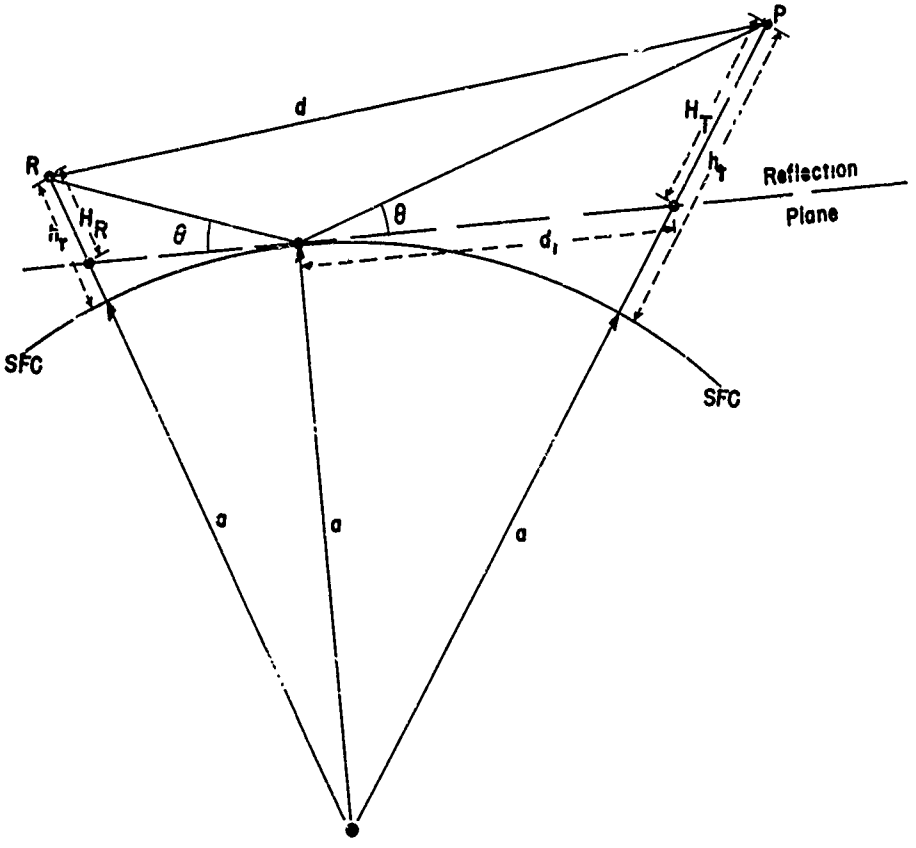

Figure 2.3. Path-Difference Geometry--Spherical Earth.

On a spherical earth, $\underline{H_R}$ and $\underline{H_T}$ are not the actual heights above the surface. Referring to figure 2.3, it may be shown that

$$H_R \cong h_r - \frac{(d - d_1)^2}{2a} , \tag{2.6}$$

and

$$H_T \cong h_t - \left(\frac{d_1^2}{2a}\right), \tag{2.7}$$

where $\underline{h_r}$ and $\underline{h_t}$ are the heights of the transmitter and target above the earth's surface and $\underline{d_1}$ is the distance from the reflection point to the projection of the target on the reflection plane. Since the angle of incidence is equal to the angle of reflection, we also have

$$\frac{d_1}{d - d_1} = \frac{H_T}{H_R} . \tag{2.8}$$

One can eliminate $\underline{H_T}$, $\underline{H_R}$ and $\underline{d_1}$ from the above four expressions, and solve for $\underline{\delta}$ in terms of $\underline{h_r}$, $\underline{h_t}$, and $\underline{d}$. The resulting expression, however, is too complicated to warrant further discussion in this manual. Domb and Pryce [12] have developed a convenient means of plotting interference patterns, to which the reader is referred for practical assistance.

The picture just described is further complicated in that the reflected ray undergoes a sudden phase shift of one-half wavelength (180°) on reflection; minimum fields, therefore, occur when the path difference is an integral number of wavelengths (1, 2, 3 ... etc), and maxima are centered at those points having 1/2, 1 1/2, 2 1/2 ... etc. wavelength path differences. Furthermore, the strength of the reflected wave is reduced by scattering if the reflecting surface is rough and by divergence if it is smooth, so that the direct and reflected waves are not of equal strength. These factors modify, but do not invalidate, the general characteristics of the interference pattern as described above.

In practice, interference patterns for a given antenna are computed for various angles of elevation of the antenna (tilt); these computed values are checked and corrected with observational data whenever possible. The weather officer should consult the electronics offi-

cer for further information concerning the characteristics of a particular antenna array. The phenomenon of interference is not affected per se by changing meteorological conditions, except that, we shall see, refractive effects may produce path length changes.

2.3.3 Diffraction

The only way in which energy can penetrate the region below the horizon line, in a homogeneous atmosphere, is by the process of diffraction (see fig. 2.2). This process results from the wave nature of the transmitted energy and is similar to simple diffraction over a knife edge. The mathematics of diffraction over a spherical obstacle is quite formidable and will not be attempted here. It turns out, however, that the depth of penetration of energy below the horizon line is proportional to the wavelength, and, at a constant height above the surface, it falls off exponentially with distance beyond the horizon point. Domb and Pryce [12] have developed relatively simple methods for computing diffraction fields, and the reader is referred to their paper for a discussion of practical computational techniques.

As was the case with interference, the mechanism of diffraction is not primarily weather-dependent, and as such its effect upon radio-radar performance is more properly a problem for the electronics engineer.

2.3.4 Reflection and Refraction

We now complicate the simple case of figure 2.2 and 2.3 by surrounding our spherical earth with a nonhomogeneous atmosphere (such as the earth's real atmosphere). Inhomogeneties produce changes in the speed of propagation of electromagnetic energy through different portions of the atmospheric envelope, giving rise to the phenomena of reflection, refraction, and scattering.

The index of refraction, n, of a medium is defined as

$$n = \frac{c}{v} , \qquad (2.3)$$

where c is the propagation velocity of electromagnetic energy in a vacuum, and v is the propagation velocity in the medium in question. The index of refraction of a medium is therefore a measure of the propagation speed (relative to the velocity of light) of an electromagnetic wave

through the medium.

(a) Reflection and Refraction at a Discontinuity

Whenever an electromagnetic wave strikes a surface of discontinuity in n (i.e., a surface across which there is an abrupt change in propagation speed) the incident wave, in general, is partially reflected and partially refracted (see fig. 2.4). The law of refraction at a discontinuity may be derived from a consideration of propagation speeds in the two media. In figure 2.4 we assume electromagnetic energy strikes the boundary between two media with indices of refraction of n_1 and n_2, where n_1 is associated with the initial medium and n_2 is greater than n_1; i.e., the propagation speed is greater in the initial than in the final medium. In a certain length of time, t, the wave front travels from position 1-2 to position 4-3, and

$$S_{2-3} = v_1 t \; ; \; S_{1-4} = v_2 t \, , \qquad (2.10\text{-}2.11)$$

where S_{2-3} is the distance traveled and v_1 is the speed of propagation in medium 1, and S_{1-4} and v_2 are the corresponding distance and speed in medium 2.

Also, we have

$$\sin \theta_i = \cos \angle 132 = \frac{S_{2-3}}{S_{1-3}} \, , \qquad (2.12)$$

and

$$\sin \theta_f = \cos \angle 413 = \frac{S_{1-4}}{S_{1-3}} \, . \qquad (2.13)$$

Therefore,

$$\frac{\sin \theta_i}{\sin \theta_f} = \frac{S_{2-3}}{S_{1-4}} = \frac{v_1 t}{v_2 t} = \frac{v_1}{v_2} \, , \qquad (2.14)$$

and, since $n = \frac{c}{v}$, we may write the law of refraction

$$\frac{\sin \theta_i}{\sin \theta_f} = \frac{n_2}{n_1} \, , \qquad (2.15)$$

where θ_i is the angle of incidence and θ_f is the angle of refraction.

It may be well to note that in figure 2.4 the direction of propagation may be reversed without invalidating the conclusions just reached so long as we interchange the designation of incident and refracted wave fronts and the angles of incidence and refraction. The incident and refracted rays lie in the same plane, and the incident rays are always bent toward the medium of higher index of refraction (i.e., lower propagation speed) in passing through a surface of discontinuity.

With the aid of Huyghens' principle one may derive the law of reflection which states that the incident and reflected rays lie in the same plane and the angle of incidence is equal to the angle of reflection; i.e., $\theta_i = \theta_r$ in figure 2.4. It will be noted that the incident wave front is inverted by reflection (the incident wave is shifted in phase 180°), as has been mentioned previously; in refraction there is no corresponding phase shift.

Whenever energy is passing through a discontinuity between a

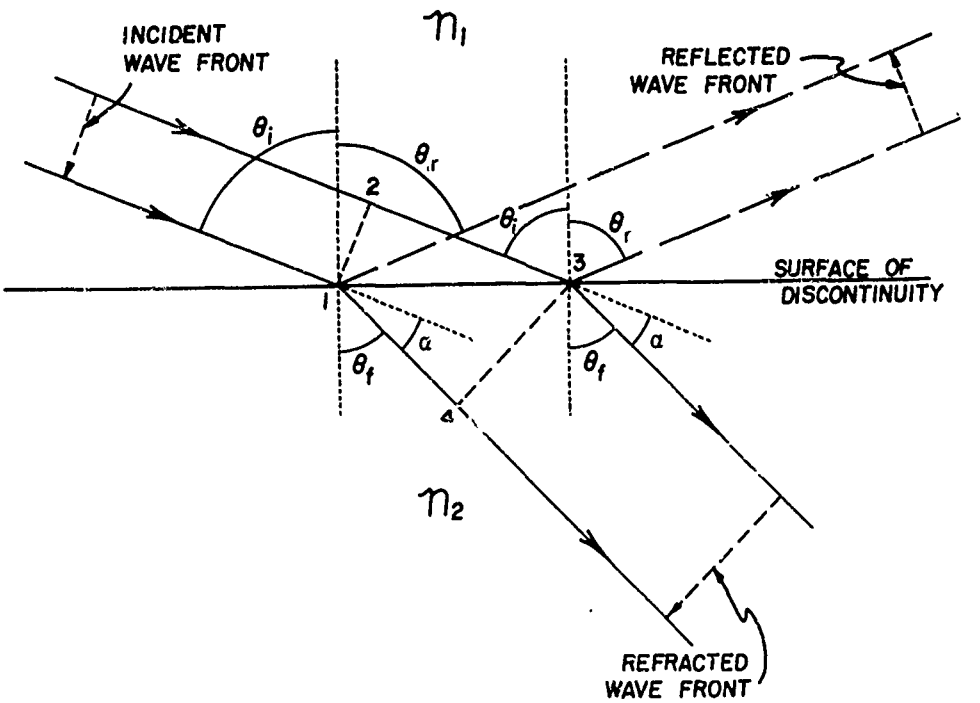

Figure 2.4. Refraction and Reflection at a Surface of Discontinuity.

medium of higher index of refraction to a medium of lower, the phenomenon of total reflection will occur when the angle of incidence exceeds a certain critical value given by

$$\theta_i = \sin^{-1} \frac{n_1}{n_2} , \tag{2.16}$$

where $n_2 > n_1$ (see fig. 2.4). At angles of incidence greater than this critical value the refracted ray is suppressed (does not emerge above the surface of the discontinuity) and the incident ray is totally reflected.

The relative amounts of energy carried in the reflected and in the refracted waves are dependent upon the transmission characteristics of the two media on either side of the discontinuity, upon the physical characteristics of the surface of discontinuity, upon the angle of incidence of the initial wave train, and upon the wavelength of the incident wave. For example, a sheet of ordinary screen wire is a good reflector of 10-centimeter radar waves but a poor reflector of electromagnetic energy in the visual spectrum; whereas, a silvered mirror is a good reflector of visible radiation but a poor reflector of gamma rays.

(b) Refraction in an Environment of Continuously Varying Inde of Refraction

If an electromagnetic wave traverses a region in which the propagation velocity (and therefore also the index of refraction) varies from point to point but in a continuous fashion; i.e., no discontinuities in n present, there will be no reflection phenomena, but refraction of the wave will occur.

In figure 2.5 the dashed vertical line at the left represents a wave front at time $t = 0$. The wave is traveling horizontally toward the right. Assume that the refractive index is n_o at the bottom of the wave front and is $n_o - \Delta n$ at the top. As the wave proceeds along, the top part will travel faster than the bottom part, because the refractive index at the top is less than at the bottom. After time Δt, the top end of the wave will have traveled

$$d_o + \Delta d = v_{top} \Delta t = \frac{c \Delta t}{n_o - \Delta n} , \tag{2.17}$$

where c is the propagation velocity in vacuum. The bottom end will

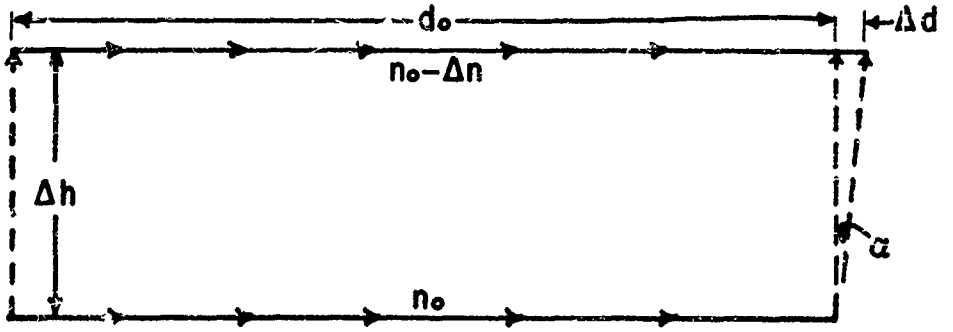

Figure 2.5. Refraction in an Environment of Continuously Varying Index of Refraction.

have travelled

$$d_o = v_{bottom}\Delta t = \frac{c\Delta t}{n_o} , \tag{2.18}$$

and, thus

$$\Delta d = c\Delta t\left(\frac{1}{n_o - \Delta n} - \frac{1}{n_o}\right) = \frac{d_o \Delta n}{n_o - \Delta n} . \tag{2.19}$$

Since $(n_o - \Delta n)$ is very close to unity we may disregard it and write

$$\Delta d \cong d_o \Delta n . \tag{2.20}$$

Since the top of the wave has travelled Δd farther than the bottom, the wave front is now tipped downward by an angle $\alpha = \Delta d / \Delta h$, where Δh is the distance increment between the top and bottom of the wave front. Substituting $\Delta d = d_o \Delta n$, one obtains the expression

$$\alpha = d_o \frac{\Delta n}{\Delta h} , \tag{2.21}$$

for the angle through which the ray is bent.

But $\frac{\alpha}{d_o}$ is simply the curvature, C, of the ray and since the bending is proportional to distance, the ray path is an arc of a circle of radius $R = \frac{d_o}{\alpha}$, so long as the n-gradient, $\frac{\Delta n}{\Delta h}$, remains constant. Thus, one can say that,

$$C = \frac{1}{R} = \frac{\Delta n}{\Delta h} \quad . \tag{2.22}$$

This is a very important expression in radio wave refraction; the curvature of a ray is equal to the gradient of the refractive index normal to the ray path. Stated another way, the angle through which a ray will be bent in passing through a refractive index gradient is equal numerically to the gradient normal to the path, times the distance travelled.

In the natural atmosphere the index of refraction becomes smaller as one proceeds to higher and higher altitudes, but abrupt changes (discontinuities) in n are not commonly observed. For this reason refractive effects in the earth's atmosphere are generally more important in the study of anomalous radio-radar performance than are reflective effects. As has already been implied, however, the surface of the earth acts as a good reflector of electromagnetic waves in the radio-radar spectrum.

(c) Snell's Law

One is frequently interested in tracing the trajectory of a ray as it travels through a medium such as the atmosphere in which the refractive index changes with height. Theory indicates that the ray will follow a trajectory having the shortest optical path. This principle is expressed in a simple mathematical form known as Snell's Law. It was originally applied to ray tracing through lenses and prisms, but applies equally well in the radio-radar case. If one assumes that the refractive index in the atmosphere changes only with height above the spherical earth, and not with horizontal distance, then Snell's Law may be expressed as

$$n\,(a + h)\cos\beta = n_s\, a \cos\alpha_0 \quad . \tag{2.23}$$

where n is the refractive index at a given height h, n_s is the refractive index at the earth's surface, a is the earth's radius, β is the ray inclination angle at height h, and α_0 is the ray inclination at the earth's surface. Figure 2.6 shows a typical ray leaving the earth at an angle α_0 and passing upwards through the atmosphere. By the time it has arrived at height h, it has been bent downward by a total angle τ, which can be calculated if one knows the way in which n changes with height. This figure will be referred to later when the method for computing

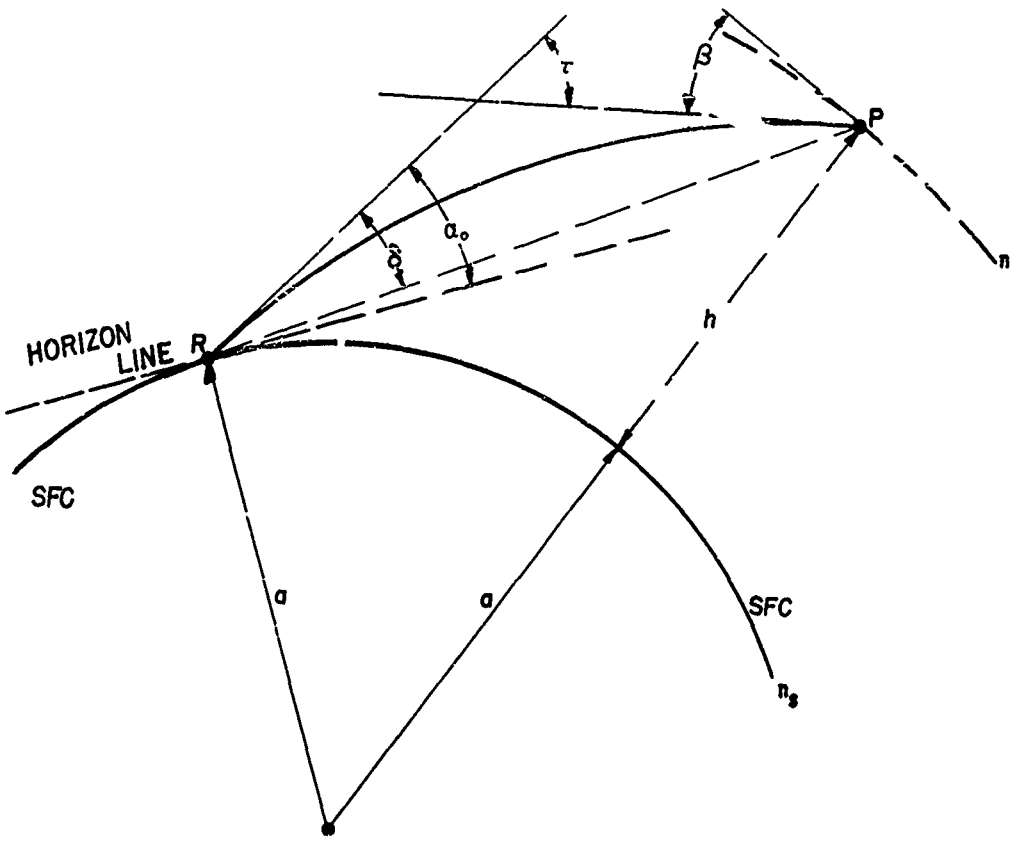

Figure 2.6. The Geometry of Ray Bending.

total bending, τ, and the associated radar elevation angle error, δ, is developed.

2.3.5 Scattering

The presence of thermodynamically dissimilar parcels of air in the atmosphere is responsible for a propagation mechanism which has not been considered previously and which is known as "scattering" It has been found experimentally that when one proceeds away from a transmitter with a receiver near the surface, the fields beyond the horizon decrease exponentially at a rate which agrees with diffraction theory for quite some distance (see fig. 7.1). As one proceeds further away from the transmitter, however, the attenuation rate suddenly decreases (the fields decrease with distance at a much slower rate). In other words, beyond a certain critical distance, the received fields are much stronger than can be accounted for by diffraction theory. The

mechanism by which these fields are produced is called scattering. Each parcel above the horizon, which is illuminated by the transmitter, scatters a small part of the incident energy in directions other than along the straight line path from the transmitter through the parcel. Most of the energy, of course, continues straight through. If a particular parcel is above the horizon for both the transmitter and the receiver, part of the scattered energy will be directed toward the receiver. The scattered field at any point may be regarded as the sum of the energies scattered by a multitude of such parcels and directed toward the point in question. Theories have been developed for computing the fields to be expected by such a mechanism; by postulating reasonable Δn values and a spectrum of parcel sizes, one can compute fields which agree well with those observed. One of the current problems in tropospheric propagation research, centers around proving or disproving this theory of scattering. Refractometer data show that at the heights required for the parcels to be visible from both terminals over long paths, the actual n fluctuations are smaller than those required by the theory to explain the observed fields. This has led to the postulation of a multiscattering mechanism, in which the energy is scattered from parcel to parcel several times before reaching the receiver. In such a model, the only parcel-height requirement is that a particular parcel be in the line of sight of the previous and the succeeding parcel, and not necessarily be in the line of sight of both terminals. This permits the scattering to occur lower in the atmosphere where the Δn values are much greater. The only difficulty with this proposal is that an analytical treatment of multiscattering becomes very complex and has in fact not yet been worked out. A further complication occurs when one considers that, because of atmospheric stability, the parcels are probably flattened like pancakes, rather than being globular. A great deal of experimental evidence exists, however, which seems to support the multiscattering hypothesis with flattened parcels.

In any case scatter fields do exist; they are stronger at night than in midafternoon, and are stronger in summer than in winter. Even at their weakest, they are much stronger than diffraction fields over paths greater than a few hundred miles in length.

2.4 Summary

In this chapter we have described briefly some of the operational anomalies actually observed in the performance of radio-radar equipment and have discussed the physical phenomena which are important

in producing the anomalous performance observed. Of these phenomena, absorption, interference, and diffraction are not significantly affected by varying atmospheric parameters and do not, therefore, produce critical weather problems in the field.

On the other hand, refraction, reflection, and scattering are most commonly (except in the case of reflection) produced by inhomogeneities in the atmosphere which in turn are attributable to variations in meteorological parameters. Of these, by far the most important in explaining or predicting the anomalous performance of naval radio-radar equipment is refraction. It is for this reason that the remaining three parts of this manual are devoted principally to a detailed discussion of atmospheric refraction.

PART II

THEORY OF ATMOSPHERIC REFRACTION

3. THE ATMOSPHERIC REFRACTIVE INDEX

3.1 Definition

It was mentioned previously that the propagation velocity of all electromagnetic energy in a vacuum is a constant ($c = 3.0 \times 10^8$ cm./sec.). In atmospheric gases this velocity is reduced slightly. The ratio of the velocity of propagation of electromagnetic energy in a vacuum to that in a particular medium, is defined as the refractive index of the medium as was described in section 2.3.4. This quantity, designated as n, generally varies with wavelength and, of course, from medium to medium. In tropospheric air (within the wavelength band from 1 cm. to 10 m.) the refractive index is, for all practical purposes, independent of wavelength and has a value slightly greater than unity. At sea level, values range from approximately 1.000250 to 1.000450, with values near 1.000350 frequently found over an ocean surface.

To facilitate numerical computation it is more convenient to define a derived index, called the "refractivity", as follows

$$N = (n - 1) \times 10^6 . \tag{3.1}$$

The atmospheric refractivity ranges from 250 to 450 N-units at sea level. It is also possible to express N as a function of total atmospheric pressure, temperature, and water vapor pressure, as follows

$$N = \frac{A}{T}\left(P + \frac{Be}{T}\right), \tag{3.2}$$

where P and e are in millibars and T is in degrees absolute. The constants, A and B, have been determined experimentally by a number of investigators; A is the dielectric constant for dry air and B is the water vapor dipole moment constant. Smith and Weintraub [22] have evaluated the results obtained by numerous investigators and have recommended the value of 77.6 for A and the value of 4,810 for B. Equation 3.2 is frequently written in the following form:

$$N = 77.6\left(\frac{P}{T}\right) + 3.73 \times 10^5\left(\frac{e}{T^2}\right) , \tag{3.3}$$

where the first and second terms are called the "dry" and the "wet"

terms, respectively. Since both P and e normally decrease with height above sea level, N also decreases with height. The exact way in which N varies with height is of course determined by meteorological processes and has a profound effect upon radio-radar propagation.

In the event that available moisture data are expressed as relative humidities, equation 3.3 may be written as follows:

$$N = 77.6\left(\frac{P}{T}\right) + 3.73 \times 10^5\left(\frac{e_s RH}{T}\right), \qquad (3.4)$$

where e_s is the saturation vapor pressure in millibars and RH is the relative humidity in percent.

It may be well to point out that both n and N are space and time functions which in general vary from place to place in the atmosphere and which in general vary with time at a particular point. The preceding formulae permit one to determine the refractivity for one particular place and time; namely, the place and time represented by the values of pressure, temperature, and humidity used. In general the path which a radio-radar ray will follow is primarily determined by the gradient of N rather than by N itself as was discussed in section 2.3.4(b). N-gradients may be determined from a series of discrete values of N in the region of interest, or the gradients may be determined by direct measurement with suitable equipment.

3.2 Methods of Measurement and Computation

Direct measurements of the propagation velocity of electromagnetic energy in a particular medium can be made and, when compared with the speed of light, give a direct measure of the refractive index or refractivity. Because of the complexity of the equipment needed, this approach is impractical for operational use.

3.2.1 Refractometer

A more practical way to measure the atmospheric refractive index was developed in the 1940's by Birnbaum [7] at the National Bureau of Standards and, somewhat later, in a slightly different form by Crain and Dean [8] at the University of Texas. The refractometer, as the instrument is called, essentially measures changes in the dielectric constant of the air inside a perforated cylindrical cavity. This is done

by feeding electromagnetic energy of about a 3-centimeter wavelength into a cavity which has been machined to resonate over a very narrow band of wavelengths. Changes in the dielectric constant of the air inside the cavity cause the resonant frequency of the cavity to change proportionally. By using two cavities (one being hermetically sealed and containing either dry air or vacuum and the other being perforated to allow passage of outside air) one can detect very small changes in the resonant frequency of the perforated cavity. Since the refractive index in this case is simply the square root of the dielectric constant, these changes can be recorded as changes in N. The sensing lag of the device is limited only by the time needed to introduce new air into the cavity. Since the volume of air contained in the cavity is very small, the speed of response may be reduced to a fraction of a second by careful design of the ventilating ducts or ports.

In spite of various simplifications which have been made in recent years, the refractometer is a relatively complex and heavy instrument, which is not yet suitable for expendable balloon borne operations. Its main use has been aboard aircraft, and many hundreds of vertical and horizontal profiles of refractive index have been recorded, particularly in the continental United States and Alaska. Very recently, refractometers have been installed in AEW-type aircraft and in certain carrier-based types. In the future refractometer data may be expected to become available to most large operational forces. It should always be used in preference to derived N-data, whenever there is a choice, because of its greater precision and because it reproduces the "fine" structure of atmospheric refractivity.

3.2.2 Temperature, Pressure, and Humidity Method

Since N is a function of P, T, and e, it follows that whenever measurements of these quantities are available they also serve to define N. At the surface the conventional barometer, thermometer, and hygrometer may be used to determine N; aloft the radiosonde provides the necessary measurements. From values of P, T, and e, N may be computed using equations 3.3 or 3.4. The particular features of the radiosonde which make it useful for propagation purposes are that it measures the required quantities as functions of height, and that record data are available which have been obtained over periods of many years and from hundreds of stations having a wide geographic distribution.

All meteorologists recognize that the radiosonde has certain de-

ficiencies which make it somewhat less than ideal, particularly in the measurement of humidity. The high lag coefficient of the humidity sensing element, particularly at low temperatures, causes the resulting N (namely, the height profile) to deviate from its true shape. The effect of these deviations on radio propagation perhaps is not as serious as it may be for other purposes. The reason for this is that, as will be shown later, anomalous propagation effects are principally conditioned by the gross features of the N-profile; the fine structure is not of first order importance. This does not mean that for propagation work, improvements in the radiosonde are unnecessary; rather, they are greatly desired (see section 3.3.3). It does mean, however, that record radiosonde data can be used to good advantage in spite of its shortcomings.

Comparisons between N-values obtained from refractometer measurements and those computed from radiosonde data are in good agreement as to the gross structure present, but of course the fine details are largely missed in the computed radiosonde values. Figure 3.1 is an example of such a comparison. Where appreciable deviations

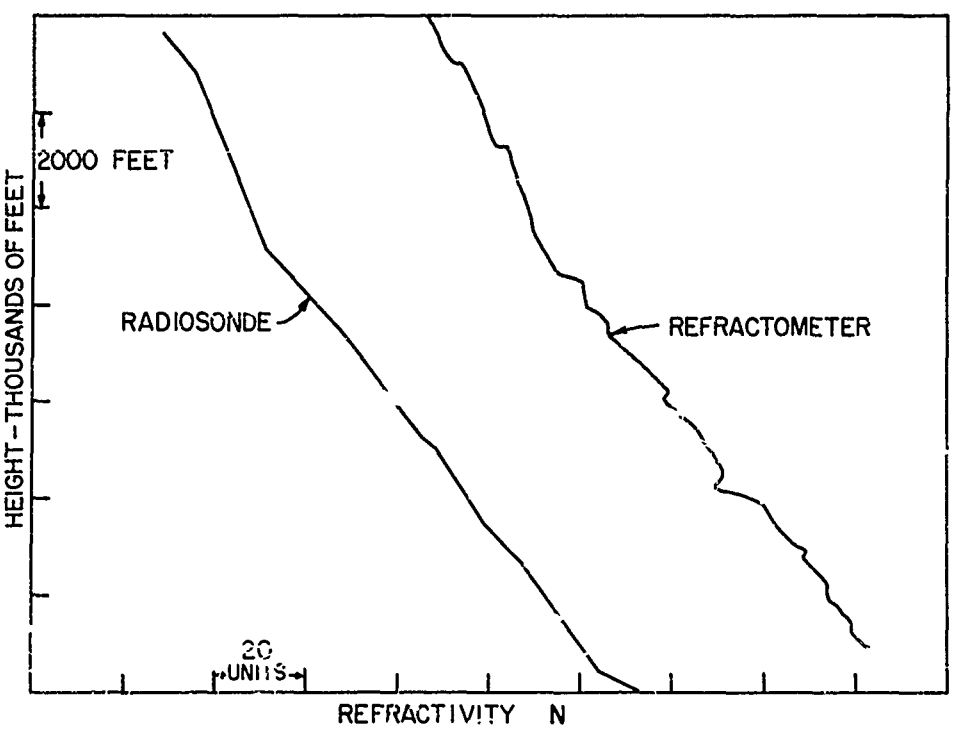

Figure 3.1. Comparison of Radiosonde and Refractometer N-Profiles.

occur, it has been found that these were caused by pronounced humidity fluctuations, as would be expected.

In propagation problems, one is continually faced with the problem of reducing P-, T-, and e-data to N-values at numerous heights. Over the years, various methods have been devised for computing N. These take the form of tables, slide rules, analogue computers, and nomograms.

(a) Refractive Index Nomogram

Perhaps the most convenient of these, for use when great precision is not required, is the nomogram shown in figure 3.2. Pressure, temperature, and humidity are shown in the units commonly used in radiosonde data tabulations; i.e., pressure in millibars, temperature in °C., and dew point in °C. It is particularly convenient in that the figure and a straight edge are all that is required. Assuming no error in entry data, the accuracy of the N-values so derived is ± 1 N-unit, which is compatible with the accuracy of radiosonde data. In addition to figure 3.2, a larger, full-size version of the refractive index nomogram is provided as a loose-leaf inclusion to this manual and is marked as chart I.

The required simple instructions for use of the nomogram appear thereon. For example, suppose the value of pressure is 1,000 millibars, the temperature is 20°C., and the dew point is 4°C. First, find the intersection of the 1,000 millibar pressure line with the 20°C. temperature line. Then connect this point with the 4°C. division on the dew-point scale and read off an N-value of 300 where the straight edge intersects the refractive index (refractivity) scale.

(b) Refractive Index Diagram

Another method for determining refractivity from pressure, temperature, and humidity data is illustrated in figure 3.3. This diagram has been designed for use in aircraft, in that the arguements used are pressure altitude in feet, dry bulb temperature in °C., and wet bulb temperature in °C. Values of N may be read directly from the diagram with a precision of ±1 N unit, assuming the entry data is without error. In addition to figure 3.3, a larger, full-size version of the refractive index diagram is provided as a loose-leaf inclusion to this manual and is marked as chart II.

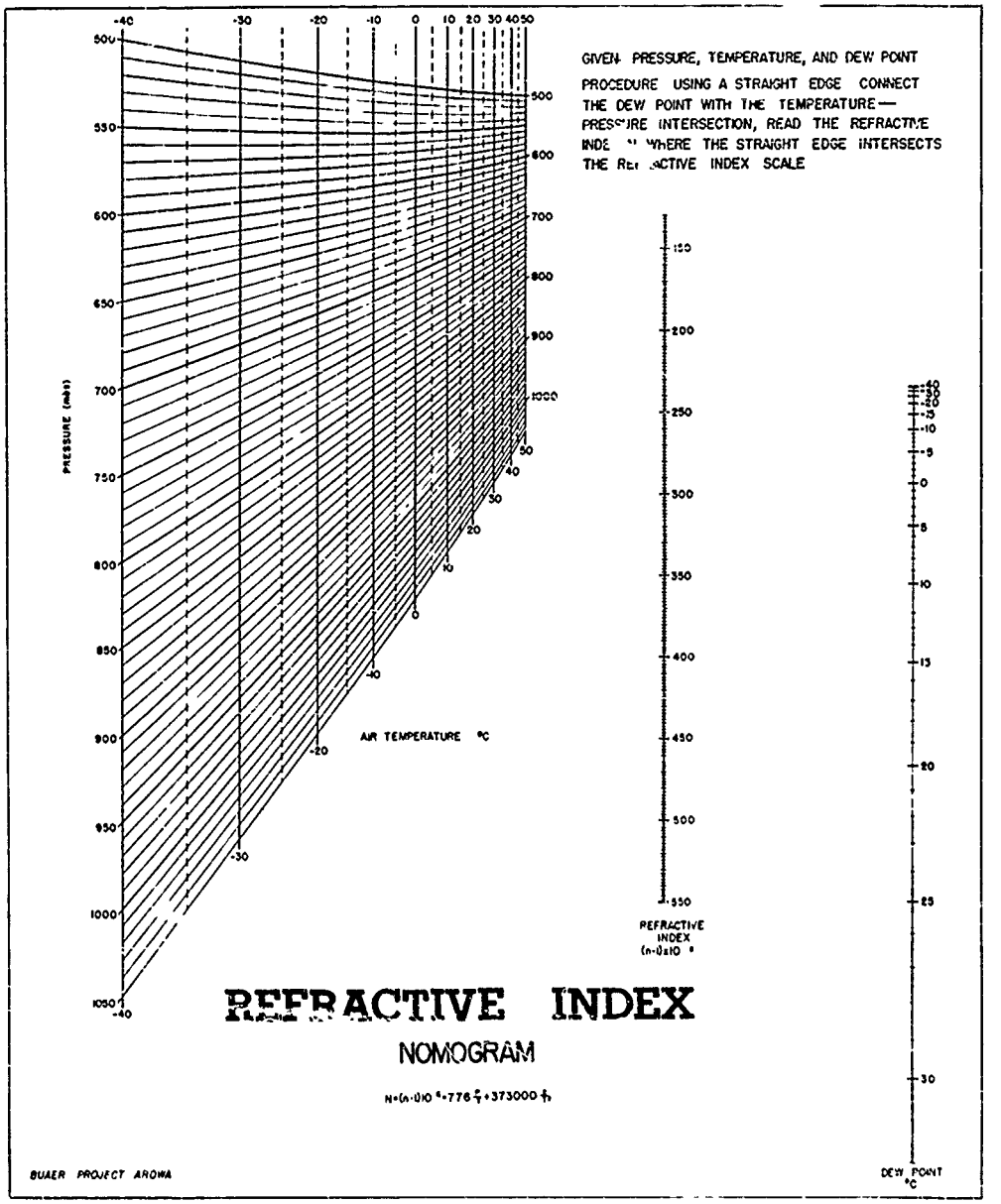

Figure 3.2. Refractive Index Nomogram. (Chart I)

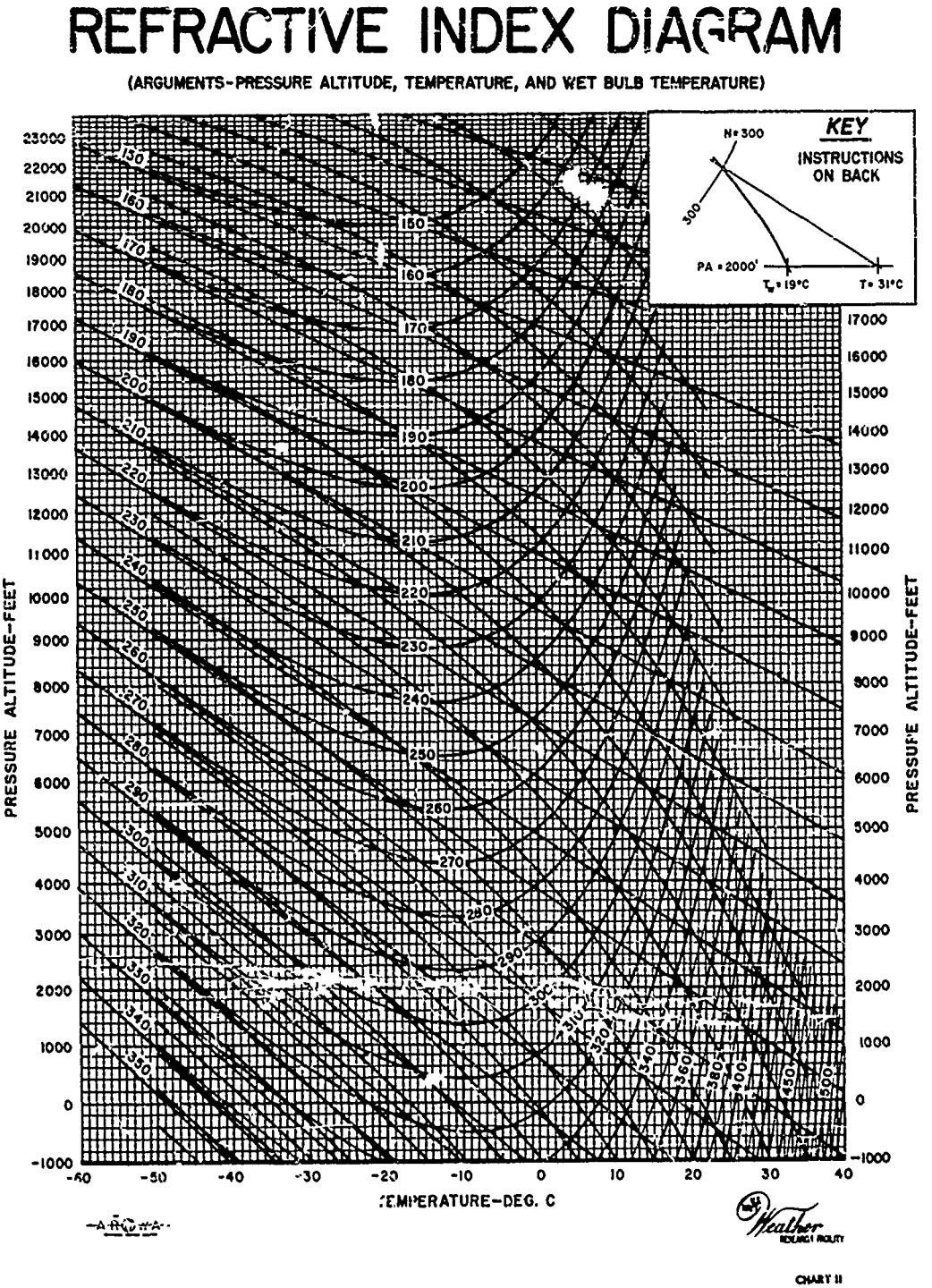

Figure 3.3. Refractive Index Diagram. (Chart II)

Use of the diagram is explained by the inset in the upper right-hand corner of figure 3.3 and in the simple instructions which appear on the back of chart II. For example, suppose the pressure altitude is 13,000 feet, the dry bulb temperature is 10°C. and the wet bulb temperature is -2°C. First locate the 10°C. and -2°C. points along the horizontal 13,000 foot pressure altitude line. Then follow the straight, sloping dry bulb temperature curve up and to the left from the 10°C. point and the curved, concave-downward wet bulb temperature curve up and to the left from the -2°C. point, until these two temperature curves intersect. At the point of intersection read off an N-value of 175 from the curved, convex-downward refractivity curves.

(c) Refractive Index Overlay (Arowagram)

Whenever pressure, temperature, and moisture data are already displayed in the form of a plotted sounding on the Arowagram (the thermodynamic chart in common use in the U. S. Navy), it is most convenient to obtain N-values for various levels of the sounding by using the refractive index overlay (see fig. 3.4). This overlay has been especially prepared for use with the large-size Arowagram; it cannot be used with other forms of thermodynamic charts.

Use of the overlay is explained in the following instructions and recommended computational procedures:

1. Plot temperature (T) and dew point (T_d) on Arowagram and place overlay in register.

   a. Carefully place a dot on the overlay in register with each plotted point (T, T_d) with a grease pencil. Connect each pair of temperature-dew-point dots at the same pressure level with a line so as to identify pairs of values.

   b. If the dew-point data is missing extend a line to the left of the plotted T-value for about 10°C.

   c. If "motorboating" is reported for the dew point; determine the saturation mixing ratio at temperature T and multiply by 15 percent to obtain a "motorboating" mixing ratio. Plot the dew point for this motorboating mixing ratio at the same pressure level. Connect the points with a line as before.

REFRACTIVE INDEX OVERLAY

FOR AROWAGRAM

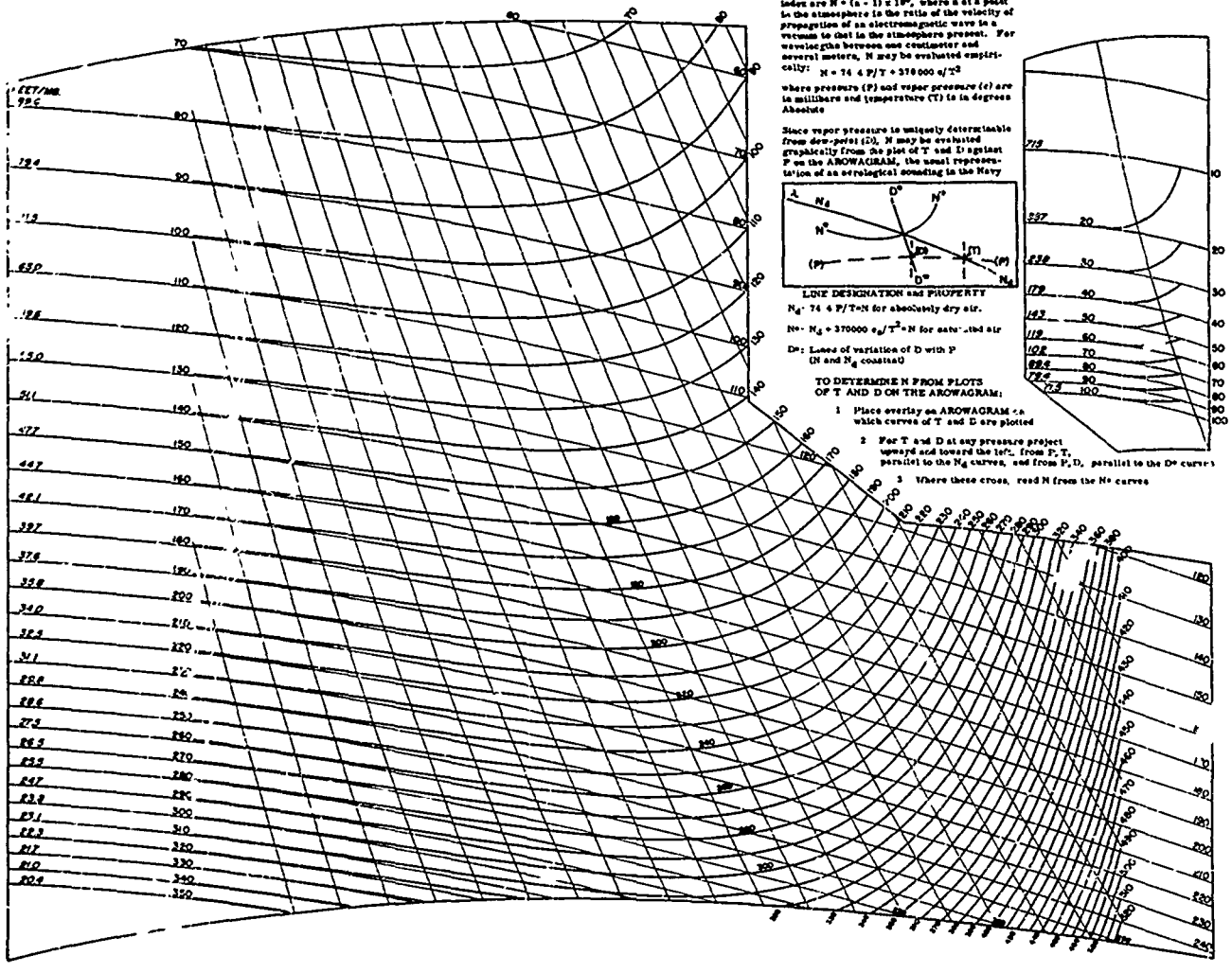

Convenient units for evaluation of refractive index are $N = (n - 1) \times 10^6$, where n at a point in the atmosphere is the ratio of the velocity of propagation of an electromagnetic wave in a vacuum to that in the atmosphere present. For wavelengths between one centimeter and several meters, N may be evaluated empirically:

$N = 74.4\ P/T + 370000\ e/T^2$

where pressure (P) and vapor pressure (e) are in millibars and temperature (T) is in degrees Absolute

Since vapor pressure is uniquely determinable from dew-point (D), N may be evaluated graphically from the plot of T and D against P on the AROWAGRAM, the usual representation of an aerological sounding in the Navy

LINE DESIGNATION and PROPERTY

N_d: $74.4\ P/T = N$ for absolutely dry air.

N^o: $N_d + 370000\ e_s/T^2 = N$ for saturated air

D^o: Locus of variation of D with P (N and N_d constant)

TO DETERMINE N FROM PLOTS OF T AND D ON THE AROWAGRAM:

1 Place overlay on AROWAGRAM so which curves of T and D are plotted

2 For T and D at any pressure project upward and toward the left, from P, T, parallel to the N_d curves, and from P, D, parallel to the D^o curves

3 Where these cross, read N from the N^o curves

2. Remove overlay and place on a white surface. Determine N by following the projection scheme given in the inset at the upper right-hand corner of figure 3.4, marking each point with a grease pencil of a different color than the one used for the T- and T_d-dots. Connect each dot as it is determined to the previous dot with a straight line. This is to avoid inverting the sequence of the dots.

3. Read the value of N from the curves and place this value alongside each dot as it is read. Interpolate to the nearest unit value of N.

4. Relabel the temperature lines in the lower left-hand corner of the Arowagram as follows: -80°C. as 100; -60°C. as 200; -40°C. as 300; -20°C. as 400, and plot the N-values as determined in (3) above at the correct pressure level on the Arowagram. Connect these points with straight line segments. This is the N-profile as a function of pressure. This plot may be directly (and easily) compared with the temperature and dew-point curves which are already plotted further to the right. The N-profile may thus be related to the existing synoptic situation.

The refractive index overlay was completed prior to the survey of the constants A and B, which was mentioned in section 3.1, and the values A = 74.4 and B = 4,973 were used in its construction rather than the currently accepted correct values (77.6 and 4,810). As a result N-values as determined from figure 3.4 are consistantly too low (5 to 15 N-units) and should not be used together with N-values determined by any other means in computing N-gradients in a layer. So long as both N-values (top and bottom of the layer) are determined from figure 3.4, the error introduced in the computed value of the N-gradient is entirely negligible. As will be seen in later paragraphs, it is the N-gradient (not the discrete values of N) which affects the performance of radio-radar equipment. For this reason the refractive index overlay may be used for most practical computations in spite of the inherent errors contained in individual N-values as determined from it.

In addition to figure 3.4, a larger, full-size overlay (for use with the large Arowagram) has been printed on transparent paper and is provided as a loose-leaf inclusion to this manual (chart III). Although

chart III can be used directly in its present form, it is suggested that working copies be made on transparent plastic stock using the Ozalid (or other) duplicating process. Routine use of chart III in its present form will soon result in its destruction.

3.2.3 Radar Method

Since variations in the vertical, refractive index structure in the troposphere are the principal cause of anomalous radar propagation one can use the measured characteristics of radar field strength versus height and range to deduce an "effective" refractive index profile. The details of an operational method for doing this are described in section 6.4. There are certain advantages and some disadvantages to using this approach. The principal advantage is that the profile deduced is an effective profile averaged over many miles, rather than one representative of a single set of points as a radiosonde ascent would be. Furthermore, one would expect such a profile to have a better correlation with propagation effects, since it was derived from actual propagation measurements. The disadvantages of this approach are that it requires radar equipment and aircraft for making the measurements, and that one can deduce only certain gross features of the refractive index profile, rather than its detailed structure. There are operational situations, however, when current radiosonde data are not available, in which the radar method can be very useful.

3.3 Refractivity Gradients

Most tropospheric propagation anomalies are caused by the bending (refraction) of radio-radar waves and such bending is in turn caused by gradients in the refractive index, rather than by the absolute value of N itself. In fact, in an atmosphere of constant N no refraction occurs irrespective of the value of N. Since gradients in pressure, temperature, and humidity exist in the atmosphere, refractivity gradients must also occur.

By far the strongest and most persistent gradients in refractivity are observed in the vertical plane. The largest and most persistent contribution to the decrease in refractivity with height is the pressure gradient which amounts to about 35 millibars in the first 1,000 feet above sea level. For a similar pressure change to take place in the horizontal plane, even in association with a deep low pressure center, would require a distance of many hundreds of miles. Similarly, vertical

gradients of temperature and humidity are usually much stronger than those in the horizontal plane. For these reasons, in the study of propagation anomalies we are primarily concerned with gradients in the vertical plane. As will be apparent to the meteorological officer, these vertical gradients are strongly affected by meteorological processes such as advection, subsidence, turbulence, radiation, and evaporation.

3.3.1 Standard Refractivity Profile

If one averages out in time the local variations in refractivity at various heights, there results what is defined as the "standard refractivity profile", such as that shown in figure 3.5. In the troposphere, the vertical decrease in $\underline{N}$ is exponential, reaching a certain constant value of $\underline{N}$ at the tropopause, regardless of the surface value. In the stratosphere a single exponential curve is sufficient to describe the average profile. The mathematical form of each of the two segments of this profile may be written as

$$N_h = N_s \exp.^{-ch} , \tag{3.5}$$

where $\underline{N_h}$ is the refractivity at height $\underline{h}$, $\underline{N_s}$ is the refractivity at the earth's surface, $\underline{h}$ is height in thousands of feet, and $\underline{c}$ is a constant which depends upon $\underline{N_s}$. If one assumes a constant value of $\underline{N}$ at the tropopause of 61.0 units at a height of 42,500 feet, the constant $\underline{c}$, in the troposphere, may be expressed as the following function of $\underline{N_s}$,

$$c = \frac{\ln N_s}{42.5} - 0.0968 . \tag{3.6}$$

Values of $\underline{c}$ corresponding to several values of $\underline{N_s}$ are given in table 3.1.

TABLE 3.1

N_s	c
N-Units	Per Thousand Feet
465	0.0478
400	0.0442
350	0.0411
318	0.0388
306	0.0375
273	0.0351
250	0.0331

Values of the Exponential Coefficient (c) for Various Values of Surface Refractivity (N_s).

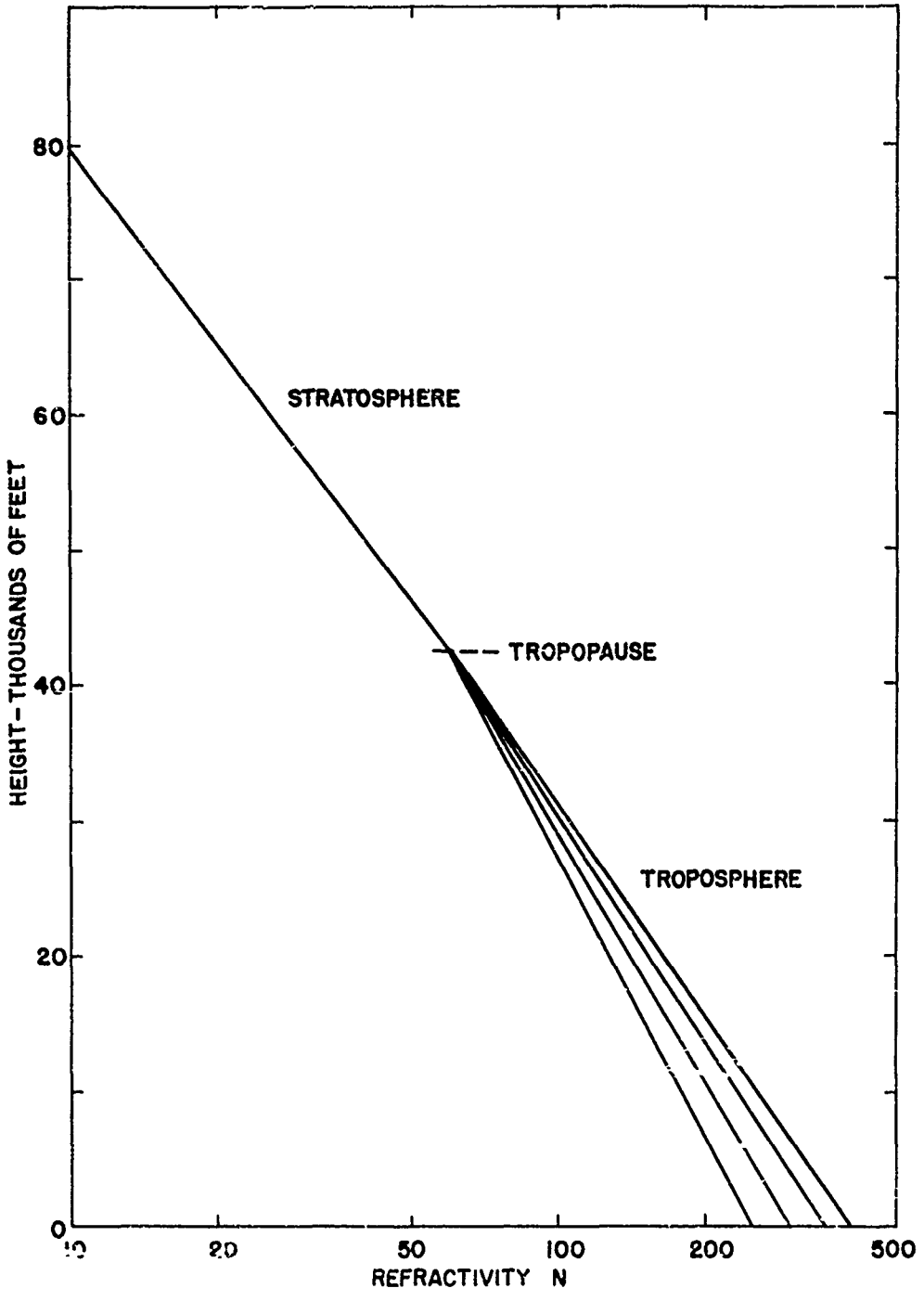

Figure 3.5. Standard Refractivity Profile.

The stratospheric segment of the standard refractivity profile may be expressed as

$$N_h = 465 \exp.^{-0.0478\ h}, \qquad (3.7)$$

where h is the height in thousands of feet.

This two-segment form of the standard refractivity profile was derived from data presented by Schulkin [20] and has been found to fit observations quite adequately. It should perhaps be noted that the standard refractivity profile here defined is not necessarily identical with either the U. S. or the ICAO Standard Atmospheres. By selecting N_S equal to the value computed from the U. S. Standard Atmosphere surface values (U. S. Standard Dry, N_S = 273 and U. S. Standard 60% RH, N_S = 318), an N-profile is obtained which agrees, in the troposphere, with that obtained by calculating N-values from U. S. Standard Atmosphere pressure, temperature, and humidity data (using equation 3.3 or 3.4).

One may construct the standard refractivity profile described above, using semilogarithmic plotting paper as follows:

1. Lay out height on the linear scale and refractivity on the logarithmic scale.

2. Plot the tropopause point at N = 61.0, h = 42,500 feet.

3. Plot a point at N = 465, h = 0 feet.

4. Lay a straight edge on these two points and draw in the stratospheric segment above h = 42,500 feet.

5. Plot a point at the desired N_S at h = 0 feet.

6. Lay a straight edge on this point and the tropopause point and draw in the desired tropospheric segment below h = 42,500 feet.

It should be realized that the structure depicted in figure 3.5 is a long-term average, and that significant departures, particularly at low altitudes, are to be expected. Furthermore the height of the tropopause varies seasonally and with latitude, but these departures will not cause

serious deviations from the N-profile as described above. The behavior of radio propagation in a standard atmosphere will be discussed in detail in the next chapter.

The gradient of refractivity, N, in a standard atmosphere, may be obtained from the general equation of the standard refractivity profile by differentiation (of equation 3.5) with respect to h as follows:

$$\frac{dN}{dh} = \frac{d}{dh} (N_S \exp.^{-ch}) ,$$

or (3.8)

$$\frac{dN}{dh} = -cN_S \exp.^{-ch} ,$$

where $\frac{dN}{dh}$ is given in N-units per thousand feet, N_S is the surface refractivity, c is the coefficient given in table 3.1, and h is the height expressed in thousands of feet.

We see that the N-gradient is negative in the standard atmosphere; i.e., the value of N decreases with height, and that the magnitude of the gradient also decreases with height. Values of N-gradient for several altitudes in the standard troposphere are given in table 3.2; surface values for pressure and temperature were taken from U. S. Standard Atmosphere with 60 percent RH; i.e., N_S = 318. It will be noted that the N-gradient in the standard atmosphere falls from an average value of about minus 12 units per thousand feet in the lowest layers to an average value of about minus 6 units per thousand feet in the midtroposphere.

TABLE 3.2

h	$\frac{dN}{dh}$
Feet	N-Units/Thousand Feet
Surface	-12.3
1,000	-11.9
10,000	- 8.4
20,000	- 5.6
30,000	- 3.8

Values of N-Gradient in the Standard Atmosphere (N_S = 318) for Several Altitudes in the Troposphere.

3.3.2 Actual Atmosphere

In order to evaluate N-gradients in the actual atmosphere it is recommended that a plot of $\underline{N}$ versus height be constructed. The height scale may be constructed in terms of geometric height, pressure altitude, pressure, etc., depending upon the application intended. For most purposes a simple linear plot of $\underline{N}$ versus geometric height or pressure altitude will suffice. It is recommended the ordinary 10x10 per inch graph paper be ruled off with height (2,000 feet to the inch) as the ordinate and with refractivity (50 N-units to the inch) as the abscissa. Such an N-profile is shown diagramatically in figure 3.6. In order to rapidly evaluate the N-gradient in the various layers of the profile an N-gradient overlay has been prepared and is shown in figure 3.7. This overlay has been designed for use with N-profiles constructed as shown in figure 3.6; it may be used on any N-profile chart having linear h- and N-scales with a ratio $\frac{\Delta h}{\Delta N}$ equal to 40. In addition to figure 3.7, an overlay has been printed on transparent paper and is provided as a loose-leaf inclusion to this manual (chart IV). As in the case of chart III it is suggested that working copies be made on transparent plastic stock.

The overlay is used by matching one of the sloping lines on the overlay with the slope of a section of the plotted N-profile (the N- and h-reference lines on the overlay must be parallel with the vertical and horizontal lines on the graph paper). The value of the selected sloping line is the estimated N-gradient for the section of the profile concerned. This process can be repeated until the gradients of all layers are determined.

In order to classify the refractive properties of layers conveniently, four zones are defined as follows:

1. Subrefractive ($\frac{\Delta N}{\Delta h} > 0$); $\underline{N}$ increases with height. Rays curve upward with reference to a straight line (opposite in sense to the curvature of the earth's surface). Radio-radar ranges are significantly reduced; occurrence quite rare.

2. Normal ($0 > \frac{\Delta N}{\Delta h} > -\frac{24}{1,000}$); $\underline{N}$ decreases with height. Rays curve downward (in the same sense as the curvature of the earth's surface) but not as sharply as in zone (3). Radio-radar performance is generally undisturbed.

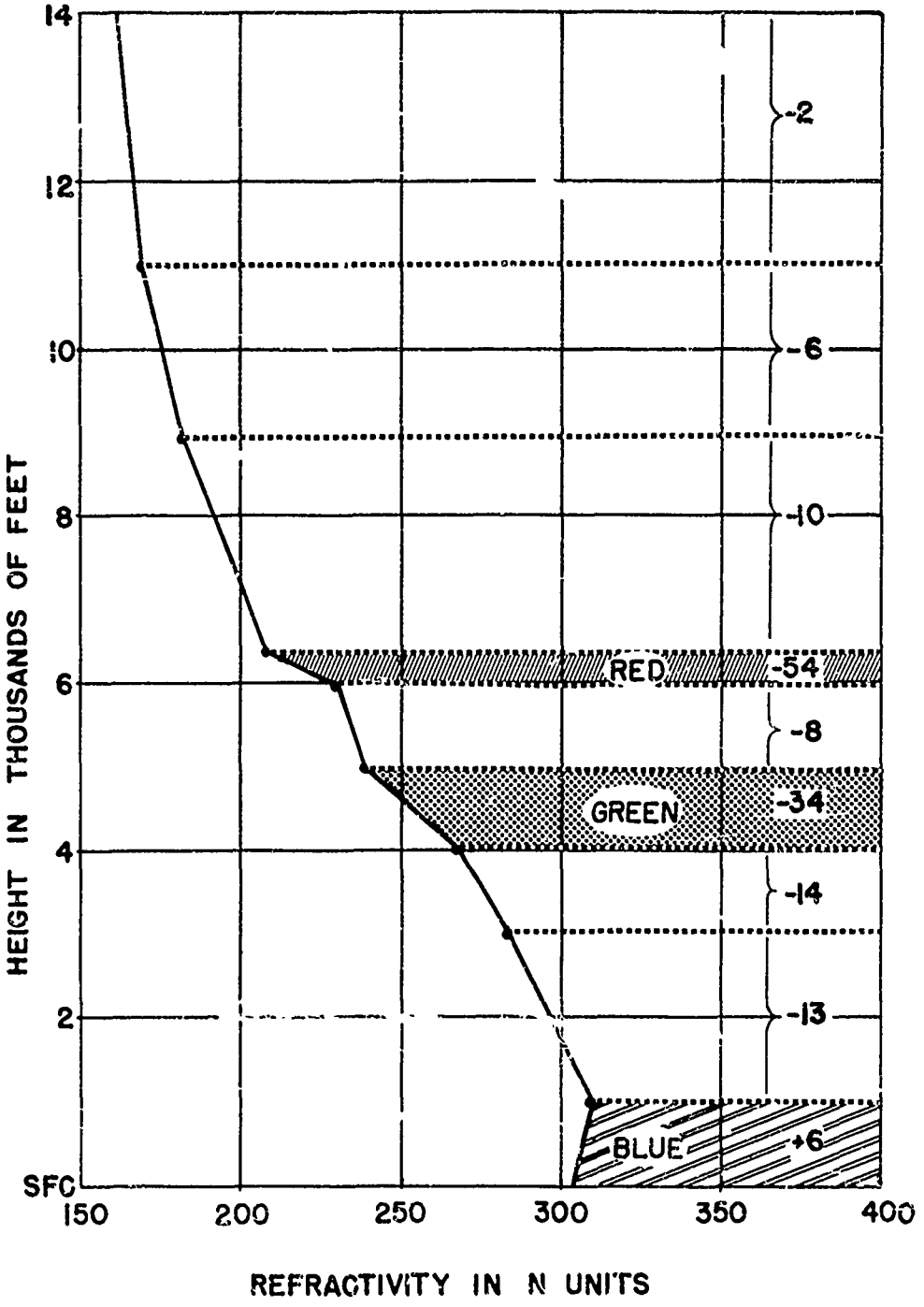

Figure 3.6. Analyzed N-Profile.

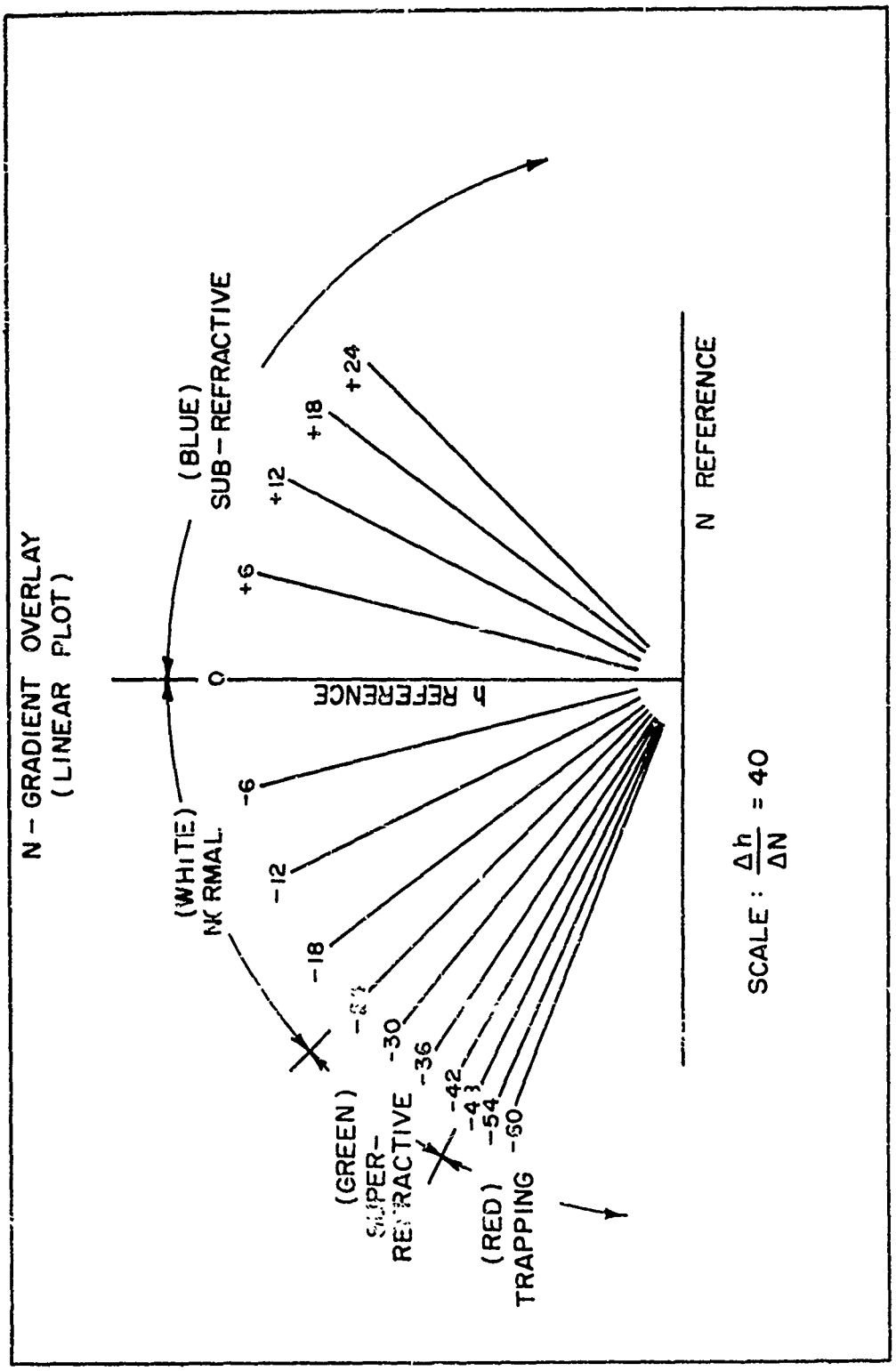

Figure 3.7. N-Gradient Overlay (Linear Plot). (Chart IV)

3. Superrefractive ($-\frac{24}{1,000} > \frac{\Delta N}{\Delta h} > -\frac{48}{1,000}$); N decreases with height. Rays curve downward (in same sense as the curvature of the earth's surface) more sharply than zone (2) but not as much as the curvature of the earth's surface. Radio-radar ranges are significantly extended; occurrence quite frequent.

4. Trapping ($-\frac{48}{1,000} > \frac{\Delta N}{\Delta h}$); N decreases with height. Rays curve downward more sharply than, and in the same sense as, the curvature of the earth's surface. Radio-radar performance is greatly disturbed; ranges extended greatly, appearance of radar holes, etc.; occurrence not frequent.

In practice construct the N-profile from refractometer values or from radiosonde data and, using the overlay (fig. 3.7), evaluate the N-gradient in each layer. Label each layer with the gradient value and designate the type of refractive zone by color shading in accordance with the color code given on the overlay (see fig. 3.6 as an example). All superrefractive and trapping layers may then easily be identified from an inspection of the completed N-profile. Each of these layers should be examined for possible influences on the particular radio-radar system in operation, using the methods described in part III of this manual. For computational purposes use the actual N-values obtained for the base and top of each layer, not the N-gradient as read from the overlay (fig. 3.7).

3.3.3 Limitations in Using Radiosonde Data

In using radiosonde data, as distinguished from refractometer data, the meteorological officer must keep certain shortcomings of the system in mind. Specifically, these are:

1. The large lag (long response time) of the humidity element which has a tendency to reduce the values of all recorded gradients, to increase the apparent thickness of all superrefractive and trapping layers, and to raise the apparent height of the top and bottom of all layers. This lag time is principally a function of temperature; decreasing with increasing temperature.

2. The sequential method of transmitting temperature,

humidity, and references which make it entirely possible to miss a superrefractive or trapping layer of anything less than about 300 feet in thickness. The response of the temperature element, while the humidity element is "off the air", can at best only given an indirect clue as to the presence of a refractive layer, since N varies only slowly with temperature.

3. The poor low-temperature response of the humidity element. At temperatures below -40°C. the response of this element virtually ceases which, along with the sequential system, makes evaluation of refractive layers in the middle and upper troposphere nearly impossible with the present instrument.

4. In cases where N-profiles are plotted from coded radiosonde reports, even when both standard and significant levels are available, errors may be introduced due to the application of the Circular "P" instructions. The criteria defining a significant level from the humidity trace operate in such a manner as to often mask out the all-important, rapid decreases in humidity. When local soundings are being evaluated, this deficiency may be overcome by instructing all raob observers to be alert for such transients and to evaluate humidity significant levels critically.

3.3.4 Radiosonde N-Gradient Overlay (Arowagram)

In order to minimize the effects of lag in the computation of N-gradients, an overlay for use with the Arowagram (fig. 3.8) has been prepared by Comdr. L. C. Clarke, USNR, and associates at U. S. Fleet Weather Facility, Argentia, Newfoundland [24]. This overlay has been designed so as to permit the analysis of N-profiles plotted on the large-size Arowagram as described in section 3.2.2(c).

The principal parameter in radio-radar meteorology which determines ray geometry (as has been shown) is the gradient dN/dh or $\Delta N/\Delta h$ where h is the true or geometric height increment. The evaluation of $\Delta N/\Delta h$ from N-profiles plotted as shown in section 3.2.2(c); i.e., refractivity versus pressure; requires reference to a pressure-height curve for the particular sounding in question. It has been shown

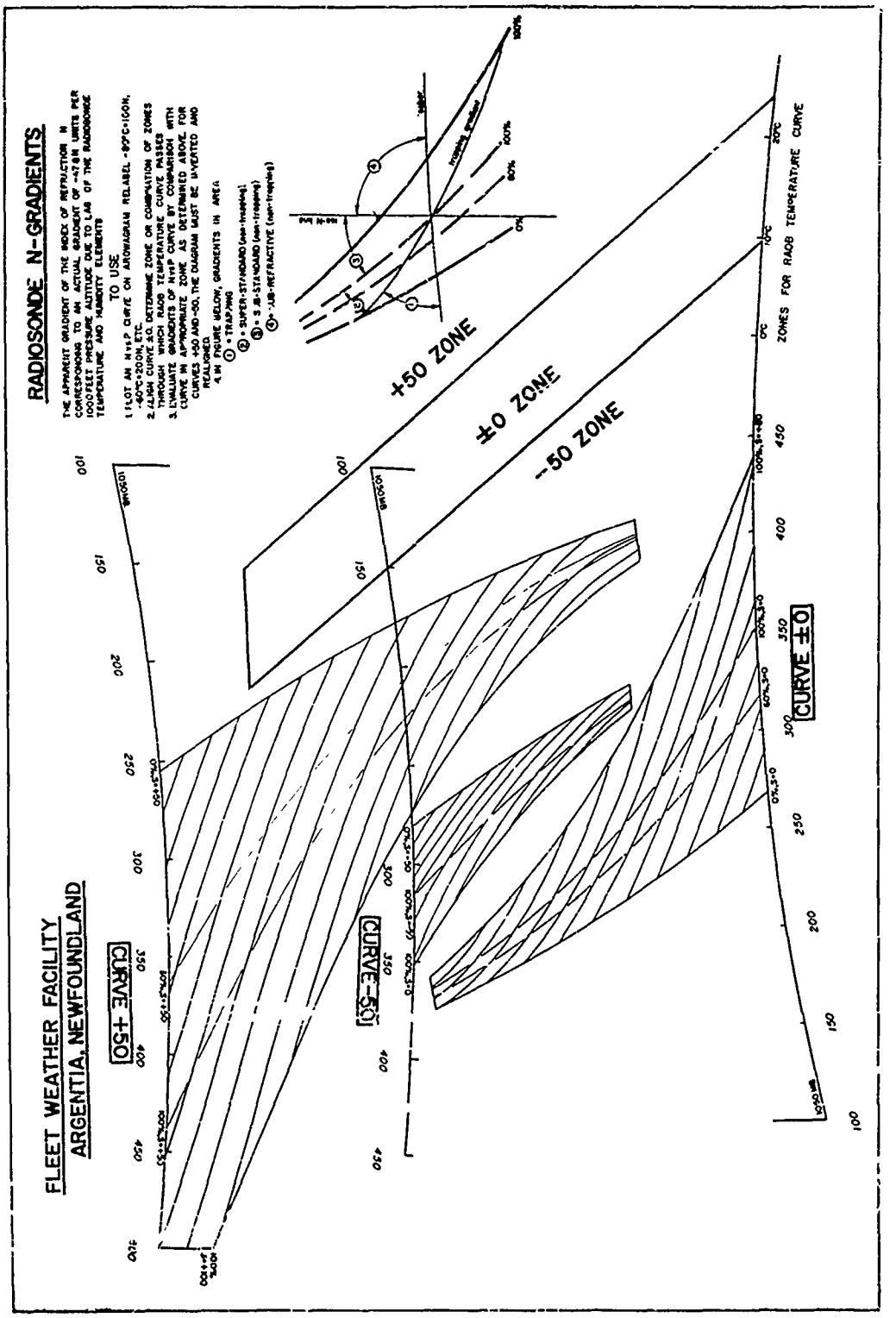

Figure 3.8. Radiosonde N-Gradient Overlay (AROWAGRAM). (Chart V)

[24] that within the range of current radiosonde inaccuracies, the gradient $\Delta N/\Delta h$ may be replaced by $\Delta N/\Delta Z_p$ (Z_p = pressure altitude) with sufficient accuracy for computational purposes.

We have by definition

$$\Delta h = \Delta Z_p + \Delta D \ , \tag{3.9}$$

then

$$\frac{\Delta N}{\Delta h} = \frac{\Delta N}{\Delta Z_p}\left(\frac{1}{1+\frac{\Delta D}{\Delta Z_p}}\right) = \frac{\Delta N}{\Delta Z_p}\left(\frac{1}{1+S}\right) \ , \tag{3.10}$$

where D is the altimeter correction and S is the specific temperature anomaly after Bellamy [5]. Possible values of S range from about plus 100 feet per 1,000 feet to minus 150 feet per 1,000 feet, with plus or minus 50 feet per 1,000 feet being probable extremes in the lower troposphere. Hence, the approximation $\frac{\Delta N}{\Delta h}$ equals $\frac{\Delta N}{\Delta Z_p}$ may be accepted without introducing errors greater than about 5 percent.

If the radiosonde actually reported true values of temperature and humidity as functions of pressure, the identification of trapping layers would require simply the construction of an overlay with isolines drawn for a gradient of minus 48 N-units per 1,000 feet (Z_p) at suitable intervals; $\Delta N/\Delta Z_p$ equal to minus 48 N-units per 1,000 feet being the critical gradient for trapping to occur. A visual comparison between the slope of these isolines and the slope of various sections of the N-profile as plotted in section 3.2.2(c) would delineate trapping layers. Because of the effects of radiosonde humidity-and-temperature-element lag, as described in section 3.3.3, many real trapping layers are not detected by this method.

Consider a radiosonde ascending at a fixed rate $\frac{\Delta Z_p}{\Delta t} = R$ (a constant), then

$$\frac{\Delta N}{\Delta Z_p} = \frac{\Delta N/\Delta t}{\Delta Z_p/\Delta t} = \frac{1}{R}\left(\frac{\Delta N}{\Delta t}\right) \ , \tag{3.11}$$

which shows that the gradient of N is a direct function of $\Delta N/\Delta t$. From equation 3.2 we have

$$N = A\left(\frac{P}{T}\right) + AB\left(\frac{e}{T^2}\right) ,$$

and by differentiation with respect to time

$$\frac{dN}{dt} = \frac{A}{T}\left(\frac{dP}{dt}\right) - \left(\frac{AP}{T^2} + \frac{2ABe}{T^3}\right)\frac{dT}{dt} + \frac{AB}{T^2}\left(\frac{de}{dt}\right) . \qquad (3.12)$$

Clarke [24] has shown that for a typical ascensional rate (R = 300 m./min. = 16.4 ft./sec.) the contribution of the first term on the right-hand side of equation 3.12 ranges from about minus 0.16 N-units per second at the surface to minus 0.10 N-units per second at 500 millibars. Similarly, the contribution of the second term in equation 3.12 is less than one N-unit per second in magnitude, while under typical tropospheric conditions the third term may have values as large as minus 10 N-units per second. Thus, the contribution of the first and second terms may be neglected in comparison with the third, and we have

$$\frac{\Delta N}{\Delta t} \cong \frac{AB}{T^2}\left(\frac{\Delta e}{\Delta t}\right) . \qquad (3.13)$$

Since most real trapping layers are quite shallow (200 to 400 ft.) we may assume that no significant temperature changes will occur within the layer. Therefore, from equation 3.11 we have

$$\frac{\Delta N}{\Delta Z_p} \cong C\left(\frac{\Delta e}{\Delta Z_p}\right) , \qquad (3.14)$$

where the "constant" $C = \frac{AB}{T^2 R}$. Thus, we have shown that the rate of change of N is principally a function of the rate of change of the vapor pressure.

The humidity element in the present radiosonde is a relatively inaccurate and slow-responding sensor. Its lag in a changing environment is a function of the temperature, the vapor pressure, and the direction of change of the relative humidity. Of these factors, temperature is the most important, and it may be taken as the only factor influencing the humidity sensor's lag, without introducing appreciable error.

Using the approximations described in the preceeding paragraph and using an error function of the form

$$\epsilon = -\left(\frac{\Delta N}{\Delta t}\right) \xi \left(1 - e^{\Delta t/\xi}\right) , \qquad (3.15)$$

where ϵ is the error in N introduced by lag and ξ is the lag coefficient in seconds, Clarke [24] has derived an expression for the apparent N-gradient in a layer (as measured by the radiosonde) required for trapping. This expression is

$$\left[\left(\frac{\Delta N}{\Delta Z_p}\right)_{\text{trapping}}\right]_{\text{apparent}} = -\left[\left(\frac{\Delta N}{\Delta Z_p}\right)_{\text{trapping}}\right]_{\text{actual}} \left(\frac{\Delta Z}{\Delta t}\right) \xi \left(1 - e^{\Delta t/\xi}\right),$$

or

$$\left[\left(\frac{\Delta N}{\Delta Z_p}\right)_{\text{trapping}}\right]_{\text{apparent}} = -48\, R\, \xi \left(1 - e^{\frac{\Delta h}{R\xi}}\right) , \qquad (3.16)$$

where R is the ascentional rate in feet per second, Δh is the layer thickness in feet, and ξ is the humidity sensor lag coefficient in seconds.

In order to compute the apparent critical N-gradient from equation 3.16, ξ must be specified and this requires a knowledge of the temperature structure. The ICAO Standard Atmosphere (S = O) can be used as an initial reference, but since the variation of ξ with T is large, auxiliary standard atmospheres for S = ±50 and S = + 100 must also be employed to provide the range of temperature structures found in the real atmosphere. Typical values of the apparent, critical N-gradients, given the N-units per 1,000 feet are:

	S = -50	S = 0	S = +50	S = +100
For Z_p = 0	-16	-26	-36	-42
For Z_p = 10,000 feet	-5	-12	-21	-31

If one remembers that the true, critical N-gradient is minus 48 N-units per 1,000 feet, the large error introduced by the lag of the humidity element is at once apparent.

In order to construct the radiosonde N-gradient overlay (fig. 3.8), the apparent, critical N-gradient was computed at selected pressure

levels and was plotted on an Arowagram at the correct N and pressure values. Since the N-values at a given temperature T are a function of the humidity, and since the ICAO Standard Atmosphere makes no provision for moisture; three values of relative humidity were used; 0 percent, 60 percent, and 100 percent in order to cover the range of all possible situations. In order that heights remain unchanged, the virtual temperature must be used. Smooth equally-spaced curves were drawn parallel to the computed gradients. These curves define three areas on the N versus P plot on the Arowagram corresponding to the three atmospheres; S = + 50, S = 0, and S = - 50. It was found convenient to extend each area to the right so as to include the adjacent portion of the next area; e.g., S = + 50 was extended to the right so as to include apparent gradients for a S = + 100 atmosphere.

Use of the radiosonde N-gradient overlay is explained in the following instructions and recommended computational procedures:

1. Carefully place the overlay in register over the Arowagram. The S = 0 curves are aligned initially.

2. Examine the temperature sounding (T vs. P) carefully to determine which layers of the sounding fall within the S = 0 parallelogram. Place grease pencil tab marks on the N-profile so as to properly delineate this (these) layer(s). Repeat this procedure for those layers which fall into the S = + 50 and S = - 50 areas.

3. Layers within the S = 0 parallelogram.

   a. Carefully compare the gradient (slope) of each straight line segment of the N-profile with the slope of the apparent trapping gradient shown on the overlay. If the slope of the N-profile is greater, then that layer is marked as being a trapping layer.

   b. If a segment of the N-profile is exactly parallel to a trapping gradient line on the overlay, mark it as being a trapping layer.

   c. If segments of the N-profile have slopes close but not equal to the apparent trapping gradient, these layers may be trapping layers. Examine the sounding to see if there are meteorological indications which suggest that a trapping layer should be present. If so, evaluate the layer (layers) as a trapping layer(s).

4. Layers S = + 50 and S = - 50.

   a. Invert the overlay. Place the appropriate curve in register and proceed to evaluate as in (3) above.

Each trapping layer identified should be examined for possible influences on the particular radio-radar system in operation, using the methods described in part III of this manual. For computational purposes use the actual N-value observed at the layer base and the actual critical N-gradient ($\frac{\Delta N}{\Delta Z_p}$ = - 48 N-units/1,000 ft.) to determine the most probable N-value at the layer top. Heights of the base and top (and layer thickness) may be determined for all layers of interest from the pressure height curve.

In addition to figure 3.8, a larger, full-size overlay (for use with the large-size Arowagram) has been printed on transparent paper and is provided as a loose-leaf inclusion to this manual (chart V). As in the case of charts III and IV it is recommended that working copies of chart V be made on transparent plastic stock.

4. THE STANDARD ATMOSPHERE

In the preceeding chapter we have defined a "standard refractivity profile" in a "standard atmosphere" and have discussed the computation of N-gradient values in both the standard and in the actual atmosphere. In this chapter we shall discuss the effect of refractive gradients in the standard atmosphere upon propagation and shall describe the various "modified" refractive indices in current use.

4.1 Refraction in a Standard Atmosphere

We have seen that N decreases exponentially with height in the standard atmosphere and that, as a consequence, electromagnetic rays are bent downward by refraction in such an atmosphere. Figure 4.1 shows a radio frequency source of electromagnetic radiation above the surface of the earth. The lit zone (or interference zone) forms the locus of all direct paths, while the crosshatched area below the grazing path is the diffraction region. Note that the radio horizon, C, lies beyond the geometric horizon, A, and the optical horizon, B. In a standard atmosphere the curvature of a radio ray is about one-fourth the curvature of the earth so that the radio horizon extends beyond the geometric horizon by about 15 percent. Tables have been calculated for radio horizon distance versus transmitter height in a standard atmosphere for several values of surface refractivity, N_s. The results of such a calculation are plotted in graphical form in figure 4.2.

4.2 The Four-Third's Earth Radius Concept

In the first few thousand feet above the surface, the exponential decrease of N with height (in the standard atmosphere) may be closely approximated by a linear decrease. The upper sketch in figure 4.3 shows the earth's surface and a tangent ray having a curvature equal to one-fourth the earth's curvature. At a given distance beyond the tangent point, a straight tangent line will be $\frac{d^2}{2a}$ above the surface, if we neglect second order terms (see fig. 2.2). At the same distance away, the straight line will be $\frac{d^2}{2}\left(\frac{\Delta n}{\Delta h}\right)$ above the curved ray. Assuming $\frac{\Delta n}{\Delta h}$ is constant and equal to $\frac{1}{4a}$, it follows that the ray will be $\frac{d^2}{2}\left(\frac{1}{a}-\frac{1}{4a}\right)$ above the earth at the distance, d. The same height-distance relationship between ray and surface may be obtained if one makes the ray straight and modifies the earth's radius to a new value a_e, such that

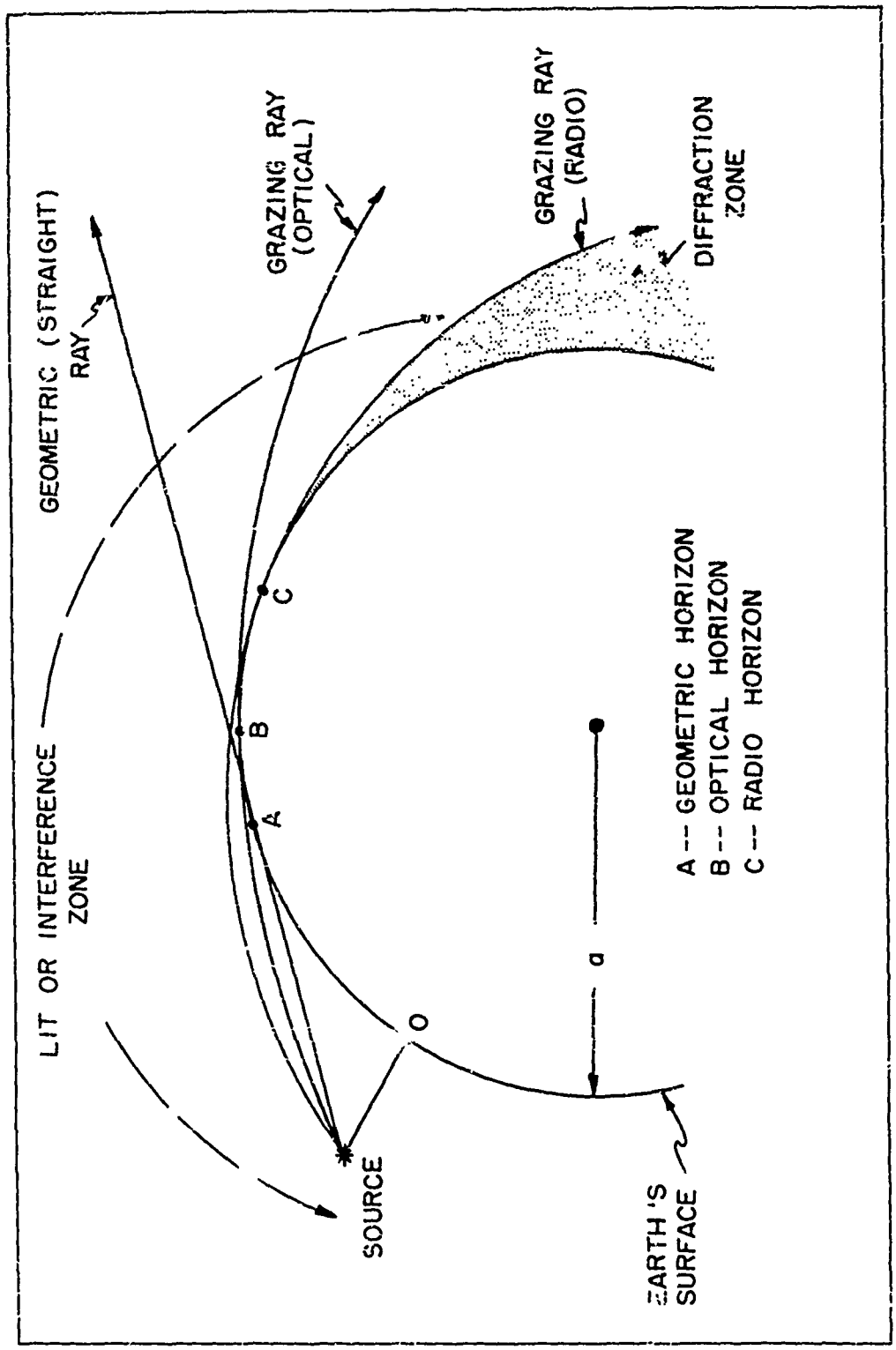

Figure 4.1. Ray Geometry for Spherical Earth--Standard Atmosphere.

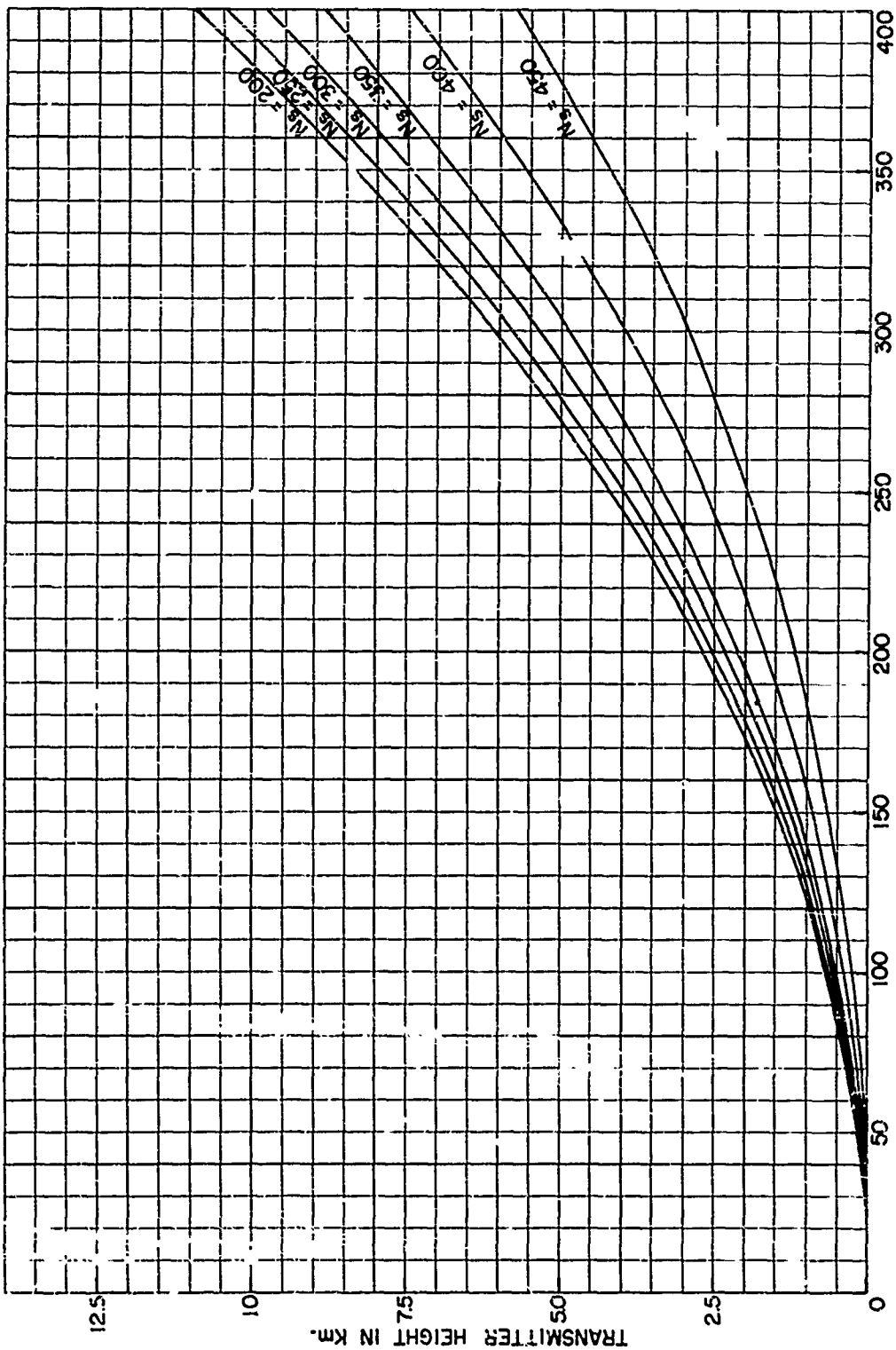

Figure 4.2 Radio Range versus Transmitter Height

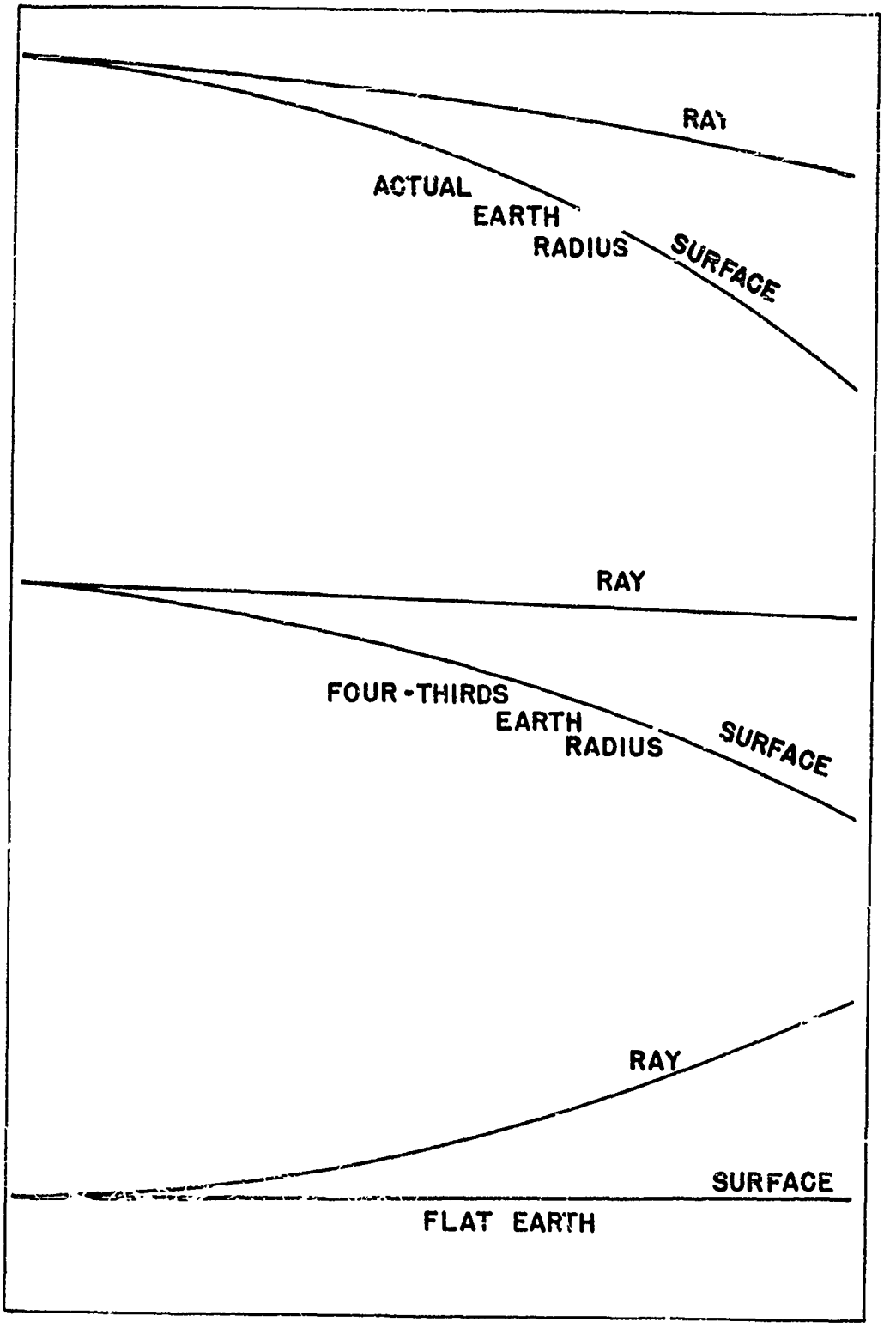

Figure 4.3. Comparative Ray Geometry.

$$\frac{1}{a} - \frac{1}{4a} = \frac{1}{a_e}$$

or

$$a_e = \frac{4}{3}a \quad . \tag{4.1}$$

Thus, by making the "effective" earth's radius four-thirds as great as the true radius, the situation has been restored to that of the homogeneous atmospheric case (straight ray and curved earth)--see middle sketch in figure 4.3. This method, advanced by Schelling, Burrows, and Ferrel [19], assumes an earth suitably larger than the actual earth and allows radio rays to be drawn as straight lines over this earth rather than as curved rays over an earth with true radius a.

In general, the effective earth's radius $a_e = ka$, where k is the effective earth's radius factor and a is the true radius of the earth. The value of k is usually assumed to be four-thirds in the United States. It is desirable, however, in some geographic areas to use a somewhat different value of k, for example in desert areas it is more nearly six-fifths. One may write in general

$$k = \frac{1}{1 + a\frac{\Delta n}{\Delta h}} \tag{4.2}$$

where $\frac{\Delta n}{\Delta h}$ is the assumed linear gradient of the index of refraction (usually negative), applying to a particular area or season and a is the sea level radius of the earth.

This method of accounting for atmospheric refraction permits a tremendous simplification in the computation of radio field strengths even though the distribution of refractive index (linear with height) implied by this method is realistic only in the lowest few thousand feet of the atmosphere.

4.3 The Flat Earth Concept

For some purposes, it is desirable to portray the earth as being flat with upward curving rays. This is done by subtracting the earth's curvature from both ray and earth. This results in an upward ray curvature equal to the downward curvature given to the earth in the situation described in section 4.2 (see bottom sketch in fig. 4.3). This rep-

resentation is not now widely used because of its unrealistic portrayal of the earth-ray relationship. However, there are instances, such as ray plotting by analogue computers, where it is advantageous to use the "flat earth" type of presentation.

4.4 Modified Refractive Indices

The B-, M-, A-, and K-modifications of refractivity are useful, particularly in ray tracing problems and in synoptic studies of refractivity. Each results in simplifications in ray geometry in certain situations, not only in plotting ray trajectories but also in the mathematical relationships describing various propagation mechanisms and in the study of climatic and synoptic relationships. There is much to be said, however, for retaining the unmodified refractivity N itself. It is a basic physical quantity, and as such is more easily understood than are B, M, A, or K. For the purposes of uniformity and initial simplicity, N-units are therefore the principle refractive index units employed in this manual (except in part IV). For reference purposes, however, a description of each of the modified indices is given in the following four subparagraphs.

4.4.1 B-Units

It was shown in section 4.2 above, that one can compensate for a linear refractive index gradient merely by changing the effective radius of the earth. The most convenient way to represent departures of a given refractivity-profile from the standard atmosphere (at least in the lowest layers where the departure of the N-gradient from the assumed constant value is negligible) is to add 12 N-units per 1,000 feet to all N-values. This modified index, B, is defined as

$$B = N_h + 0.012\,h \tag{4.3}$$

where N_h is the value of refractivity at any height h in feet. A B-profile will have zero gradient in the lower layers of a standard atmosphere. The B-modification, therefore, is a logical consequence of the four-third earth radius concept described in section 4.2 because the B-gradient is zero for the same situation where the ray curvature is zero. A standard atmosphere B-profile is compared with standard N-, A-, and M-profiles in figures 4.4 and 4.5. Note that in the lowest few thousand feet B has a zero gradient but at higher levels (where the departure of $\frac{\Delta N}{\Delta h}$ from an assumed constant surface value of minus 12 N-

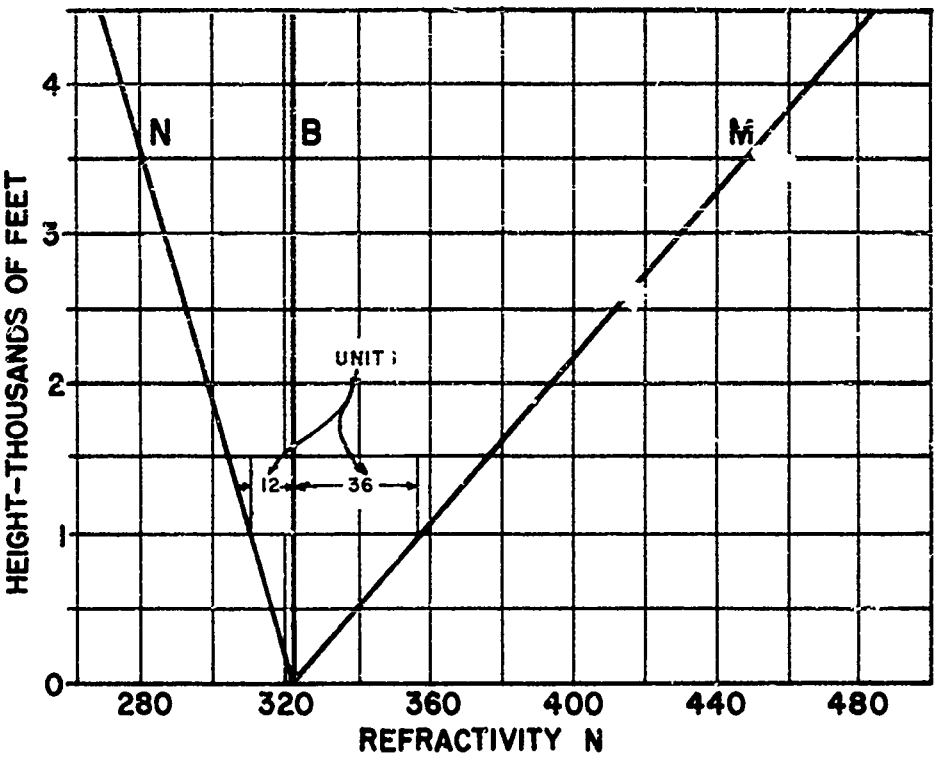

Figure 4.4. N-, B-, and M-Profiles for a Standard Atmosphere.

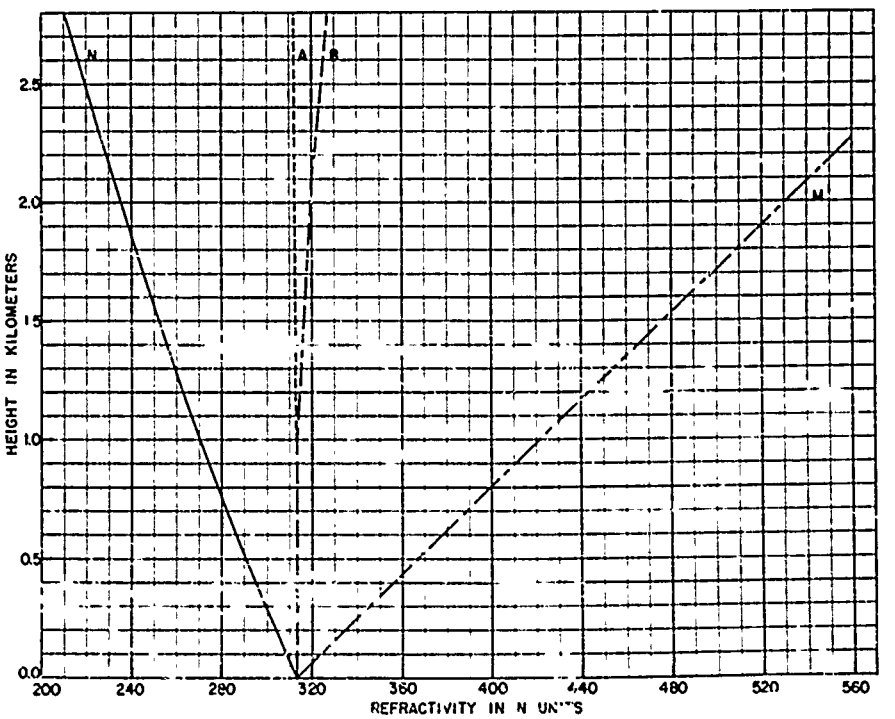

Figure 4.5. N-, A-, B-, and M-Profiles for a Standard Atmosphere.

units per 1,000 feet has become appreciable) B shows a small positive gradient.

4.4.2 M-Units

Another form of modified refractive index has been widely used, and is associated with the flat earth concept of section 4.3. In this case, one adds 48 N-units per 1,000 feet to all N-values. This modified index, M, is defined as

$$M = N_h + 0.048h \quad , \tag{4.4}$$

where N_h is the value of refractivity at any height h in feet. When the M-gradient is zero the ray curvature is zero in the flat earth case. This is another way of saying that when the N-gradient is minus 48 units per 1,000 feet, the ray has the same curvature as the earth. Thus, if the earth's surface is represented as a straight line, the ray will also be straight. Figures 4.4 and 4.5 show a standard atmosphere profile, expressed in terms of N-, A-, B-, and M-units for comparison purposes.

4.4.3 A-Units

As we have seen the B-unit modified index overcorrects for the decrease in N with height in the standard atmosphere as shown in figure 4.5 by the increase of B with height. This overcorrection results from the assumption of a constant N-gradient (i.e., linear N-profile) with a value representative of the lowest few thousand feet of the standard atmosphere. A modified refractive index (potential refractivity) expressed in A-units has been defined by Bean, Riggs, and Horn [4] in order to eliminate this overcorrection. The expression for A, which is written in terms of an exponential height function, is given by

$$A = N_h + N_s \left[1 - \exp.^{ch}\right],$$

or

$$A = N_h + 313 \left[1 - \exp.^{-0.144h}\right], \tag{4.5}$$

where N_h is the refractivity at height, h, in kilometers. The decay coefficient c = - 0.144 was determined so as to correspond best with the average station value of N_s = 313 for the United States. Figure 4.5

shows a comparison between the standard atmosphere profile expressed in terms of N-, A-, B-, and M-units.

To facilitate the transformation from N-units to A-units, a potential refractivity chart was prepared and is given in figure 4.6. This chart eliminates the necessity of using exponential tables in each individual calculation of $\underline{A}$ and thus lends considerable ease to the preparation of charts of the new parameter.

4.4.4 K-Units

In order to remove the height-dependent variations of refractivity in homogeneous air (the problem for which Bean proposed the A-unit modification) and to develop a modified index from fundamental meteorological relationships (rather than from essentially empirical considerations as Bean has done), a modified index (potential refractive index) expressed in K-units has been defined by Jehn [16]. The expression for $\underline{K}$ is given by

$$K = \left(\frac{1{,}000}{P}\right)^{0.714} \left[N_d + \left(\frac{P}{1{,}000}\right)^{0.286} N_m\right], \qquad (4.6)$$

where $\underline{N_d}$ is the conventional "dry" term and $\underline{N_m}$ the conventional "wet" term in the refractivity equation and $\underline{P}$ is the pressure in millibars at the point in question. Tables or graphs of the two multipliers could be prepared to facilitate the conversion from N-units to K-units, but as yet these are not available.

It should be noted that K-values are referred to the 1,000 millibar pressure surface, and as a result the station-to-station variability of refractivity occasioned by differences in station elevation are strongly suppressed. In synoptic radio-meteorology this becomes an important factor.

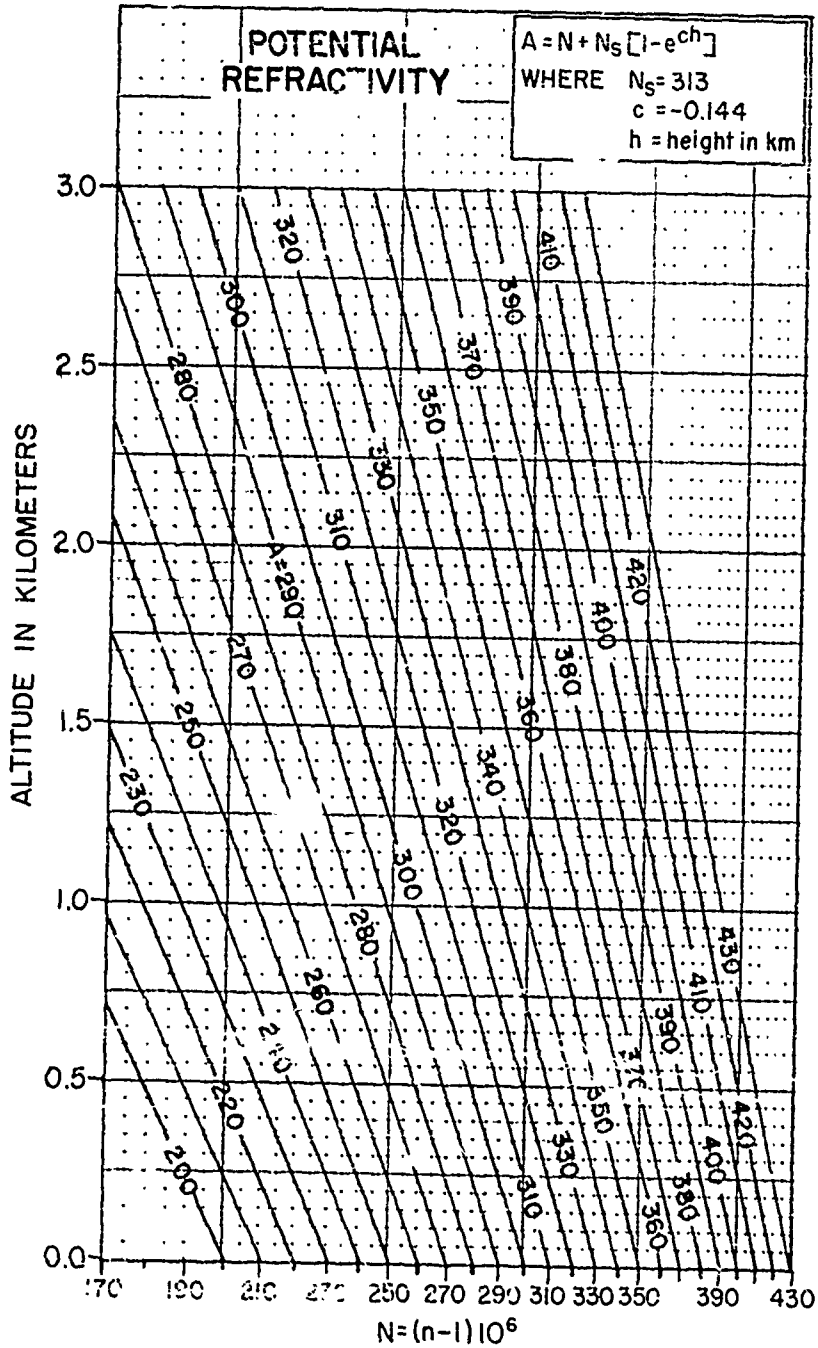

Figure 4.6. Potential Refractivity Chart.

5. THE ACTUAL ATMOSPHERE

Thus far, the discussion has been concerned with the propagation of radio waves under two artificial situations; an earth enveloped by a homogeneous atmosphere, and one with an atmosphere in which refractivity decreases smoothly (linearly or exponentially) with height. As a final step, it is now in order to consider the actual atmosphere and its effects on propagation.

There are numerous ways in which the troposphere departs from the simple linear or exponential gradient model. In a well mixed troposphere, for example, there are a myriad of small random variations in $\underline{N}$, both in vertical and horizontal planes. Even at a fixed point, $\underline{N}$ is found to vary in a random way about some mean value. These fluctuations are caused by parcels of air with different temperatures and/or vapor pressures than their surroundings. Most parcels are caused by unequal heating, during the daytime, of air in contact with the ground. The warmer parcels rise convectively and drift with the wind until they are broken up and eventually lose their identity through turbulent mixing with the surrounding air. Similarly, air overlying lakes, rivers, and oceans becomes more moist than its surroundings and rises because of its lower density. Refractometer measurements show that the root mean square value of the $\underline{N}$ fluctuations decreases exponentially with height in a well mixed atmosphere. This is a priori evidence that the source of the small-scale variability of $\underline{N}$ is at the surface.

5.1 Anomalous Propagation

In some cases the actual refractive index profile in the atmosphere departs from the linear and exponential models enough to cause radio and radar fields to be much stronger well beyond the horizon than would be expected from standard refraction and diffraction. These situations are generally caused by the presence of steep, negative, vertical gradients of refractivity in layers, which in turn cause the radio waves to be bent downward sufficiently to continue some distance on around the figure of the earth. A discussion follows of the development and of the characteristics of these so-called "trapping" or "ducting" layers.

5.1.1 Surface Layers

The actual troposphere departs most frequently from standard in

the lowest few hundred feet. These surface layers, in which the N-gradient is much steeper than minus 12 units per 1,000 feet, are caused by nocturnal radiational cooling, by evaporation or by advection. Frequently the N-gradient, particularly just above the ground, is considerably stronger than minus 48 units per 1,000 feet, such that a ray actually has a downward curvature greater than the earth's curvature. If the layer is thick enough compared to the propagation wavelength, energy is guided around the figure of the earth in the layer, causing fields beyond the horizon to be very much stronger than normal. Because of the wave nature of radio energy, it turns out that the layer thickness must exceed a certain critical value, which is a function of wavelength and of the shape of the N-profile, before guiding or "ducting" of the wave can occur.

When the layer becomes particularly intense, the horizontally directed energy from a transmitter located within the layer will be completely contained in the layer; in this instance the fields will decrease as the square root of distance rather than as the first power of distance. At some distance beyond the horizon, these fields would then theoretically not only be stronger than the diffracted fields, but would even be stronger than the free space fields. Such intense layers have not actually been found in the atmosphere. The strongest fields observed in surface ducts have been about equal to the free space fields. When the fields approach this level, the energy is said to be "trapped". The refractivity profile requirements for trapping radio energy of various wavelengths are described in more detail in section 6.1.

(a) Radiation Ducts

Nocturnal radiational cooling of the ground surface may produce "radiation" ducts. They are particularly intense over dry or desert areas, where there is little water vapor in the air to intercept and return outgoing, longwave radiation back to the ground. Calm nights tend to intensify duct formation because there is little mechanical turbulence to mix the cool lower layers with the warmer air above. The typical N-profile is exponential in shape, merging with the standard gradient at heights of a few hundred feet. Measurements in southwestern Arizona by Day and Trolese [10] showed that usually the profile is standard at sunset, with the surface N value increasing as the night progresses. At sunrise, the surface N-value has typically increased by about 15 units while the values above 500 feet have increased by only 2 or 3 units. Usually the top of the duct is arbitrarily taken to be the height where

the gradient is minus 48 units per 1,000 feet. A typical value of this height at sunrise in Arizona is about 50 feet. Such a duct would be expected to trap wavelengths shorter than about 30 centimeters, and experimental results [10] show this to have been the case.

(b) Evaporation Ducts

Over the ocean, surface refracting layers are caused by a different process than that described in (a) above. Diurnal temperature changes over large bodies of water are usually quite small. This is because solar energy penetrates well beneath the sea surface. Therefore, a relatively large amount of heating is required to change the sea surface temperature. Radiational cooling, which does occur, makes the surface water heavier than the underlying water, so it sinks, bringing up warmer water from below. The surface temperature, therefore, remains practically constant night and day. Daytime heating can cause a thin surface layer of higher temperature, but wave action usually rapidly mixes this layer with the cooler water below.

Evaporation from the sea surface, on the other hand, causes air parcels to be carried aloft by buoyancy, and thus gives rise to a steep gradient of water vapor pressure (and hence of N) in the first few hundred feet above the sea. While instantaneous N-profiles show wide fluctuations, the average over several minutes shows a profile which is exponential in shape when the air and sea are the same temperature. When the air is warmer than the sea the profile is more nearly linear; i.e., the N-gradient changes more slowly with height. In the unstable case (sea warmer than air), the gradient decreases more rapidly with height than in the neutral case (sea and air temperature the same). An interesting consequence of the physical processes which take place in the formation of an evaporation duct, is that in the stable case, low wind speeds favor strong duct formation; while in the unstable case, high wind speeds favor strong ducts. These hypotheses have been verified in data taken over the Irish Sea by Anderson and Gossard [1]. Criteria are presented in section 6.1.3 which enable one to determine from meteorological measurements at bridge elevation, whether or not a given wavelength will be trapped by the oceanic duct.

(c) Advection Ducts

Another process by which surface layers with superstandard N-gradients can be formed, is the advection of dry air over the sea. If

the air is colder than the sea, vertical convection takes place which tends to disperse air parcels with high refractivity upward, thus producing a weak but thick surface layer which does not usually affect propagation appreciably.

However, if the air is warmer than the sea, stability will keep the cool, moist (high $\underline{N}$) air confined to a thinner layer. This gives rise to surface layers in which the N-gradient can be strong enough for "trapping" and at the same time be thick enough to affect longer wavelength energy than is the case with evaporation ducts. This situation is prevalent over the Mediterranean, Red Sea, and Gulf of Arabia.

5.1.2 Elevated Layers

Thus far, processes which cause persistent departures of $\underline{N}$ in atmospheric layers close to the earth or sea surface have been considered. These layers are caused by processes taking place at the surface itself. There is another class of phenomena which gives rise to strong N-gradients at some height above the surface. Refractometer studies have shown that these elevated layers exist to some extent over wide geographic areas. In fact, very few refractometer profiles have been taken which do not show the presence of at least one elevated layer within 10,000 feet of the earth's surface.

Most of these layers are only a few hundred feet in thickness and the change of $\underline{N}$ from top to bottom averages about 10 units. Some layers can be traced for tens of miles in horizontal extent while others, particularly the weaker ones, are less than 10 miles in extent. Figure 5.1 shows an N-profile through an idealized elevated layer. Several parameters of interest are shown; the intensity, $\underline{\Delta N_L}$, the thickness, $\underline{\Delta h}$, and the heights of the top and bottom of the layer, $\underline{h_T}$ and $\underline{h_B}$, respectively. It will be noted that the N-gradient is shown as being standard below and above the layer. This is usually the case although nominal departures from standard are often found.

Figure 5.2, shows the effect of such an elevated layer on rays emanating from a transmitter located well below the layer bottom. The four-thirds earth's radius modification has been used in constructing the earth and layer boundaries. Since (as shown in fig. 5.1) the N-gradient is standard outside the layer, the ray paths above and below the layer are straight lines. In the layer itself, the N-gradient exceeds standard, therefore, the rays bend downward.

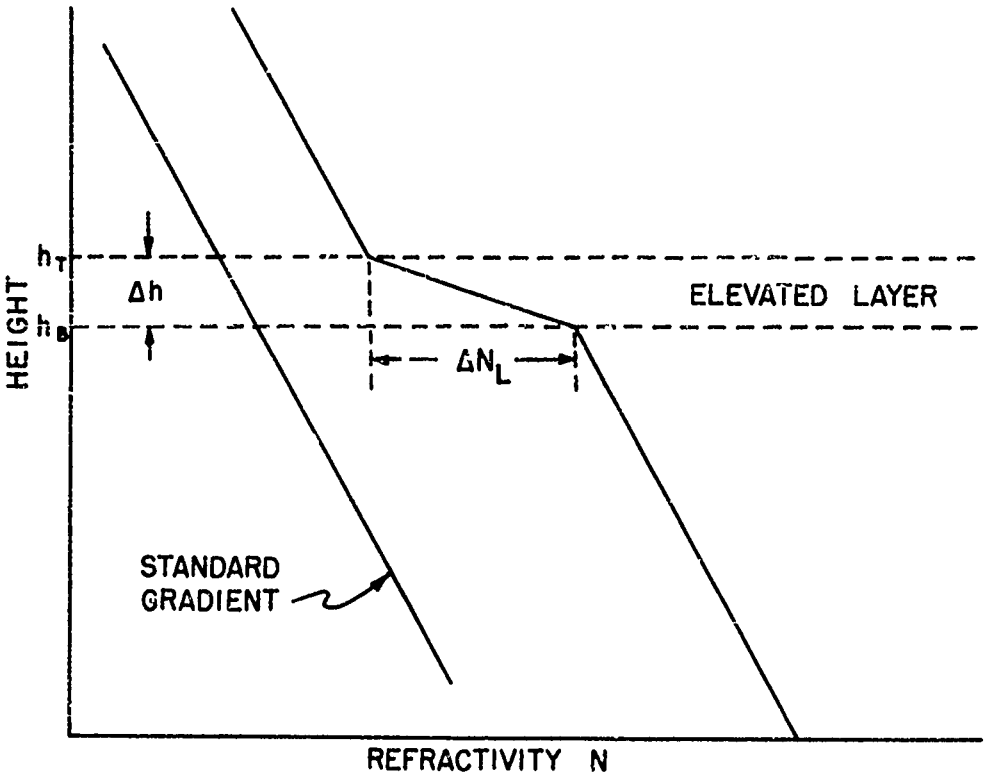

Figure 5.1. N-Profile--Elevated Layer.

Using these geometric considerations and Snell's Law, and with the help of expressions previously derived for ray bending in a medium of constant N-gradient, one obtains the following expressions for the distance, d, between the radar and the point of entry into the layer, and Δd, the distance the ray travels in the layer,

$$d = a_e \left[-\alpha_o + \sqrt{\alpha_o^2 + \frac{2(h_B - h_R)}{a_e}} \right] \qquad (5.1)$$

and

$$\Delta d = \frac{\sqrt{\alpha_o^2 - 2\Delta n_L + \frac{5}{2}(\Delta h/a_e) + 2(h_B - h_R)/a_e} - \sqrt{\alpha_o^2 + 2(h_B - h_R)/a_e}}{\left(\frac{\Delta n_L}{\Delta h} - \frac{5}{4a_e} \right)}, \qquad (5.2)$$

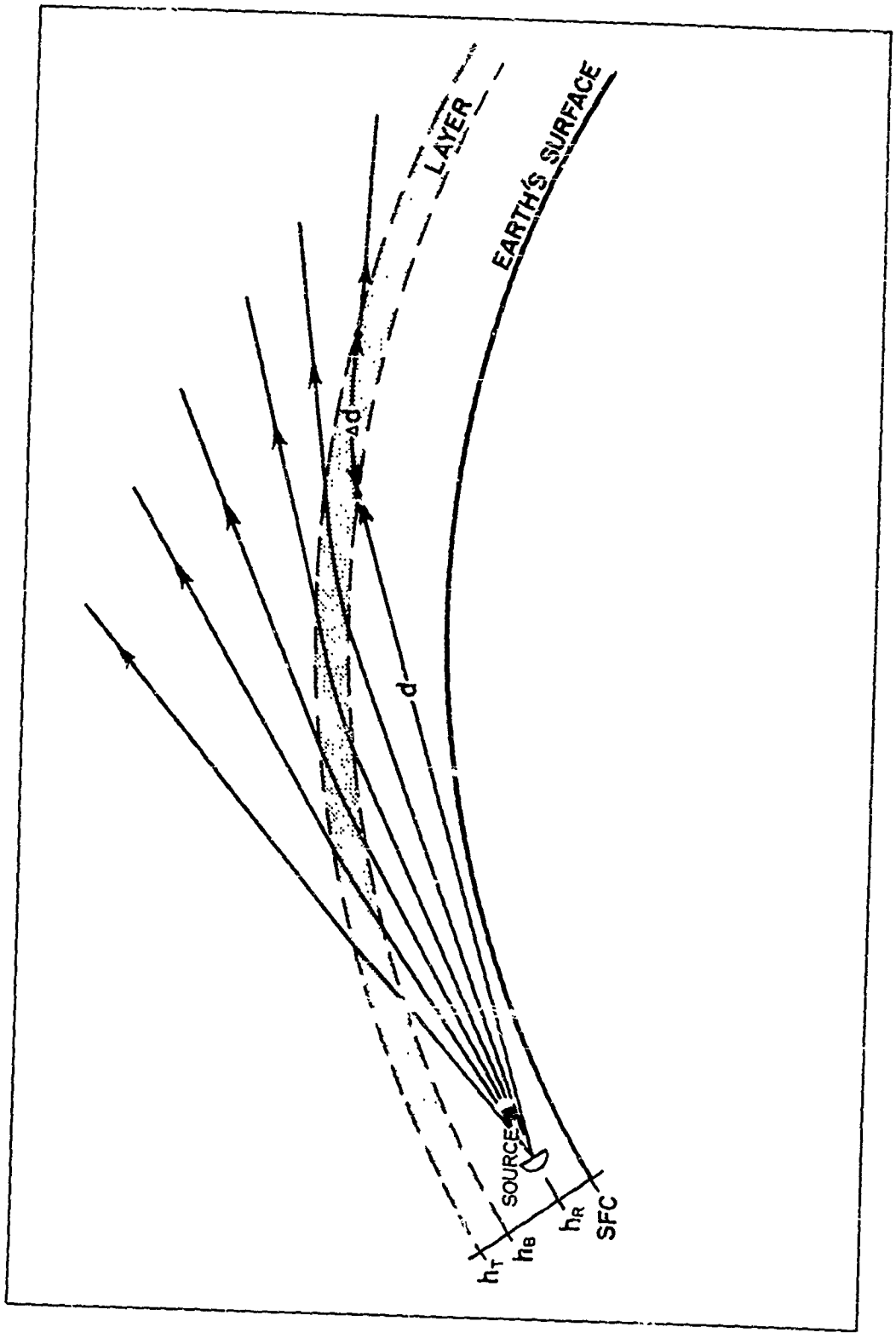

Figure 5.2. Ray Refraction by an Elevated Layer--Radar Well Below Layer.

where a_e is the effective earth's radius, α_o is the inclination angle of the ray as it leaves the transmitter, h_B and h_R are the heights of the layer base and the transmitter respectively, Δh is the layer thickness, and Δn_L; i.e., $(\Delta N_L \times 10^{-6})$; is the change in the index of refraction through the layer (see figs. 2.6 and 5.2). The distance from the transmitter at which the ray emerges is simply the sum of these two expressions. From this point, the ray proceeds in a straight line as shown in figure 5.2. Figure 5.2 also illustrates the behavior of the rays as the elevation angle, α_o, is changed. For high elevation rays (above 2°) the bending is slight, but as α_o becomes smaller, the rays are deflected more and more from their original direction.

Figure 5.3, illustrates the effect of raising the transmitter height (or lowering the layer height). The high angle rays still penetrate the layer as before, but now, as α_o is decreased, the rays are bent more and finally (in the third ray from the left) emerge tangent to the layer top. If α_o is decreased even further, the rays do not penetrate the layer at all, but are totally refracted back down toward the surface again. The reason for this will be evident from a consideration of the expression for Δd. If $(h_B - h_R)$ and α_o are sufficiently small, the first radical becomes imaginary, signifying no emergent ray. When this radical is just equal to zero, the emergent ray is tangent to the layer top. However, as α_o becomes negative, there will again be a value of α_o^2, which is larger than the remaining terms in the radical, and rays will again emerge from the layer top. This situation is depicted in figure 5.3 by the lowest ray in the bundle. Between the two emerging tangent rays is a region where no energy penetrates the layer. A radar target in this region would not be detected, nor would communications be possible between an airplane in the region and a surface-located transmitter. This region is called a "radio or radar hole." A discussion of methods for locating these regions, as well as avoiding them, is given in section 6.3.1.

In figure 5.4, the transmitter is above the layer. In this case, the upper rays do not intersect the layer at all, and are unaffected by it. There are, however, two rays which again define a "radio hole" in this situation. The first is the ray tangent to the layer top, and the second is a ray going down at a steeper angle, which comes back up through the layer farther out. The distance from the transmitter to the tangent point (start of the radio hole) is simply

$$d' = \sqrt{2a_e (h_R - h_B)} \quad , \tag{5.3}$$

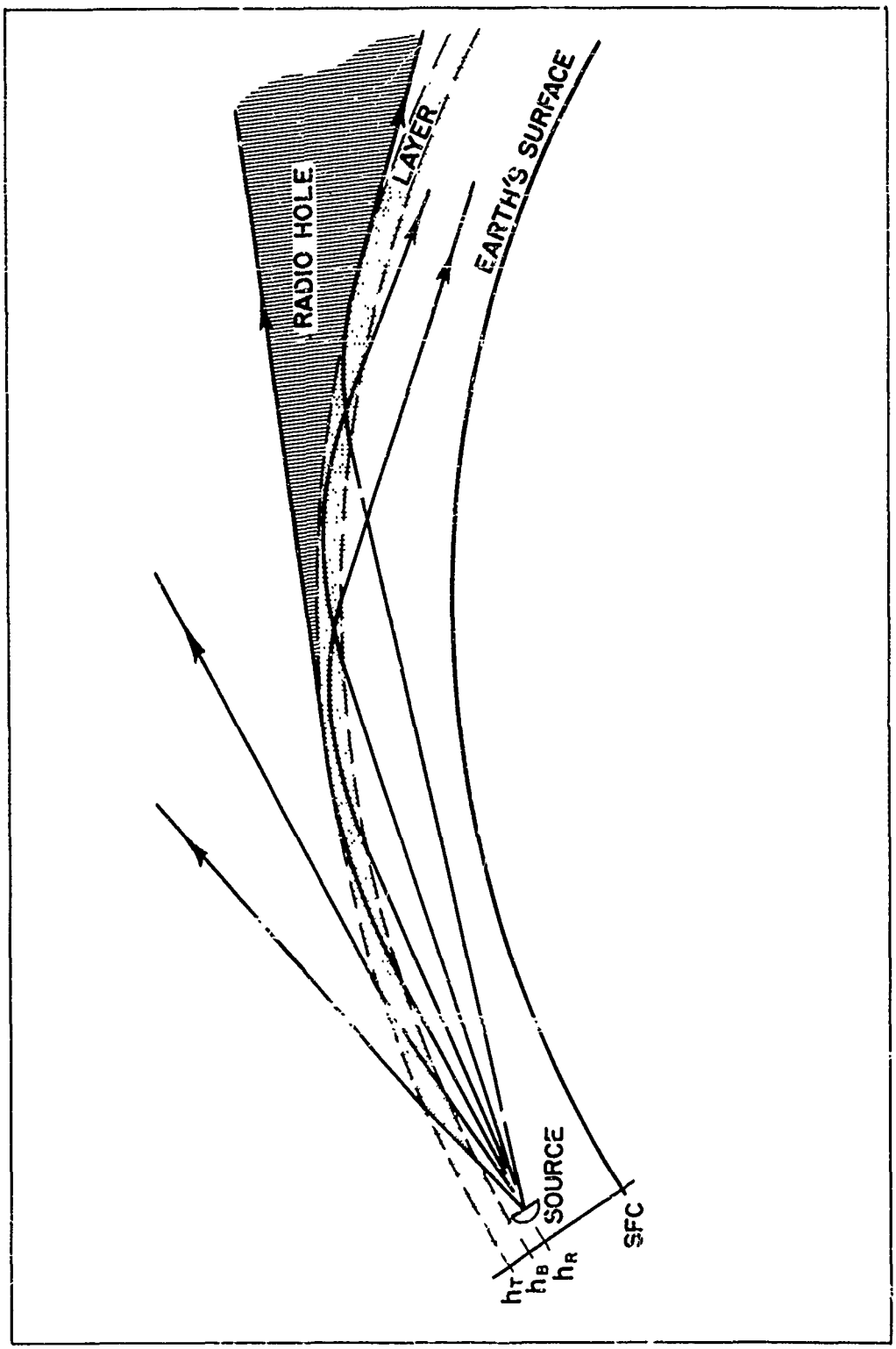

Figure 5.3. Ray Refraction by an Elevated Layer--Radar Just Below Layer.

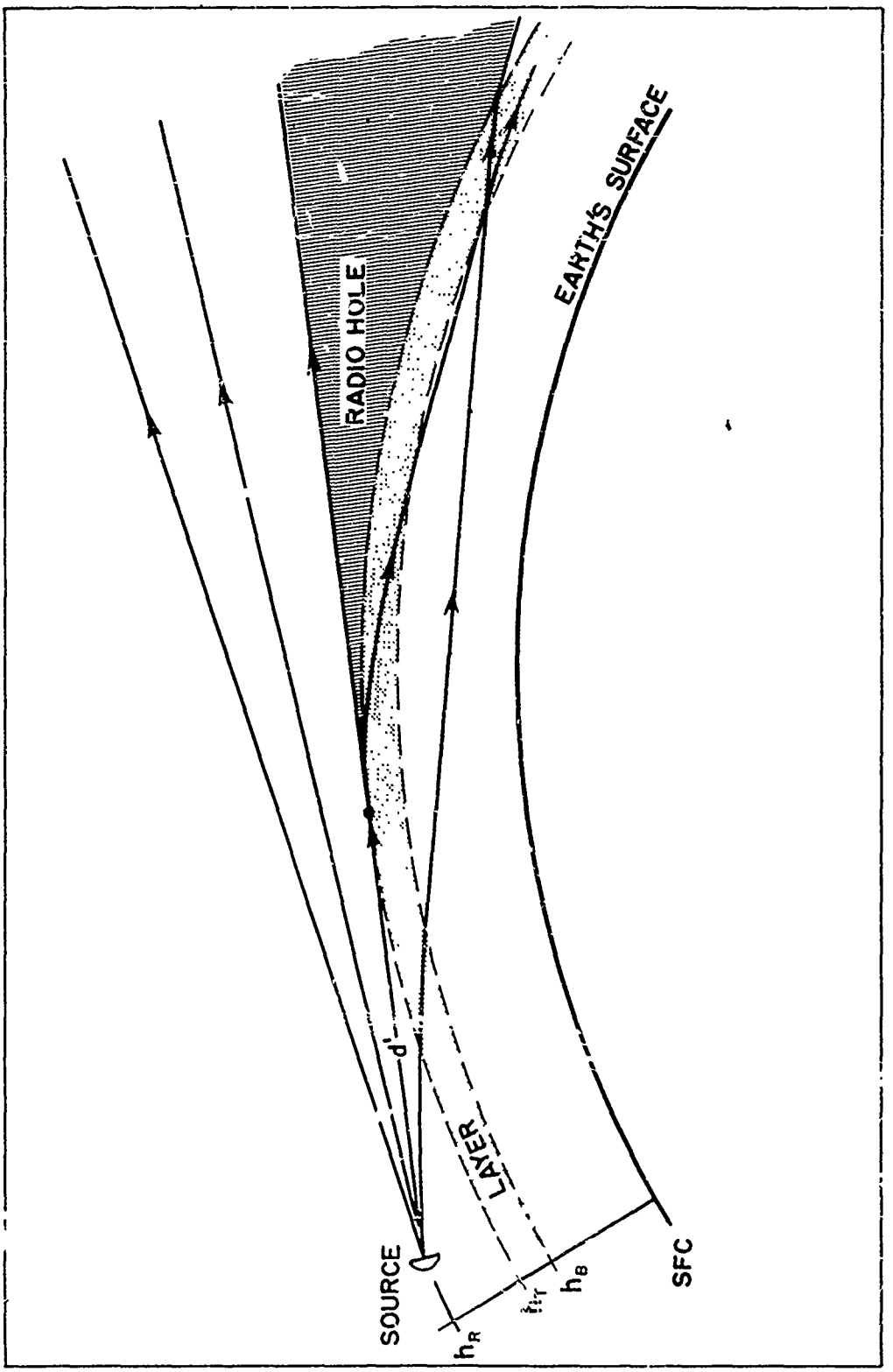
RADIO HOLE
EARTH'S SURFACE
SOURCE
d'
LAYER
h_R
h_T
h_B
SFC

where h_T and h_R are the heights of the layer top and transmitter respectively and a_e is the effective earth's radius. The width of the radio hole is more complicated to express in this case, than when the transmitter is below the layer. In section 6.3.1, practical methods are presented for operational use.

The main difference between the transmitter being below the layer and being above the layer, is that in the former case one can eliminate the radio hole completely by lowering the transmitter far enough below the layer. If $h_B - h_R$ is large enough, all rays will emerge from the layer regardless of α_0. When the transmitter is above the layer, on the other hand, raising the transmitter moves the hole further away and gradually narrows it but can never eliminate it.

Substituting 10 units for ΔN_L; ($\Delta n_L = 10 \times 10^{-6}$); and 200 feet for Δh in the expression for Δd, shows that if the transmitter is more than 80 feet below the layer base, there will be no radio hole. It can be seen then that a typical elevated layer will have little effect until the transmitter is nearly at layer height. For the same layer, with the radar 80 feet above the layer, a radio hole would exist at radar height between 22 and 60 miles from the transmitter.

The ray tracing expressions discussed above, are theoretically valid only when the layer is smooth and has a uniform N-profile over a large horizontal area surrounding the transmitter. Even though actual elevated layers rarely are as smooth as the mathematical model requires, the results of many experimental flights above and below such layers give results as indicated by Doherty [11], which are in surprisingly good agreement with theory. Field strengths in radio holes are found to be considerably lower than outside them, and the distances to the boundaries agree very well with those calculated from ray theory and measured N-profiles.

In certain geographical areas, strong subsidence of dry air from aloft gives rise to intense elevated inversions (layers) with ΔN's of the order of 40-60 units and heights of less than 3,000 feet. These areas are near 30°N. (and S.) latitude in those belts where atmospheric subsidence is strongest. In the Northern Hemisphere, the areas of occurrence of the strongest elevated inversion (layers) are located where the 30°N. latitude belt intersects the west coasts of large continents; namely, southern California, northern Mexico, and Morocco. Little data is available for the Southern Hemisphere, although such evidence as

exists indicates that similar areas will be found on the west coasts of the continents in that hemisphere as well. Ducts of this intensity are frequently able to trap energy from surface radar and also at communication wavelengths.

In layers where ΔN_L is large, causing the total refraction of rays with relatively large α_o's, the roughness of the layer becomes a very important factor in feeding energy into the radio holes. In experimental studies off southern California, it has been found that in such situations, the field strength in the radio hole is weaker than it is above or below the hole, but it is stronger than when no layer is present. This comes about because of the Rayleigh criterion of roughness, as follows:

$$h = \lambda/8 \sin \alpha_o \ , \tag{5.4}$$

where h is the permissible height of random roughness elements for a reflecting surface to appear smooth at wavelength λ and with the incident angle equal to α_o.

Suppose, for example, that a layer has the following characteristics:

$$\Delta N = 50 \ ,$$

and

$$\Delta h = 200 \text{ feet} \ .$$

We find that total refraction will occur for α_o as large as 9.3 milliradians. In this case, the roughness elements must be less than 13 wavelengths in height for the layer to appear smooth. On the other hand, if ΔN is 10 units, as it was in our previous layer, α_o can only be as large as 2.4 milliradians, giving a permissible roughness element height of 53 wavelengths. From this, it is evident that a strong elevated layer, which is capable of trapping energy incident at rather large angles, must also be much smoother than is usually found in nature in order to give a well defined radio hole. Weaker layers, which require small ray angles for radio holes to form, can be relatively much rougher and still produce well defined holes.

5.2 Ray Bending

The previous section considered the behavior of rays in the pres-

ence of steep N-gradients. Of primary concern were those rays which were bent sufficiently to emerge tangent to the top of the layer. Now we wish to consider situations where the bending is not so drastic. It should be realized, of course, that such bending occurs in any atmosphere where N changes with height. If N decreases with height, as it does over the earth, the rays are bent downward. As was seen in section 2.3.4, this bending, τ, at any point along the ray trajectory is proportional to the N-gradient normal to the ray path.

In order to determine τ exactly, one must know how N varies with height. In general this relationship cannot be expressed in simple analytical form. Furthermore, the N-profile changes from place to place and from time to time. In practice, it is more satisfactory to approximate a given N-profile by a series of straight lines and then to determine the incremental bending caused by each segment. The total bending up to a given height is simply the sum of the individual increments up to that height. This procedure is particularly suited to N-profiles derived from radiosonde data, since significant levels are originally specified using linear interpolation between levels to recover the original trace.

Using this approach, one may express the incremental bending $\Delta\tau$ caused by a layer with constant N-gradient as,

$$\Delta\tau \text{ (milliradians)} = \frac{(N_B - N_T)}{500\,(\tan\beta_B + \tan\beta_T)}, \qquad (5.5)$$

where the subscript B refers to the bottom of the layer and T refers to the top of the layer (see fig. 2.6). The values of tan β are determined at each level in terms of α_o, $N_s - N_h$, and h, using Snell's Law. Figure 5.5 gives values of 500 tan β in terms of these parameters.

5.2.1 Elevation Angle Errors

In tracking targets with radars capable of measuring elevation angles very accurately one is more interested in correcting the apparent elevation angle, α_o, to the true angle, than in the value of τ itself. Figure 2.6, shows this correction or error angle, δ. If one knows the total bending, τ_t, between radar height and target height, h_t, then,

$$\delta_t \text{ (milliradians)} = \frac{\tau_t \tan\beta_t + \left(\frac{\tau_t^2}{2}\right) - (N_s - N_t)}{\tau_t + \tan\beta_t - \tan\alpha_o}. \qquad (5.6)$$

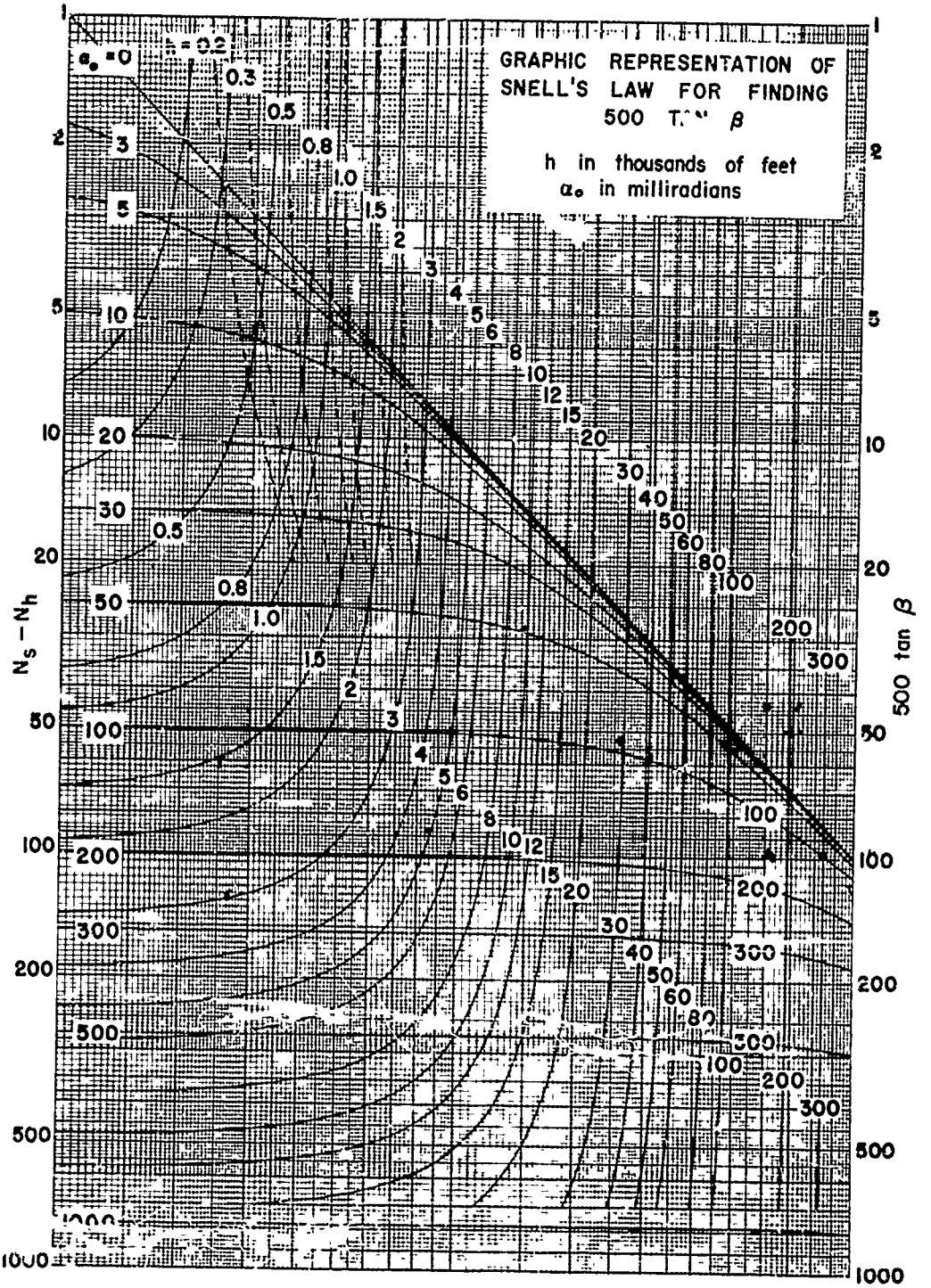

Figure 5.5. Graphical Representation of Snell's Law.

For low target heights, where the atmosphere may be regarded as a single layer of constant N-gradient, $\underline{\delta}$ is exactly half of $\underline{\tau}$. At great heights $\underline{\delta}$ approaches the value of $\underline{\tau}$. These two limits are frequently useful in estimating $\underline{\delta}$'s without the necessity of carrying out detailed computations.

Figure 5.6 shows curves of both $\underline{\tau}$ and $\underline{\delta}$ for various $\underline{\alpha_o}$'s, over a height range of 1,000 to 1,000,000 feet. These values were computed assuming $N_s = 350$, and an N-profile as shown in figure 3.5. It can be seen that a ray departing tangentially from the earth ($\alpha_o = 0°$) is bent almost 1° in traversing the entire troposphere. At an elevation angle of 30°, the tropospheric bending amounts of 2' of arc. It is obvious that the bending falls off rapidly as the elevation angle increases. Even at 1°, the bending is only two-thirds of the tangential value, and at 5° it is one-fourth of the tangential value. It is interesting to note that at low angles, most of the bending takes place at low altitudes, while at higher angles, the contributions at greater heights are relatively more important. To a first order of approximation, one may regard total bending as proportional to $\underline{N_s}$; this is quite true at angles above 10°. At very low angles, $\underline{\tau}$ varies more rapidly with respect to $\underline{N_s}$, but the linear approximation is still reasonably good.

The values shown in figure 5.6 refer to a standard atmosphere, with an exponential decrease of $\underline{N}$ with height. When layers exist which have steeper N-gradients, additional bending will occur. Layers close to the surface are much more effective in increasing $\underline{\tau}$ and $\underline{\delta}$ than are those at heights of several thousand feet. The additional bending caused by such layers is confined largely to the lowest few degrees. Above 5°, even a trapping layer will cause no additional bending. This is because the distance the ray travels in the layer falls off rapidly with increasing elevation angle. The bending caused by any given profile of refractive index may be computed as a function of the ray elevation angle $\underline{\alpha_o}$ at the radar, using the method described above. The additional $\underline{\delta}$ caused by several typical layers is discussed in section 6.2.2 and is shown in figure 6.11.

It should be pointed out that the above discussion of radio ray bending has been confined to refraction caused by the troposphere. When the radar target is in or above the ionosphere (heights above 100 miles), additional bending is caused by ionospheric layers. Total bending by the ionosphere is roughly equal to the tropospheric contribution at 100 megacycles ($\lambda = 3$ meters). At shorter wavelengths the ionospheric

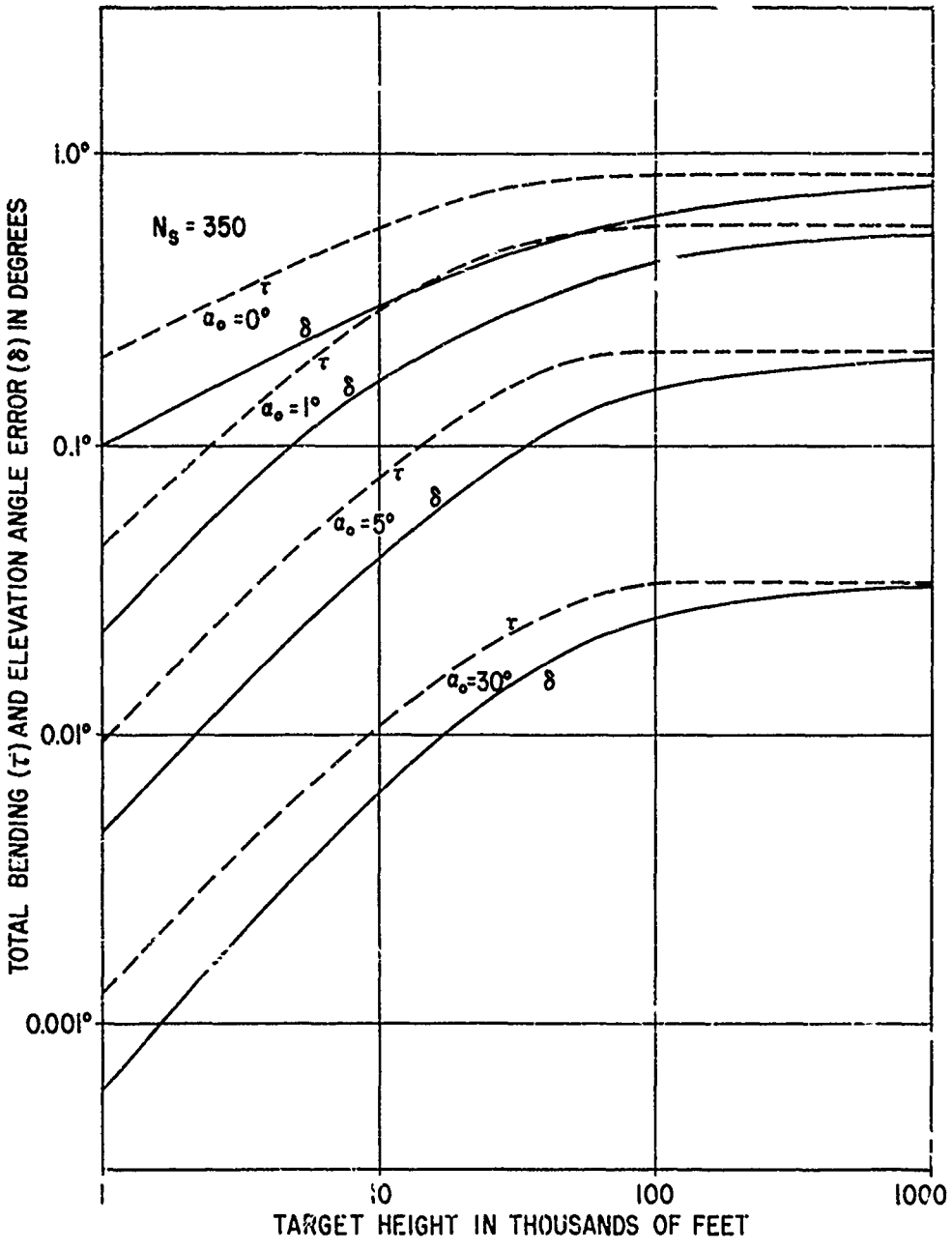

Figure 5.6. Total Bending and Elevation Angle Error for a Standard Atmosphere.

bending decreases as the square of wavelength.

5.2.2 Range Errors

Because radar waves travel slower in the atmosphere than in a vacuum and since radar range calibrations are made using the vacuum velocity as a reference, measured ranges are slightly larger than actual. These range errors are for most purposes entirely negligible. A method for determining range errors is given, however, in section 6.2.3.

PART III

THE COMPUTATION OF ATMOSPHERIC REFRACTIVE EFFECTS ON RADIO-RADAR PERFORMANCE

6. RADAR PERFORMANCE

In parts I and II of this manual the various mechanisms were discussed by which radar or radio energy is propagated from a transmitter to a distant point in space. Also considered were the several ways in which meteorological variables affect these propagation mechanisms. It was seen that relatively simple ray-tracing concepts are useful in describing the behavior of radio energy in various situations. In this chapter, these concepts are put to practical use in order to solve the operational problem of determining the variations in radar performance caused by meteorological variables.

6.1 Surface-to-Surface Situations

6.1.1 "Normal" Detection

A surface radar, such as those on ships or low shore installations, normally is limited to detecting targets above the horizon line (see fig. 4.1). Its antenna pattern is characterized by interference maxima and minima as shown in figure 6.1. Inside the fingers the fields are above the free space fields, because the direct and reflected waves reinforce one another, and in the regions between fingers the fields are less than free space fields, because the two waves partially cancel one another. For low radar heights, the vertical angles of the center lines of maximum strength are given by

$$\alpha_{max.}(\text{milliradians}) = (n - \tfrac{1}{2}) \frac{1{,}000\ \lambda}{2h_R} , \qquad (6.1)$$

where n is 1, 2, 3, etc., h_R is the radar height, and λ is the wavelength, both expressed in the same units. Thus, for a radar height of 60 meters and a wavelength of 0.5 meters, the interference maxima will occur at 2.5, 7.5, 12.5, etc., milliradians. The minima occur at 5, 10, 15, etc., milliradians. The range at which the tips of the fingers occur is taken arbitrarily as the maximum detection range of the radar; this range depends, of course, on transmitted power, size of target, and other factors not related to propagation itself.

It is evident that surface targets will not be detected unless they are high enough to protrude into the lowest maximum of the pattern. This will occur under normal atmospheric conditions at, or just beyond,

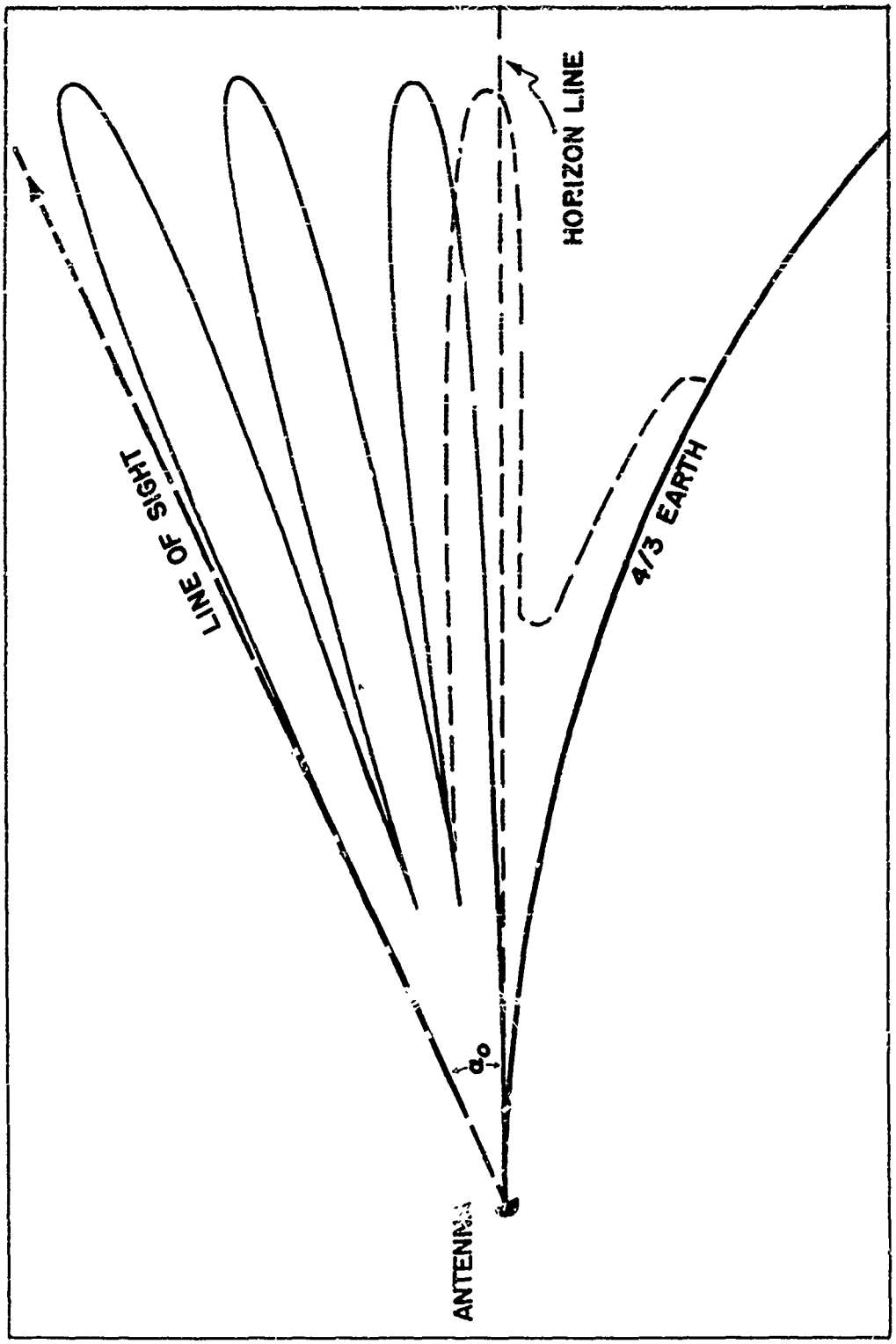

Figure 6.1. Vertical Coverage Pattern--Surface Radar.

the horizon range for most shipboard radar installations and most surface targets. Other things being equal, a short-wavelength radar will detect surface targets farther away because its lowest interference lobe lies closer to the horizon than that of a longer-wavelength radar. In the presence of strong surface or elevated ducts, the lower finger of the pattern may be bent downward considerably as shown by the dashed pattern in figure 6.1. The lower side of the bottom finger extends well beyond the horizon in this case.

6.1.2 Evaporation Ducts (Surface)

Evaporation or "oceanic" ducts are not particularly effective in extending the coverage of most shipboard radars because they are usually shallow (75 ft. is about average). In order for such a duct to be effective, the radar must be within 50 feet of the sea surface and its wavelength must be shorter than 30 centimeters. Submarine radars of 3-centimeter (X-band) and 10-centimeter (S-band) wavelengths as well as similar radars on small craft are the only ones which are usually affected by the evaporation duct. The normal practice of installing radars on the highest point on the ship places most radars above evaporation ducts which may be present. For low-sited radars, however, the duct is often useful in extending the normal limit of coverage. It turns out that one can determine, from simple meteorological data, whether such a radar at a particular wavelength will have extended coverage or not.

The Ductogram, figure 6.2, was designed at Bureau of Aeronautics Project AROWA [25] to facilitate the prediction of extended radar coverage associated with an oceanic (evaporation) duct. Use of the Ductogram is limited to low-level oceanic ducts. For input data, the Ductogram utilizes surface observations of air, dew point, and sea water temperatures taken onboard the ship. The quantity $\Delta N'$ is the approximate difference between the refractivity, N, at the elevation of shipboard observation (bridge height) and the refractivity, N_S, at the water surface.

In an air mass which has stagnated over an ocean surface for some time, the values of N at observation height (determined from air and dew point temperature) and N_S at the ocean surface (determined from the sea water temperature) normally do not differ by more than one or two units. However, when the meteorological conditions favor extended surface radar propagation, the gradient of N may reach much

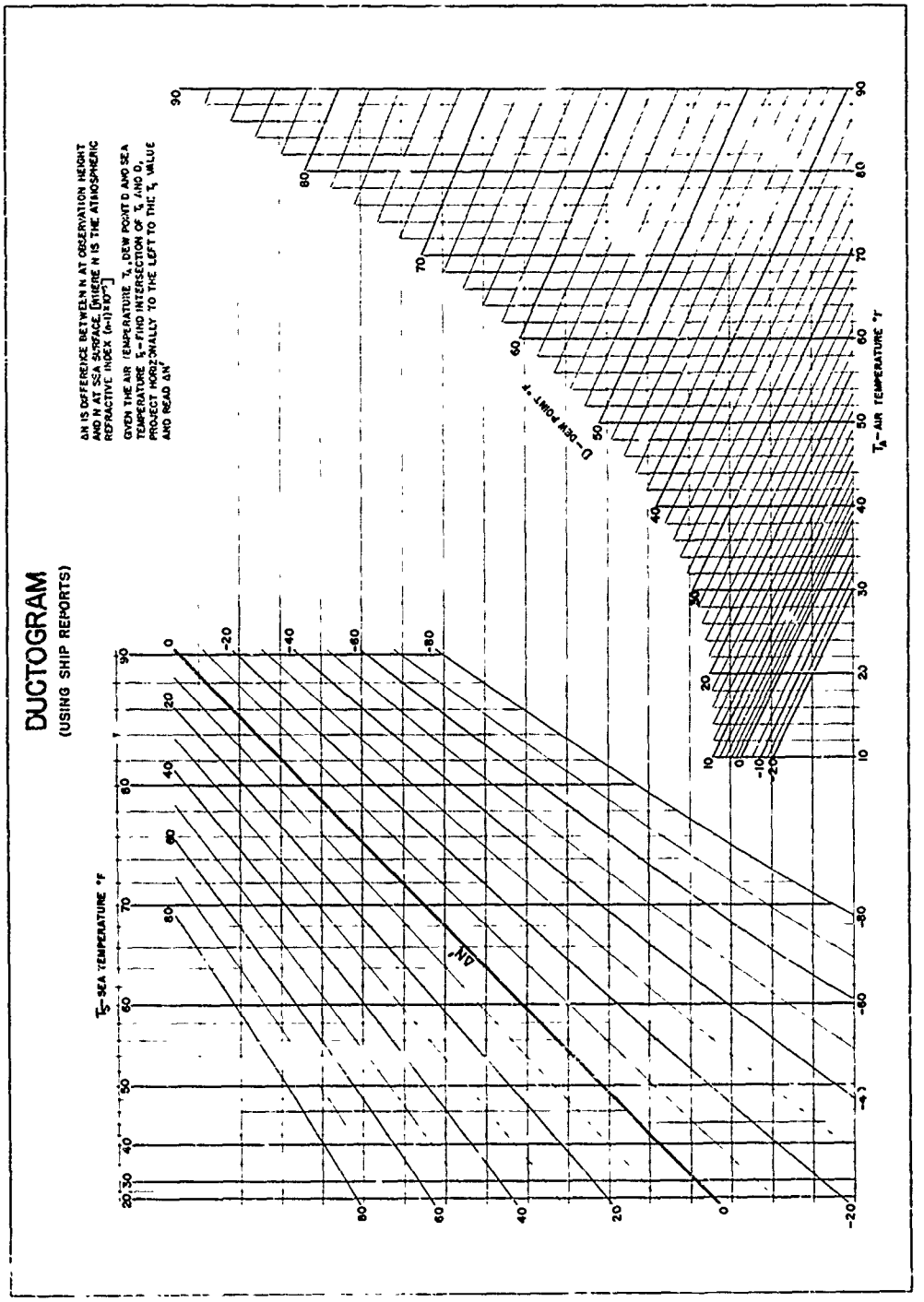

Figure 6.2. Ductogram.

larger values and is especially pronounced in the lowest few feet of the atmosphere. Thus, when $\Delta N'$ is large, the gradient of N for a depth of several hundreds of feet will also be large. For this reason, $\Delta N'$ is introduced as a parameter to be used in estimating the presence of an oceanic duct. The magnitude of $\Delta N'$ necessary for extended radar ranges varies with the wavelength of the radar, ranging from 67 units for the L-band, to 36 for the S-band, and 16 for the X-band. For longer wavelengths, such as the P-band (100-500 m), the oceanic duct will be ineffective, and one must use the methods presented in the following section to determine whether trapping will occur. Since air turbulence affects the gradients of temperature and moisture throughout the layer in which surface ducting occurs, the surface wind velocity is introduced as a factor in the prediction of surface ducting.

The procedure to be used with the Ductogram is as follows: given the air temperature, the dew point, and the sea water temperature (all in °F.), find the intersection of the pertinent air temperature and dew point lines and project horizontally to the left to the given sea water temperature. Read the resulting $\Delta N'$-value from the sloping lines at the point. Then, refer to figures 6.3, 6.4, and 6.5, to obtain the minimum $\Delta N'$-value required for ducting as a function of radar wavelength, surface windspeed, and the air-water temperature difference (in °C.).

Although the vertical extent of an oceanic duct may be estimated from local observations, it should be pointed out that the horizontal space distribution of refractive conditions must be analyzed from a number of ship observations or from a consideration of the synoptic situation (see part IV). Unless ducting conditions are expected to prevail over a large horizontal area, extended ranges should not be predicted. In those instances when ducting is indicated, the amount of range extension cannot be accurately computed. However, one may safely estimate that radar coverage will be extended to at least double the normal range. For particularly favorable conditions (strong duct, low antenna, short wavelength) the range may be extended as much as five times normal.

6.1.3 Advection Ducts (Surface)

As was discussed in section 5.1.1, ducts may occur when warm, dry air flows out over a cool sea. They do not extend more than 100 miles or so from land unless there is a strong advection wind carrying the air offshore. Usually these ducts are found over seas lying close

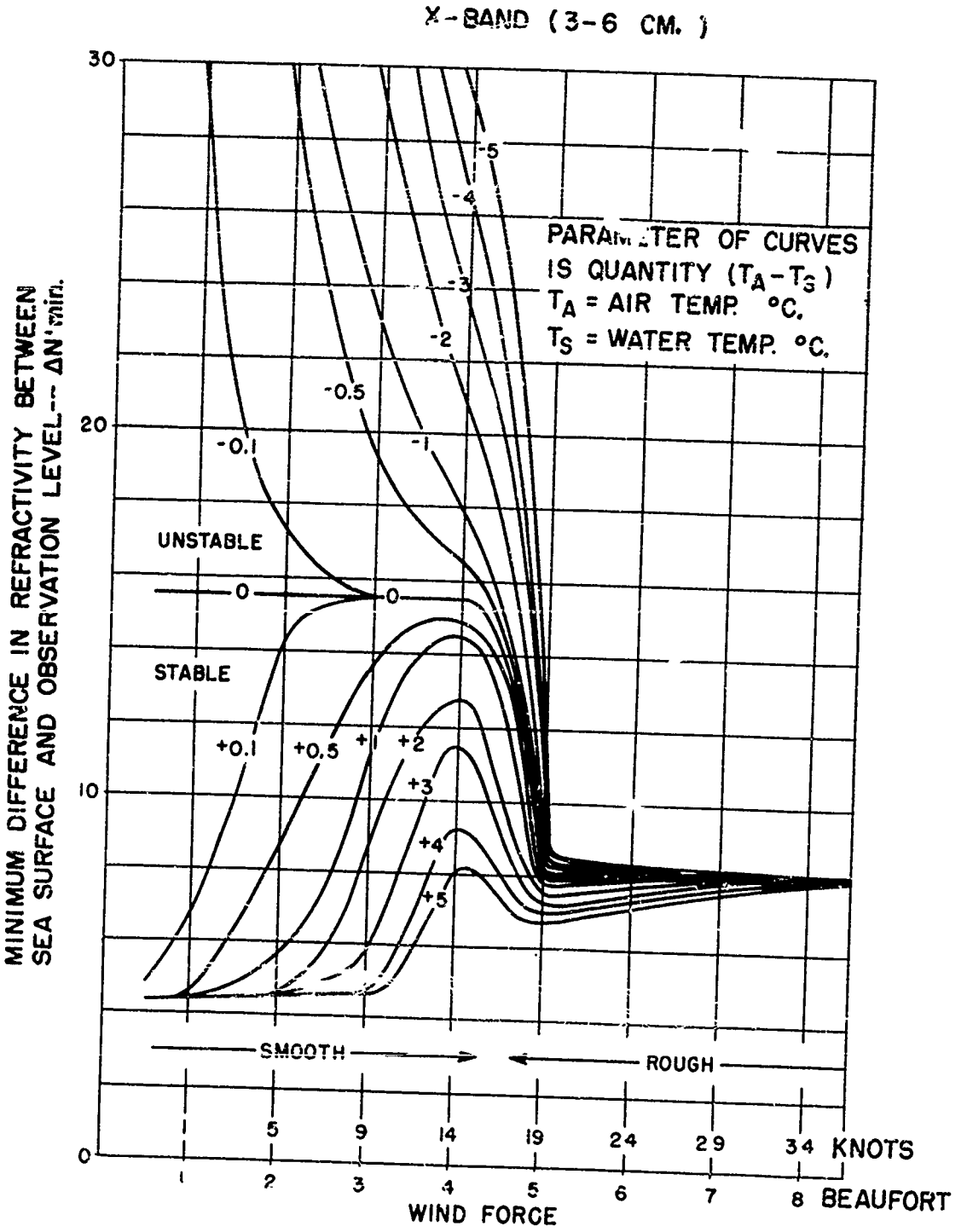

Figure 6.3. X-Band Trapping Criteria--Oceanic Duct.

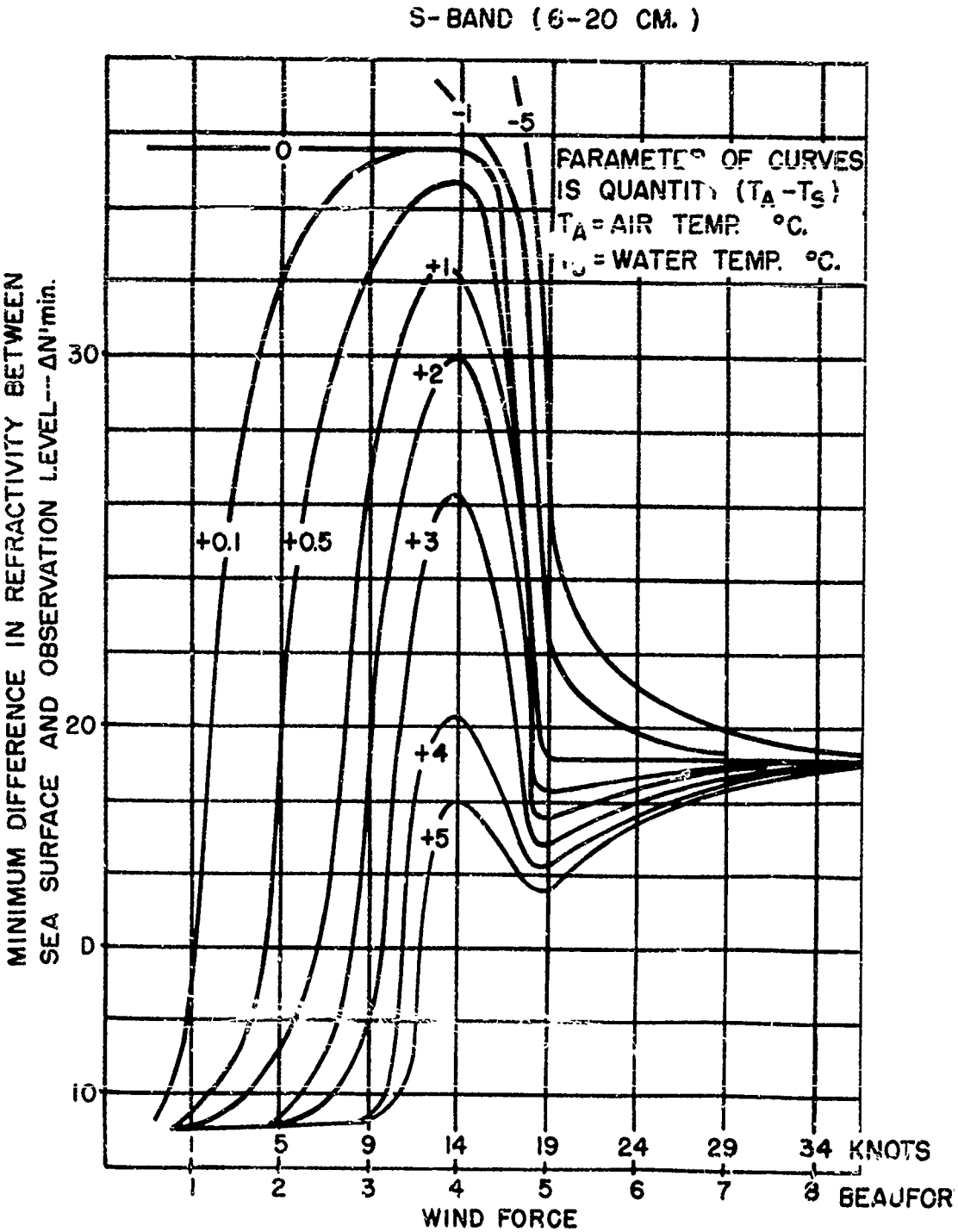

Figure 6.4. S-Band Trapping Criteria--Oceanic Duct.

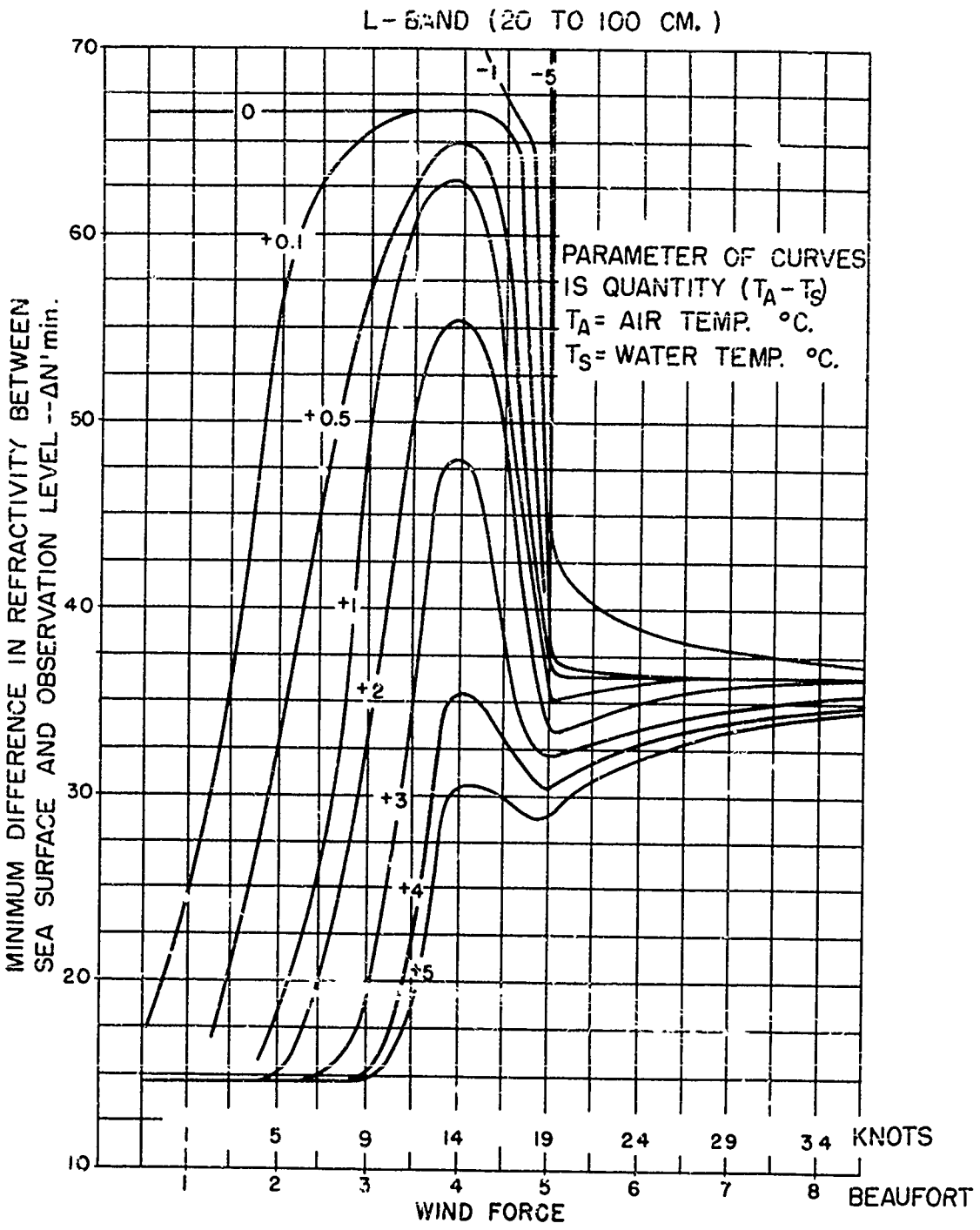

Figure 6.5. L-Band Trapping Criteria--Oceanic Duct.

to desert areas, such as in the Mediterranean, Red Sea, Gulf of Arabia, and similar areas. To assess their effects on propagation, one needs shipboard radiosonde or other data from which to plot an N-profile to heights of 500 feet or more. In order to determine whether the duct is capable of trapping energy of a particular wavelength (and hence whether extended radar coverage may be expected), the N-profile is plotted and the height of the layer top, h_T, and ΔN_L for the layer are determined as shown in figure 6.6. Using the criterion curves in figure 6.7, one can determine whether a particular wavelength will be trapped. If a point corresponding to the measured h_T and ΔN_L lies to the right of the curve corresponding to the radar frequency in question, the duct will trap the emitted energy and give extended range coverage. The farther to the right of the curve the point lies, the greater will be the radar coverage extension.

The difference between the trapping criteria presented in figure 6.7 and those given in figures 6.3, 6.4, and 6.5 lies in the fact that figure 6.7 is applicable to any duct, but one must have an N-profile to de-

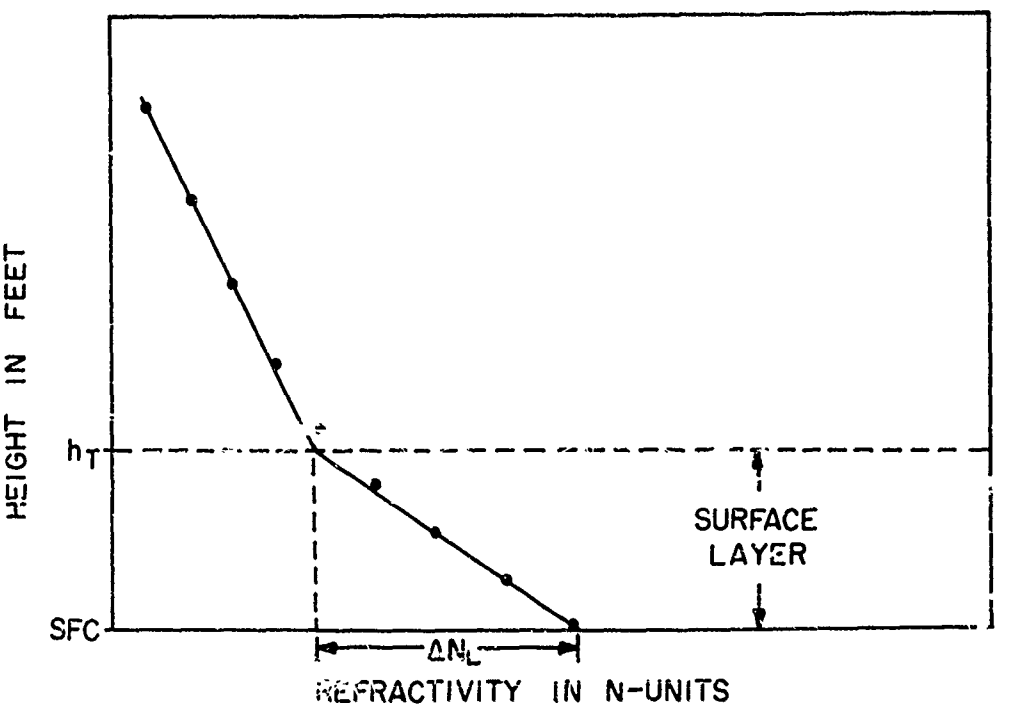

Figure 6.6. N-Profile--Surface Layer.

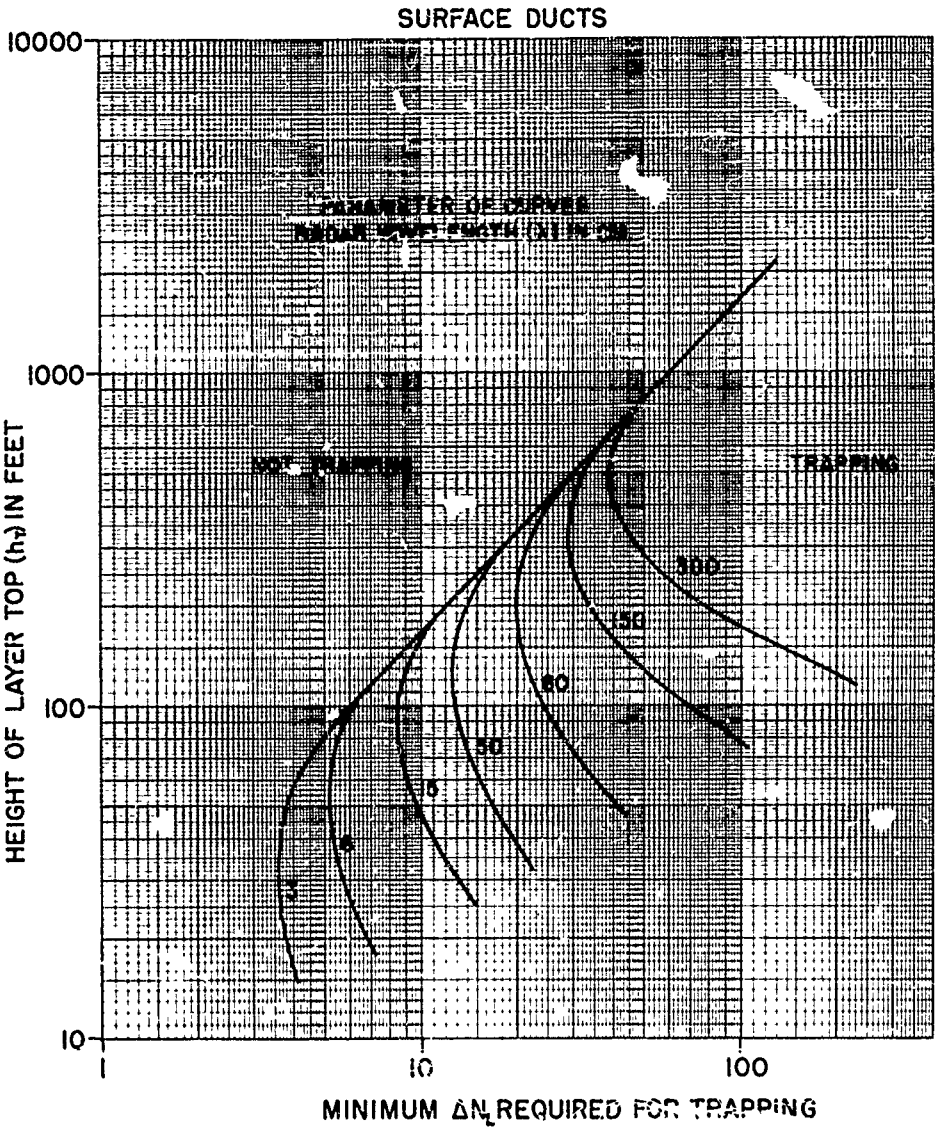

Figure 6.7. Trapping Criteria for Surface and Elevated Layers.

termine whether or not a given wavelength will be trapped. In figures 6.3, 6.4, and 6.5, on the other hand, one needs only N-values at the sea surface and at bridge height. From these two values, one can deduce the N-profile if it is assumed that the air has been over the sea a long enough time for equilibrium to have been established. In general, the criteria shown in figures 6.3, 6.4, and 6.5 are applicable far from land, while those in figure 6.7 are applicable anywhere. No comprehensive comparison between the two methods is yet available.

6.1.4 Elevated Ducts

One may use a similar procedure for analyzing the effect of elevated ducts on radar performance. In this case, plot an N-profile as before; figure 6.8 illustrates an elevated duct. Figure 6.7 may again be used as the trapping criterion if one plots the point corresponding to the height of the layer top divided by two, $(\frac{h_T}{2})$ and ΔN_L for the layer. If the point lies to the right of the radar frequency curve in question, trapping will occur and radar coverage will be extended. As in the case

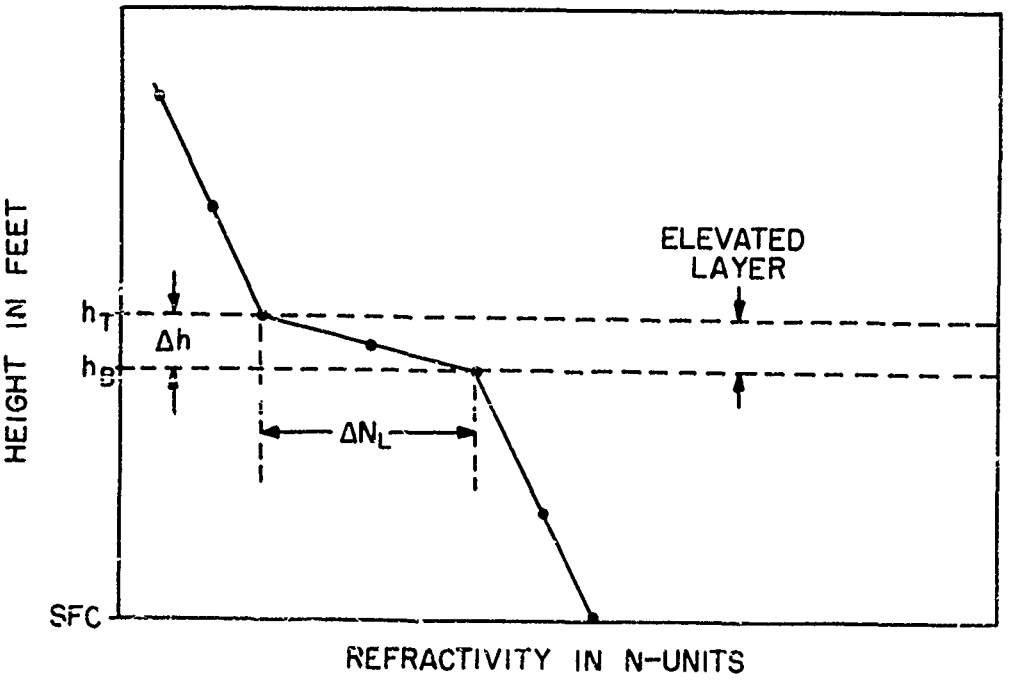

Figure 6.8. N-Profile--Elevated Layer.

of evaporation and advection ducts, one cannot accurately predict the extent of anomalous coverage, but only whether or not it will occur. With experience one may estimate whether there will be a large extension (up to 5 times normal range) or a moderate one (twice normal) according to how far the plotted point lies to the right of the pertinent radar frequency curve.

The criteria curves shown in figure 6.7 are based on a theoretical treatment of the guiding of radio-radar energy by ducts. Numerous attempts have been made to treat the problem theoretically, but this particular method, by S. A. Schelkunoff of Bell Telephone Laboratories [18], has been the only one to successfully stand the test of experimental verification.

6.2 Surface-to-Air and Air-to-Surface Situations

In the previous discussion it was noted that various types of N-profiles with strong gradients could channel radar energy near the surface and thus illuminate targets which were well below the horizon line. The propagation effects of refractive layers when one terminal is well above the ground are considerably different from those when both terminals are low. In principle, the coverage pattern of a surface radar looking at a high-flying target, should be the same as that of an airborne radar looking at surface targets. One significant difference, however, is that in the air-to-surface situation "sea clutter" complicates detection, particularly of small surface targets.

6.2.1 Sea Clutter

The myriad of echoes frequently observed by airborne radars looking over a sea surface is called "sea clutter" or "scope clutter". Its effect is to increase the background of echoes against which one must detect the surface target, and, in the case of small targets such as submarine snorkels and small craft, it can seriously interfere with detection. Sea clutter is caused by reflection from individual waves. As one would expect, it is worse in heavy seas than in calm ones, and the echoes are stronger for shorter wavelengths than for longer ones. Furthermore, the echo intensity increases as the cube of the angle of incidence. Thus, clutter echoes extend from the sea surface directly under the aircraft out to some distance, as given in figure 6.9, depending upon the altitude of the aircraft and the sea state. The presence of strong N-gradients has little effect on the extent of the clutter echoes.

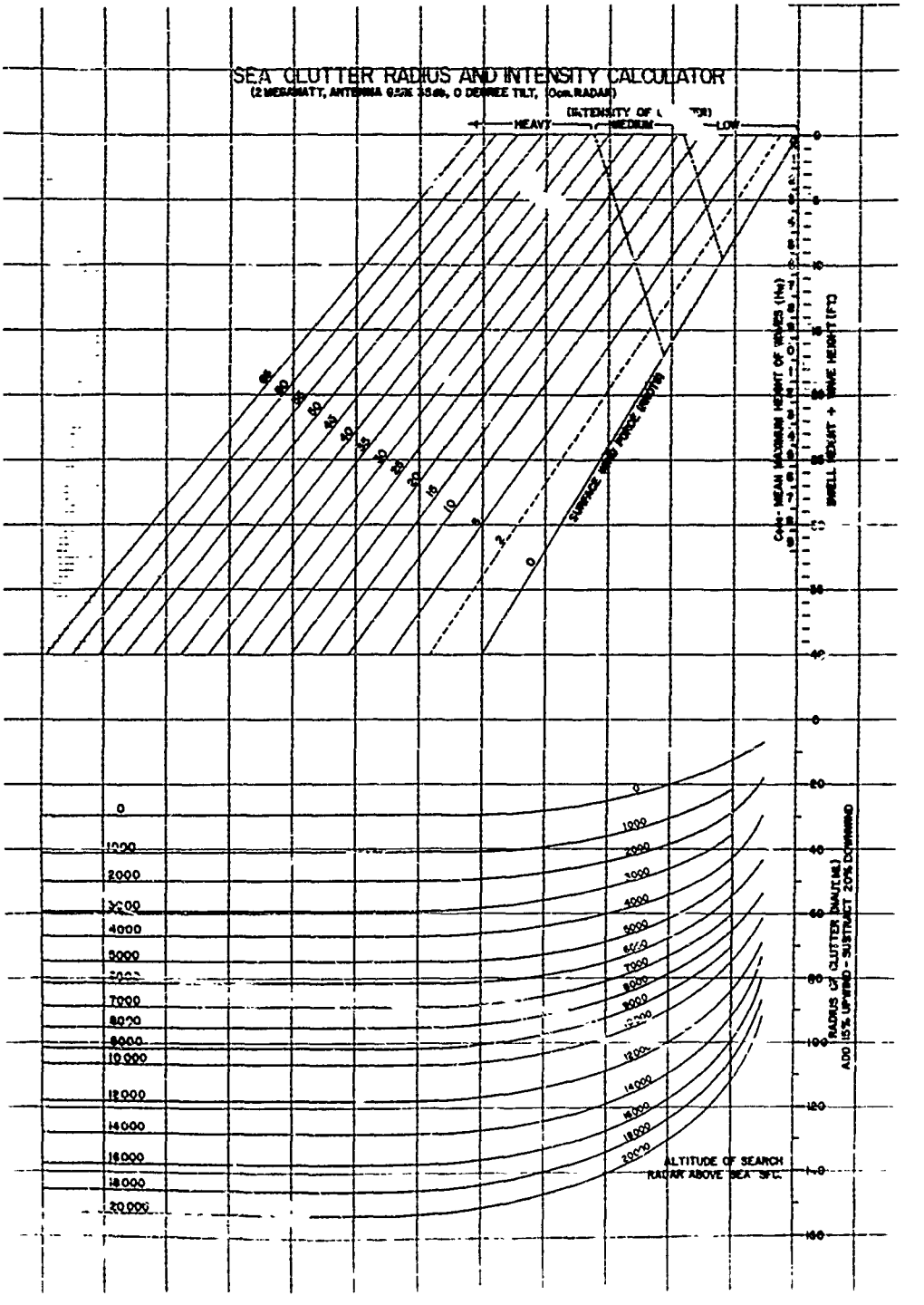

Figure 6.9. Graph for Estimating the Radius and Intensity of Sea Clutter.

Figure 6.9 was adapted from a chart originally produced by Lockheed Aircraft Company [23]. It was modified to its present form, on the basis of in-flight sea-clutter data, by personnel of the U. S. Fleet Weather Central, Argentia [24]. To use the figure:

1. Enter at upper right with swell height plus wave height in feet, or with the coded value of H_W, mean maximum height of waves.

2. Proceed horizontally to the appropriate surface wind speed line in knots.

3. Proceed vertically down to the appropriate aircraft altitude curve.

4. Read the sea clutter radius on the scale at lower right in nautical miles.

For example, suppose the wave height plus swell height is 8 feet and the surface wind is 10 knots:

> If the aircraft is at 5,000 feet, R (the radius of clutter) = 64 miles.
> If the aircraft is at 10,000 feet, R (the radius of clutter) = 93 miles.
> If the aircraft is at 20,000 feet, R (the radius of clutter) = 134 miles.

Because of the effect of wave shape on the reflected energy, one should add 15 percent to the clutter radius in the upwind area and subtract 20 percent in the downwind area.

As stated on the chart, the values given are for a 2 megawatt, 10-centimeter radar having an antenna gain of 35 decibels. To obtain clutter ranges for other wavelengths multiply the indicated ranges by

$$\left[\frac{10}{\lambda\ (\text{cm.})}\right]^{3/2} ;$$

for other radar powers multiply the indicated ranges by

$$\left[\frac{P\ (\text{mw.})}{2}\right]^{1/3} ;$$

and for other antenna gains multiply the indicated ranges by the antilog of $\{0.067\ [G\ (db) - 35]\}$.

6.2.2 Elevation Angle Error

An important problem encountered in surface, air search radar operation is that of elevation angle error. The standard N-profile causes radar rays to bend downward as they travel through the troposphere. The total ray bending along the tangent line amounts to about 3/4° as the ray proceeds from the surface up through the stratosphere. About 90 percent of this bending takes place between the surface and 30,000 feet; as a result an air-search radar capable of measuring precise elevation angles will always indicate higher elevation angles than the true ones.

The elevation angle error, $\underline{\delta}$, is a function of the measured elevation angle, $\underline{\alpha_o}$, the N-profile and the target height, $\underline{h_t}$. Standard atmosphere corrections can be made to take average bending into account (see fig. 5.6). In the presence of layers where the N-gradient is stronger than standard, however, the bending error can be increased considerably. If one has a refractivity profile, the radar elevation angle error may be determined quite accurately, according to Weisbrod and Anderson [26], in the following way:

1. Subtract all N-values (computed from radiosonde data) from the refractivity at the surface (radar height), $\underline{N_s}$. Tabulate the resulting $N_s - N_h$ values for each height, $\underline{h}$, above the radar.

2. Using figure 5.5, determine 500 tan β at each height. This is done by entering the left margin of the figure with the proper $N_s - N_h$. Next, move horizontally to the curve corresponding to the height, $\underline{h}$, which is expressed in thousands of feet. Now, proceed vertically to the curve corresponding to the measured elevation angle, $\underline{\alpha_o}$, which is expressed in milliradians. Finally, read 500 tan β by moving horizontally to the right-hand scale. This is a graphical solution of Snell's Law (see section 3.2). Occasionally, $N_s - N_h$ will be negative; in this case enter the left margin with $N_s - N_h$ and use the dashed height curves, proceeding as above to determine 500 tan β.

3. By dividing the atmosphere into layers whose boundaries are the radiosonde heights tabulated above, the ray bending $\Delta\tau$ caused by each layer can now be determined from the expression

$$\Delta\tau \text{ (milliradians)} = \frac{\Delta N_L}{500 \tan \beta_T + 500 \tan \beta_T} ,$$

where 500 tan β_B is the value tabulated at the lower boundary of a given layer and 500 tan β_T is the value tabulated for the next higher level; ΔN_L is equal to N at the bottom of the layer minus N at the top of the layer. For each consecutive pair of heights one gets a value of $\Delta\tau$ in milliradians.

4. Add the $\Delta\tau$ s from the radar height (surface) to the target height, h_t. The sum is τ_t in milliradians.

5. Compute δ corresponding to the assumed α_o and target height, h_t, by

$$\delta \text{ (milliradians)} = \frac{1000\,\tau_t \tan \beta_t - (N_s - N_t) \times 10^{-3} + \frac{\tau_t^2}{2}}{\tau_t + 1000 \tan \beta_t - 1000 \tan \alpha_o}, \quad (6.2)$$

where N_t is the refractivity at target height and 1,000 tan β_t is twice the value of 500 tan β at target height.

6. This will give a value of δ corresponding to the assumed α_o and target height. It must be repeated from step 2 on for other α_o's and target heights to cover a useful range of conditions

The procedure outlined above is straightforward though tedious. It is, however, quite exact, and is the simplest way (short of using an electronic computer) for determining δ from radiosonde data.

One can, however, estimate the values of δ to be expected under conditions reasonably close to the standard atmosphere by using figure 6.10. The values shown are for an N_s of 350. To convert to other values of surface refractivity, multiply the indicated elevation angle errors by $\frac{N_s}{350}$. The presence of refractive layers can cause significant

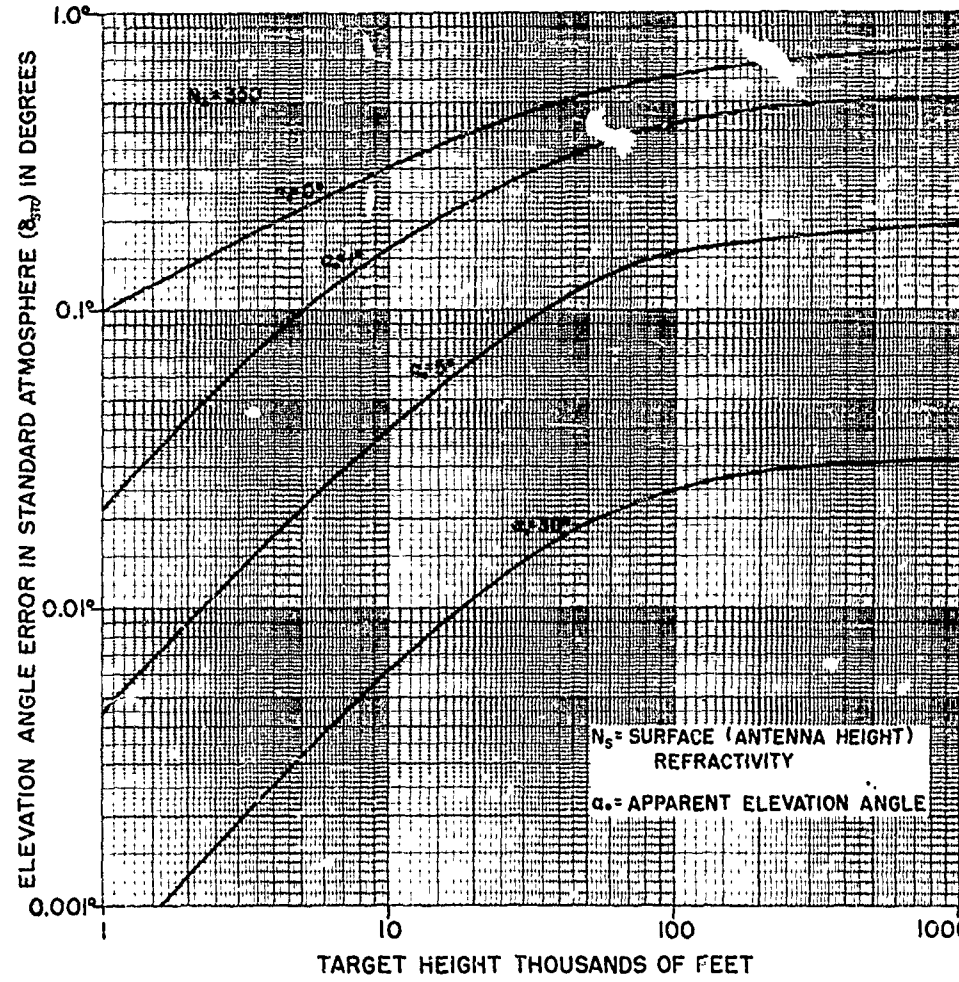

Figure 6.10. Elevation Angle Error in a Standard Atmosphere; N_S = 350.

departures from these values, particularly at low elevation angles. In figure 6.11, the differences between the elevation angle error under layered and standard-atmosphere conditions, $\delta_{layered}$ minus $\delta_{standard}$, are shown for several types of refractive layers. To estimate refraction effects then, one adds the values obtained from figure 6.11 to those found in figure 6.10 to obtain values of the total elevation angle error.

6.2.3 Range Error

Because radar waves in the atmosphere travel slower than they do in a vacuum, a range error results. Since radar range calibrations are made using the vacuum velocity as a reference, the measured ranges are always slightly larger than the actual. The resulting error, ΔR, is usually too negligible to be considered in practical air search operations. It amounts to approximately 700 feet for the round trip to a target above the stratosphere with $\alpha_o = 0$. Figure 6.12 shows the one-way range error as a function of measured range, R, for several α_o's and assuming N_s is 350. For other N_s's one may assume that ΔR is proportional to N_s with sufficient accuracy for most practical purposes. The effect of strong N-gradients on range error is at most a few percent of the values shown in figure 6.12 so it can safely be ignored.

6.2.4 Radar Holes

The occurrence of radar holes or blind spots in a surface, air-search radar coverage pattern is infrequent. It was noted in section 5.1.2, that intense elevated layers cause such holes but that the fields in them are stronger than when the layer is absent, so they do not reduce radar coverage. Weak elevated layers are incapable of causing surface radar holes unless they are just a few hundred feet above the radar. Surface ducts caused by advection, however, can cause surface, air-search radar holes. The ray tracing results for this case also apply to low, weak elevated layers. In both cases, the radar is below the top of the layer. The near edge of the radar hole will be located at the top of the layer at the distance

$$d = h_T \sqrt{\frac{2}{\Delta N_L - 0.048\, h_T}}, \qquad (6.3)$$

where h_i is the height of the top of the layer above the surface and ΔN_L is equal to N at the surface minus N at the top of the layer, $N_S - N_T$. It can be seen that unless the N-gradient between the radar antenna

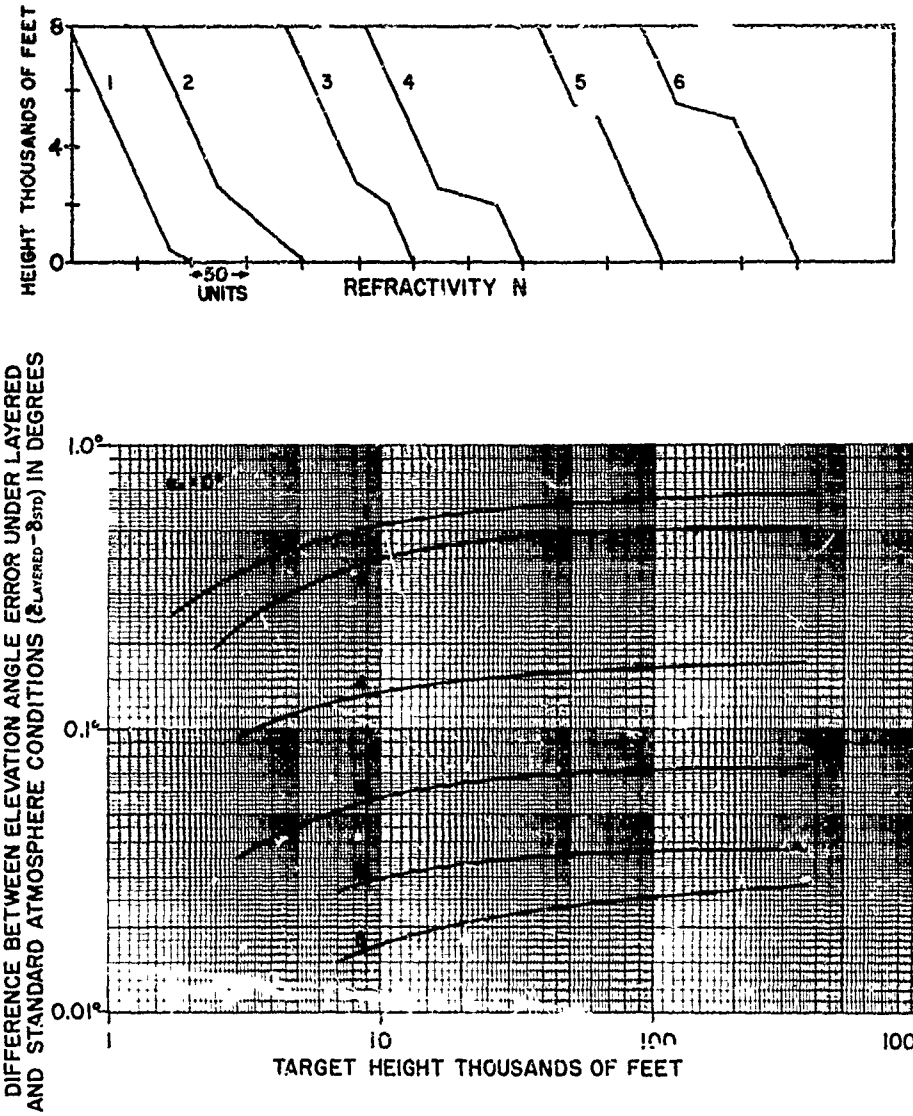

Figure 6.11. Excess Elevation Angle Error Due to Layers; $\alpha_o = 0°$.

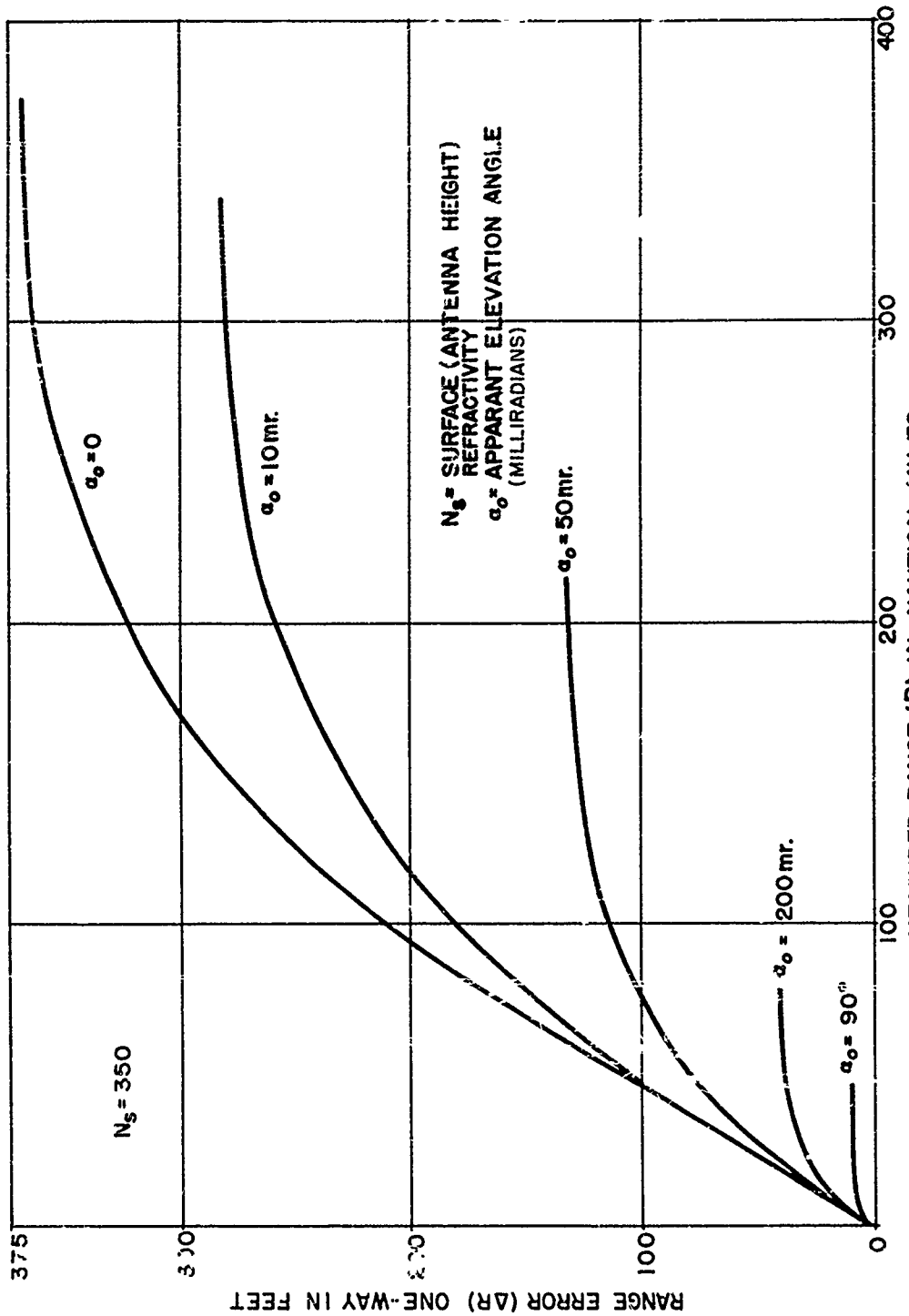

Figure 6.12. Range Error in a Standard Atmosphere; N_S = 350.

height (surface) and the top of the layer is greater than 48 units per 1,000 feet, d will be imaginary and no radar hole will be present. The same expression applies to evaporation ducts, although in this case ΔN_L as defined above will almost never be large enough to give a radar hole.

6.2.5 Summary

The general effects of refractive layers on surface-to-air (and air-to-surface) radar performance are summarized following:

1. In air-to-surface situations the presence of "sea clutter", which is produced by reflections from individual waves, may seriously interfere with the detection of small surface targets.

2. Actual ray bending may be considerably in excess of standard-atmosphere bending. This will cause radar elevation angle errors on the order of a large fraction of a degree.

3. Range errors, which can be as great as 700 feet over a range of 200 miles in a standard atmosphere, are not significantly changed by the occurrence of strong N-gradients.

4. Radar holes or blind spots in the radar coverage pattern are rarely observed in surface-to-air situations, but may occur occasionally in the case of advection ducts.

6.3 Air-to-Air Situations

Since both the radar and the target are usually well above the sea surface, evaporation and advection layers have little, if any effect, on radar performance in this instance. Such layers are too far below the line of sight to affect propagation, and even when the line of sight grazes the horizon, they have little effect for the reasons discussed in the preceeding paragraph.

6.3.1 Radar Holes

Elevated layers, on the other hand, can be quite effective in causing

radar holes. It was shown in chanter 5, that radar rays can be totally refracted when the radar is below the layer, thereby causing a region into which little energy can penetrate.

(a) Location of Holes (Radar Below Layer)

The distances, $\underline{R}'$ and $\underline{R}''$, from the radar to the near edge and to the far edge of the radar hole, respectively (at the top of the layer) can be expressed in terms of the refractivities $\underline{N}_R$, $\underline{N}_B$, and $\underline{N}_T$ at the radar, layer base, and layer top, respectively, together with the three corresponding heights $\underline{h}_R$, $\underline{h}_B$, and $\underline{h}_T$ (see fig. 6.13). For this purpose two parameters $\underline{D}_1$ and $\underline{D}_2$ are defined

$$D_1 = \frac{0.232\ (h_T - h_B)}{N_B - N_T - 0.048\ (h_T - h_B)}\ , \tag{6.4}$$

and

$$D_2 = \frac{0.232\ (h_B - h_R)}{N_R - N_B - 0.048\ (h_B - h_R)}\ , \tag{6.5}$$

where $\underline{D}_1$ and $\underline{D}_2$ are in nautical miles and $\underline{h}_T$, $\underline{h}_B$, and $\underline{h}_R$ are in feet. It can be shown that

$$R\ (\text{naut. miles}) = (D_1 - D_2)\sqrt{N_B - N_T - 0.048\ (h_T - h_B)} \pm D_2\sqrt{N_R - N_T - 0.048\ (h_T - h_R)}\ . \tag{6.6}$$

Subtracting the two terms gives $\underline{R}'$, the range to the near edge of the hole, and adding them gives $\underline{R}''$, the range to the far edge (see fig. 6.13). It should be noted that $\underline{D}_2$, which is determined by the N-gradient below the layer, will usually be negative, since the gradient will be less than 48 units per 1,000 feet; on the other hand $\underline{D}_1$ will always be positive when there is a radar hole. When the radar is at the height of the layer base, the two radicals are equal. When the radar is within the layer, $\underline{D}_1$ and $\underline{D}_2$ are equal, and the range to the near edge of the radar hole is given by the last term of the range equation.

The width of the radar hole, $\underline{W}$, at the level of the top of the layer is approximately given as follows:

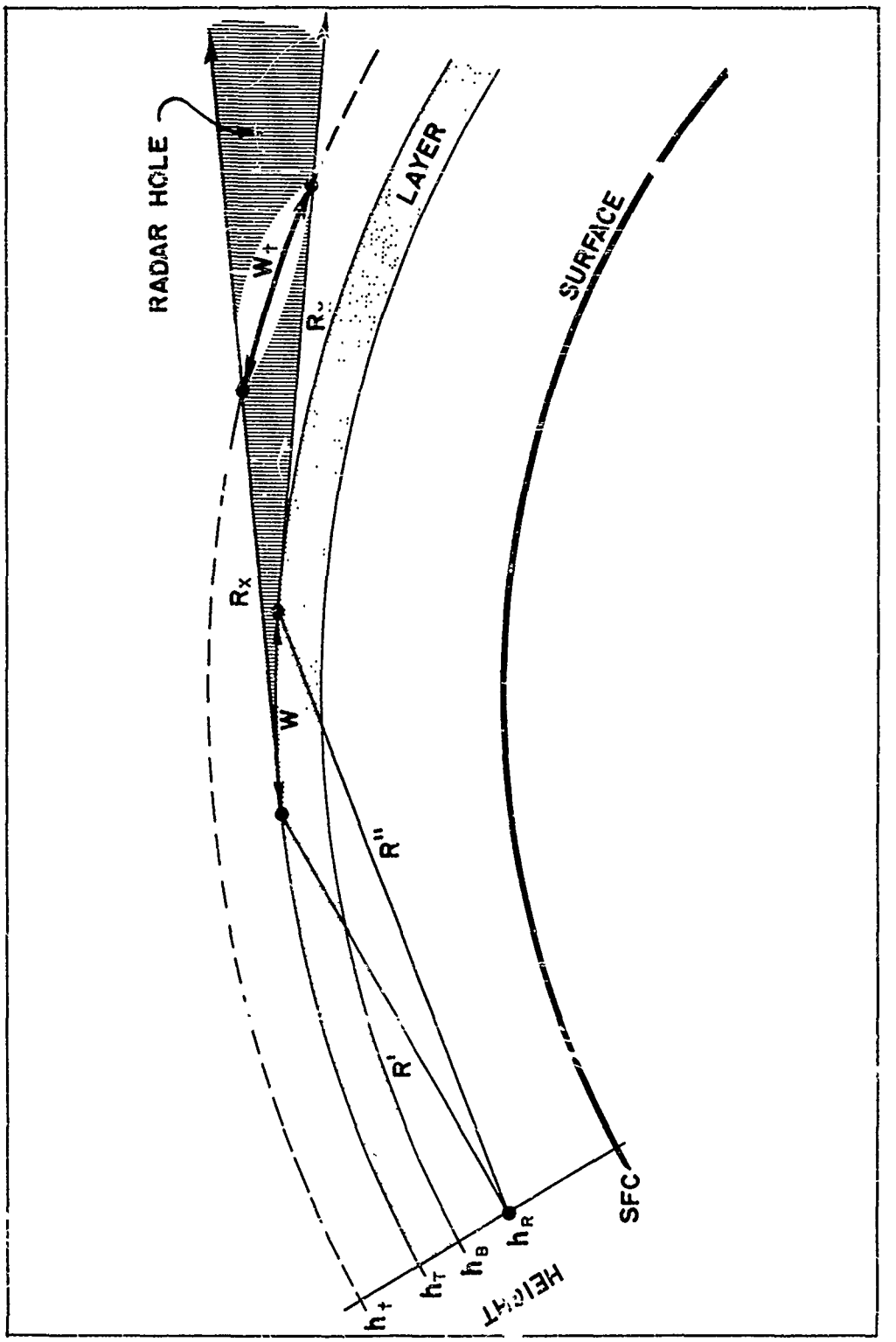

Figure 6.13 Idealized Radar Hole Geometry: Radar Below Layer

$$W \text{ (naut. miles)} \cong 2 D_2 \sqrt{N_R - N_T - 0.048 (h_T - h_R)} \quad . \qquad (6.7)$$

The foregoing equation assumes the radar hole width is equal to the range to the far edge minus the range to the near edge; i.e., $W = R'' - R'$. In figure 6.13, we see that this is only strictly true if the angle between R' and R'' equals zero; in all practical cases this angle will be small and the error introduced by the assumption will be entirely insignificant.

(b) Avoidance of Holes (Radar Below Layer)

It was pointed out in chapter 5, that if the radar is sufficiently far below the layer, there will be no radar hole at all. This can be seen from equation 6.5; if $\left[0.048 (h_T - h_R)\right]$ becomes equal to $\left[N_R - N_T\right]$, the radical will be equal to zero, and the radio hole will have zero width. For a still lower h_R, the hole width will become imaginary and no hole will exist. The radar height at which a radar hole will first appear is therefore,

$$h_R \text{ (max.)} = h_B \left[\frac{0.048 h_T - N_S + N_T}{0.048 h_B - N_S + N_B} \right] , \qquad (6.8)$$

where N_S is the surface refractivity.

(c) Location of Holes (Radar Above Layer)

When the radar is above the elevated layer, the distances to the near and to the far edges of the radar hole are given at radar height instead of at the height of the layer top as was done previously (see fig. 6.14). The near edge distance, R', is given by

$$R' \text{ (naut. miles)} = \frac{0.465 (h_R - h_T)}{\sqrt{0.048 (h_R - h_T) - (N_T - N_R)}} , \qquad (6.9)$$

where all heights are expressed in feet. The width of the radar hole, when the radar is above the elevated layer, turns out to be a complex expression, which is plotted graphically in figure 6.15. The abscissa is C_2/C_1 where C_1 and C_2 are defined as

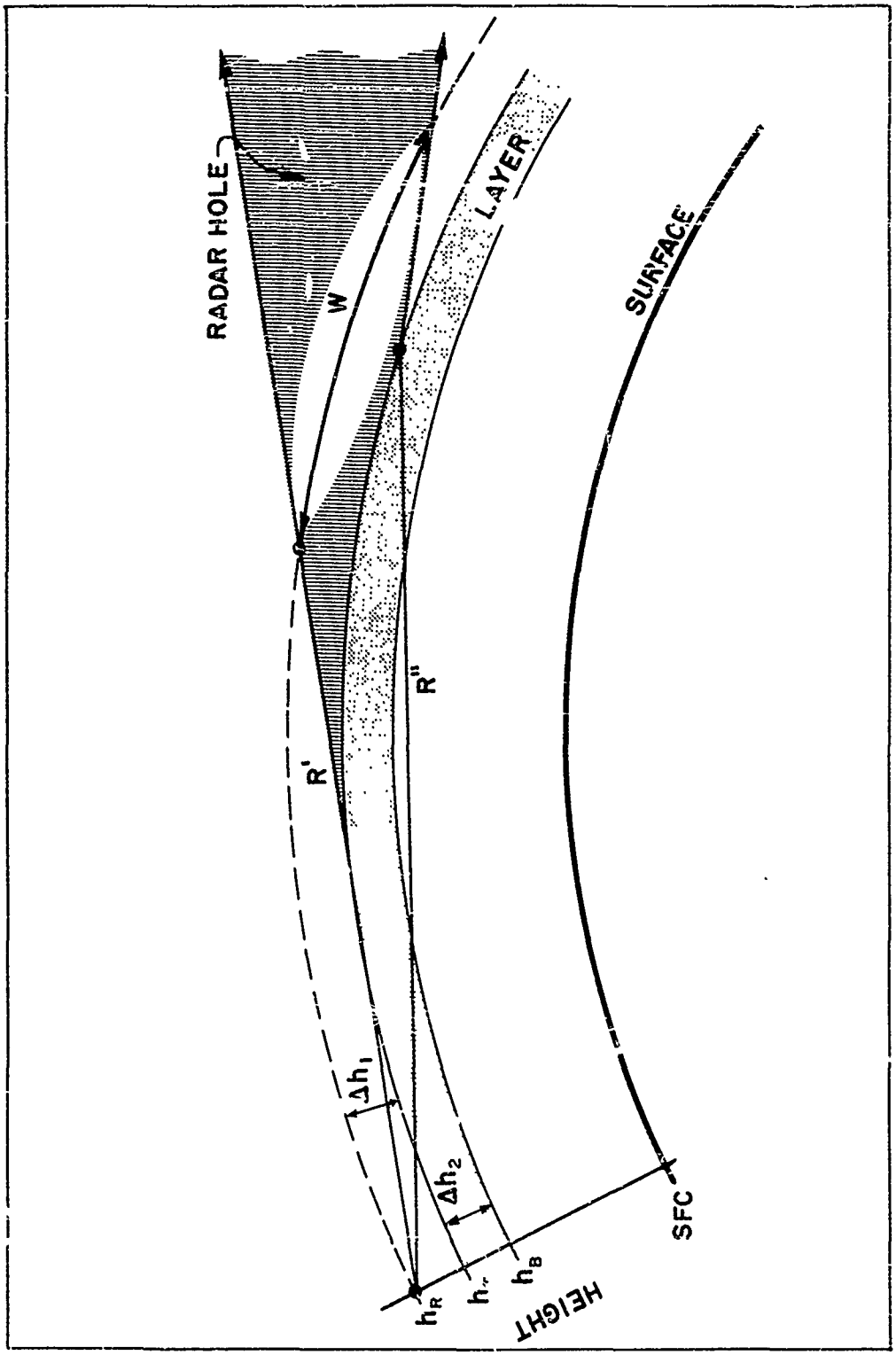
RADAR HOLE
W
LAYER
SURFACE
R'
R''
Δh1
Δh2
SFC
HEIGHT
hR
hB

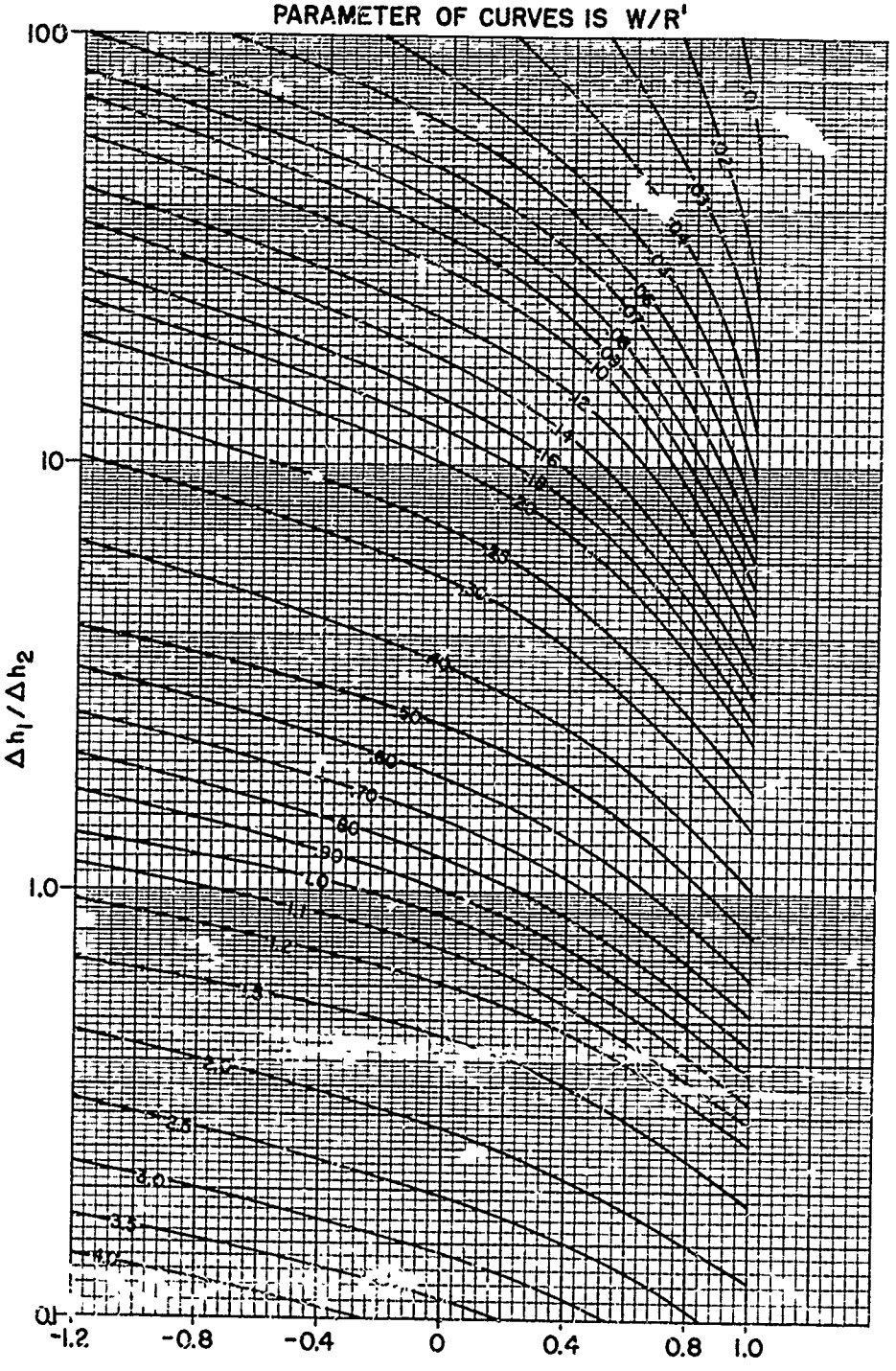

Figure 6.15. Width of Radar Hole Chart--Radar Above Layer.

$$C_2 = \frac{N_T - N_B}{h_T - h_B} + 0.048 \quad , \tag{6.10}$$

and

$$C_1 = \frac{N_R - N_T}{h_R - h_T} + 0.048 \quad . \tag{6.11}$$

The ordinate is $\Delta h_1 / \Delta h_2$, where Δh_1 is the height of the radar above the layer top, $(h_R - h_T)$, and Δh_2 is the layer thickness, $(h_T - h_B)$. The family of curves give hole width, W, at radar height, divided by R', the distance to the near edge of the hole at radar height.

In the expressions for C_1 and C_2 above, it will be seen that C_1 is always positive, but that for strong layers C_2 can become negative. Thus, in figure 6.15, negative values of C_2/C_1 refer to strong layers and positive values to weak layers. When C_2/C_1 is zero, the N-gradient in the layer is equal to the earth's curvature, and when C_2/C_1 is equal to positive one, the layer becomes indistinguishable since its N-gradient is equal to that above the layer.

The curves of figure 6.15 were adapted from theoretical work carried out at Cornell University [11], and the results have been compared with actual flight data taken by the Wright Air Development Center. It was found that actual elevated layers produce radar holes whose location and width agree quite well with the theory. Furthermore, it was found that appreciable radar holes occur even when C_2/C_1 is as much as 0.9 (as indicated by radiosonde data). Since this value of C_2/C_1 is associated with an N-gradient in the layer only 30 percent greater than standard, it is evident that even very weak elevated layers can cause significant radar holes.

(d) Numerical Examples

It is likely that the descriptions given in paragraphs 6.3.1(a), (b), and (c) above for locating radar holes involve concepts unfamiliar to the reader. To clarify these concepts, numerical examples are given in the following subparagraphs. Suppose the radiosonde data given in table 6.1 is representative over the area where radar holes are to be located.

TABLE 6.1

Pressure	Temperature	Dew Point	Height	N
mb.	°C.	°C.	ft.	N-Units
1,013	15.0	12.0		336
902	8.4	7.0	3,260	296
885	12.2	-13.0	3,760	250
850	9.5	-18.0	4,900	240
700	-1.3	-35.0	9,900	201

Sample Radiosonde Data, Heights, and N-Values for the Numerical Examples.

The first step is to compute $\underline{N}$ at each level, using chart I or chart II; these values are tabulated in the last column above. Next plot $\underline{N}$ versus height to obtain a refractivity profile as described in section 3.3.2 (see fig. 6.16).[1] From this profile the parameters of the trapping layer, which is present, are determined to be

$$N_B = 296 \qquad h_B = 3{,}260 \text{ feet}$$

$$N_T = 250 \qquad h_T = 3{,}760 \text{ feet}$$

$$\Delta N = N_B - N_T = 46 \qquad \Delta h = h_T - h_B = 500 \text{ feet}$$

(i.) Radar Below the Layer

To determine the radar hole location when the radar is below the layer, substiiute the above values into equations 6.4, 6.5, and 6.6 as follows:

$$D_1 = \frac{0.232\,(500)}{46 - 0.048\,(500)} = \frac{116}{46 - 24} = 5.28 \text{ nautical miles},$$

[1] The method described in section 3.3.4 will give somewhat different numerical answers. For the purposes of illustration the simpler presentation (of N-profile) is used.

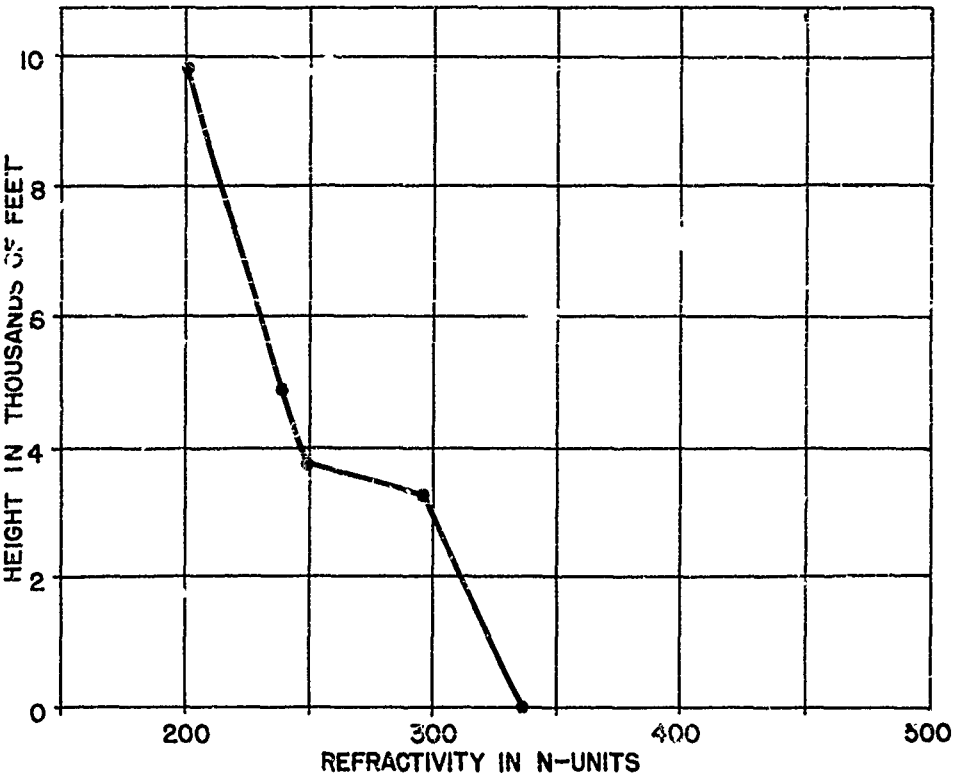

Figure 6.16. N-Profile--Numerical Example.

$$D_2 = \frac{0.232\,(3{,}260 - h_R)}{N_R - 296 - 0.048\,(3{,}260 - h_R)} ,$$

and

$$R = (5.28 - D_2)\sqrt{46 - 24} \pm D_2\sqrt{N_R - 250 - 0.048\,(3{,}760 - h_R)} .$$

To determine the actual location of the radar hole, assume a radar height h_R and read off N_R at that height from figure 6.16.

Example 1

Suppose h_R = 3,000 feet; N_R (taken from fig. 6.16) is then 301. D_2 now becomes $\frac{0.232\,(260)}{5 - 12.5}$ = -8.05 nautical miles,

$$R = 13.3\sqrt{22} \pm 8.0\sqrt{51 - 36.5}\ ,$$

$$R = 62 \pm 30 \text{ nautical miles}\ .$$

The near edge of the radar hole, R', at the layer top (3,760 ft.) is thus at 62 - 30 = 32 nautical miles and the far edge, R'', is at 62 + 30 = 92 nautical miles.

Example 2

Now lower the radar height to 2,500 feet; (from fig. 6.16) then N_R = 307. D_2 becomes $\frac{0.232\ (760)}{11 - 36.5}$ = -6.9 nautical miles,

$$R = 12.2\sqrt{22} \pm 6.9\sqrt{57 - 60.5}\ .$$

Since the quantity under the second radical is negative, the term is imaginary, and there will be no radar hole.

From the above examples, it is seen that a radar hole is present when the radar height is not far below the layer base, but is absent when the radar is lowered an additional 500 feet. For this particular layer, one may find the maximum radar height which will not produce a radar hole. Substituting the parameters of the example into equation 6.8 we have

$$h_R\ (\text{max.}) = \frac{3{,}260\ (180 - 86)}{156 - 40} = 2{,}640 \text{ feet}\ .$$

In this example, a radar height of 2,640 feet will give a radar hole width of zero; at greater heights a radar hole will appear. This then is the critical height for avoiding a radar hole for the particular profile of the example. Using equation 6.8 one can readily compute h_R (max.) for any elevated layer, using appropriate values of h_B, h_T, N_s, N_B, and N_T.

(ii.) Radar Above the Layer

Consider now the problem of locating the radar hole when the radar is above the same layer as specified in figure 6.16.

Example 3

For comparison with example 1 above, assume $(h_R - h_T)$

in the present case is equal to $(h_B - h_R)$ in the previous case, or h_R = 4,020 feet; then from figure 6.16, N_R = 248 and substituting into equations 6.9, 6.10, and 6.11 we have

$$R' = \frac{0.465\ (260)}{\sqrt{0.048\ (260)-2}} = \frac{121}{3.2} = 38 \text{ nautical miles},$$

$$C_2 = \frac{-46}{500} + 0.048 = -0.044,$$

and

$$C_1 = \frac{-2}{260} + 0.048 = 0.040.$$

Then $C_2/C_1 = -1.1$, and

$$\Delta h_1/\Delta h_2 = \frac{260}{500} = 0.52.$$

Entering these values in figure 6.15 gives $\frac{W}{R'} = 1.8$. Thus, the hole width at radar height is given as

$$W = 1.8\ (38) = 68 \text{ nautical miles.}$$

The distance to the near edge of the radar hole at radar height is 38 nautical miles, and to the far edge it is 68 plus 38 or 106 nautical miles.

Example 4

In this example, assume $(h_R - h_T)$ is equal to $(h_B - h_R)$ in example 3, namely 760 feet. Then h_R = 4,520 feet and from figure 6.16, N_R = 243. In this case, from equation 6.9, we have

$$R' = \frac{0.465\ (760)}{\sqrt{0.048\ (760)-7}} = \frac{354}{5.4} = 66 \text{ nautical miles},$$

and C_1 and C_2 will be the same as in example 3 above ($C_2/C_1 = 1.1$). The ratio $\Delta h_1/\Delta h_2$ will now be $\frac{760}{500} = 1.5$ and

from figure 6.15, $\frac{W}{R'} = 0.94$. Thus,

$$W = 0.94\ (66) = 62 \text{ nautical miles},$$

and

$$R'' = 66 + 62 = 128 \text{ nautical miles}.$$

The results obtained in examples 3 and 4 show that, when the radar is not far above the layer top (260 ft.), the near edge of the radar hole is 38 nautical miles away and has a width of 68 nautical miles. Raising the radar height 500 feet, moves the near edge of the hole out to 66 nautical miles, but does not remove the hole. When, however, the radar is an equal height below the layer base (example 2), the hole disappears entirely. This illustrates the statement made previously; namely, if the radar is above the layer, raising its height moves the hole outward and narrows it slightly, but does not eliminate it. When the radar is below the layer, one can eliminate the hole entirely by locating the radar several hundred feet below the layer base.

(e) Shape of Radar Holes

The previous paragraphs have discussed the location of the radar hole (1) where it intersects the top of the elevated layer, for the case where the radar is below the layer, and (2) where it intersects the radar altitude, for the case where the radar is above the layer. Since the radar target will rarely be at either of these particular altitudes, one would like to be able to locate the boundaries of the hole at any target height.

(i.) Radar Below the Layer

When the radar is below the layer, this is particularly simple. Since the rays defining both edges of the hole emerge tangent to the layer top, they will remain the same distance apart at all heights above the layer top; in other words, the width of the radar hole above the layer is constant with altitude. This effect is illustrated in figure 6.13. At a height, h_t, (above the top of the layer) the radar hole width is equal to W_t; comparison will show that $W \cong W_t$. The only problem then is to define the range beyond the layer top, R_x, versus altitude (above the layer top) relationship of one edge of the hole (see fig. 6.13), and the problem is completely solved. Figure 6.17 shows various curves de-

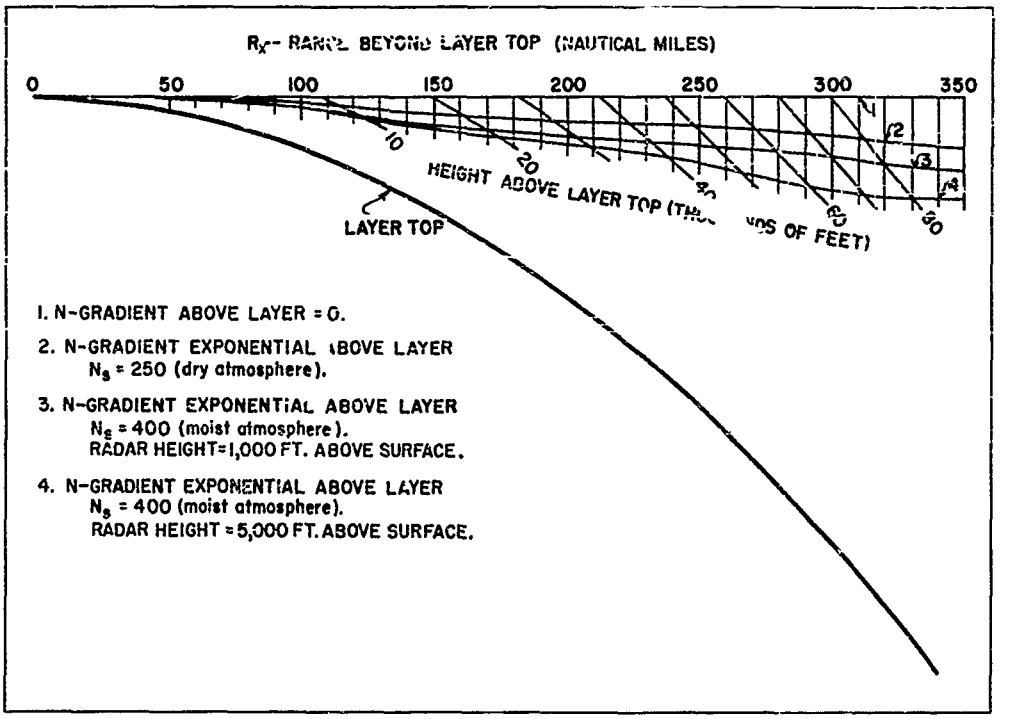

Figure 6.17. Shape of Radar Hole Chart.

fining this relationship for several different refractive conditions. In the figure, the layer top is shown, together with segments of curves drawn at 10,000-foot increments above the layer top. The range scale, R_x, is in nautical miles beyond the point where the ray emerges from the layer top. The exact trajectory of the ray will depend on the characteristics of the N-profile above the layer. The upper straight line, curve 1, assumes no change of N with height above the layer, which of course is unrealistic. The second curve, 2, assumes a reasonably dry atmosphere above the layer, which corresponds to an exponential profile with N_S equal to 250. The next two curves assume a very high surface N of 400. In these cases the amount of atmosphere below the source is of importance; thus, the third curve, 3, is for a radar height of 1,000 feet, and the fourth curve, 4, is for a radar at 5,000 feet. An exponential decrease of N with height above the layer, as portrayed in figure 3.5, has been assumed in all cases except the top line. The proper curve to use in most cases will lie between 2 and 3, and probably closer to curve 2.

(ii.) Radar Above the Layer

In this situation, the near edge of the radar hole is again defined by figure 6.17, since this edge is tangent to the layer top. The far edge of the hole is defined by the next ray emerging from the layer top, which emerges at a small upward angle rather than being exactly tangent (see fig. 6.14). The hole, therefore, gets narrower (width decreases) with increasing altitude above the layer, at a rate which depends on the layer characteristics. The parameter given in figure 6.15 is the ratio of hole width, W, to the distance to the near edge, R', at the same altitude as the radar antenna. It turns out that above this altitude the hole narrows very slowly with altitude; thus, if one predicts a hole of constant width, he will be a little pessimistic in that the hole at greater heights will actually be somewhat narrower than predicted.

(f) Practical Limitations

In applying ray tracing techniques to practical propagation problems, several limitations should be kept in mind. First, elevated layers as they occur in nature are rarely uniform over the 100-200 mile ranges called for in the foregoing ray treatment. Even if one had an accurate refractive index profile at one point along the propagation path, this would not necessarily be representative of the layer characteristics 100 miles, or even 50 miles, away. Usually elevated layers can be regarded as being reasonably uniform, but one must remember that a single radiosonde ascent may not be representative of the layer in question. It is always necessary to consider carefully all available synoptic information.

Another characteristic of layers is that they have small-scale irregularities which make them more like a ground glass mirror than a smooth mirror in the region of total refraction. This has the effect of scattering energy into the radar hole from adjacent rays. This "filling in" of the theoretical well-defined radar hole is more apparent at the edges of the hole, particularly at shorter wavelengths, since these wavelengths are more affected by small-sized roughness elements. For example, the southern California subsidence inversion layer looks quite smooth at a 3-meter wavelength, but it looks quite rough to 0.5-meter energy. As pointed out in chapter 5, weaker layers appear smoother than intense layers; for this reason when a hole is present due to a weak layer it is less likely to be filled in by scattering; i.e.,

it will have more well defined boundaries.

Another complicating factor, which is particularly common over the sea, is that energy is reflected from the sea surface. This energy will be incident upon the layer at much steeper angles than the direct ray and thus will not be affected by the layer to any appreciable extent. Energy reflected from the sea will, therefore, tend to fill in radar holes, particularly at longer wavelengths (due to more efficient reflection). The fact that deep radar holes are observed, however, even over sea paths, attests to the fact that one should not rely on sea reflections to eliminate radar holes but rather only to reduce their intensity.

The above remarks are not intended to convey the impression that atmospheric structure is so erratic that useful predictions of its effect on radio or radar propagation cannot be made. It is wise, however, to realize that various complicating factors are operating to modify the simple assumptions on which the computations are based. Observational evidence shows that radiosonde and refractometer data are usually adequate for practical performance calculations.

6.3.2 Extended Radar Ranges

In the case of air-to-air layered situations, it is found that the energy in the region just beyond the far edge of the radar hole is stronger than when no layer is present. Theory [11] predicts that this should be the case, and experimental evidence supports the theory. As the target closes range it will first pass through this region, which is usually about the same width as the radar hole. As it moves in, the target passes through numerous narrow fingers of alternately high and low illumination. The field in the maxima increases as the far edge of the radar hole is approached, and usually detection probability increases markedly over that expected if no layer were present. Finally, when the far edge of the radar hole is passed, the target will be lost until it emerges from the near edge of the radar hole at relatively close range. The layer, therefore, serves to extract radar energy from the region of the radar hole and to concentrate it in the region beyond. As mentioned above, the enhancement is strongest just beyond the radar hole; it decreases gradually through a distance about equal to the hole width, and merges with the free space field beyond.

When a layer is present which causes a radar hole, the best operational procedure is to fly the radar above the layer at a height such

that the far edge of the radar hole coincides with the radar's normal detection range. In this way, the enhancement beyond the radar hole will serve to increase the detection range by at least half the width of the radar hole.

6.4 Method for Determining Refractive Characteristics from Radar Performance Data

Under certain circumstances, such as in aircraft carrier operations during radio silence, one may not be able to obtain radiosonde data from which to make predictions, and at the same time airborne refractometers may not be available. It may be feasible, however, to obtain initial detection ranges on incoming aircraft at several altitudes with surface search radar. Such information will serve to define the shape of the radar horizon line and thus indicate the presence of an elevated layer.

It was stated in chapter 5, that the range to the radio horizon in an atmosphere with a linear N-gradient is

$$R = \sqrt{2a_e h_R} + \sqrt{2a_e h_T} \ ,$$

where a_e is the effective earth's radius for the N-gradient present, h_R is the radar height, and h_t the target height. If one plots R versus h_t, for various N-gradients, the result is shown in figure 6.18. The distance is made up of two parts, corresponding to the two terms expressed above. The first term is the distance from the radar to the radio horizon ($\sqrt{2a_e h_R}$) and is plotted to the left of zero. Since this term is usually quite small compared to the second term, the effect of varying a_e is insignificant, and the standard N-gradient of 12 units per 1,000 feet, has been assumed. If the radar is at a height of 100 feet, the horizon distance is 12 miles. If the N-gradient is constant, the total horizon distance for a given target height is then 12 miles plus the horizon distance at which the curve corresponding to the existing gradient intersects the target height, h_t.

6.4.1 Layer Characteristics

If one has initial detection range data at several target heights and plots them on figure 6.18 (after subtracting the radar height term), the points will lie on a single curve if no elevated layers are present.

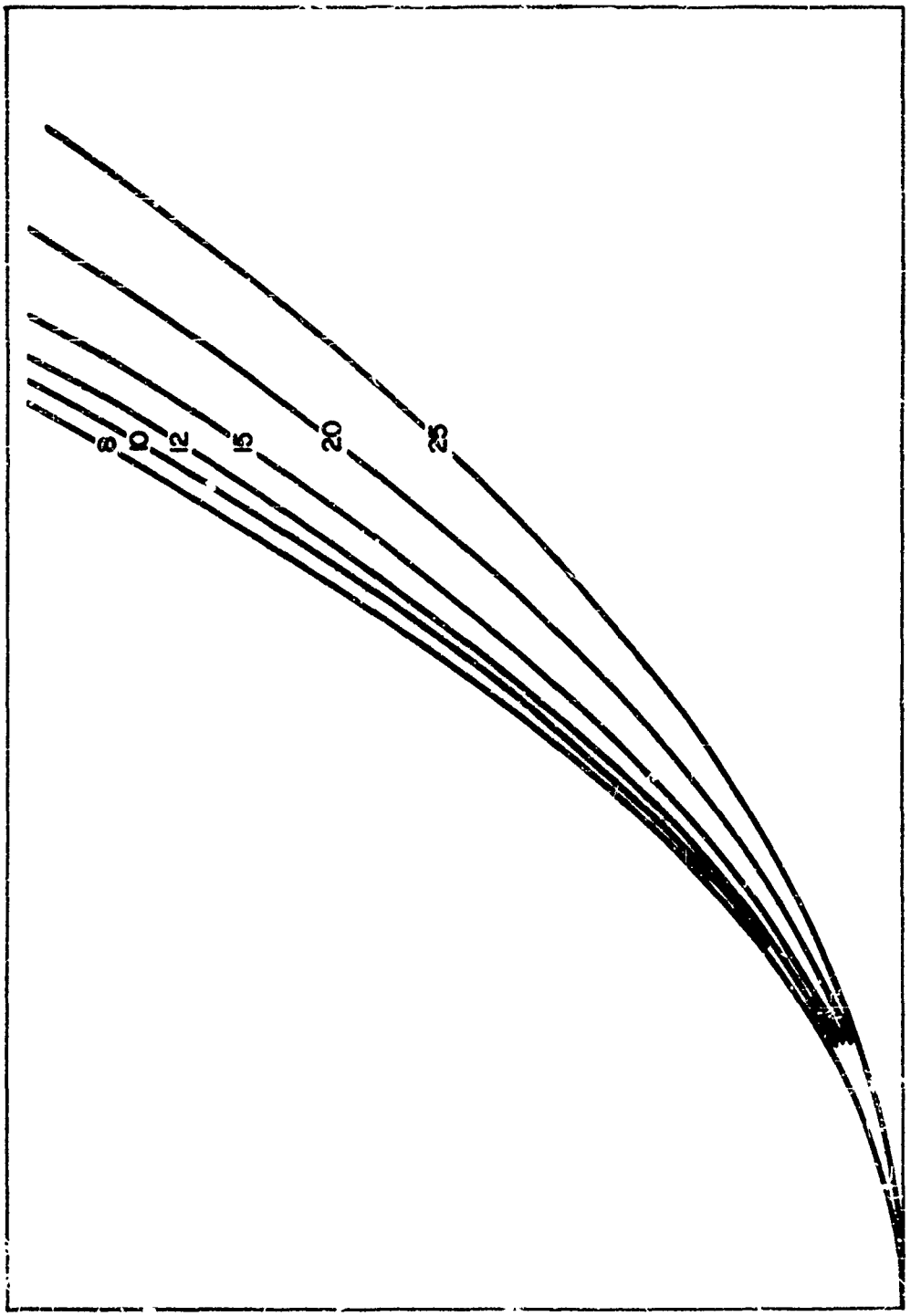

Figure 6.19. Overlay for Figure 6.18. (Chart VII)

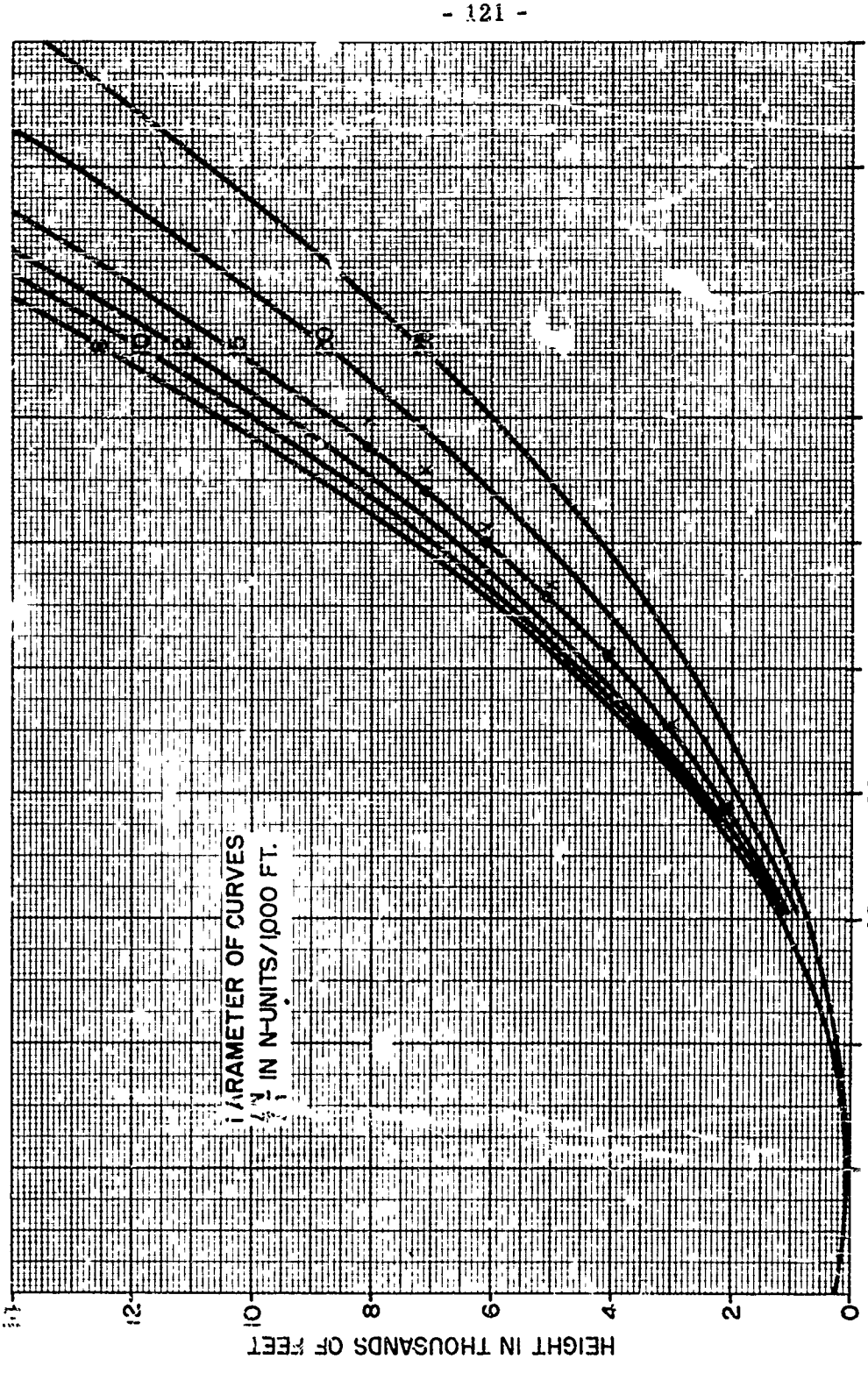

Figure 6.12 Height of Radar Horizon versus Range and Refractivity Gradient. (Chart VI)

In this case the position of the plotted points, as shown by the circles, in relation to the curves already plotted on figure 6.18, enables one to determine the N-gradient directly.

When an elevated layer is present, the points observed for the targets (aircraft) below the layer height will lie on a single curve as before. When the targets are above the layer, however, the points will lie further out, as shown by the crosses in figure 6.16. The reason for this is that, as the rays penetrate the layer they are bent downward (as illustrated in fig. 5.2), thus extending the horizon somewhat.

Using points plotted as in figure 6.18, one can determine the layer characteristics in a particular situation in the following way:

1. Observe that the lower points (crosses) lie on the curve corresponding to an N-gradient of 15 units per 1,000 feet. Thus, one can say that this is the N-gradient below the layer.

2. Next, place the overlay (fig. 6.19) on top of figure 6.18. This overlay is simply a duplicate of the curves plotted in figure 6.18 to the right of the origin (h = 0, R = 0). Now move the overlay up and to the right, keeping the axis at the bottom parallel to the horizontal lines in figure 6.18. A position of the overlay will be found such that the upper points (crosses) fall on one of the overlay curves. When this position is found, the overlay curve corresponding to the plotted points indicates the N-gradient above the layer ($\frac{\Delta N}{\Delta h}$ = 12 in this case).

3. Read off the height h_1, and range R_1, where the two curves intersect ($\frac{\Delta N}{\Delta h}$ = 15 of figure 6.18 and $\frac{\Delta N}{\Delta h}$ = 12 of the overlay). In this case h_1 = 3,500 feet and R_1 = 76 miles.

4. Read off the height h_2, and distance R_2, of the overlay origin (cross). In this case h_2 = 1,100 feet and R_2 = 16 miles.

5. The intersection height of the two curves $\underline{h_1}$, is the layer height. The total change of $\underline{N}$ through the layer is determined by

$$\Delta N_L = 0.0541 \left[\left(\frac{h_1}{R_1} \right)^2 - \left(\frac{h_1 - h_2}{R_1 - R_2} \right)^2 \right] , \qquad (6.12)$$

where $0.0541 \left(\frac{h_1}{R_1}\right)^2 = N_1$ and $0.0541 \left(\frac{h_1 - h_2}{R_1 - R_2}\right)^2 = N_2$. In this case

$$\frac{h_1}{R_1} = \frac{3{,}500}{76} = 46.0 \text{ feet/mile} ,$$

and

$$\frac{h_1 - h_2}{R_1 - R_2} = \frac{3{,}500 - 1{,}100}{76 - 16} = \frac{2{,}400}{60} = 40.0 \text{ feet/mile} .$$

6. Figure 6.20 is a plot of $\underline{N_1}$ (or $\underline{N_2}$) versus $\frac{h}{R}$. $\underline{N_1}$, corresponding to $\left(\frac{h_1}{R_2}\right) = 46.0$, is 115, and $\underline{N_2}$, corresponding to $\left(\frac{h_1 - h_2}{R_1 - R_2}\right) = 40.0$, is 87. Thus, $\Delta N_L = N_1 - N_2 = 115 - 87 = 28$ units.

In summary, the points plotted on figure 6.18 indicate that the N-profile has a gradient of 15 units per 1,000 feet up to 3,500 feet, then a decrease of 28 units, followed by an N-gradient of 12 units per 1,000 feet above this height. It is not feasible to determine the layer thickness from detection range data. One would need a large number of very precisely measured points and would have to assume a smooth, absolutely uniform layer in order to derive the layer thickness. Instead, one has obtained the effective ΔN which the layer would have if it had zero thickness; i.e., if it were a very sharp (thin) layer.

In addition to figures 6.18 and 6.19, full-size reproductions (without the plotted data shown) have been printed on transparent paper and are provided as loose-leaf inclusions to this manual (charts VI and VII). Although charts VI and VII may be used in their present form, it is suggested that working copies be made on transparent plastic stock using the Ozalid (or other) duplicating process. Routine use of these charts in their present form will soon result in their destruction.

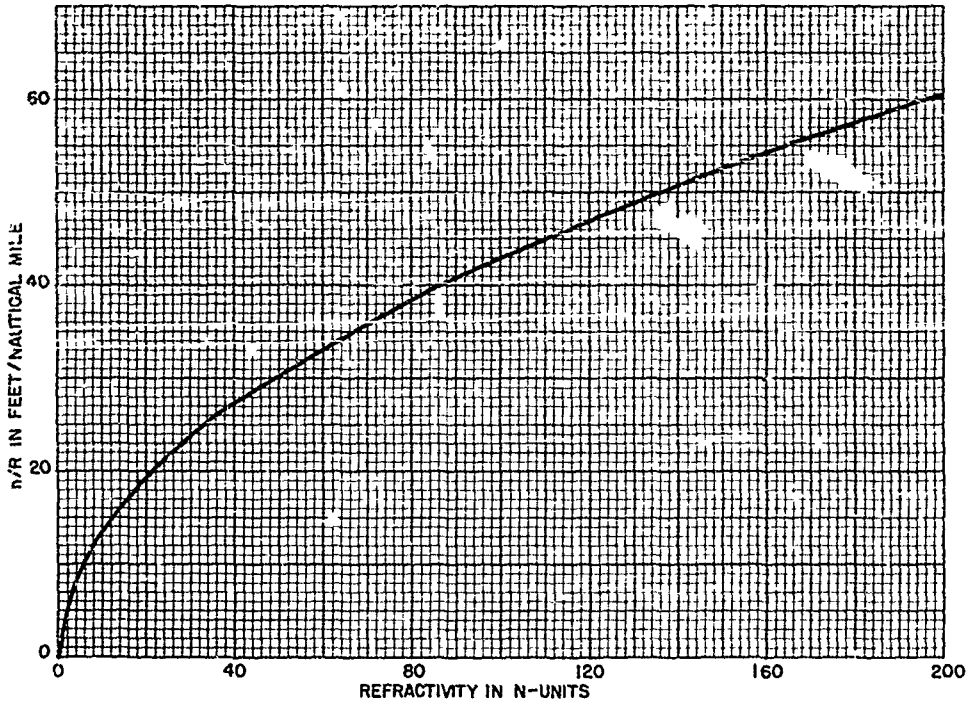

Figure 6.20. Refractivity versus h/R.

6.4.2 Prediction of Radar Holes

(a) Radar Below the Layer

When an airborne radar is h' feet below a sharp layer, the distances, R' and R'', to the boundaries of the radar hole are given by

$$R \text{ (naut. miles)} = \frac{4.87}{1 - 0.0209\left(\frac{\Delta N}{\Delta h}\right)_1}\left[\sqrt{\Delta N_L} \pm \sqrt{\Delta N_L - 0.048h'\left[1 - 0.0209\left(\frac{\Delta N}{\Delta h}\right)_1\right]}\right], \quad (6.13)$$

where $\left(\frac{\Delta N}{\Delta h}\right)_1$ is the N-gradient below the layer in units per 1,000 feet and ΔN_L is the change of N in the layer itself. Using the minus sign before the second radical gives the distance, R', to the near edge of the hole at layer height, and using the plus sign gives the distance, R'', to the far edge.

Using the figures given in the preceding example we obtain

$$R = \frac{4.37}{1 - 0.0209(15)} \left[\sqrt{28} \pm \sqrt{28 - 0.048[1 - 0.0209(15)]h'} \right] , \quad (6.13)$$

$$R = 7.1 \left[5.3 \pm \sqrt{28 - 0.033h'} \right] ,$$

or

$$R = 37.5 \left[1 \pm \sqrt{1 - .0118h'} \right] .$$

If the radar height is 850 feet or more below the layer, the radical will be imaginary and no hole will be found. If it is closer to the bottom of the layer than this, say 500 feet below the layer, there will be a hole between 13.5 miles and 61.5 miles.

(b) Radar Above the Layer

When the radar is above a sharp layer, the distance to the near edge of the radar hole at radar height is similar to that given in section 6.3, namely,

$$R' \text{ (naut. miles)} = 14.8 \sqrt{\frac{h''}{48 - \left(\frac{\Delta N}{\Delta h}\right)_2}} , \quad (6.14)$$

where h'' is the radar height in feet above the layer and $\left(\frac{\Delta N}{\Delta h}\right)_2$ is the N-gradient in N-units per 1,000 feet above the layer. The distance R'' to the far edge of the hole (again at radar height) is obtained from figure 6.21. In this figure, it is assumed that

$$\left(\frac{\Delta N}{\Delta h}\right)_1 = \left(\frac{\Delta N}{\Delta h}\right)_2 = 12 \text{ units/1,000 feet} ,$$

which will be reasonably well satisfied most of the time. This figure is similar to figure 6.15, which applies to layers of finite thickness, and gives the ratio of hole width W to R' in terms of ΔN_L and radar height, h'', above the layer.

(c) Summary

To summarize the use of the radar method for obtaining refractive characteristics, one finds that if initial detection ranges on incoming aircraft are available for at least four different aircraft altitudes,

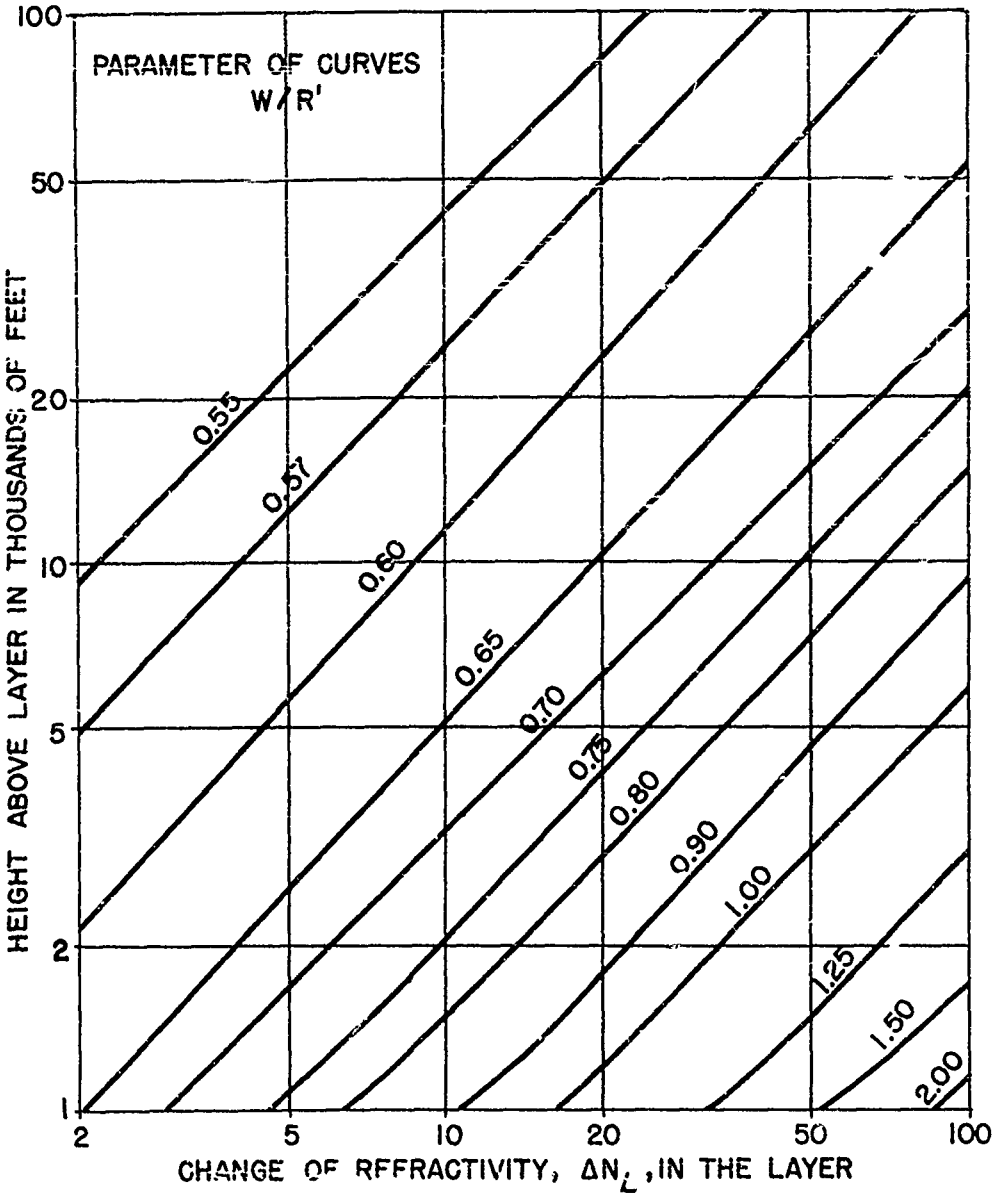

Figure 6.21. Width of Radar Hole Chart--Radar Above a Sharp Discontinuity in N-Gradient.

it is possible to deduce the effective characteristics of the N-profile. These characteristics are: (1) the N-gradient, $(\frac{\Delta N}{\Delta h})_1$, below the layer, (2) the layer height, (3) the effective change of $\underline{N}$ through the layer, $\underline{\Delta N_L}$, and (4) the N-gradient, $(\frac{\Delta N}{\Delta h})_2$, above the layer. The effective $\underline{N}$ change in the layer is based on a thin layer, and it is not practical to attempt to determine layer thickness. Using the derived characteristics,

one can predict the location and extent of radar holes for airborne radars. In order to do this without layer thickness information, one must modify the methods of section 6.3 as has been shown.

It should be emphasized that the N-profile characteristics derived in this way are dependent upon the accuracy with which the horizon line of ship-borne radar can be defined. As can be seen in figure 6.18, errors of a mile or so in defining this line above the layer will cause appreciable errors in the derived layer characteristics. It is, therefore, much better to use refractometer or radiosonde data if it is available.

7. RADIO PERFORMANCE

The physical concepts of radio wave propagation, which were developed in parts I and II of this manual, apply equally well whether one is concerned with radar detection or with radio communication. The application of these concepts, however, is somewhat different in the two cases. Since radar detection involves reflection of energy from the target and a return trip to the radar antenna, a great deal more power is required for the detection of a target at a given distance than for radio communication over the same distance. Furthermore, the meteorological effects needed to increase radar detection ranges are much stronger than those needed to extend communications ranges by the same amount. In this section, the principles presented in parts I and II are applied to the problem of radio communications over the ocean. Before proceeding, however, it is necessary to become familiar with the term, "decibel".

Since radio power or field strength may vary over a very large range, covering many orders of magnitude, it is convenient to express these quantities on a logarithmic scale. In most radio propagation work, the power or field strength is expressed in "decibels below free space". To understand this and similar terms, one must bear in mind that decibels always refer to a ratio. The definition of decibel (db) is

$$\text{db} = 10 \log \frac{P_o}{P} = 20 \log \frac{F_o}{F} , \qquad (7.1)$$

where P is power (or intensity) and F is field strength (or amplitude). The zero subscript refers to a reference power or field. If the reference is the free space power or field at a given distance from the transmitter, then expressing the power at "x" decibels below free space, means that ten times the log of the ratio of "free space" to "measured power" at a given distance is equal to "x". For example, suppose the measured power received at 20 miles from a transmitter is one-fifth of the computed free space power at 20 miles. Then $\frac{P_o}{P} = 5$, but log 5 = 0.70; thus, on a decibel scale the measured power is 10 (0.7) = 7 decibels below free space. In the same example, since $\frac{P_o}{P} = 5$, then $\frac{F_o}{F} = \sqrt{5} = 2.24$, but log 2.24 = 0.35, and 20 (0.35) = 7 decibels. Thus, the decibel value is the same whether the power ratio or the amplitude ratio is used. The following sections discuss the effects of meteorological variables on radio communications.

7.1 Surface-to-Surface Situations

7.1.1 Linear N-Profile

Consider now the case of two ships proceeding away from each other with omnidirectional antennas radiating at a wavelength, λ, and located H feet above the sea surface. How does the rad. signal strength, as measured at one of the ships, vary with distance? The result is shown schematically in figure 7.1.

At very close range, there is interference between the direct and surface-reflected rays. This will cause the field to pass through maxima and minima as the ships move apart. At distances where the two waves arrive just out of phase the received signal will be very low. These distances are $d = \frac{2H^2}{n\lambda}$ where n is an integer (1, 2, 3, etc.). The greatest distance where a minimum will occur corresponds to n = 1 or $d = \frac{2H^2}{\lambda}$. Suppose for example that H = 100 feet and λ = 1 meter (300 mc.); then d = 1.0 nautical mile. At twice this distance the signal will

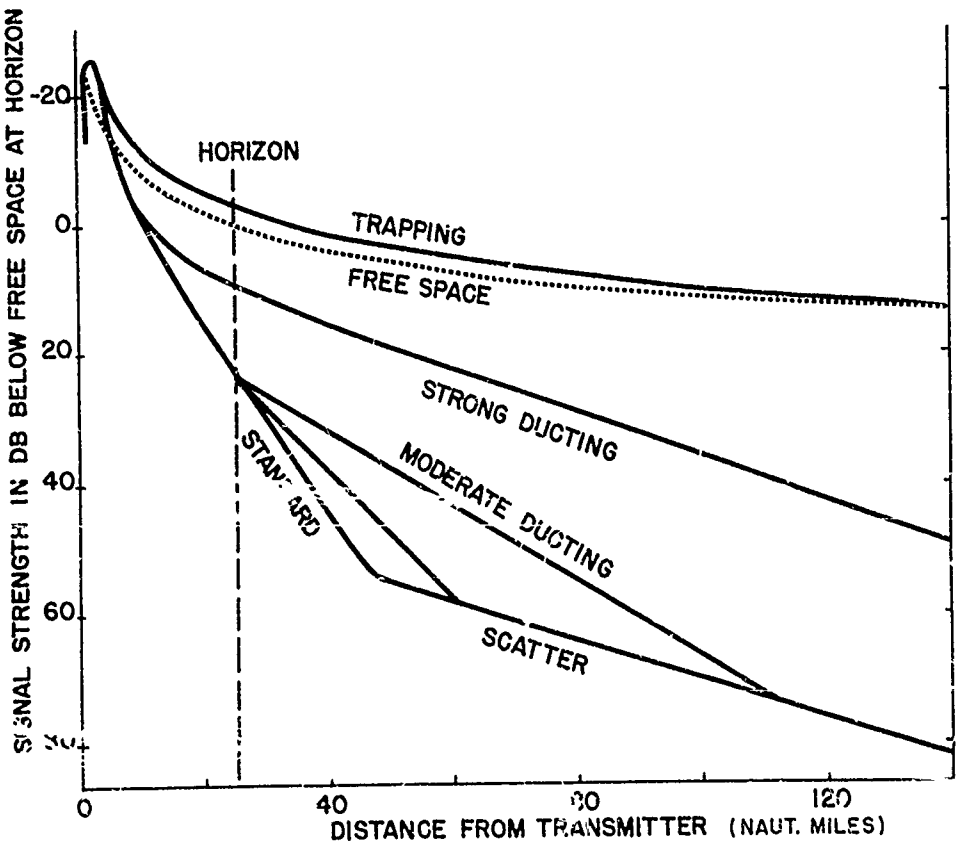

Figure 7.1. Radio Field Strength versus Distance for Various Propagation Conditions.

again pass through a maximum. Since the two waves are in phase the signal amplitude will be double the free space field at this point (power will be 4 times free space). Thus, the field is 10 log 4 = 6 decibels above free space. From this point on, the signal will decrease steadily with increasing distance. When the distance is doubled again ($d = \frac{8H^2}{\lambda}$, or 4.0 miles in the example above), the field will be equal to the free space field. At this point the two waves arrive 90° out of phase with each other, so the measured field is simply that of either wave alone.

As the ships continue to separate, they will reach the horizon distance. Since both antennas are assumed at equal height this distance is

$$d_h = 2\sqrt{2a_eH} = 2.2\sqrt{\frac{H}{1 - 0.0209(\frac{\Delta N}{\Delta h})}}, \qquad (7.2)$$

where H is the antenna height in feet and $\frac{\Delta N}{\Delta h}$ is the N-gradient in the layer below the antenna. For H = 100 feet and $\frac{\Delta N}{\Delta h}$ = 12 units per 1,000 feet, d = 25.5 nautical miles. The signal strength at the horizon distance turns out to be very nearly constant (when expressed as db below free space) over a wide range of wavelengths and N-gradients. Figure 7.2 shows the horizon signal strength versus λ for a substandard N-gradient (8 units/1,000 ft.) and for a superrefractive gradient (30 units/1,000 ft.). The solid curves represent 100-foot antenna heights, and the dashed curves represent 50-foot antenna heights. It can be seen that a value of 24 ± 1 decibels below free space represents the horizon signal (field) strength for all but the shortest wavelengths quite closely. The main effect of changing the N-gradient is to increase the horizon distance according to the above expression.

Beyond the horizon distance, the radio waves enter the diffraction region in which the attenuation rate (decrease of field strength with distance) in decibels per nautical mile is constant. The attenuation rate, A, in this region is

$$A \text{ (db/naut. mile)} = 0.72 \left[\frac{\left(1 - 0.0209\frac{\Delta N}{\Delta h}\right)^{2/3}}{\lambda^{1/3}}\right], \qquad (7.3)$$

where λ is the wavelength in centimeters and $\frac{\Delta N}{\Delta h}$ is the N-gradient below antenna height. Using the previous example (λ = 100 cm., $\frac{\Delta N}{\Delta h}$ = 12 units/1,000 ft.) gives a rate of 1.3 decibels per nautical mile; smaller λ's and smaller N-gradients will increase the rate. Table 7.1 shows

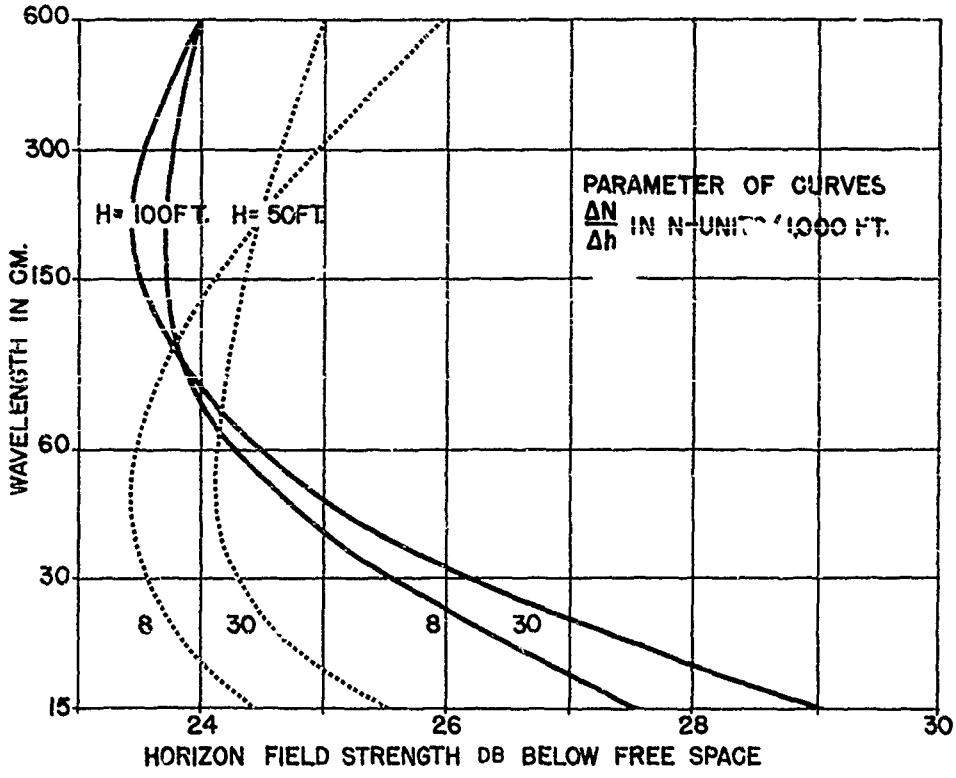

Figure 7.2. Horizon Field Strength versus Wavelength.

the attenuation rate for various λ's and N-gradients. This constant attenuation rate will control the fields out to a distance of about 50 miles (for shipboard antenna heights).

From this point on, the radio waves enter the "scatter" region, in which the dominant propagation mechanism is scattering from atmospheric inhomogeneities. The attenuation rate in this region has been found experimentally to be about 0.15 of a decibel per nautical mile and is reasonably independent of wavelength. The scatter region is not usually of particular interest in shipboard communications because the fields are so weak that very high-power transmitters and large, highly-directional antennas are required to obtain a usable signal. Shore installations, between islands for example, often use such measures, and find that scatter communications are very reliable. The fields in temperate latitudes are usually somewhat stronger in summer than in winter, because the presence of more water vapor results in more intense scattering parcels.

TABLE 7.1

λ	$\frac{\Delta N}{\Delta h}$ (units/1,000 ft.)						
cm.	8	10	12	15	20	25	30
600	0.73	0.71	0.68	0.65	0.58	0.50	0.43
300	0.93	0.90	0.87	0.84	0.74	0.64	0.55
150	1.17	1.13	1.09	1.05	0.93	0.81	0.69
60	1.58	1.53	1.47	1.42	1.25	1.09	0.93
30	1.99	1.92	1.86	1.79	1.57	1.37	1.17
15	2.51	2.43	2.34	2.25	1.98	1.73	1.48

Attenuation Rate in the Diffraction Region (db/naut. mile) for Linear N-Gradients.

7.1.2 The Effect of Layers

Thus far, the effects of constant N-gradients on communications have been considered. Under these circumstances diffraction theory may be applied quite easily, since a linear N-profile may be closely approximated by simply changing the effective earth's curvature. In the case of nonlinear N-profiles, with surface and/or elevated layers, theory has not been so well verified by experimental evidence. It is necessary, therefore, to resort to semiempirical methods, as derived by Gossard and Anderson [14], to obtain useful results. In practice, one is not interested in the signal strength as such, but in how much additional communicating distance will result from given layer characteristics. This additional distance is given by

$$\Delta D \text{ (naut. miles)} = (D_o - 2.55\sqrt{H}) \left[\left(\frac{105}{A + B \log \Delta N_L + C \log h_T} \right) - 1 \right], \quad (7.4)$$

where D_o is the normal communicating distance in nautical miles, H is the antenna height in feet, ΔN_L is the change in N through the layer, h_T is the layer-top height in feet, and A, B, and C are given in figure 7.3 as functions of wavelength.

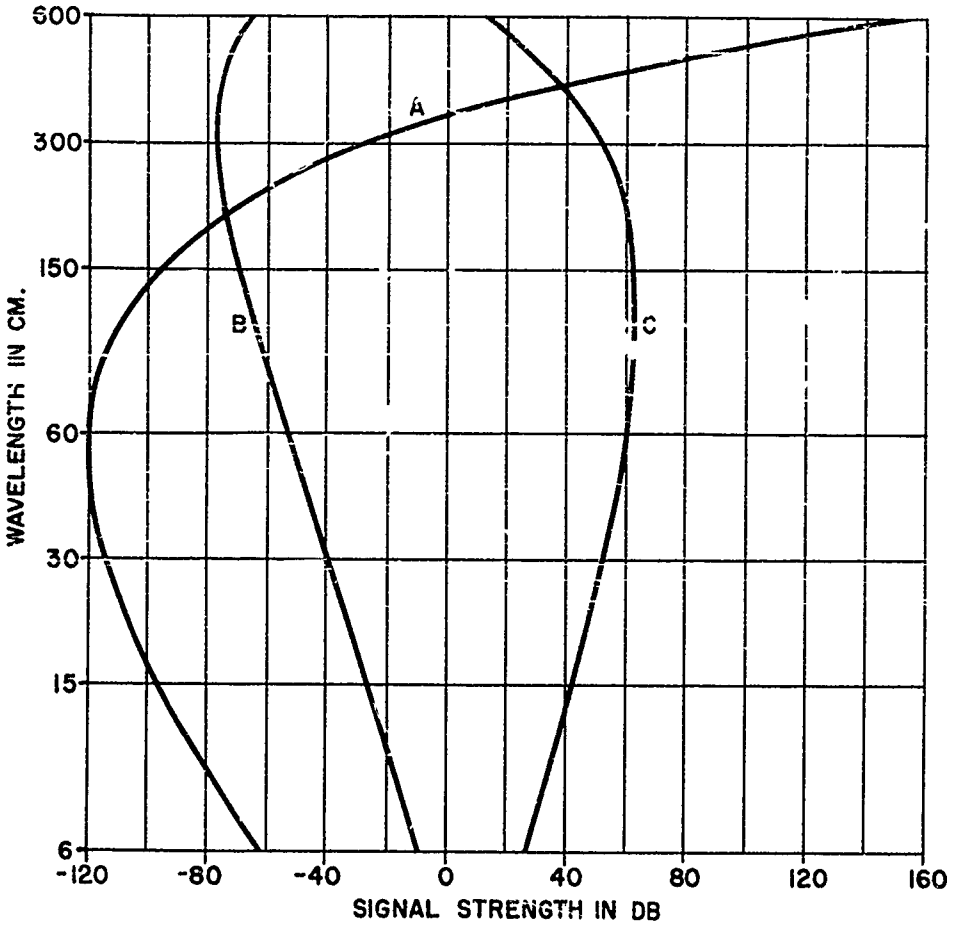

Figure 7.3. Attenuation Coefficients versus Wavelength.

Numerical Example

Suppose for example λ = 100 centimeters, H = 75 feet, and D_o = 35 miles, and the layer characteristics are h_T = 2,000 feet and ΔN_L = 10. From figure 7.3; A = -116, B = -62, C = +63

$$\Delta D = (35 - 22)\left(\frac{105}{30} - 1\right) = 32.5 \text{ nautical miles .}$$

Increasing the layer-top height to 3,000 feet makes

$$\Delta D = 20 \text{ nautical miles.}$$

Equation 7.4 applies only over a limited range of elevated layer characteristics. It would not be used under strong ducting conditions; i.e., when, $A + B \log \Delta N_L + C \log h_T$, is less than about 10 decibels. Under these conditions, the assumption of a constant signal at the horizon distance becomes invalid. For conditions between standard and moderate ducting, and for extended ranges within 100 miles from the transmitter, equation 7.4 will be reasonably reliable.

When layers are present which give very large (or negative) ΔD's using the above expression, there is no method (empirical or otherwise) for predicting the expected extension in communicating distance. When trapping layers are encountered, the fields at the horizon and beyond are found to be nearly at the free space level for great distances. When the h_T and ΔN_L of a layer exceed the trapping criteria shown in figure 6.7, it is safe to conclude that communication signals will be very much stronger than usual, and that communications may be carried out between ships at much greater distances than normal.

7.2 Surface-to-Air and Air-to-Surface Situations

The meteorological effects on surface-to-air communications will be considerably less pronounced than those described in chapter 6. The region of maximum signal enhancement caused by atmospheric layers extends from the sea surface up to the top of the layer. Since strong effects are rarely caused when the layer top is above a few thousand feet, the aircraft will usually be well above the region where strong effects occur.

In cases where appreciable surface-to-surface effects occur, the signals above the layer will also be enhanced, but to a degree which falls off rapidly with height. Experimental evidence shows that in cases of strong ducting, the field for the first few thousand feet above the layer top is appreciably stronger than when no duct is present. Also, when the aircraft is at high altitudes (30,000 - 40,000 ft.), the radio horizon distance is increased by as much as 5 percent of its standard value of $1.23 (\sqrt{H_R} + \sqrt{H_T})$, where H_R and H_T are the two terminal heights.

No systematic study has been made for intermediate altitudes. It is likely, however, that the degree of communication range extension will not exceed a few percent whenever the aircraft is more than a few thousand feet above the layer top.

In the absence of layers capable of causing appreciable surface-to-surface signal enhancement, the surface-to-air enhancement will be negligible. One can conclude, therefore, that the meteorological effects on surface-to-air communications will generally be very much less than over surface-to-surface paths, and that they will be appreciable only when the aircraft is at low altitude (such that surface-to-surface criteria apply).

7.3 Air-to-Air Situations

When both terminals of a communications link are well above the surface, the effects of weak elevated layers become more important than they are when one terminal is near the surface. In this situation, radio holes can play a significant role in redistributing the transmitted energy.

In section 6.3 (air-to-air radar), it was noted that radio holes, caused by relatively weak elevated layers, can cause radio energy to be very weak in the radio hole, and that beyond the hole, for a distance roughly equal to the hole width, the energy is stronger than usual. Thus, as two aircraft move apart, the signal will decrease at the free space rate until the near edge of the hole is reached. Then it will decrease markedly for a distance of many miles, until the far edge of the radio hole is passed. At this distance, the signal will increase markedly in intensity, pass through a maximum, and then will gradually fall off to the free space values at a distance roughly equal to the width of the radio hole. Beyond this, the layer will have little effect, and the signal strength will again decrease at the free space rate (6 db per octave of distance). The methods for locating the boundaries of the radar hole which were developed in section 6.3, are of course equally valid for the radio hole, since the phenomena are identical.

It should be emphasized that all of the above effects occur within the radio horizon as determined by $d = 1.23\left(\sqrt{H_R} + \sqrt{H_T}\right)$. This distance for high altitude aircraft is rather large (350 miles at 20,000 ft for example), so free space attenuation will usually limit the communication range before the earth's shadow becomes effective.

PART IV

METEOROLOGICAL STUDIES

OF THE

ATMOSPHERIC REFRACTIVE INDEX

8. REFRACTIVE INDEX CLIMATOLOGY

In part II of this manual we have discussed methods for describing the refractive properties of an atmosphere in terms of various refractivity profiles, and in part III we have outlined procedures for predicting radio-radar performance in terms of specific refractivity conditions.

In the absence of specific information and particularly for planning purposes, it is useful to develop a knowledge of the climatology of refractivity. An understanding of the refractive properties of air masses will also be helpful in answering questions as to the horizontal extent and time persistence of refractive layers. For these reasons such a climatology is presented in the following paragraphs.

8.1 Seasonal Distribution of Refractivity Near the Surface

If we examine the first term, the "dry" term, on the right-hand side of equations 3.3 or 3.4, we see that it is proportional to air density. From typical atmospheric data, it can also be shown that the "dry" term constitutes at least 60 percent of the value of $\underline{N}$. For these reasons the refractivity is strongly affected by pressure changes.

In order to study the distribution of refractivity at the surface, it is desirable to suppress those variations produced solely by surface topography. For this purpose we use a technique analogous to that of reducing station pressures to sea level. Solving the expression for the standard refractivity profile, equation 3.5, for $\underline{N}_S$ we have

$$N_O = N_S \exp.^{ch} ,$$

where $\underline{N}_S$ is the refractivity at the earth's surface, $\underline{N}_h$ is the refractivity at height $\underline{h}$ above the surface and $\underline{c}$ is the exponential coefficient of a particular standard profile. We then define a datum refractivity, $\underline{N}_O$, as follows

$$N_O = N_S \exp.^{ch_S} , \qquad (8.1)$$

where $\underline{N}_S$ is the surface refractivity, $\underline{h}_S$ is the height of the surface, and c is again the exponential coefficient of a particular standard profile. The datum refractivity is then the value obtained if one extrapolates the surface value along a standard refractivity profile to zero height.

In order to facilitate the reduction of surface refractivity values to the zero-height datum figure 8.1 has been prepared, using the value of c = 0.1057 as arbitrarily adopted by Bean and Riggs [3] as being the most representative standard profile. Equation 8.1 then becomes

$$N_0 = N_S \exp.^{0.1057\, h_S} ,$$

where N_0, N_S, and h_S (in kilometers) are defined as in equation 8.1. In use, one locates the point on figure 8.1 corresponding to the surface refractivity, N_S, and the surface elevation, h_S. By laying a straight edge through the point and parallel to the set of sloping, dashed lines, the datum refractivity, N_0, may be read from the ordinate scale. Other values of the exponential coefficient, c, could be represented on figure 8.1 by additional sets of sloping, dashed lines of different slopes.

Using the reduction method described above Horn, Bean, and Riggs [15] have prepared world-wide maps of datum refractivity for various months and seasons. Figures 8.2 and 8.3 show these results for the months of February and August. It can be seen that N_0 varies from 390 in humid tropical areas to 290 in desert and plateau regions. Continental interiors and mountain chains in middle latitudes are reflected by low values of N_0 as compared to coastal areas. Such major climatic details as the Indian monsoon and orographic rain shadows are also indicated by the N_0 contours.

Figure 8.4 illustrates the climatic response of surface refractivity and shows a world-wide analysis of the annual range of monthly mean values of N_S. Climatic controls, such as the prevailing transport of maritime air inland over the west coasts of North America and Europe, are indicated by relatively small annual ranges of N_S (20 to 30 units). On the other hand, a range of 40 to 50 units or more along the east coast of the United States reflects the frequent invasion into this area of such diverse air masses as continental arctic and maritime tropical. The largest annual ranges of N_S (90 units) are observed in the Sudan of Africa and in regions affected by the Indian monsoon.

8.2 Refractive Index Characteristics of Air Mass Types

Air masses, having approximately homogeneous horizontal distributions of temperature, humidity, and lapse rate, have been defined [6] and are commonly identified by the practical meteorologist in his study of daily weather development. Nearly uniform characteristics

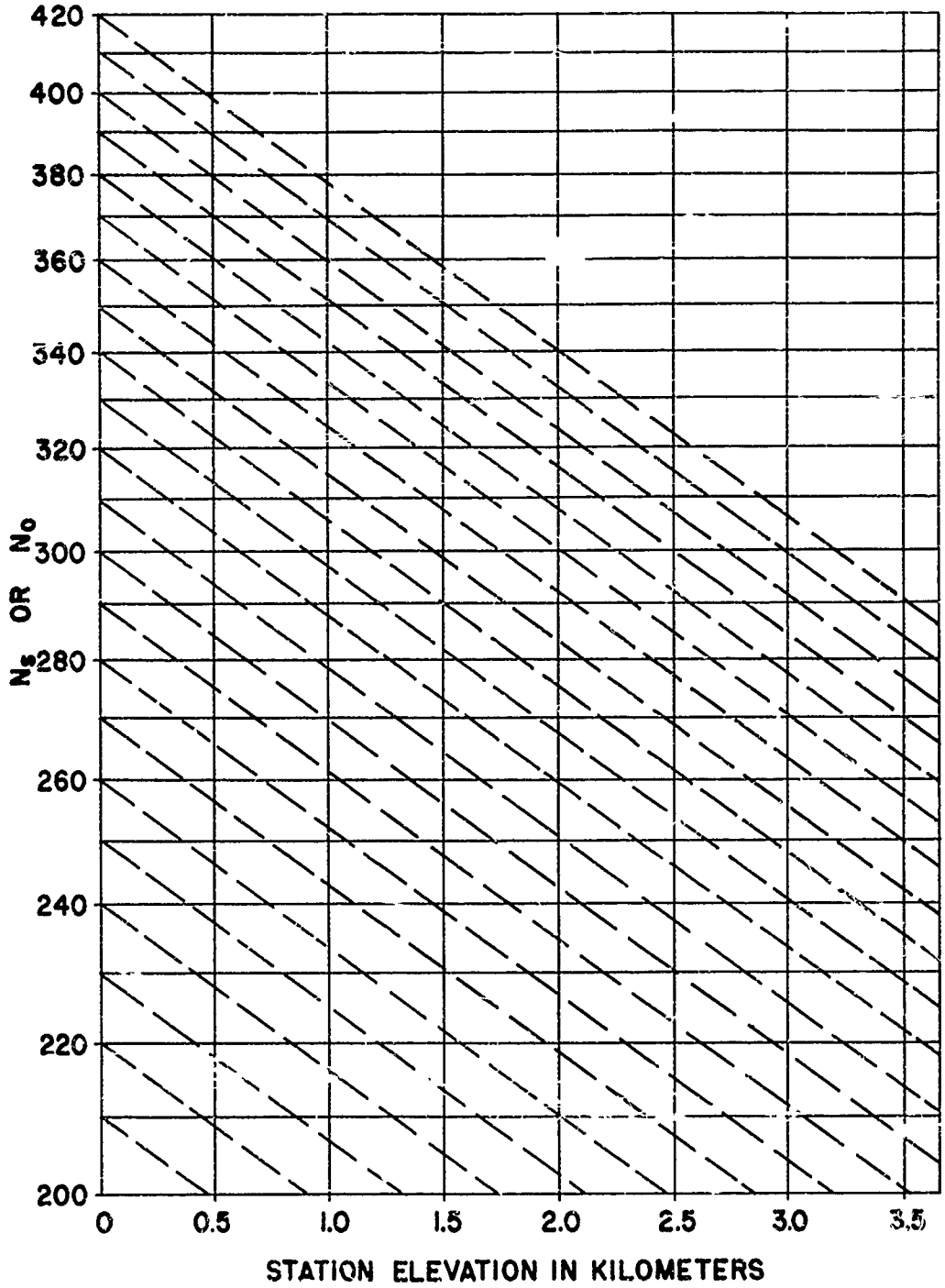

Figure 8.1. Chart for the Reduction of N_s-Values to N_o-Values.

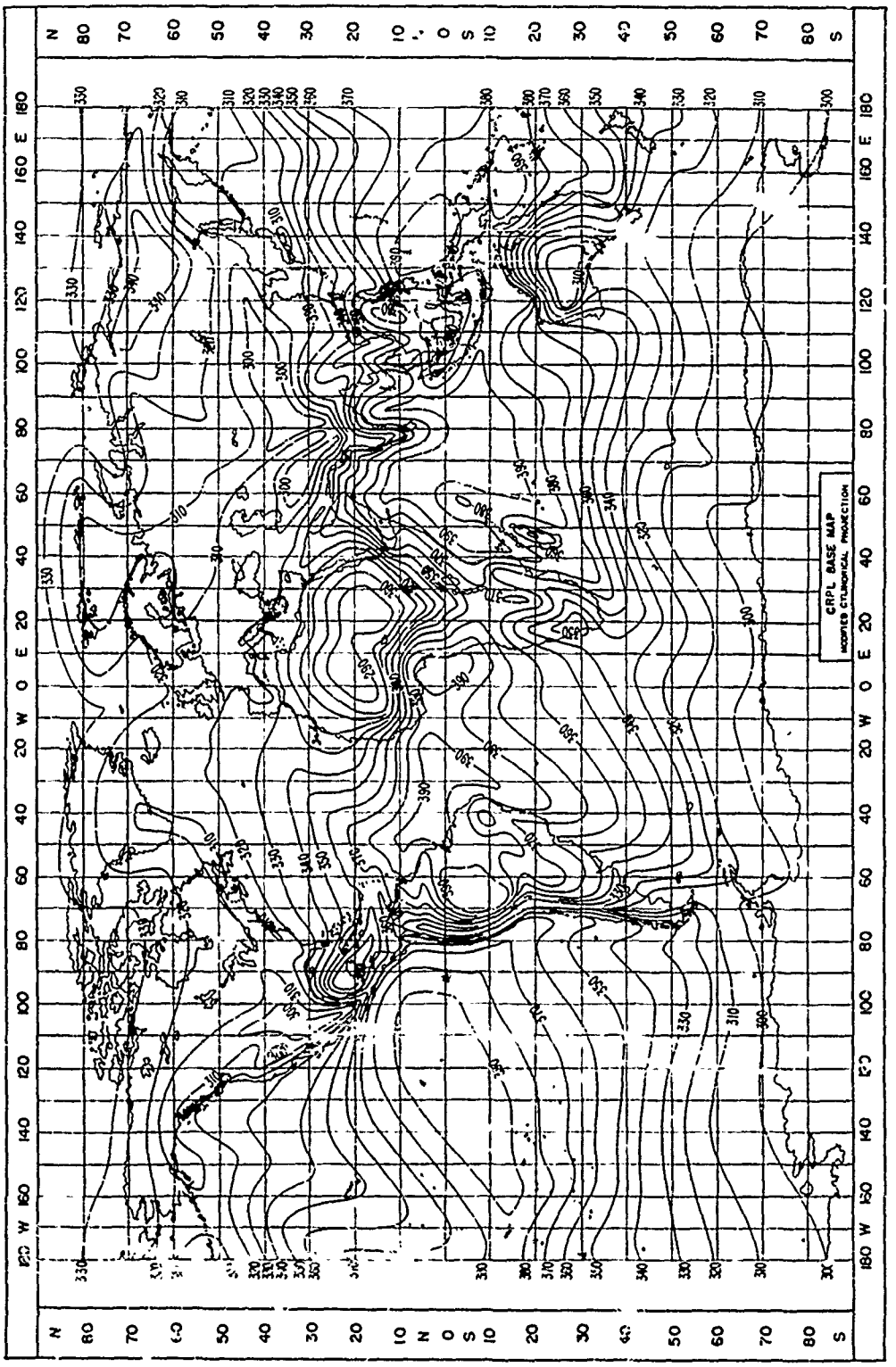

Figure 8.2. World-Wide Distribution of Datum Refractivity, N_0, for the Month of February.

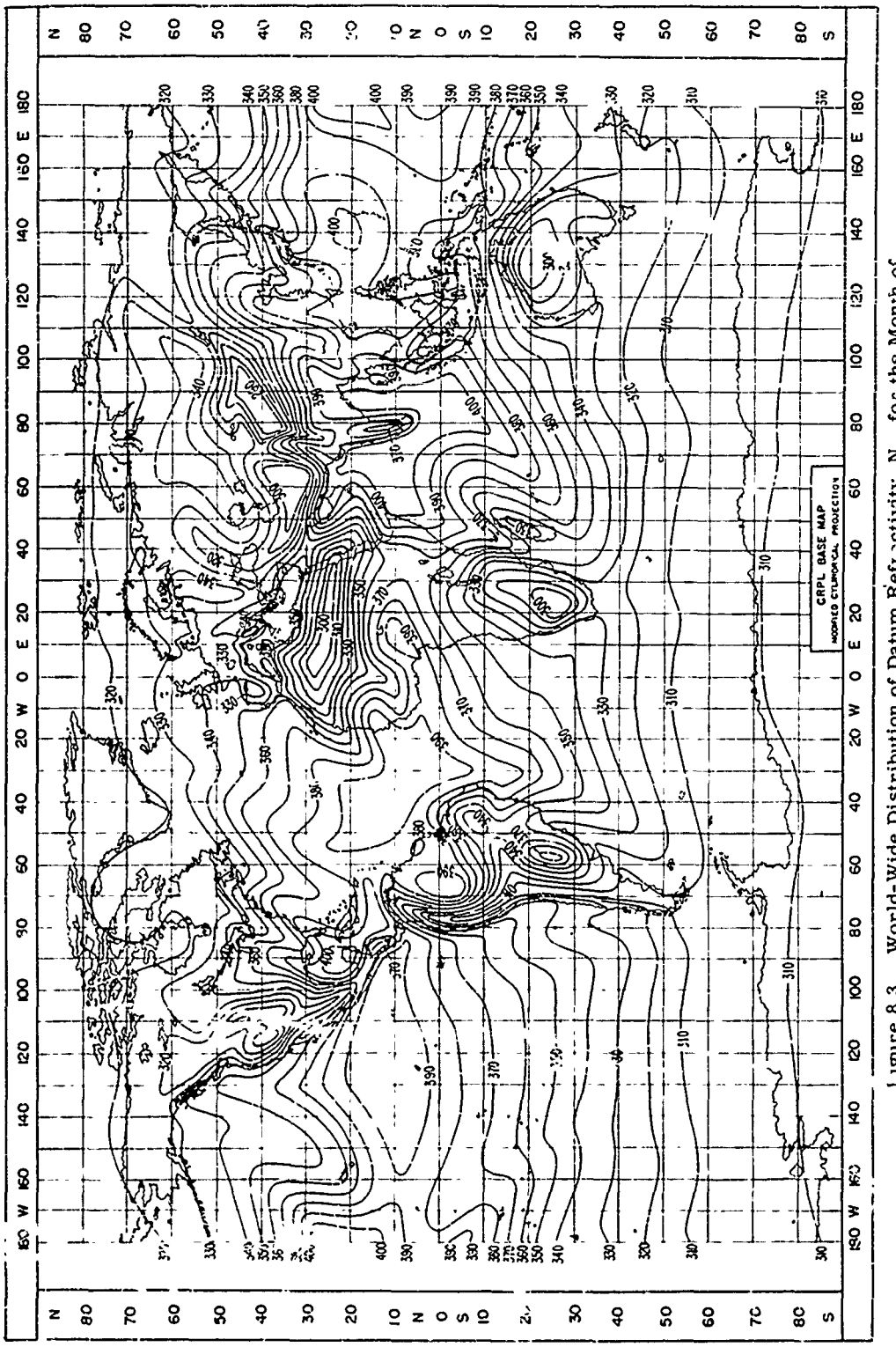

Figure 8.3. World-Wide Distribution of Datum Refractivity, N_0, for the Month of August.

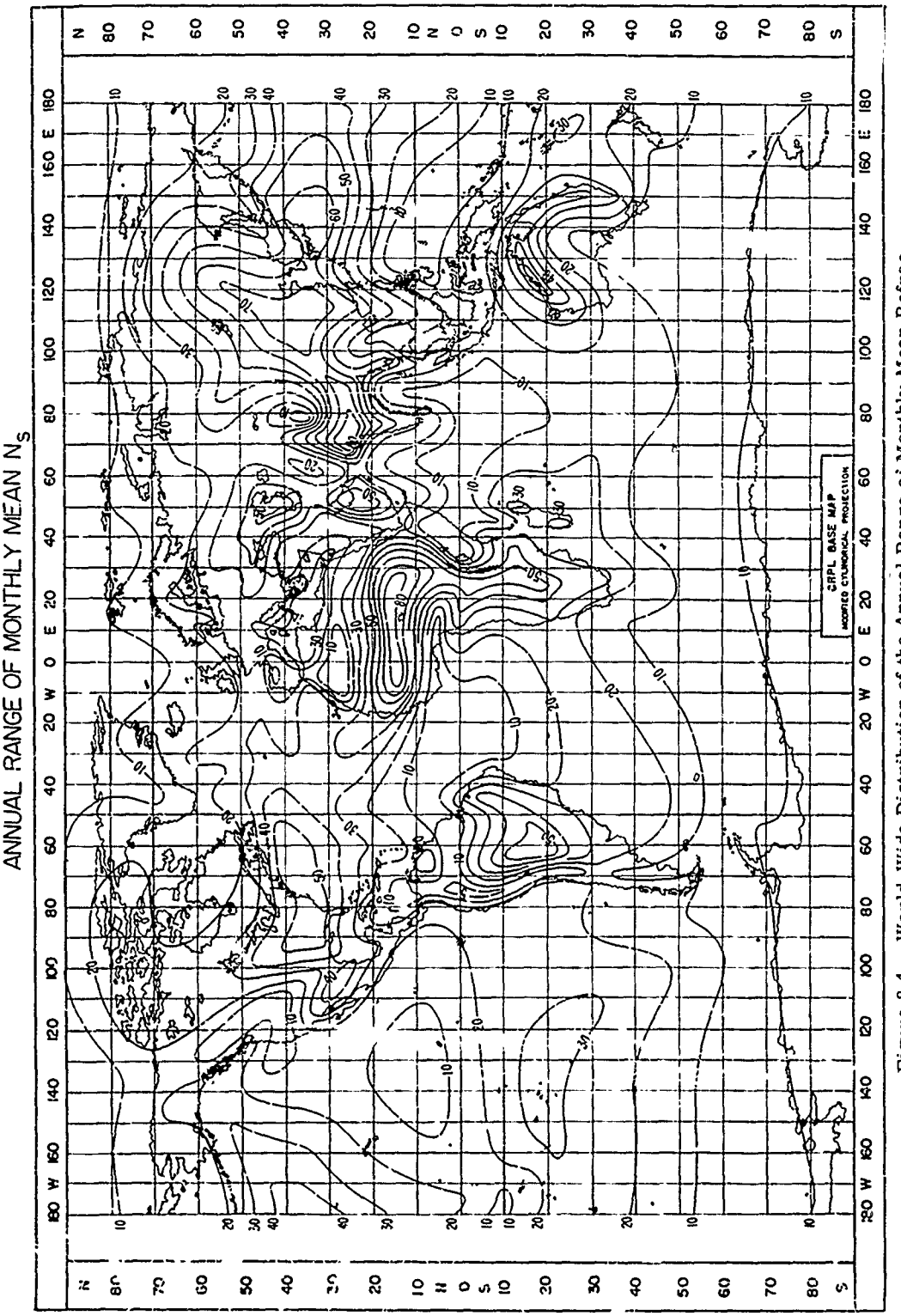

Figure 8.4. World-Wide Distribution of the Annual Range of Monthly Mean Refractivity at the Surface, N_S.

are acquired when air remains over a large source region, with uniform surface temperature and humidity conditions, until equilibrium is reached through the action of convection and radiative processes. Because refractive properties are also determined by the distribution of temperature and humidity, each air mass may be associated with characteristic refractivity values and profiles. These air mass characteristics will now be described.

Because it is desired to suppress the pressure-height variations in refractivity, the A-unit presentation of refractive index (see section 4.4.3) will be used in constructing all profiles. The profiles thus become more sensitive indicators of changes in temperature and humidity.

8.2.1 Continental-Arctic and -Polar Air Masses

Continental-arctic air masses are produced over the arctic (and antarctic) fields of snow and ice and over the snow-covered portions of the continents, where the wind systems are predominantly anticyclonic and large-scale subsidence is typical. Physical modification of continental arctic air as it moves southward over the continents changes it, by warming, into a continental-polar air mass in which the temperature regime is less severe.

The refractivity profiles of the two air masses, continental arctic and continental polar, are similar as indicated in figure 8.5, which shows representative profiles for both summer and winter. Continental polar air is characterized summer and winter by a profile showing a very slight increase in refractivity with height. Continental arctic air shows the same slight increase with height above one-half kilometer, but exhibits a sharp increase in the lowest levels above the ground. Large surface values in continental arctic air indicate extremely low ground temperatures characteristic of a pronounced arctic inversion.

When continental polar air is found away from its arctic source region (in the United States for example), it has usually been modified, and the strong surface inversion has been erased. A nearly linear profile, resembling the standard refractivity profile, results and superrefractive effects are reduced. On the other hand, ducting occurs relatively frequently near the ground in the arctic source region.

8.2.2 Maritime-Polar Air Masses

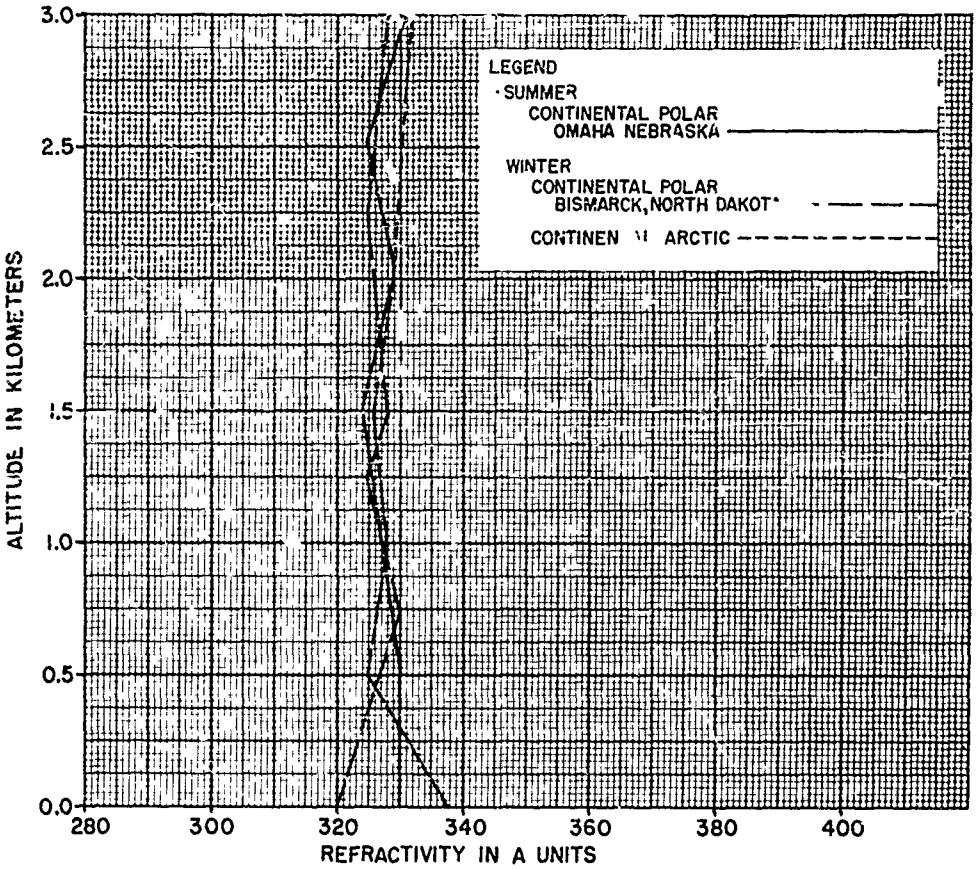

Figure 8.5. Representative Profiles for Continental Air Masses.

The maritime polar source region is in reality an oceanic zone of transition separating the tropical maritime source from the polar and arctic continental source. During the winter, maritime polar air over land exhibits a linear profile above about the 1-kilometer level with a decrease in refractivity in the lower layers (see fig. 8.6), due to the drying-out effects of an over-land trajectory. Summertime profiles over land and oceanic profiles show an increase in refractivity near the ground due to the addition of water vapor (at warmer temperatures).

As a consequence, winter profiles over land generally produce standard or even substandard refractive conditions, while summer and oceanic profiles tend to become superrefractive.

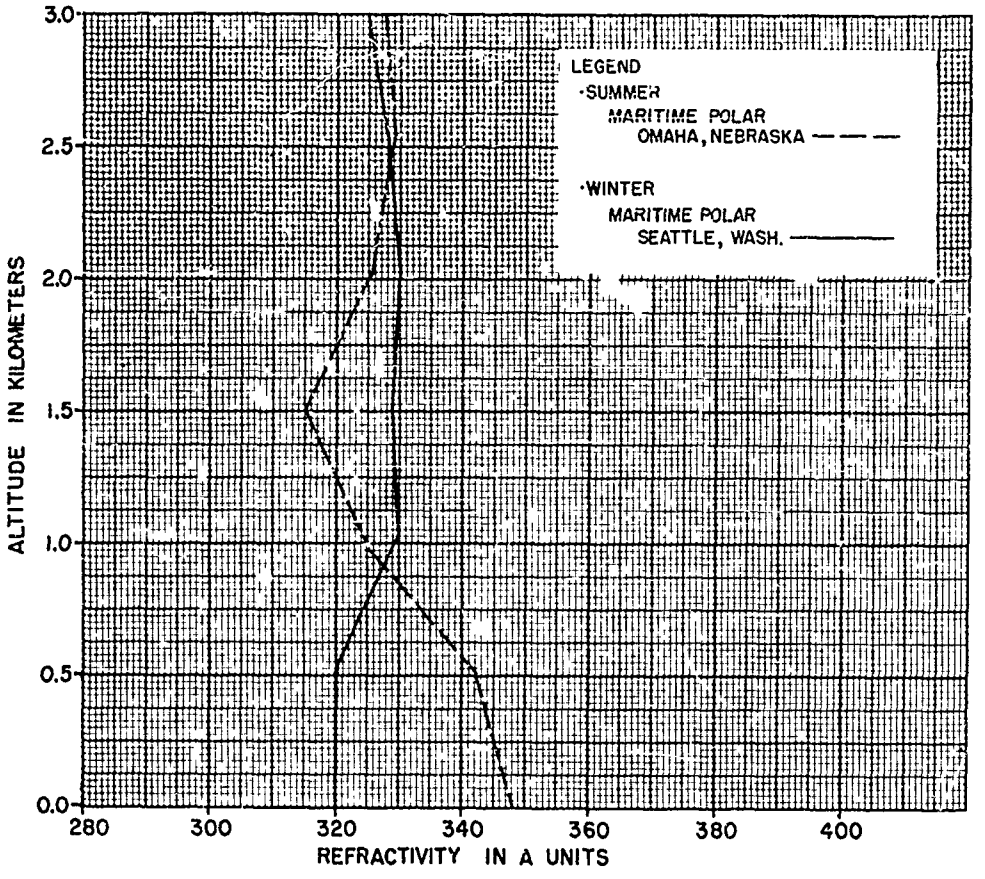

Figure 8.6. Representative Profiles for Maritime-Polar Air Masses.

8.2.3 Continental-Tropical Air Masses

Source regions for these air masses are found in the Northern Hemisphere over the large land masses of North Africa, Asia, southwestern United States, and southern Europe in summer; and over North Africa in winter.

Refractivity profiles for continental tropical air show a decided increase in refractivity with height and typically have surface values under 300 units, as shown in figure 8.7. A positive gradient of about 50 A-units per kilometer exists aloft. The extremely low surface refractivity values reflect the prevailing high temperatures, extensive vertical mixing, and extreme dryness typical of the desert source re-

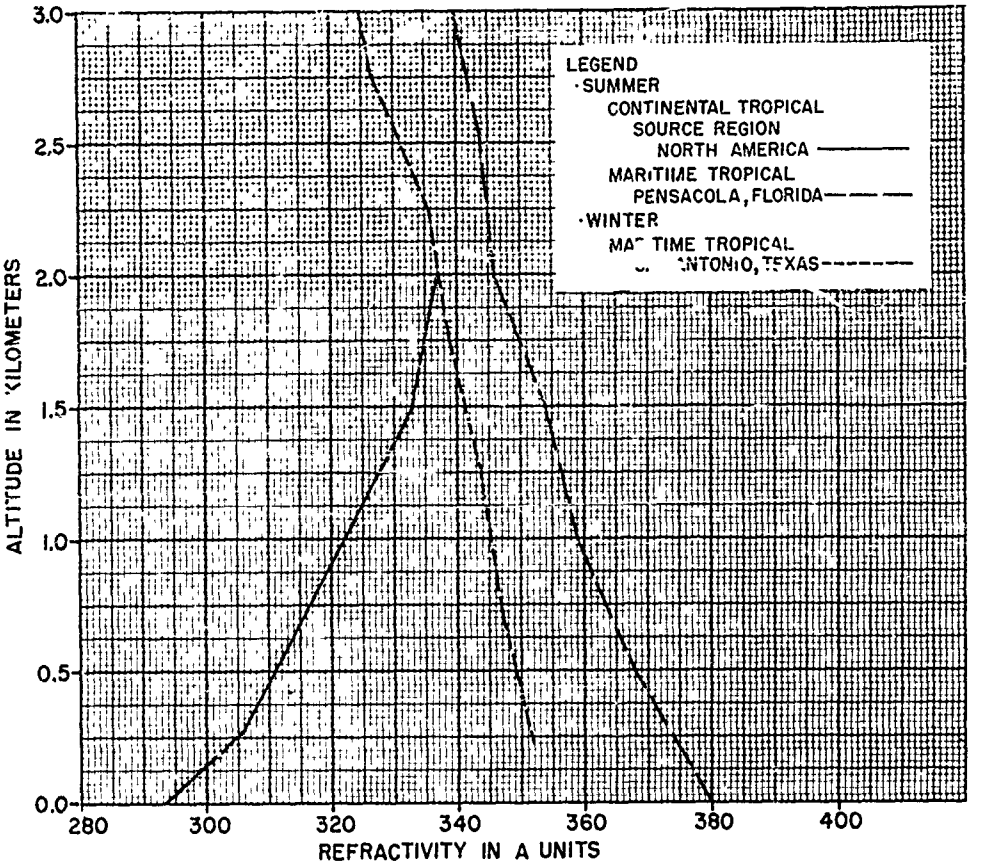

Figure 8.7. Representative Profiles for Tropical Air Masses.

gions of this air mass. Continuous subrefractive effects can be expected in continental tropical air in view of the large positive A-gradient.

8.2.4 Maritime-Tropical Air Masses

The maritime tropical source region comprises the oceanic areas on the equatorial side of the subtropical high-pressure belt in both hemispheres.

As shown in figure 8.7, profiles for this warm, humid air mass show a marked decrease in refractivity with height, often amounting to 40 A-units or more at the 3-kilometer level. Surface refractivity values are about 10 A-units higher in summer due to the increased insolation

over Northern Hemisphere source regions. Superrefractive effects can be expected within this air mass both summer and winter, but they can be expected to be more pronounced in summertime due to the increased water vapor gradient.

8.2.5 Superior Air Masses

Superior air is essentially a high-level air mass, although it may appear at the surface. It appears most frequently over the southwestern part of North America and is believed to be created largely by large-scale subsidence aloft.

This air mass is characterized by a near-linear profile, as shown in figure 8.8. A slight decrease of refractivity with height is evidenced

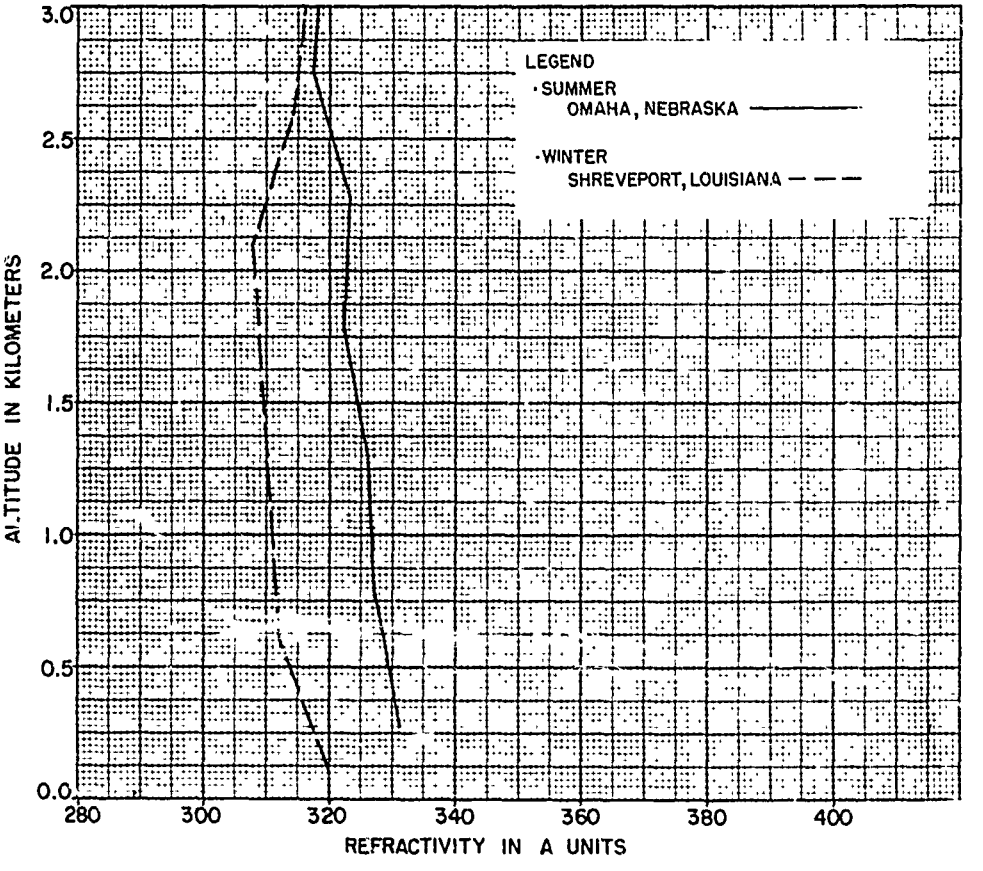

Figure 8.8. Representative Profiles for Superior Air Masses.

in most summer profiles. Winter profiles typically show about the same rate of decrease to the 2-kilometer level, above which a slight increase in refractivity is observed. Superior air mass profiles approximate the standard refractivity profile, with only a slight tendency toward superrefraction. Normal propagation at microwave frequencies can be expected within a superior air mass; ducting is most unlikely due to the dryness of superior air.

8.2.6 Air Mass Summary

In order to summarize the salient refractive characteristics of each of the several air masses discussed in the preceding paragraphs table 8.1 has been prepared for convenient reference.

TABLE 8.1

Air Mass	A-Profile Characteristics	Summer		Winter	
		N_o	A at 3 km.	N_o	A at 3 km.
Continental Arctic	Near-Linear (above surface inversion)	330	330	340	330
Continental Polar	Near-Linear	330	330	320	325
Maritime Polar	Near-Linear (above 1 km.)	340	330	320	330
Continental Tropical	Strong Positive A-Gradient	300	340	290	330
Maritime Tropical	Negative A-Gradient	380	340	360	330
Superior	Near-Linear	330	320	310	310

Typical Air Mass Refractivity Characteristics Between the Surface and 3 Kilometers.

8.3 Mechanisms of Air Mass Modification

We have described, in very general terms, the refractive properties of the six most commonly identified air masses. These properties are typical for each air mass in or near its source region. As an air mass moves from its source region it is modified by various physical mechanisms which come into play. In order to predict the probable characteristics of such a transient air mass we shall now discuss each mechanism in turn.

8.3.1 Radiation

An important physical process, producing nocturnal atmospheric stratification, is the continuous loss of energy by long-wave radiation from the surface. For an average earth temperature of 287° K. this radiation has its maximum intensity at 10 μ in the infrared portion of the electromagnetic spectrum. Most of this outgoing radiation is captured by the carbon dioxide and water vapor absorption bands in the atmosphere, so that the ground cools after sundown at a relatively slow rate. Through conduction and convection processes the air layer next to the ground also loses heat. An inversion layer several hundred meters thick may be produced in this fashion. Conditions favoring the formation of strong nocturnal radiation inversions are clear skies, low humidity, and light surface winds. Large humidity gradients are also common in radiation inversions, so that superrefractive conditions and, occasionally ducting, result from the large negative refractivity gradients produced.

Over ocean surfaces the effects just described do not occur to any appreciable extent since as surface water cools, it becomes heavier, sinks, and is replaced by warmer water from below the surface. Thus, ocean surface temperatures do not vary appreciably from day to night.

8.3.2 Turbulence and Convection

During the day surface heating is produced by insolation. Surface heating is at a maximum on hot, clear, summer afternoons when the ground may reach temperatures of 70°C. and higher, as shown by Sinclair [21]. The atmosphere above this superheated ground surface is warmed by conduction and small-scale convection. Eventually, superadiabatic gradients are produced in the air layer above the ground, and overturning occurs. This process, together with the turbulence created by winds moving over rough land surfaces, produces large-scale atmospheric mixing which tends to destroy vertical stratifications. Accordingly, standard or subrefractive profiles are the rule during daytime hours over land areas with clear skies and/or where the terrain is rough and moderate to strong winds exist.

As in the case of radiational cooling, the effects described above are not observed over ocean surfaces. Insolation striking a deep water surface is not absorbed in a shallow surface layer but rather, penetrates to moderate depths. Thus, the surface temperature, together

with that of a thick layer of water, is raised only slightly. Also, the roughness coefficient of even heavy seas is small compared to that of most land surfaces.

8.3.3 Subsidence

Subsidence is defined as a large-scale downward motion superimposed on the horizontal air motions in the atmosphere. Its occurrence is common in the eastern portions of the semiperma[illegible] anticyclones of the Northern Hemisphere. The lower limit of subsidence is well defined, and the base of the subsiding layer is usually found between 800 and 900 millibars. The subsiding air is warmed by compressional heating and is characterized by a temperature inversion and a large dew point depression, as shown by Petterson, Sheppard, and Priestly [17]. Since the air below the subsidence layer is usually moist, excellent conditions for the formation of superrefractive layers aloft are present. The California coast of the United States, under the eastern end of the Pacific anticyclone, is noted for the persistence of superrefractive, elevated layers during the summer months.

8.3.4 Evaporation and Condensation

The addition of water vapor from a warm water surface to overlying cold air, takes place rapidly because of the higher vapor pressure of the water surface. At the outset of this process, shallow superrefractive or ducting layers may be formed close to the surface. However, as the evaporation process continues and the moisture has been mixed through a fairly thick layer (by convective processes) the uniform distribution of moisture precludes the formation (or maintenance) of superrefractive layers.

Such evaporative effects may also occur inland when a cold, dry air mass moves over moist soil or heavily vegetated areas. The Florida Everglades, for example, have about the same evaporation rate as the ocean.

8.3.5 Advection

An air mass moving over a surface of dissimiliar physical characteristics (warmer, cooler, wetter, dryer) will be modified through the action of surface heating or cooling, convection, evaporation, etc. The results to be expected in any particular case may be deduced from

the discussion given in the preceding paragraphs and are discussed in considerable detail in NAVAER 50-1P-527 [8].

8.4 Climatology of Ground-Based Ducts

For the purposes of this section atmospheric ducting (trapping) is defined to occur whenever geometrical optics indicates that a radio ray leaving the earth's surface is sufficiently refracted that it eventually travels back toward or parallel to the earth's surface. This criterion has been applied by Bean [2] to several years of radiosonde observations from stations typical of polar, temperate, and tropical climates in order to derive estimates of the variation of the occurrence of radio ducts with climatic conditions.

Approximately 3 years of radiosonde data typical of a polar climate (Fairbanks, Alaska), a temperate climate (Washington, D. C.), and a tropical climate (Swan Island, W. I.) were examined by means of a digital computer for the occurrence of ducts during the months of February, May, August, and November. The percentage occurrence of ducts is shown in figure 8.9 for these three locations. The maximum occurrences of 13.8 percent for August at Swan Island and 9.2 percent for Fairbanks in February are significantly greater than the values observed at other locations and times of the year. The Washington data display a summertime maximum of 4.6 percent. These data indicate that the tropical zone, maximum incidence occurs in late summer and is nearly three times the temperate zone, summertime maximum; while the arctic zone maximum occurs in midwinter and is about twice as large as the temperate maximum.

The results of an analysis of refractivity gradients observed during ducting are given in figure 8.10. The maximum gradient of 420 N-units per kilometer was observed during February at Fairbanks, Alaska; with a value of 396 N-units per kilometer observed during August at Washington, D. C. The gradient observed during ducting at Swan Island, W. I. reached a maximum (285 N-units per km.) both during August and November. The annual mean values of N-gradient appear to show a small latitudinal trend from a high value of 230 N-units per kilometer at Fairbanks to a value of 190 N-units per kilometer at Swan Island.

Another property of radio ducts is their thickness; typical thickness values are shown in figure 8.11. Again a small latitudinal trend is observed as the median thickness increases from 66 meters at Fair-

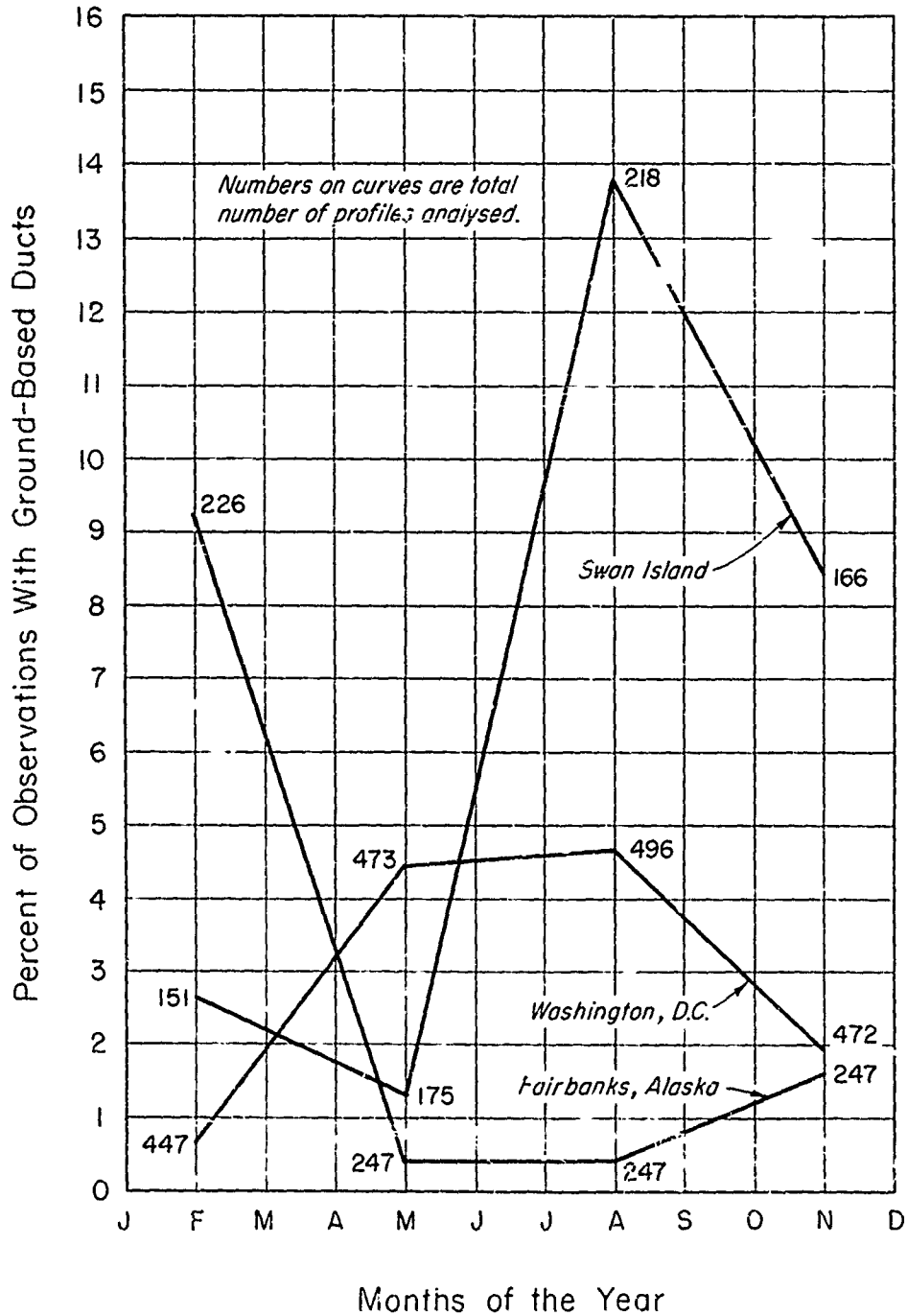

Figure 8.9. Frequency of Occurrence of Ground Based Ducts.

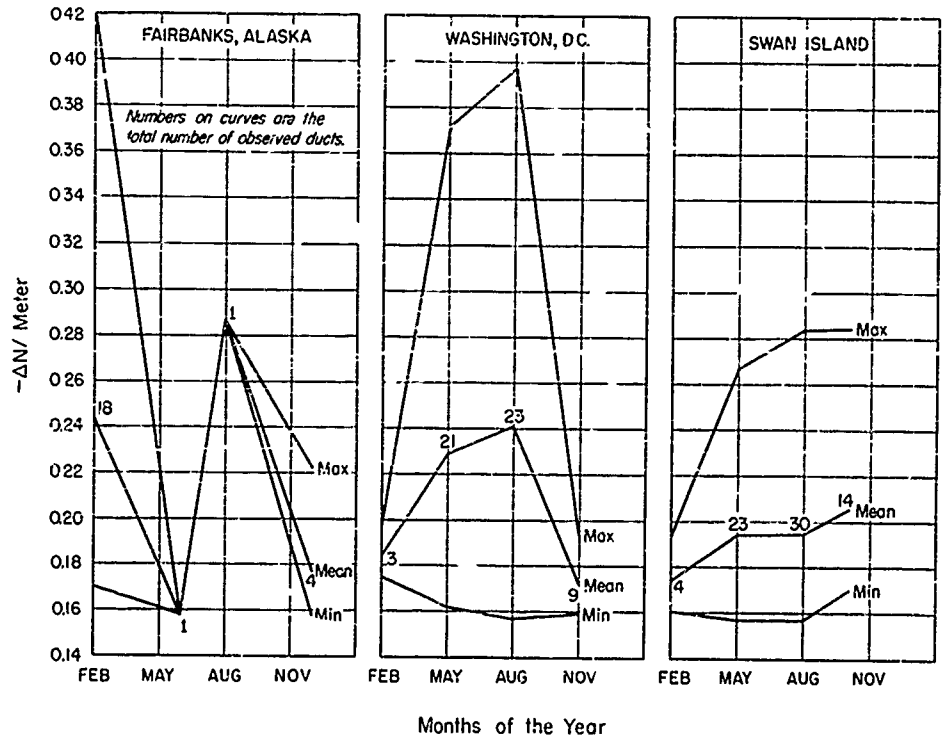

Figure 8.10. Typical Refractivity Gradients of Ground-Based Ducts.

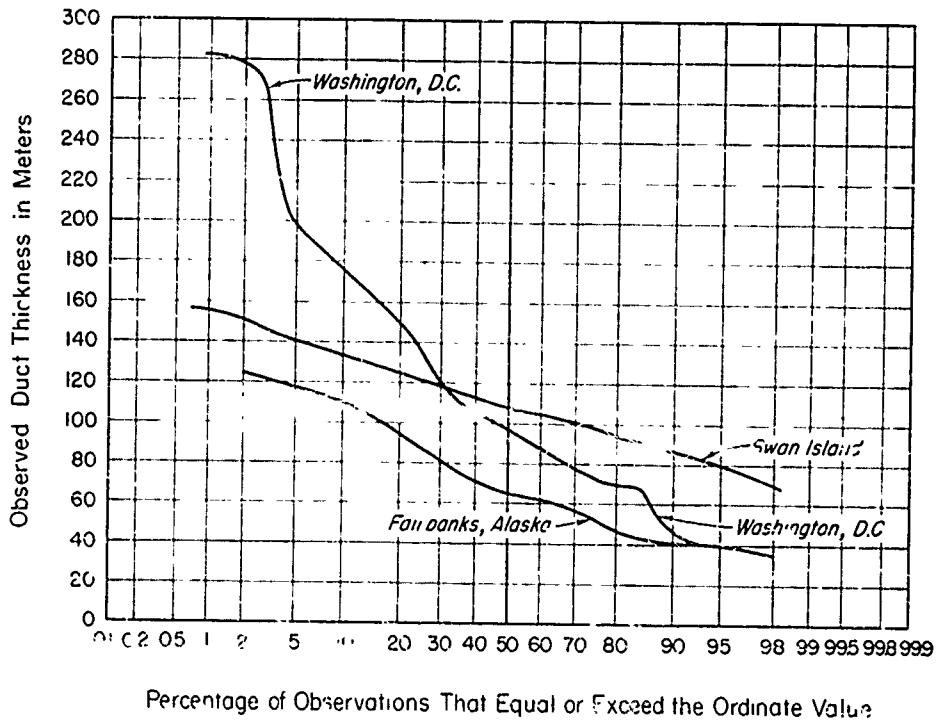

Figure 8.11. Observed Ground-Based Duct Thickness.

banks to 106 meters at Swan Island.

We may summarize the data of figures 8.10 and 8.11 by saying that polar climates (Fairbanks) are characterized by shallow layers with relatively intense gradients, tropical climates (Swan Island) are characterized by thick layers with relatively weak gradients, and temperate climates (Washington, D. C.) lie in between.

It is interesting to consider the temperature and humidity distribution that accompanies a radio duct. An example typical of each station is given in figure 8.12. The polar duct illustrated was accompanied by a surface temperature of -25°C. with a strong temperature inversion and a slight humidity lapse, indicating an inversion associated with wintertime cooling of the air next to the ground. The temperate example appears to be typical of a temperate zone, temperature inversion. The tropical profile, however, shows a moderate lapse of both temperature and humidity. This apparent inconsistency is explained by the strong lapse in vapor pressure which is associated with a moderate lapse in temperature and humidity when the surface temperature is near 30°C. This strong, vapor pressure lapse presumably arises from evaporation from the sea surface.

The structure of ducts was further examined by studying the percentage of the total N-gradient in each duct, contributed by the gradient of the "dry" and "wet" terms. The median contribution of the "dry" term gradient, summarized in table 8.2, displays strong seasonal and

TABLE 8.2

Month	Fairbanks (Polar)	Washington, D.C. (Temperate)	Swan Island (Tropical)
February	103%	73.0%	9.5%
May	40.5%	33.5%	2.0%
August	37.0%	26.5%	4.5%
November	62.0%	55.0%	6.0%

Median Contribution of $\frac{\Delta D}{\Delta h}$ to $\frac{\Delta N}{\Delta h}$ for Ducting Conditions.

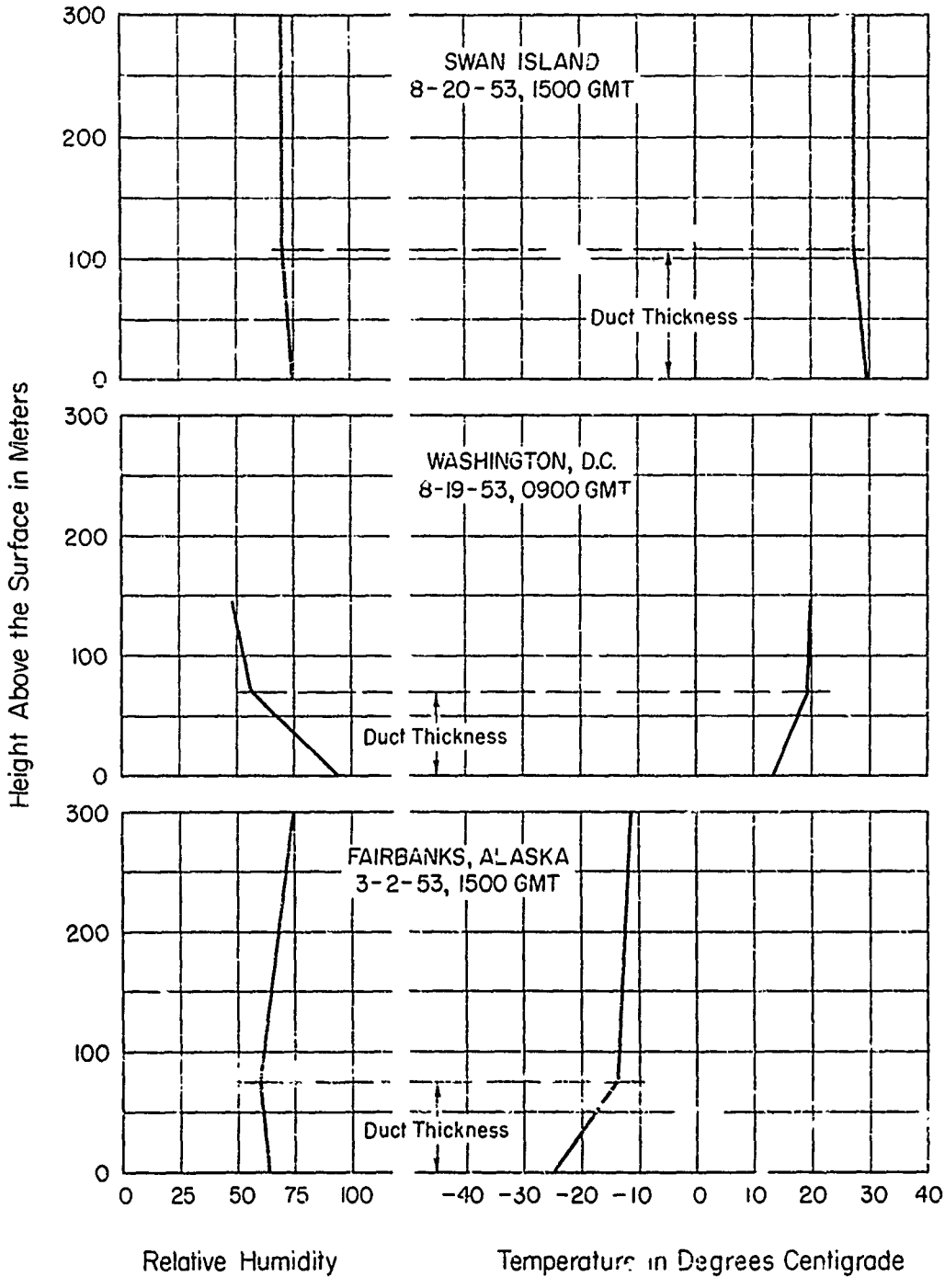

Figure 8.12. Temperature and Humidity Profiles for Typical Ground-Based Ducts.

geographic differences. The "dry" term contribution decreases from winter to summer and from arctic to tropical climates. The tropical ducting gradients are then at least 80 percent due to humidity lapse, while the polar wintertime maximum is due to the strong temperature inversion which is associated with very low surface temperatures. In fact, under these conditions vapor pressure increases with height, and the dry term contributes more than 100 percent of the ducting gradient.

8.5 Climatology of Superrefractive Elevated Layers

Although no systematic study of elevated layers has been completed on a scale large enough to support statistically valid conclusions, a few general statements may be made. The great majority of all strong, superrefractive, elevated layers are associated with subsidence in the atmosphere. Since subsidence involves an adiabatic process, a given layer may, therefore, be associated with a certain, constant potential temperature. In other words, the layer is in an isentropic surface. This concept may be used operationally to estimate the horizontal extent of strong superrefractive layers by indicating the particular heights most likely for layer occurrence at points removed horizontally from the known sounding. It must be remembered, however, that the existence of the "same" potential temperature alone is not sufficient evidence for extending an elevated layer horizontally into "unknown" areas; other considerations must also indicate a "good" probability for its existence.

In maritime-polar air masses over the western Atlantic and North Pacific, the boundary between the moist, lower, mixed layer and the unmodified, dry, upper layer can frequently become an elevated superrefractive layer. When the existence of such a layer has been established by measurement, the tops of the convective clouds in the mixed lower layer can be assumed to be at the height of the layer base.

9. SYNOPTIC STUDIES OF REFRACTIVE PROPERTIES

As indicated in the introduction, no practical techniques exist which will permit one to make useful predictions of the refractive state of the atmosphere beyond a 6- to 12-hour range. For such "short" periods one may properly, either assume no change in measured conditions, or predict trends in the modification of observed refractivity profiles expected as a result of forecast meteorological changes.

One approach to the problem of longer-range refractivity forecasting lies in the direction of predicting the detailed pressure, temperature, and humidity structure at several points within the area of interest, and from these predictions calculate the required refractivity profiles. The precision realized in 12- to 36-hour forecasts of P, T, and RH with present-day methods is not sufficient to produce useable refractivity predictions for these forecast intervals. This approach, for periods in excess of 18 hours, can be expected to lie beyond the "state of the art" for many years to come.

Another approach would be to attempt to develop 3-dimensional models of refractivity which could be directly associated with the classical synoptic features (fronts, highs, lows, etc.) and which would be sufficiently representative of the real refractive situation to permit useful forecasts to be made from a knowledge of expected synoptic developments. In order to explore this approach to the refractivity forecasting problem, a detailed case study has been completed by Horn, Bean, and Riggs [15] and is described in the following paragraphs.

9.1 Analysis of the Storm of 18-21 February 1952

A wintertime storm, displaying strong contrasts of continental polar and maritime tropical air, was chosen for study of the refractivity model problem. This particular storm commenced with an outbreak of polar air across the Great Plains from the 18th to the 21st of February 1952, during which time a pronounced cold front developed and moved rapidly across the United States.

9.1.1 Description of the Synoptic Development

At the start of the period a frontal system had come in from the Pacific Northwest and was composed of a cold front extending from

northern Utah southward into Arizona, with a stationary front extending northeastward into Wyoming. This frontal system had moved very slowly for several days prior to the start of the sequence. With a fresh outbreak of polar continental air east of the Rocky Mountains this old front became more active and (moving ahead of the fast-moving, polar continental front sweeping across the Great Plains) was reported as a squall line by the time it crossed the Mississippi River early on the morning of the 20th of February. During the latter part of the period the polar-maritime cold front/squall line was located in the developing warm sector of the polar-front wave. The entire frontal ensemble of cold front, polar-front wave, and squall line had moved rapidly to the east coast by the morning of the 21st, which is the last day of the period studied.

This storm sequence is a rather well developed one, with strong temperature and humidity contrasts between the air masses within the warm sector and behind the cold front. The existence of this strong contrast was one of the main reasons for studying this particular period, because if refractivity is not a good synoptic indicator in this case there is little hope of its being one in more subtle synoptic disturbances.

9.1.2 Datum Refractivity (N_0) Analysis

In order to supress the effects of topography, the datum refractivity, $\underline{N}_0$, (see section 8.1) has been used as the refractive parameter plotted in all horizontal analyses. Charts of $\underline{N}_0$ were prepared from surface observations taken every 12 hours from 0130 EST, February 18 until 1330 EST, February 20, 1952, or, in other words, every 12 hours during the period studied. These $\underline{N}_0$ charts are presented in figures 9.1 through 9.6. Each chart shows the $\underline{N}_0$ field with the U. S. Weather Bureau frontal analysis (surface) superimposed; conventional frontal symbols have been used in these figures. The cold front which originally extended from Utah southward appears to be rather weak, since it is not associated with an appreciable N_0-change across the front. In the early stages of our sequence the lack of air mass contrasts is evidenced by the slight change in the position of the 290 N_0-contour (encircling the west Texas and New Mexico area) as the frontal system moves through that area. By comparison, the cold front which later sweeps down across the Great Plains has a rather marked N_0-gradient across the front; due in large measure to the northward flow of warm, moist air into the warm sector, which had formed by 1330 EST on the 19th. It is perhaps significant that the N_0-contours show the various frontal

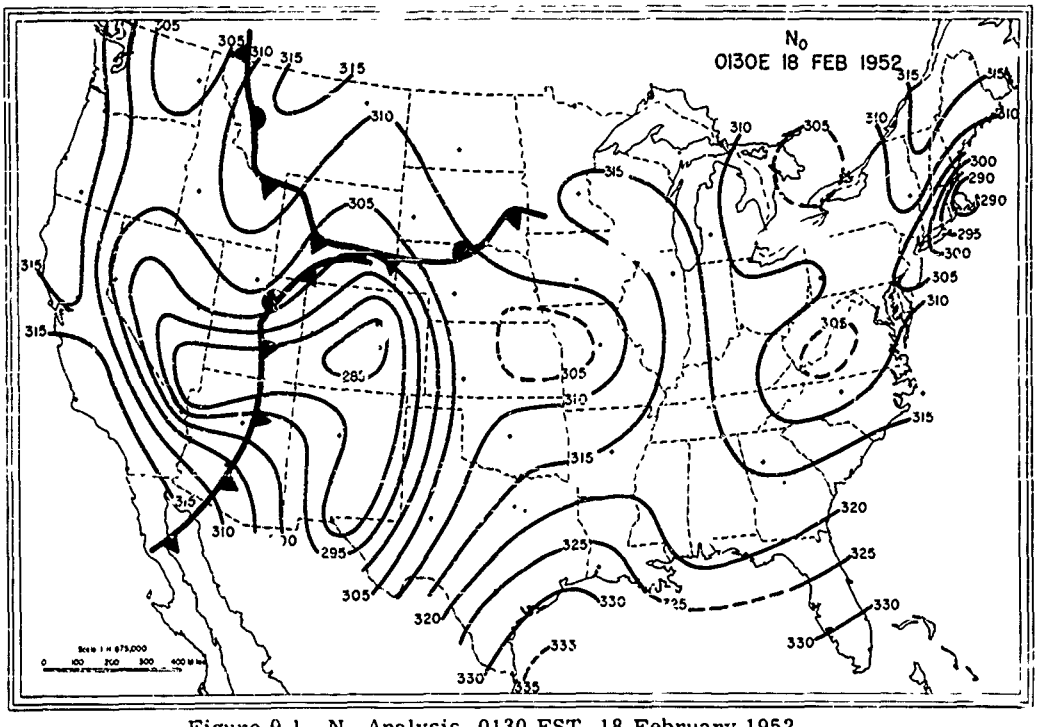

Figure 9.1. N_0 Analysis, 0130 EST, 18 February 1952.

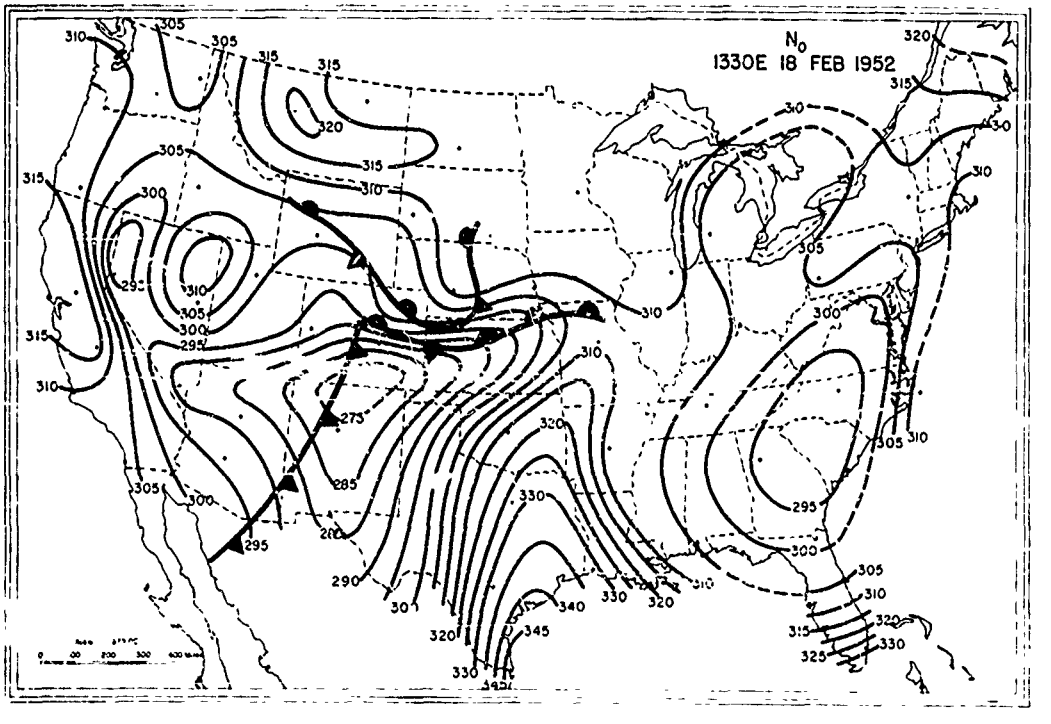

Figure 9.2. N_0 Analysis, 1330 EST 18 February 1952.

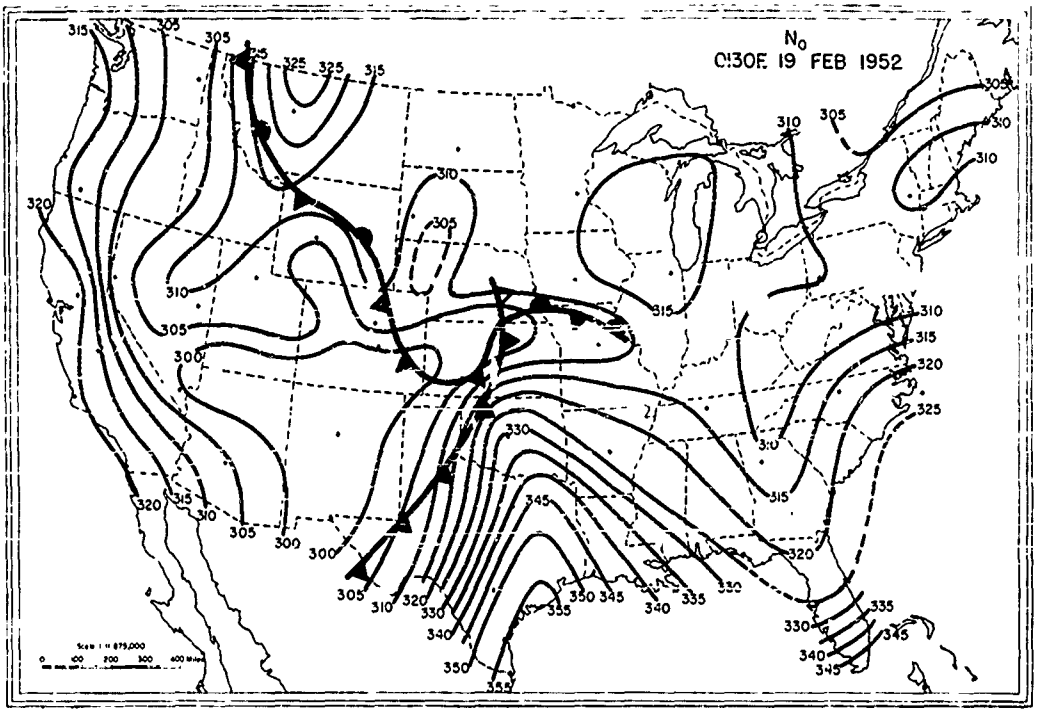

Figure 9.3. N_0 Analysis, 0130 EST, 19 February 1952.

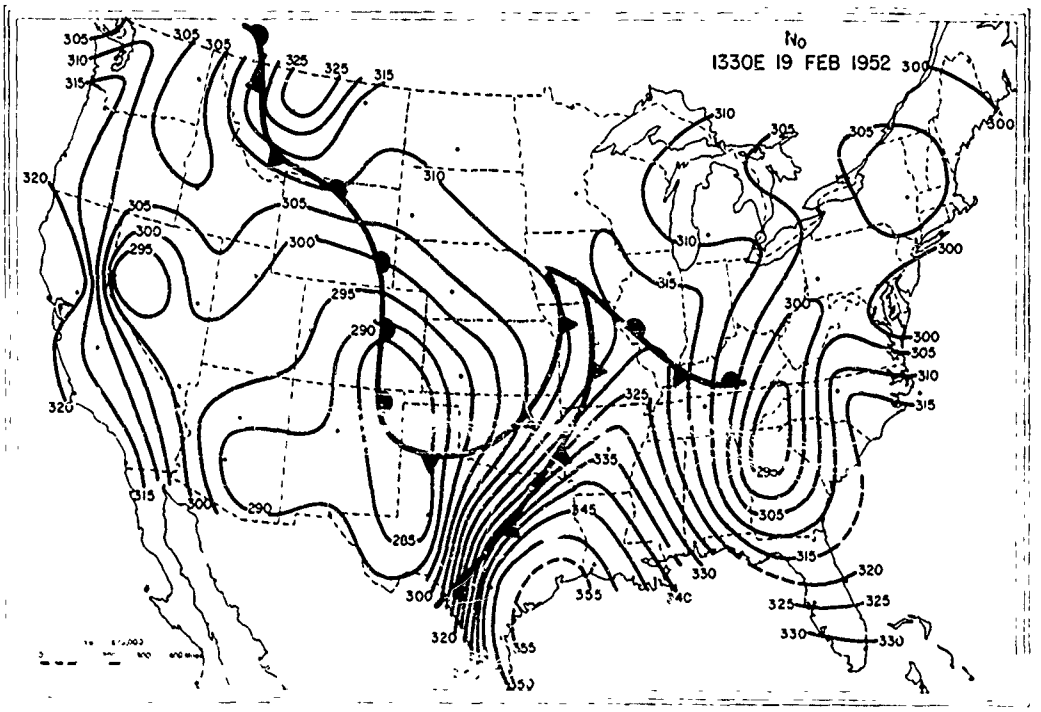

Figure 9. . N_0 Analysis, 1330 EST, 19 Feb ary 1952.

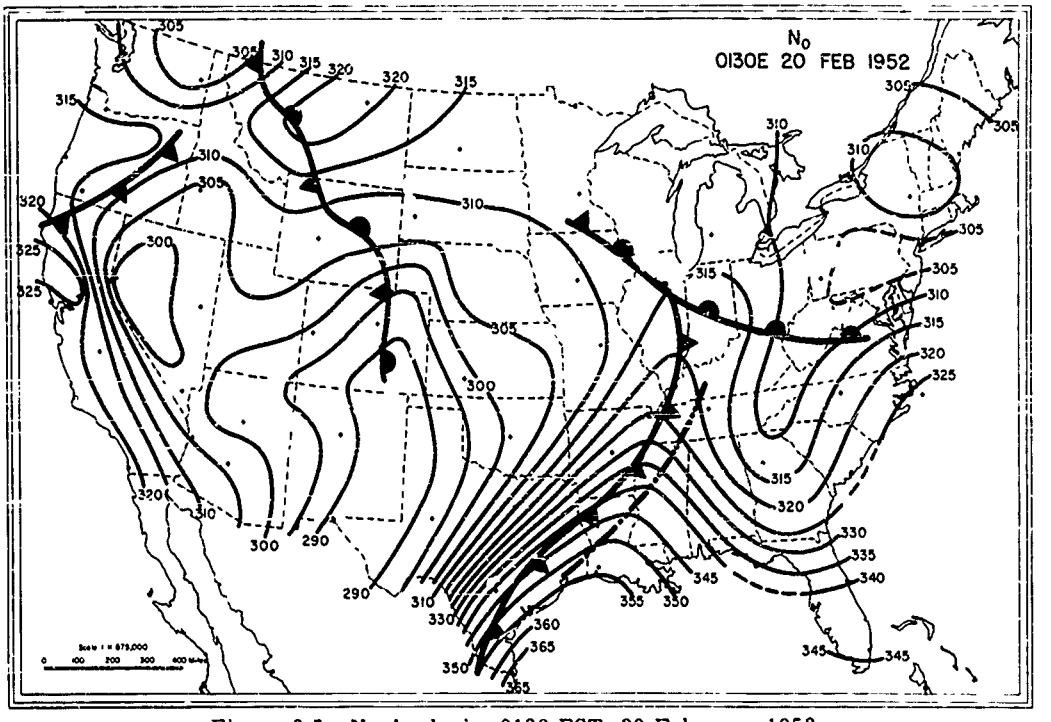

Figure 9.5. N_0 Analysis, 0130 EST, 20 February 1952.

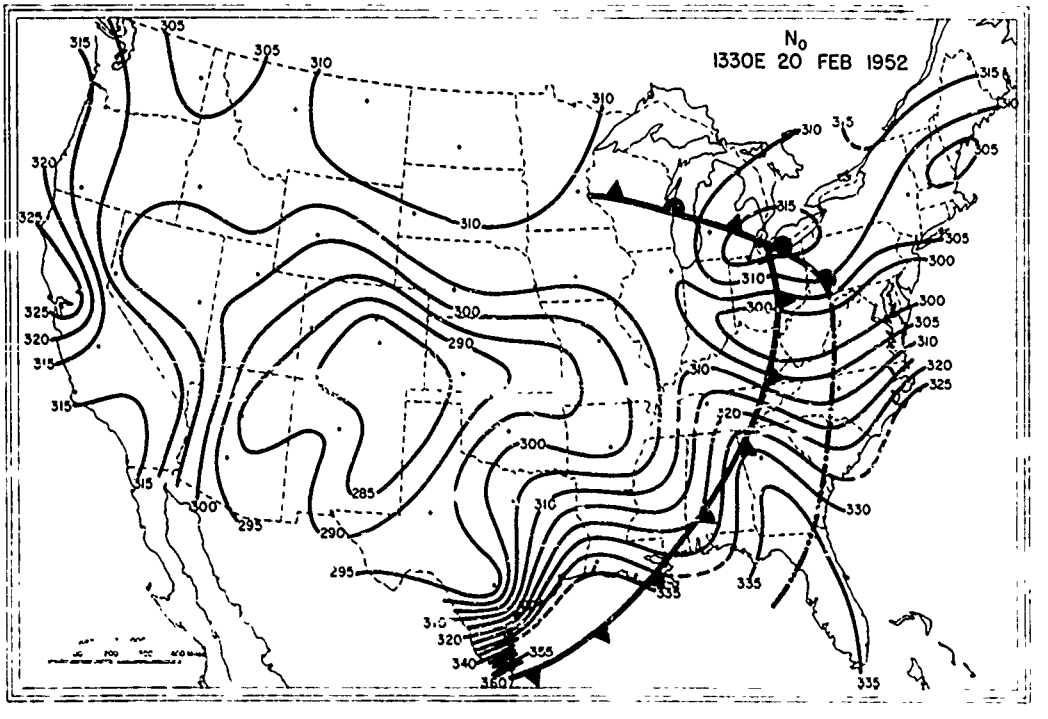

Figure 9.6. N_0 Analysis, 1330 EST, 20 February 1952.

systems as transition zones rather than as sharply defined discontinuities.

Figures 9.1 through 9.6 appear to indicate that $\underline{N}_o$ does reflect frontal system changes and that, with extensive studies of many cases, a system of direct objective forecasting from this parameter might be developed. Although this conclusion is based on a study of a single storm, it appears to be borne out by preliminary analysis of other frontal systems.

9.1.3 Vertical Cross Section A-Unit Analysis

Another aspect of this case study is illustrated in a series of charts displaying vertical cross sections of the storm of 18-21 February 1952 in terms of A-units, which are largely free from a pressure-height dependency (see section 4.4.3). The height distributions of refractivity along the base line of the particular cross section shown in figure 9.7 were computed for every 12 hours during the 4-day period. Examples representing the early, mature, and late stages of the outbreak are reproduced as figures 9.8, 9.9, and 9.10. At the outset of the period of observation, the A-unit gradient was quite flat around the polar front. By 1000 EST on the 18th of February, figure 9.8, the polar front was located midway between Glasgow, Mont. and Dodge City, Kans. The contrast between the southerly extension of polar air and the northerly advection of tropical maritime air, from the Gulf of Mexico into the developing warm sector of the polar-front wave, is evidenced by the relatively large A-gradients in the vicinity of Dodge City. The core of tropical maritime air has evidently not progressed far enough northward to displace the warm but dry air that had been over the Great Plains prior to the outbreak. As a result, a region of low A-values is found between the front and the tropical maritime air. Twenty-four hours later, figure 9.9, the core of tropical maritime air has become more extensive and now reaches to an altitude of 3 kilometers. A second cold front was now reported on the daily weather map, and the area of low A-values is confined between it and the main cold front. Finally, by the morning of February 20, figure 9.10, the front has passed to the south of Lake Charles, La. and the polar air just behind the front is characterized by relatively low A-values.

9.1.4 Epic Chart Analysis

The use of space cross sections does not always yield measure-

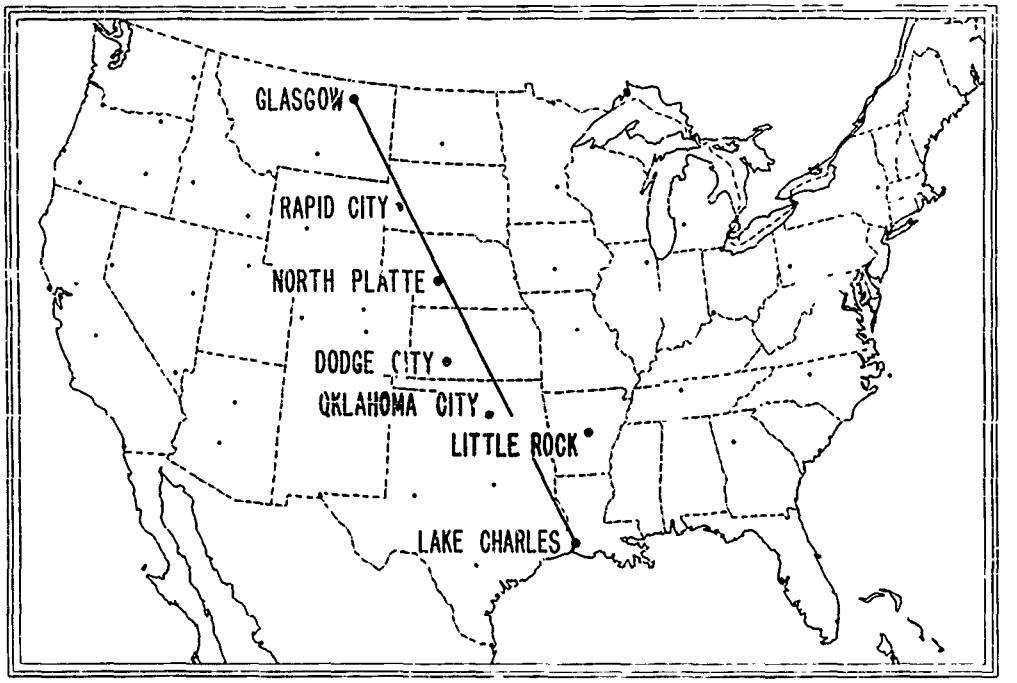

Figure 9.7. Location of Cross-Section.

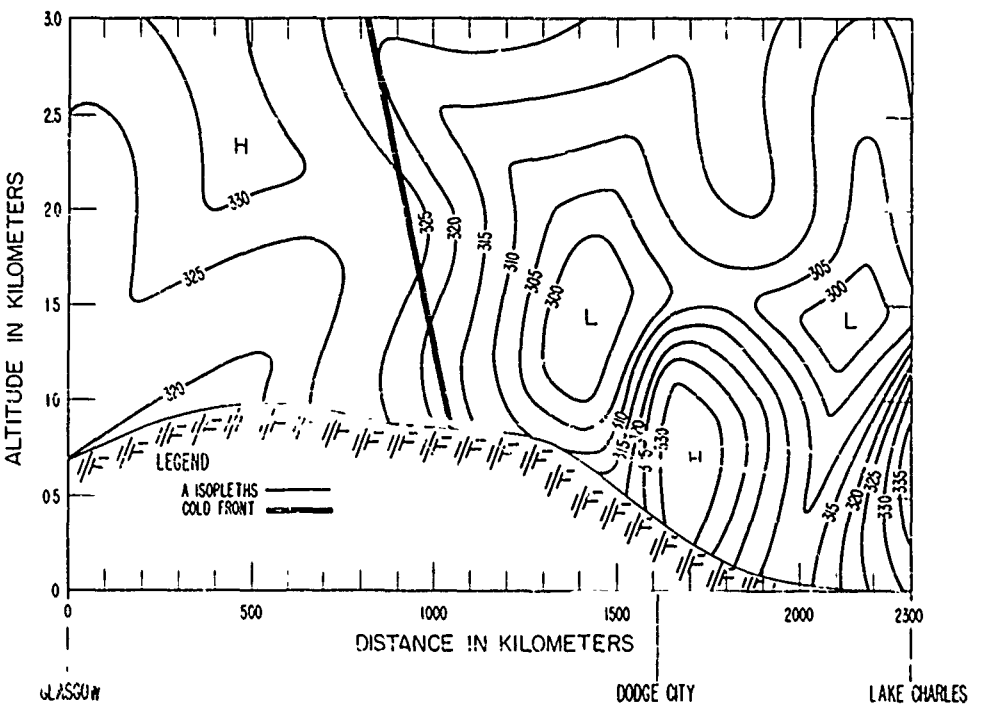

Figure 9.8. Space Cross-Section in A-Units, 1000 EST, 18 February 1952.

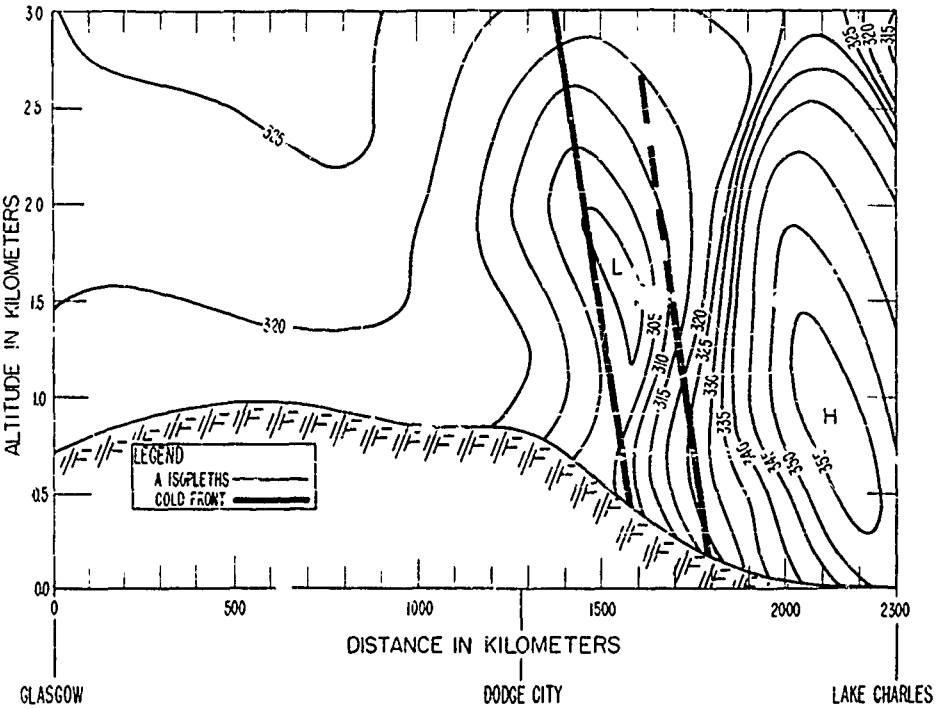

Figure 9.9. Space Cross-Section in A-Units, 1000 EST, 19 February 1952.

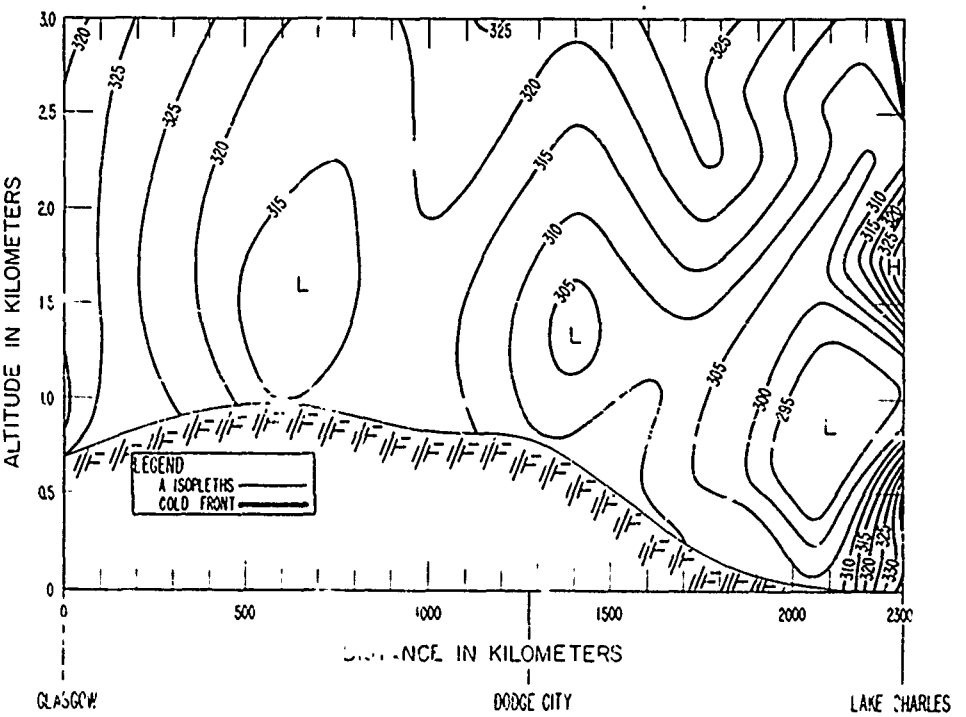

Figure 9.10. Space Cross-Section in A-Units, 1000 EST, 20 February 1952.

ments at the most desirable points along a frontal interface. Another method of determining the refractive index structure in a frontal zone is to construct a time cross section from the series of radiosonde observations taken at a single station. Thus, as the frontal system advances and passes over the station, one obtains a time-history of the structure of the frontal zone. Such cross sections may be drawn using time, or the distance from the station to the front (at the surface), as abscissa. In the latter case, the presentation is referred to as an epic chart since the observations are normalized with respect to the frontal passage. Epic charts are illustrated in figures 9.11 and 9.12. Figure 9.11 represents a typical continental station located in the polar continental air throughout the storm sequence under study. The essential

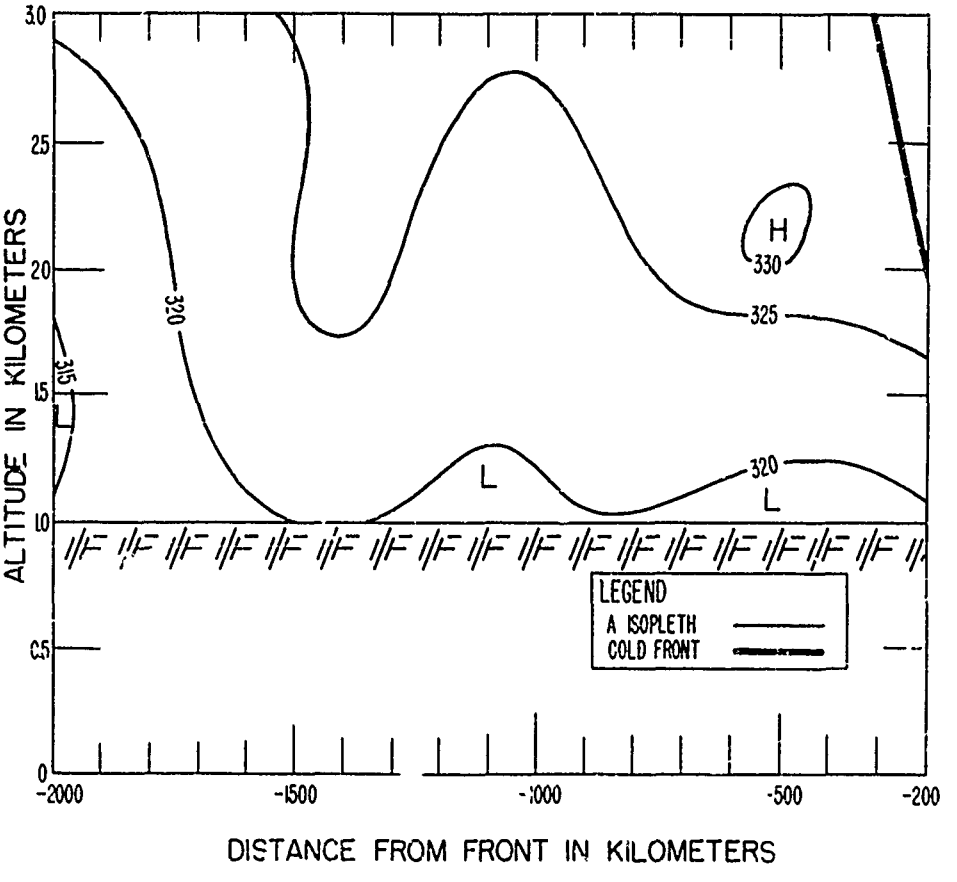

Figure 9.11. Epic Chart in A-Units, Rapid City, South Dakota.

feature here is the absence of detail in the A-structure due to the presence of a uniform air mass over the station. Compare this with the epic chart for Oklahoma City, Okla., figure 9.12, which clearly shows a strong prefrontal A-unit high, a strong gradient across the frontal interface, and an A-unit low behind the front. Figure 9.12 was constructed for a station located at the point of confluence of virtually unmodified polar continental and tropical maritime air.

9.2 Conclusion

Although no general conclusions should be drawn from this single case study, it appears probable that 3-dimensional refractivity models

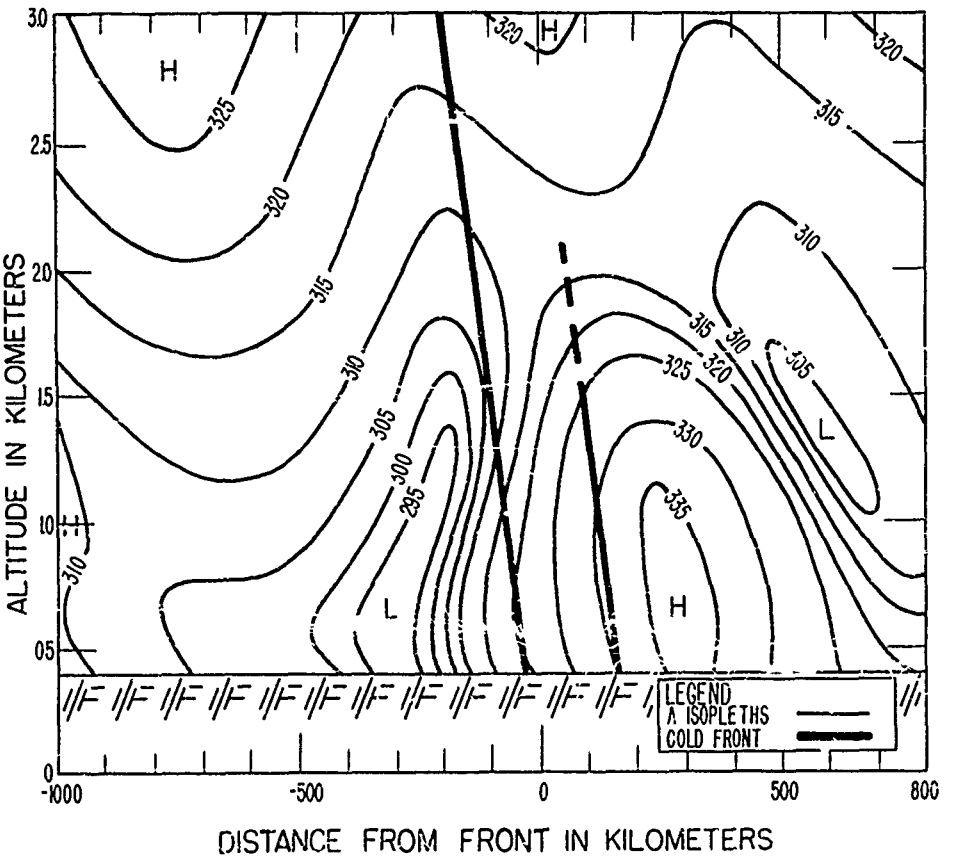

Figure 9.12. Epic Chart in A-Units, Oklahoma City, Oklahoma.

could be developed which could be directly associated with synoptic features and which were generally representative of the refractive properties of the real atmosphere. With this object in mind preliminary models for an idealized, continental, fast-moving cold front and for an idealized, continental warm front have been constructed by Bean, Riggs, and Horn [4] and are shown in figures 9.13 and 9.14. The figures are drawn in the form of cross sections normal to the front and show the frontal surfaces, the directions of motion, and the refractivity fields in the form of A-unit contours. Great care must be exercised in the application of these models, until such time as the details of their construction can be verified by the analysis of a statistically valid number of cases.

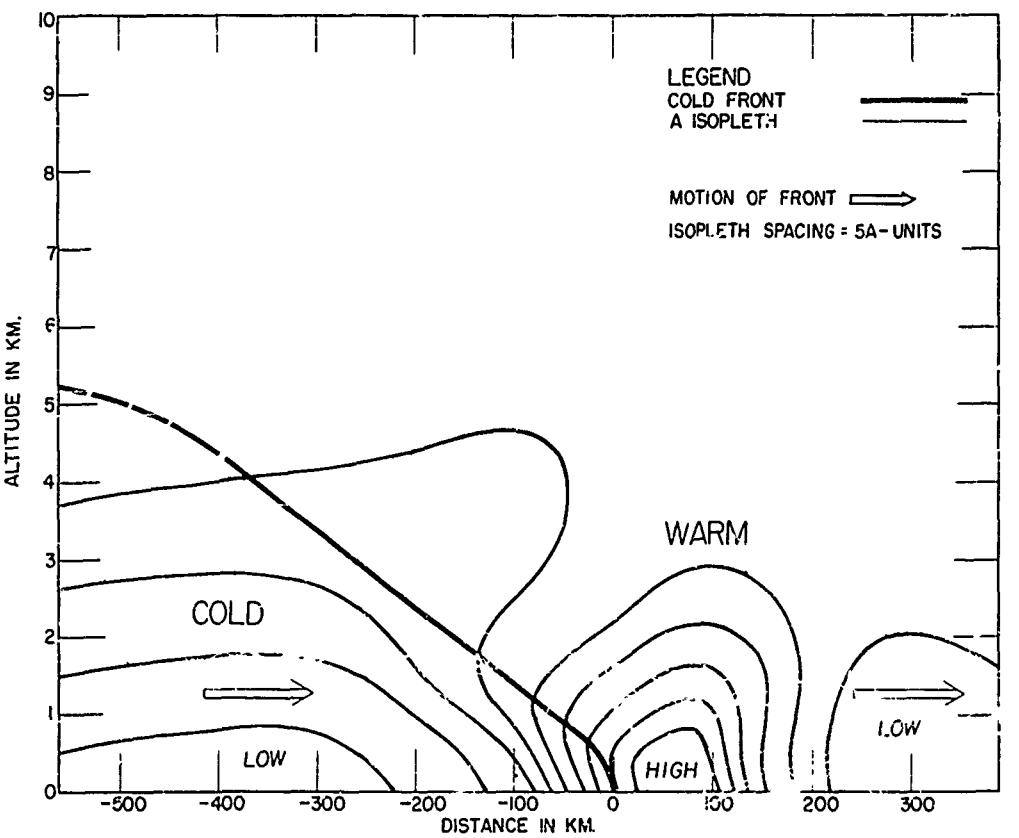

Figure 9.13. Refractive Index Structure Through an Idealized Continental, Fast-Moving Cold Front in A-Units.

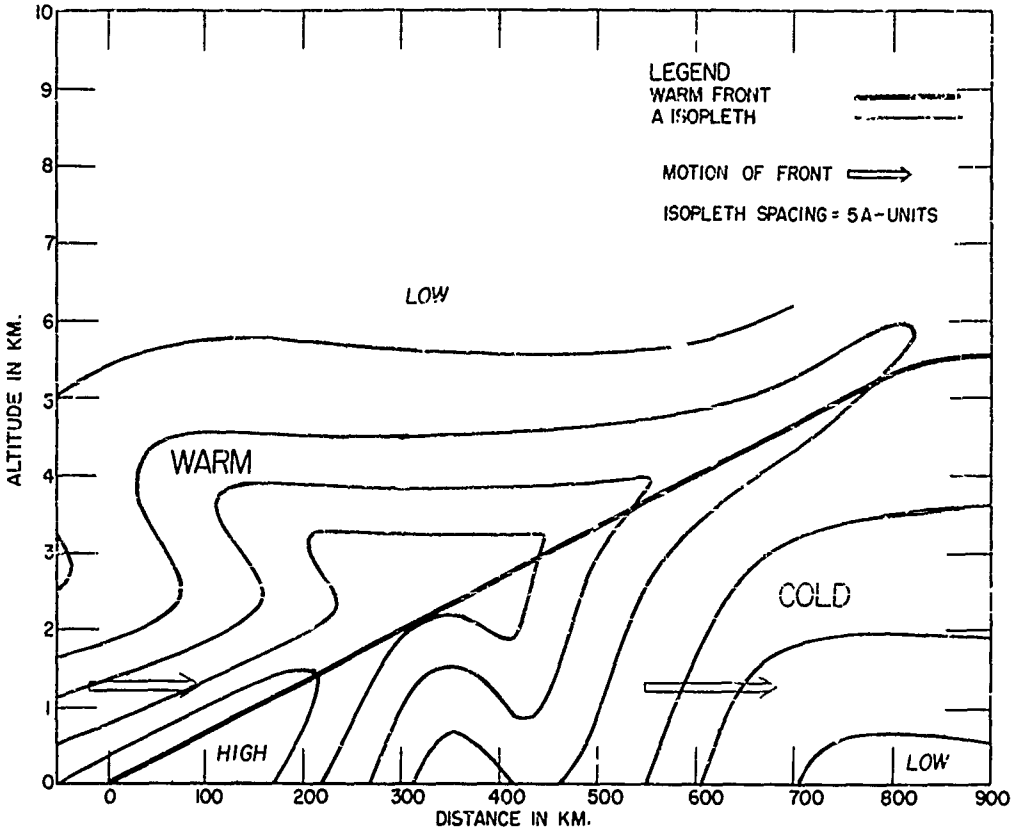

Figure 9.14. Refractive Index Structure Through an Idealized Continental Warm Front in A-Units.

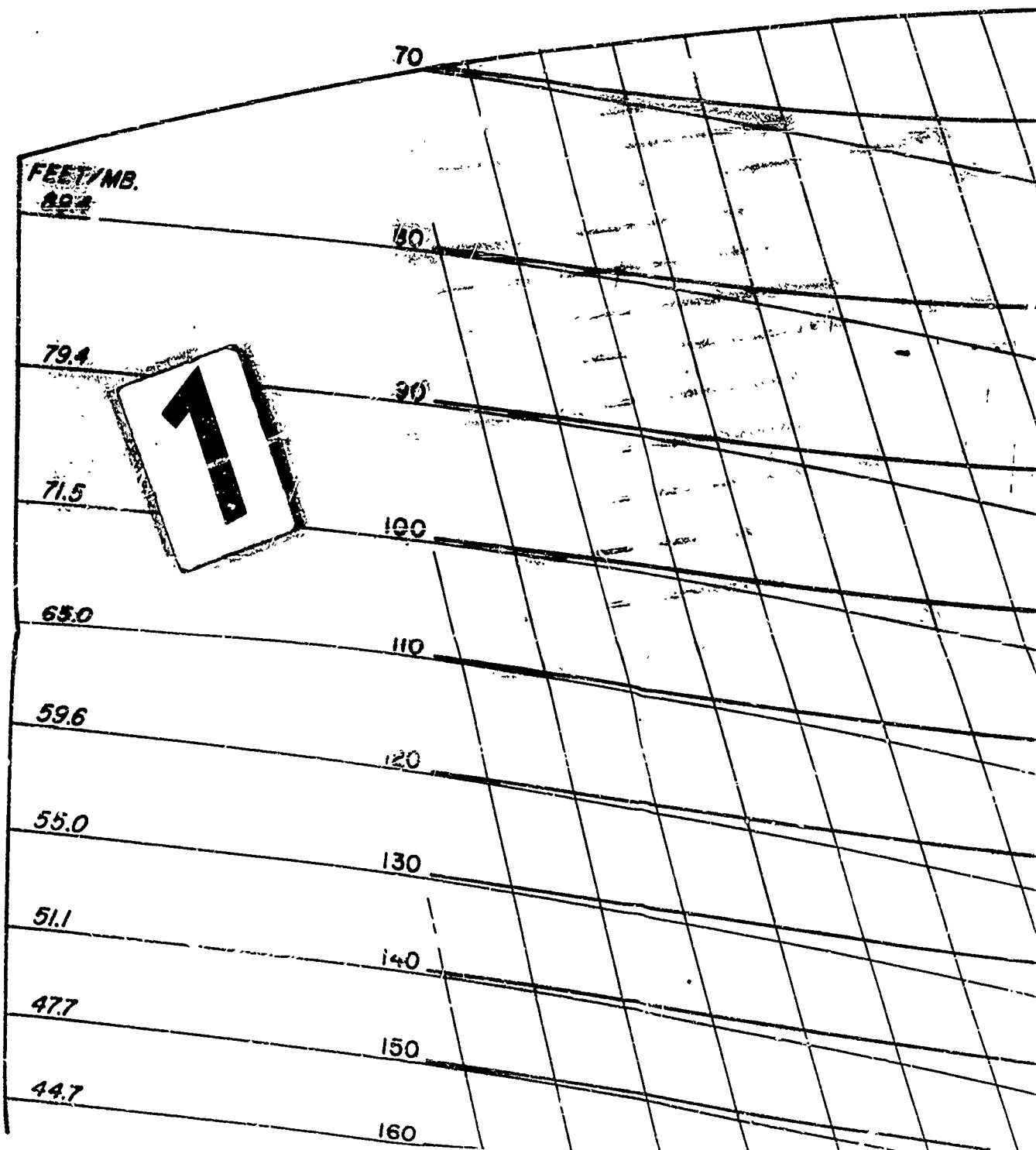
70
FEET/MB.
80.4
80
79.4
90
71.5
100
65.0
110
59.6
120
55.0
130
51.1
140
47.7
150
44.7
160

RACTIVE INDEX OVERLAY

FOR AROWAGRAM

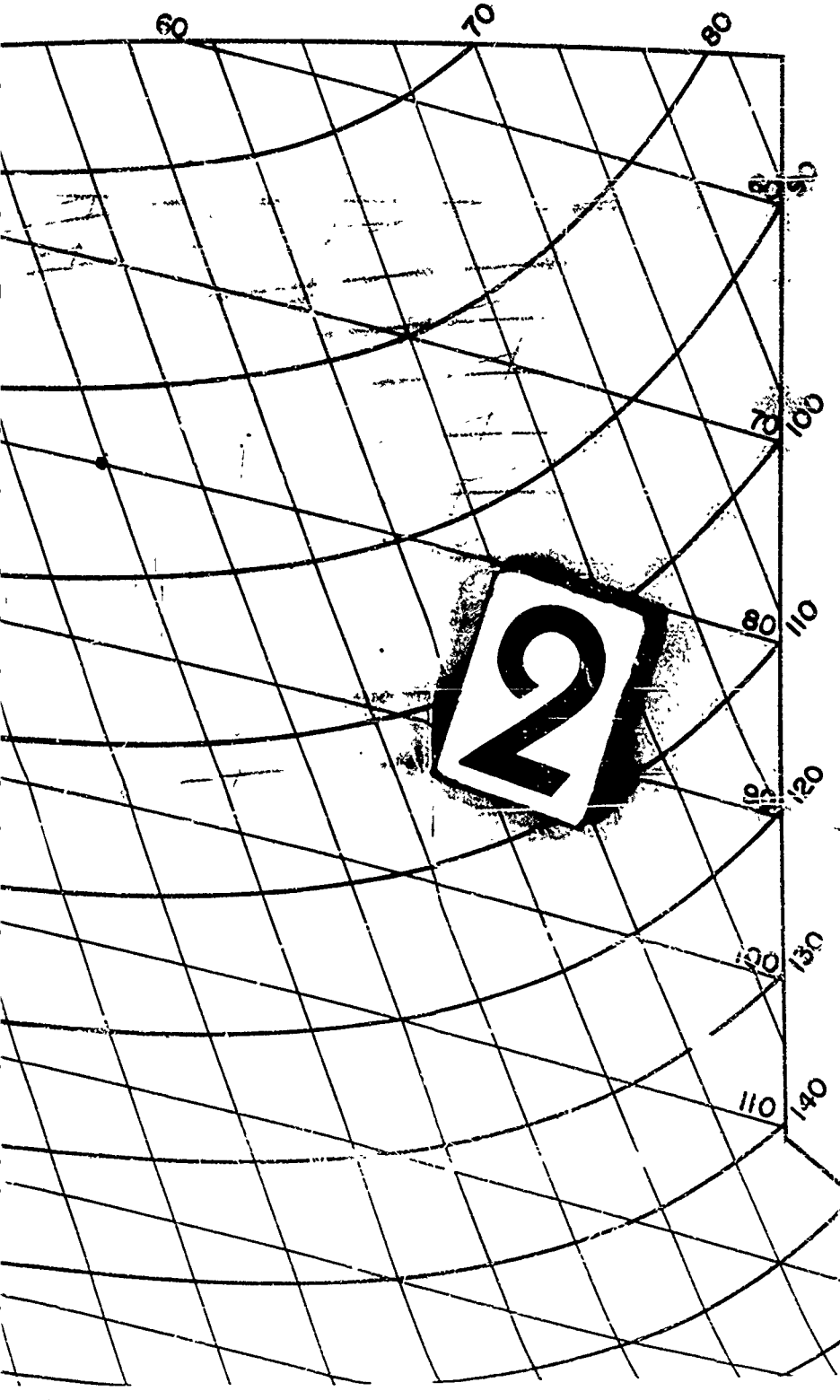

Convenient units for evaluation o
index are $N = (n - 1) \times 10^6$, whe
in the atmosphere is the ratio of
propagation of an electromagnet
vacuum to that in the atmospher
wavelengths between one centim
several me[illegible], N may be evalu
cally: $N = 74.4\ P/T + 370000$

where pressure (P) and vapor p
in millibars and temperature (T
Absolute.

Since vapor pressure is uniquel
from dew-point (D), N may be e
graphically from the plot of T a
P on the AROWAGRAM, the usu
tation of an aerological sounding

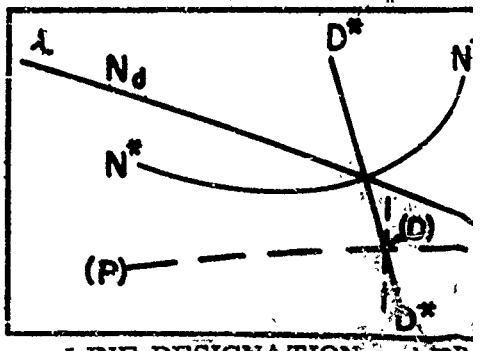

LINE DESIGNATION and PR

N_d: $74.4\ P/T = N$ for absolutely

N^*: $N_d + 370000\ e_s/T^2 = N$ for

[illegible]: Lines of variation of D wit
(N and N_d constant)

TO DETERMINE N FROM
OF T AND D ON THE A

1. Place overlay on
which curves of T

2. For T and
upward and
parallel to

3. Wher

Convenient units for evaluation of refractive index are $N = (n - 1) \times 10^6$, where n at a point in the atmosphere is the ratio of the velocity of propagation of an electromagnetic wave in a vacuum to that in the atmosphere present. For wavelengths between one centimeter and several meters, N may be evaluated empirically: $N = 74.4\ P/T + 370\,000\ e/T^2$

where pressure (P) and vapor pressure (e) are in millibars and temperature (T) is in degrees Absolute.

Since vapor pressure is uniquely determinable from dew-point (D), N may be evaluated graphically from the plot of T and D against P on the AROWAGRAM, the usual representation of an aerological sounding in the Navy.

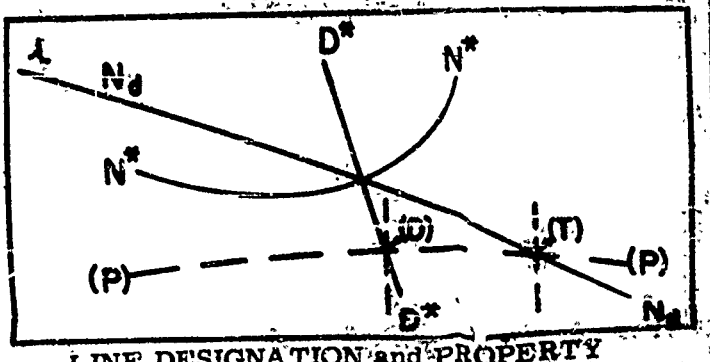

LINE DESIGNATION and PROPERTY

N_d: $74.4\ P/T = N$ for absolutely dry air.

N*: $N_d + 370000\ e_s/T^2 = N$ for saturated air.

D*: Lines of variation of D with P (N and N_d constant)

TO DETERMINE N FROM PLOTS OF T AND D ON THE AROWAGRAM:

1. Place overlay on AROWAGRAM on which curves of T and D are plotted.
2. For T and D at any pressure project upward and toward the left, from P, T, parallel to the N_d curves, and from P, D, parallel to the D* curves.
3. Where these cross, read N from the N* curves.

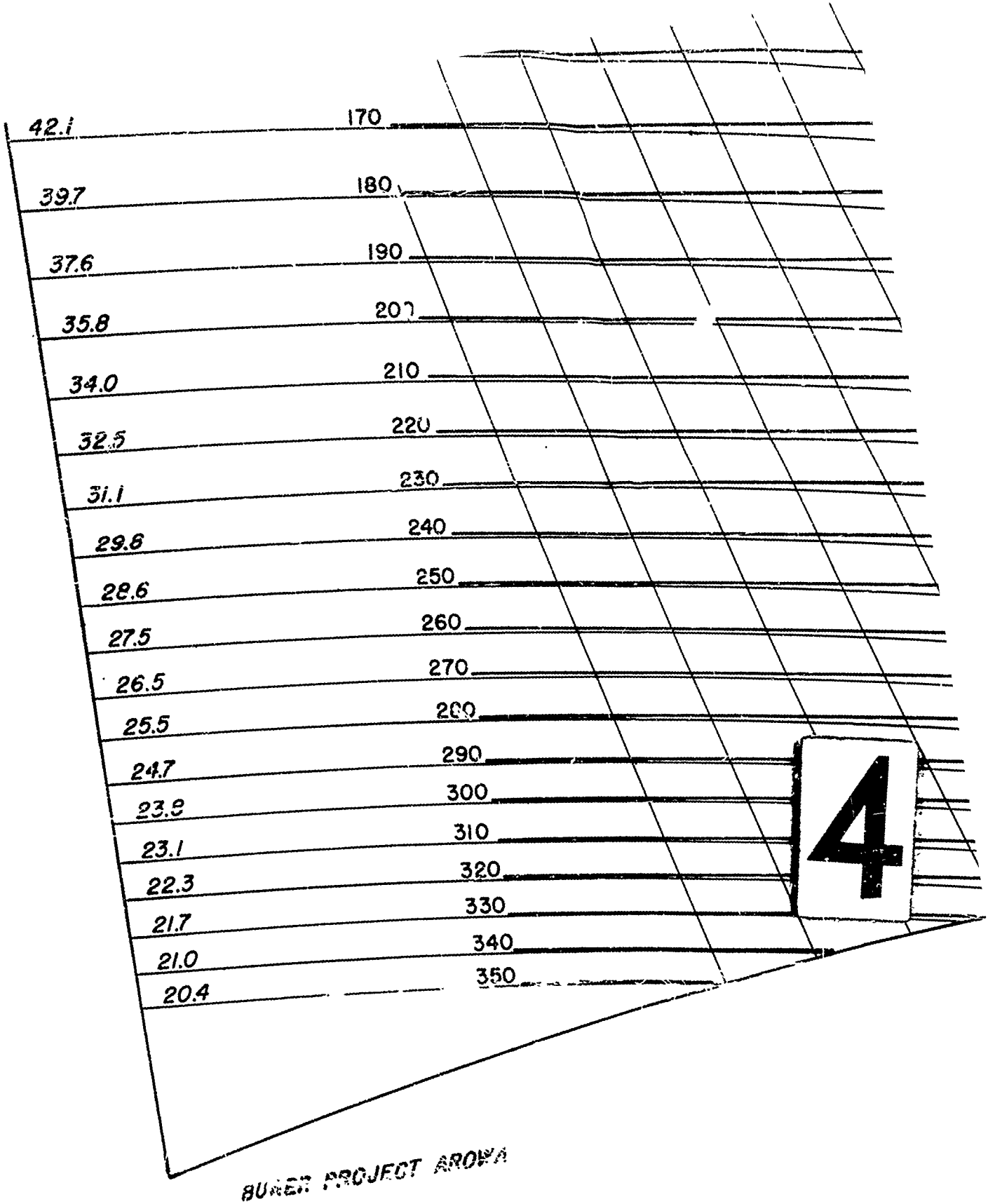
42.1
170
39.7
180
37.6
190
35.8
200
34.0
210
32.5
220
31.1
230
29.8
240
28.6
250
27.5
260
26.5
270
25.5
280
24.7
290
23.9
300
23.1
310
22.3
320
21.7
330
21.0
340
20.4
350
4
BUNKER PROJECT AROWA

160
180
200
220
240
260
280
300
320
330
340
350
360
5

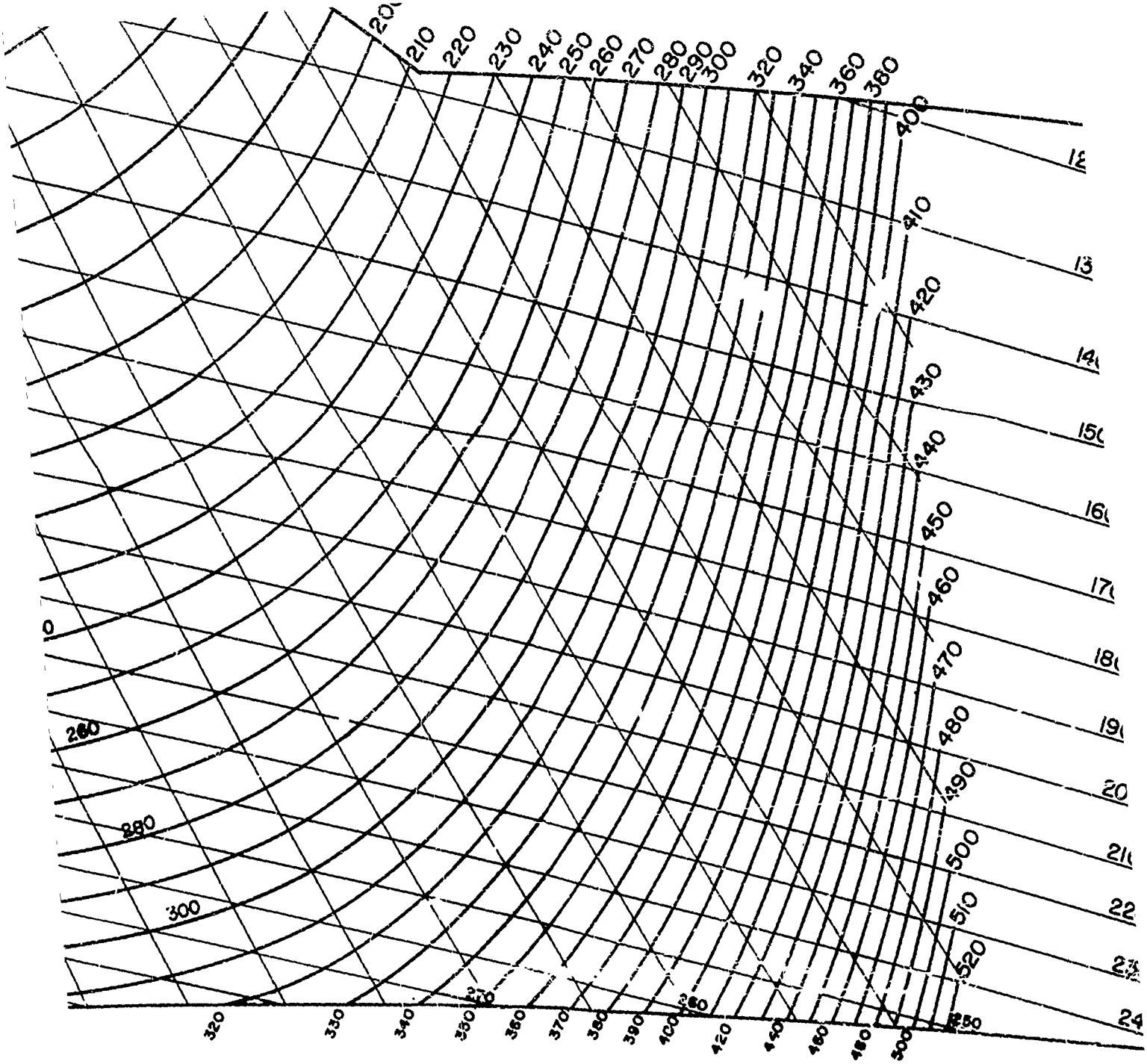
210
220
230
240
250
260
270
280
290
300
320
340
360
380
400
410
420
430
440
450
460
470
480
490
500
510
520
260
280
300
320
330
340
350
360
370
380
390
400
420
440
460
480
500

6

CHART 1

REFERENCES

1. ANDERSON, L. J. and E. E. GOSSARD, "The Effect of the Oceanic Duct on Microwave Propagation." Transactions of the AGU. Vol. 34, pp. 695-700, October 1953.

2. BEAN, B. R., "Climatology of Ground-Based Radio Ducts." Journal of Research of the NBS. Vol. 63D, No. 1, pp. 29-34, July-August 1959.

3. BEAN, B. R. and L. P. RIGGS, "Synoptic Variation of the Radio Refractive Index." Journal of Research of the NBS. Vol. 63D, No. 1, pp. 91-97, July-August 1959.

4. BEAN, B. R., L. P. RIGGS, and J. D. HORN, "Synoptic Study of the Vertical Distribution of the Radio Refractive Index." Journal of Research of the NBS. Vol. 63D, No. 2, pp. 249-254, September-October 1959.

5. BELLAMY, J. C., "The Use of Pressure Altitude and Altimeter Corrections in Meteorology." Journal of Meteorology. Vol. 2, No. 1, pp. 1-79, March 1945.

6. BERRY, F. A., E. BOLLAY, and N. F. BEERS, "Handbook of Meteorology." New York: McGraw-Hill Book Company. pp. 604-621, 1945.

7. BIRNBAUM, G., "Fluctuations in the Refractive Index of the Atmosphere at Microwave Frequencies." Physical Review. Vol. 82, pp. 110-111, April 1951.

8. CHIEF OF NAVAL OPERATIONS, "Meteorological Refractive Effects Upon Radar Wave Propagation." NAVAER 50-1P-52, July 1954.

9. CRAIN, C. M. and A. P. DEAN, "An Airborne Microwave Refractometer." Review of Scientific Instruments. Vol. 23, pp. 149-151, April 1952.

10. DAY, J. P. and L. G. TROLESE, "Propagation of Short Waves over Desert Terrain." Proceedings of the IRE. Vol. 38, pp. 165-175, February 1950.

REFERENCES (Continued)

11. DOHERTY, L. H., "Geometrical Optics and the Field at a Caustic, With Applications to Radiowave Propagation Between Aircraft." Final Report on Contract AF 33(038)-1090, Part V. Ithica, N. Y.: Cornell University, School of Electrical Engineering. September 1952.

12. DOMB, C. and M. H. L. PRYCE, "The Calculation of Field Strengths Over a Spherical Earth." Journal of the IEE. Vol. 94, Part III, pp. 325-336, September 1947.

13. DURST, C. S., "Meteorological Factors in Radio Wave Propagation." Physical Society London and Royal Meteorological Society: Report of 1947 Radio Climatology Conference Held 8 April 1946 at Royal Institution, London. pp. 193-212, 1947.

14. GOSSARD, E. E. and L. J. ANDERSON, "The Effect of Superrefractive Layers on 50-5,000 mc. Non-Optical Fields." IRE Transactions. PGAP AP-4, pp. 175-178, April 1956.

15. HORN, J. D., B. R. BEAN, and L. P. RIGGS, "Some Meteorological Aspects of the Radio Refractive Index." NBS Report 6066. Boulder, Colo.: National Bureau of Standards, Boulder Laboratories. August 1959.

16. JEHN, K. H., "The Use of Potential Refractive Index in Synoptic-Scale Radio Meteorology." Electrical Engineering Research Laboratory, Report No. 6-29 on Contract AF 19(604)-2249. Austin, Texas: University of Texas. September 1959.

17. PETTERSON, S., P. A. SHEPPARD, C. H. B. PRIESTLY, and K. R. JOHANNESSEN, Report on an Investigation of Subsidence in the Free Atmosphere, M.R.P. 207, September 1944.

18. SCHELKUNOFF, S. A., Bell Telephone Laboratory Report MM-44-110-53. July 1944.

REFERENCES (Continued)

19. SCHELLING, J.C., C.R. BURROWS, and E.B. FERRELL, "Ultra-Short-Wave Propagation." Proceedings of the IRE. Vol. 21, No. 3, pp. 427-463, March 1933.

20. SCHULKIN, M., "Average Radio Ray Refraction in the Lower Atmosphere." Proceedings of the IRE. Vol. 40, pp. 554-561, May 1952.

21. SINCLAIR, J. G., "Temperature of the Soil and Air in a Desert." Monthly Weather Review. Vol. 50, pp. 142-153, 1922.

22. SMITH, E. K. and S. WEINTRAUB, "The Constants in the Equation for Atmospheric Refractive Index at Radio Frequencies." Proceedings of the IRE. Vol. 41, pp. 1035-1037, August 1953.

23. SMITHSON, J.A. and G.L. ARNOLD, "Suggested Operational Procedure for Selection of AEW Flight Altitudes." Appendix B to Memorandum Report 7106. Lockheed Aircraft Corporation, Military Operations Research Division. June 1956.

24. U.S. FLEET WEATHER CENTRAL, "Operational Radar Meteorology." Argentia, Newfoundland. July 1957.

25. U. S. NAVY WEATHER RESEARCH FACILITY, "Some Aids for Estimating Atmospheric Refractive Conditions." Report No. NWRF 31-0658-003. Norfolk, Va., June 1958.

26. WEISBROD, S. and L. J. ANDERSON, "Simple Methods for Computing Tropospheric and Ionospheric Refractive Effects on Radio Waves." Proceedings of the IRE. Vol. 47, pp. 1770-1777, October 1959.

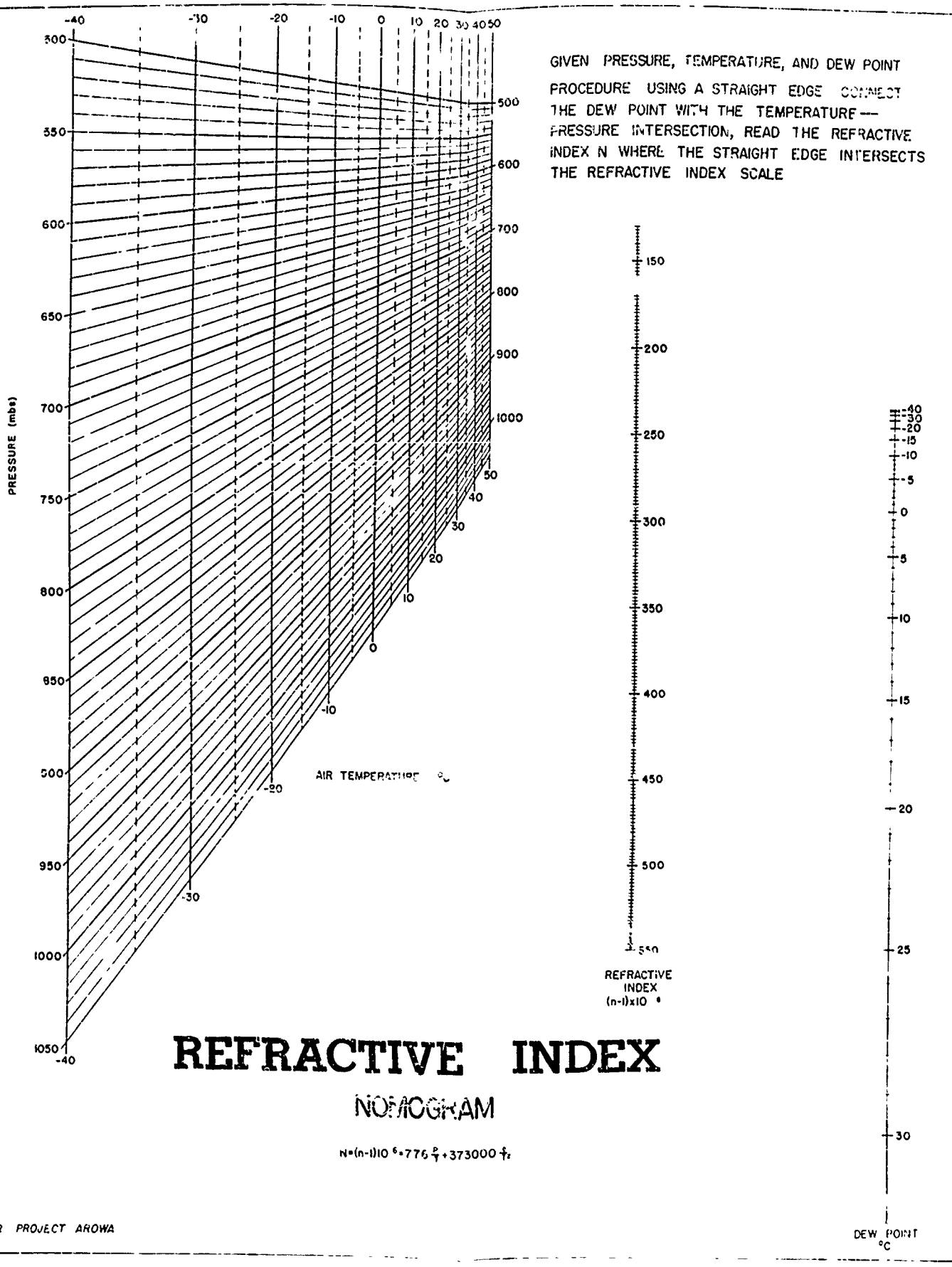

GIVEN PRESSURE, TEMPERATURE, AND DEW POINT PROCEDURE USING A STRAIGHT EDGE CONNECT THE DEW POINT WITH THE TEMPERATURE — PRESSURE INTERSECTION, READ THE REFRACTIVE INDEX N WHERE THE STRAIGHT EDGE INTERSECTS THE REFRACTIVE INDEX SCALE

REFRACTIVE INDEX

NOMOGRAM

$N=(n-1)10^6=776\frac{p}{T}+373000\frac{f}{T}$

BUAER PROJECT AROWA

CHART I

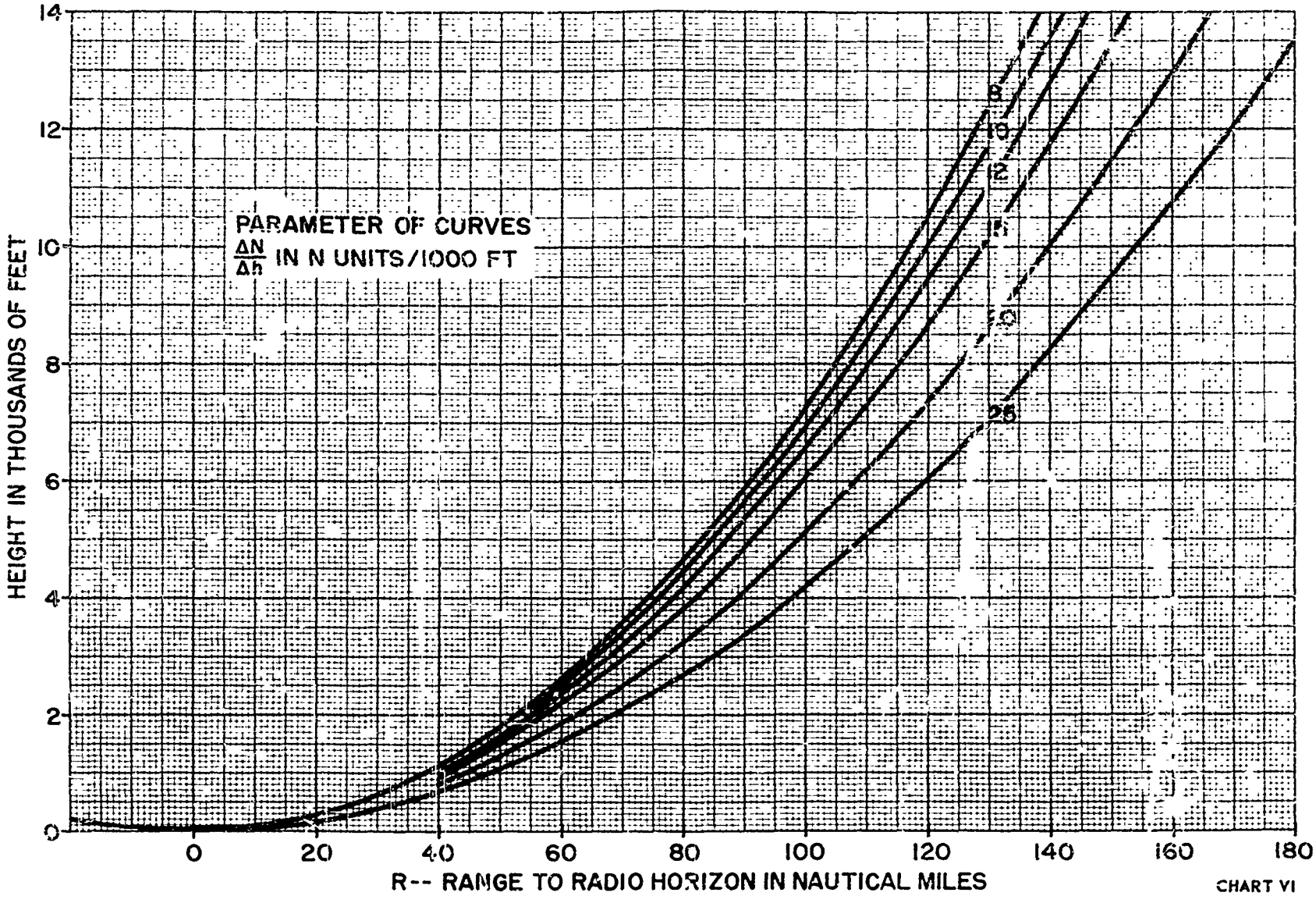
PARAMETER OF CURVES
ΔN/Δh IN N UNITS/1000 FT
8
10
12
15
20
25
HEIGHT IN THOUSANDS OF FEET
0
2
4
6
8
10
12
14
0
20
40
60
80
100
120
140
160
180
R-- RANGE TO RADIO HORIZON IN NAUTICAL MILES

CHART VI

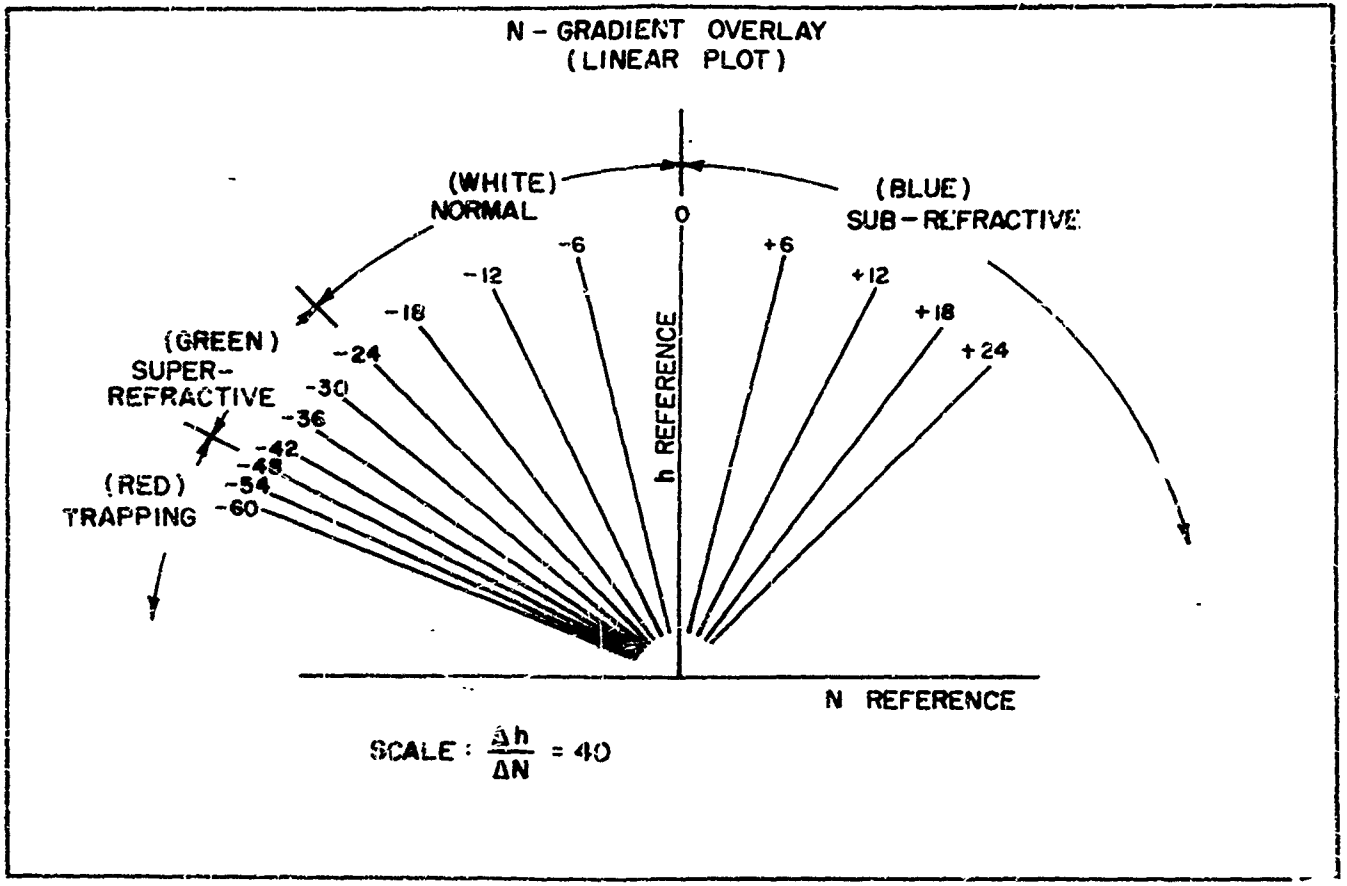
N - GRADIENT OVERLAY
(LINEAR PLOT)
(WHITE)
NORMAL
0
(BLUE)
SUB - REFRACTIVE
-6
+6
-12
+12
-18
+18
+24
(GREEN)
SUPER-
REFRACTIVE
-24
-30
-36
-42
-48
-54
-60
(RED)
TRAPPING
h REFERENCE
N REFERENCE
SCALE : Δh/ΔN = 40

CHART IV

FLEET WEATHER FACILITY
ARGENTIA, NEWFOUNDLAND

RADIOSONDE N-GRADIENTS

THE APPARENT GRADIENT OF THE INDEX OF REFRACTION N CORRESPONDING TO AN ACTUAL GRADIENT OF -47.8N UNITS PER 1000 FEET PRESSURE ALTITUDE DUE TO LAG OF THE RADIOSONDE TEMPERATURE AND HUMIDITY ELEMENTS.

TO USE

1. PLOT AN N vs P CURVE ON AROWAGRAM. RELABEL -80°C=100N, -60°C=200N, ETC.
2. ALIGN CURVE ±0. DETERMINE ZONE OR COMBINATION OF ZONES THROUGH WHICH RAOB TEMPERATURE CURVE PASSES.
3. EVALUATE GRADIENTS OF N vs P CURVE BY COMPARISON WITH CURVE IN APPROPRIATE ZONE AS DETERMINED ABOVE. FOR CURVES +50 AND -50, THE DIAGRAM ... BE INVERTED AND REALIGNED.
4. IN FIGURE BELOW, GRADIENTS IN AREA:
   - ① = TRAPPING
   - ② = SUPER-STANDARD (non-trapping)
   - ③ = SUB-STANDARD (non-trapping)
   - ④ = SUB-REFRACTIVE (non-trapping)

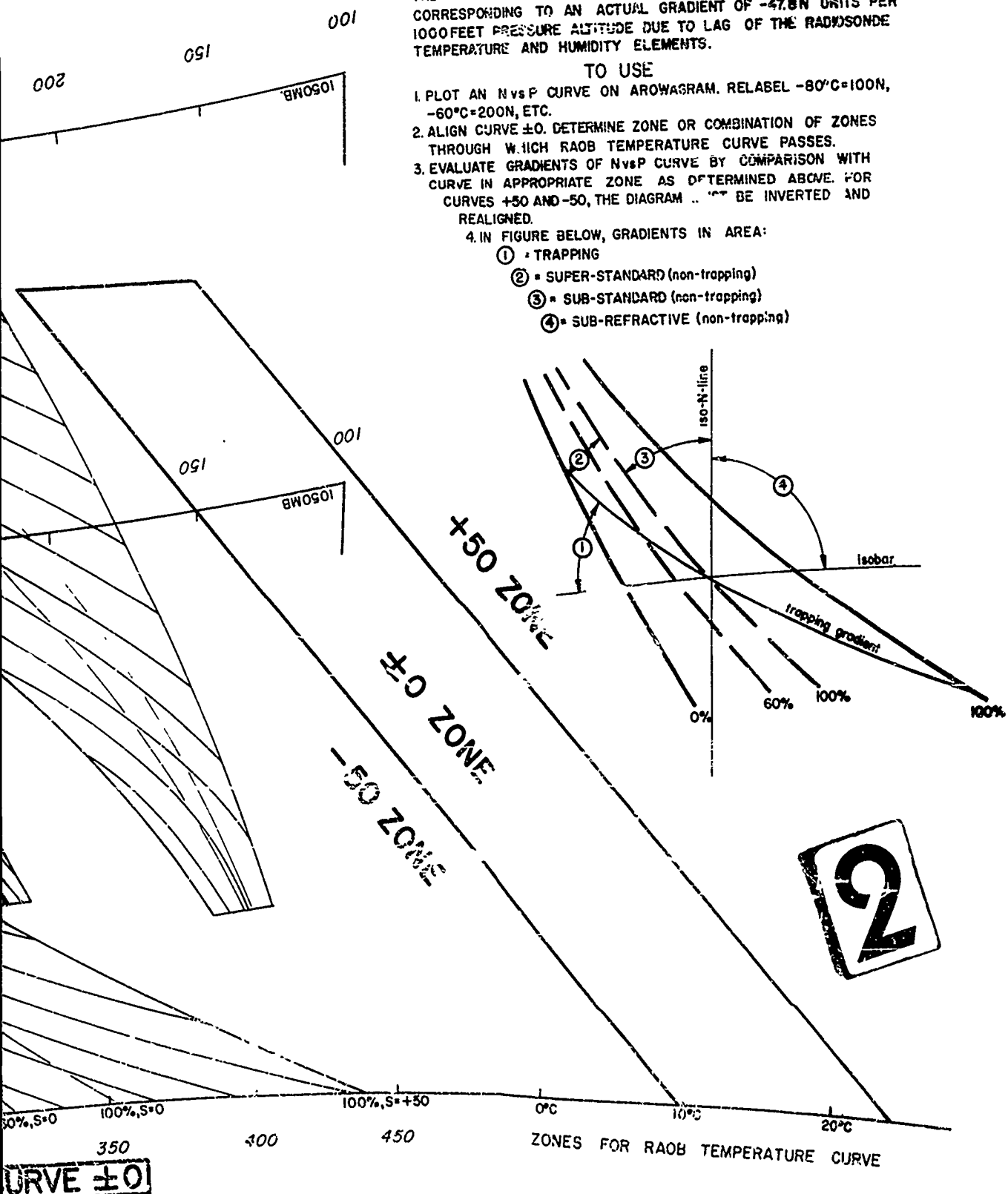

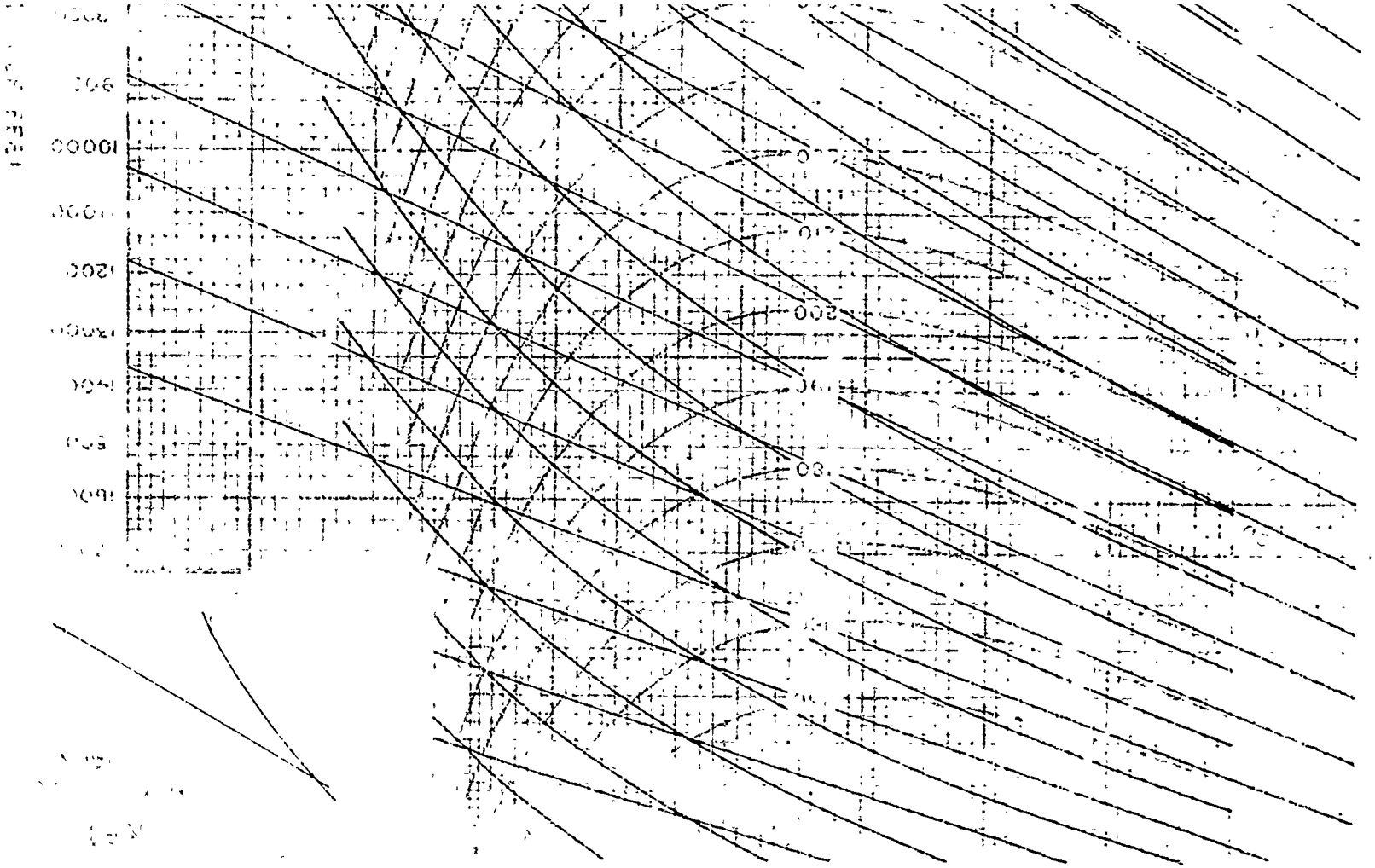

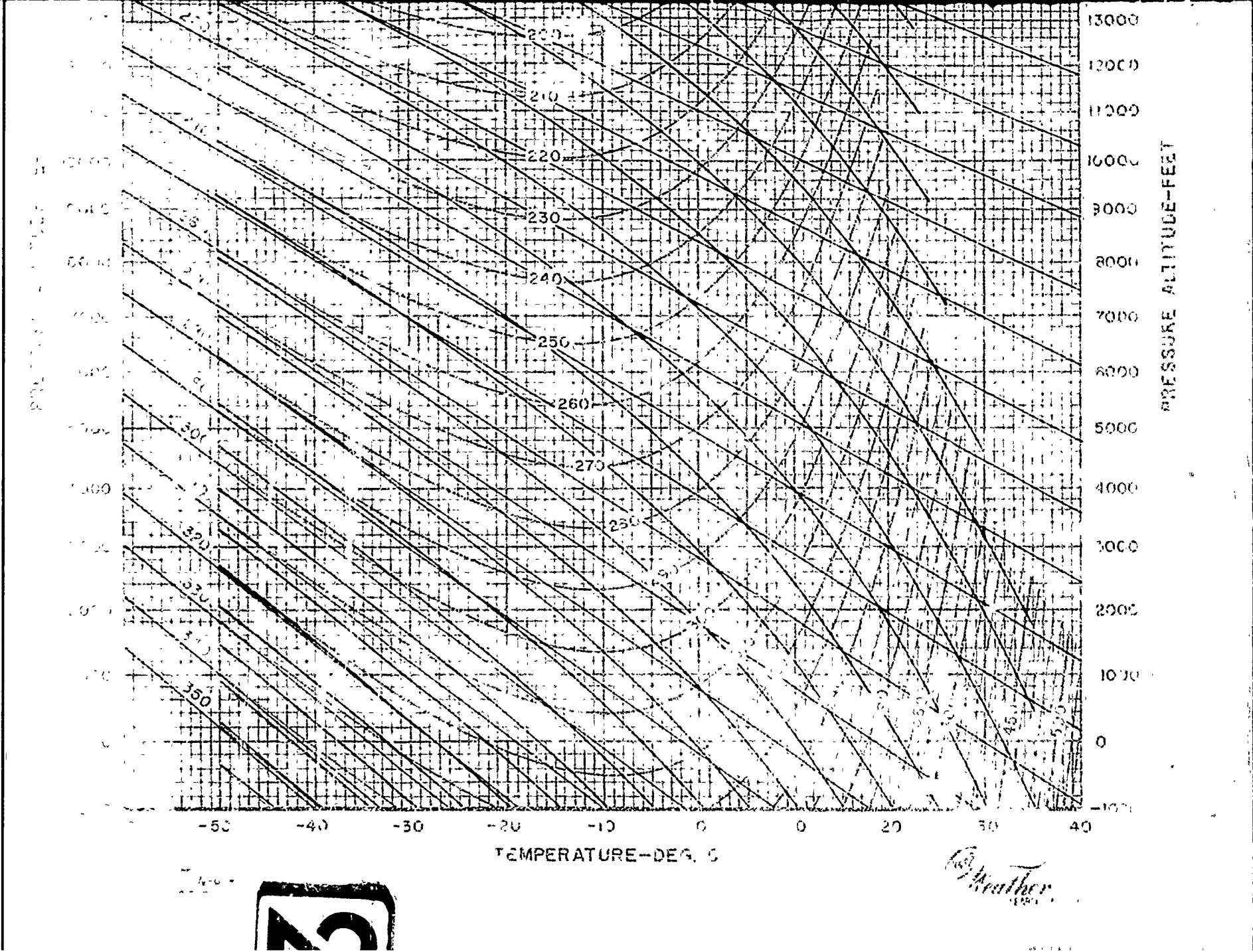
200
210
220
230
240
250
260
270
280
290
300
310
320
330
340
350
13000
12000
11000
10000
9000
8000
7000
6000
5000
4000
3000
2000
1000
0
-1000
PRESSURE ALTITUDE-FEET
-50
-40
-30
-20
-10
0
10
20
30
40
TEMPERATURE-DEG. C

INSTRUCTIONS FOR THE USE OF THE REFRACTIVE INDEX DIAGRAM

A. Description:

The most common index of atmospheric conditions used in studies of radar propagation is the refractivity, N. Its exact definition in relation to the classical index of refraction is shown in section C below, where a formula for its determination from observed values of pressure, temperature, and the partial pressure of water vapor is also shown. Since the vapor pressure is difficult to measure directly from an aircraft, a requirement has existed for a convenient method of computing N from the directly observable quantities: PA (pressure altitude - altimeter reading when the altimeter is set to standard sea-level pressure), T (temperature), and T_w (wet bulb temperature). The REFRACTIVE INDEX DIAGRAM has been designed to fulfill this requirement.

The ordinate of the diagram is pressure altitude, in feet, labeled along both sides of the diagram. The absissa is temperature, labeled in degrees C. The heavy brown lines, concave upward and labeled both near the center of each line and near the left hand margin, are curves from which values of N are finally read. The two sets of blue lines are used as guide lines in the determination of N. One set of these blue lines, the straight ones, share with the brown N lines the set of labels just inside the left margin, and show by that label the N value of perfectly dry air of any given PA and T. The other, curved, set of blue lines is related to T_w, but carries no labels.

B. To Use:

1. From the point (T, PA), project a straight line upward and to the left following the straight blue lines (the dry N lines).
2. From the point (T_w, PA), project a curved line upward and to the left using the curved blue lines as a guide.
3. At the intersection of the two projected lines, read the refractivity from the N curves.

C. Design Equation:

The classical index of refraction, n, is the ratio of the speed of light or electro-magnetic propagation in vacuo to the speed through the medium actually traversed. Since in the atmosphere the significant range of n is greater than unity by only a few parts in a million, it is convenient to name and define a quantity expressing the departure of n from unity in millionths. This quantity has been named refractivity, and its relation to n is

$$N = (n - 1) \times 10^6 .$$

It has been found that N can be closely determined as a function of P (pressure, measured in millibars), T (temperature, measured in degrees C.), and e (partial pressure of water vapor, measured in millibars), by the equation:

$$N = \frac{77.6}{273.16 + T} \left(P + \frac{4810e}{273.16 + T}\right) . \qquad \text{Eq. 1}$$

According to the Sixth Revised Edition of the Smithsonian Meteorological Tables, the vapor pressure may be expressed in terms of pressure, temperature and wet bulb temperature as follows:

$$e = e' - [0.000660\ (1 + 0.00115\ T_w)]\ P\ (T - T_w)$$

in which T_w is wet bulb temperature in degrees C., and e' is the saturation vapor pressure at temperature T_w. Substituting this into Eq. 1 gives

$$N = \frac{77.6\ P}{273.16 + T} + \frac{77.6 \times 4810e'}{(273.16 + T)^2} - \frac{77.6 \times 4810[0.000660(1 + 0.00115\ T_w)]\ P(T - T_w)}{(273.16 + T)^2} . \qquad \text{Eq. 2}$$

Since e' is a function of T_w only, N is expressed as a function of P, T, and T_w by Eq. 2. The Refractive Index Diagram provides a solution to Eq. 2, except that the ordinate of the diagram has been labeled to permit entry of PA instead of P.

D. Accuracy:

The diagram is accurate for computations for either dry or saturated air. For moist unsaturated air the solution is approximate, but it is rarely in error by more than four N units. In any event, errors in observing pressure, temperature, and wet bulb temperature aboard an aircraft in flight are almost certain to contribute greater errors in N than the approximation in the diagram will contribute.